The Oceanography and Modelling of the Pontevedra Ria (NW Spain)

A. W. Dale

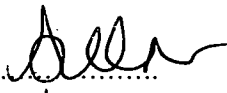Ph.D   2003

Copyright

This copy of the thesis has been supplied on condition that anyone who consults it is understood to recognise that its copyright rests with the author and that no quotation from the thesis and no information derived from it may be published without the author's prior written consent.

Signed...

Date......1|9|03

The Oceanography and Modelling of the Pontevedra Ria (NW Spain)

By

Andrew W. Dale M.Sc, B.Sc. (Hons)

A thesis submitted to the University of Plymouth in partial fulfilment for the degree of

Doctor of Philosophy

Department of Environmental Sciences
Faculty of Science

In collaboration with:

Instituto de Investigaciones Marinas (CSIC)
Vigo, Spain

The Oceanography and Modelling of the Pontevedra Ria (NW Spain)

Andrew William Dale

Abstract

A multidisciplinary study the oceanography of the Pontevedra Ria (NW Spain), including hydrography, biogeochemistry and biogeochemical modelling, has been performed. The hydrographical variability of the Pontevedra Ria was dependent on freshwater inputs and upwelling of nutrient-rich East North Atlantic Central Water from the shelf. Intrusions of the Poleward Current were also detected during winter. A stratified box model approach predicted that upwelling water fluxes into the ria of $2\text{-}4 \times 10^3$ m^3 s^{-1}, of which >30% rises to the surface waters inside the ria. Freshwater residence time varied from ~4-9 d in the central ria and 1-4 d in the internal ria.

Nutrients concentrations showed a strong fluvial and oceanic signal, with a clear zone of near-bed aerobic remineralisation in the internal ria. Nutrient flux experiments showed that high nutrient fluxes, particularly ammonium (3.5 mg N m^{-2} h^{-1}), coincided with period of high water influx to the ria. These were related to stirring of quasi-benthic phytodetrital fluff. Denitrification was a major fate for particulate organic nitrogen in the sediment, averaging 2.5 mg N m^{-2} h^{-1} for the spring and dry season. A non-steady state nutrient budget revealed that the central and internal zones of the Pontevedra Ria display different biogeochemical characteristics. Net community production (*NCP*) based on phosphate uptake was spatially and temporally variable, with rates of 9.6 and 20.2 mg C m^{-2} h^{-1} in central and internal rias in spring, respectively, and 30.3 and 29.0 mg C m^{-2} h^{-1} in the dry season. Previously unquantified benthic nutrient inputs were important, and up to 25% of *NCP* was due to the sediment nutrient flux in the dry season. Denitrification calculated with the nutrient budget equalled 1.82 and 5.66 mg N m^{-2} h^{-1} in the dry season in the central and internal ria, respectively, and was equal to 27 and 42% of dry season *NCP*. The robustness of the box model was questioned, and found to be an unsuitable modelling approach for the Rias Bajas. This had clear implications for predicting *NCP* and net nutrient budgets to the coastal zone.

Salinity and temperature were simulated with the commercially-available simulation shell, ECoS, to within the analytical error of the observed data. Inorganic nutrient concentrations and benthic effluxes were qualitatively and quantitatively agreeable with observed data. Phytoplankton growth in ECoS was limited by up to 30% by phosphorus rather than nitrogen, as previously believed. The annual evolution of *NCP* was successfully reproduced by examining the chlorophyll-normalised rate of organic carbon production. Mean *NCP* in the spring and dry season was 46.5 and 147 mg c m^{-2} h^{-1}, which agreed well with the literature. There were clear discrepancies between box model and ECoS-derived nutrient export to the Atlantic ocean. The definitions of constituent uptake and remineralisation processes between the two approaches were examined in the context of biogeochemical modelling and environmental management of the Rias Bajas.

Acknowledgements

Declaration

At no time during the registration for the degree of Doctor of Philosophy has the author been registered for any other University Award.

This study was jointly financed by Plymouth Environmental Research Centre (PERC) and the Comisión Interministerial de Ciencia y Tecnología (CICYT, Spain). The Spanish funds were provided under the multidisciplinary, project "CICYT-MAR96-1782: The hydrodynamics and biogeochemical cycle of silicate in the Pontevedra Ria". The project field work was conducted between October 1997 and October 1998 and the assistance of all those involved is duly and gratefully acknowledged. This thesis is founded on the data collected during the sampling campaigns – the author was not responsible for the analytical procedures followed or sample analysis. A substantial part of this thesis has been published or submitted for publication. Published papers by the author while registered for the research degree can be found at the end of this thesis.

Publications: Peer reviewed

- **Dale, A. W.** & Prego, R. 2003 Tidal and seasonal nutrient dynamics and budget in the Chupa Estuary, White Sea, Russia. *Estuarine Coastal and Shelf Science* **56**, 377-389.
- **Dale, A. W.** & Prego, R. 2002. Physico-biogeochemical controls on benthic-pelagic coupling of nutrient fluxes and recycling in a coastal inlet affected by upwelling. *Marine Ecology Progress Series* **235**, 15-28.
- Prego, R., **Dale, A. W.** et al. 2001 Hydrography of the Pontevedra Ria: Intra-annual spatial and temporal variability in a Galician coastal upwelling system (NW Spain). *Journal of Geophysical Research* **106 (C9)**, 19845-19858.
- **Dale, A. W.** & Prego, R. Modelling net community metabolism in the Pontevedra Ria (NW Spain) upwelling system. *Estuarine Coastal and Shelf Science. In revision.*
- González, A. F., Otero, J., Guerra, A., Prego, R., Rocha, F. J. & **Dale, A. W.** Influence of the oceanographic regime on the planktonic phase of *Octopus vulgaris* in a seasonal upwelling region. *Marine Ecology Progress Series. Submitted.*
- **Dale, A. W.,** Prego, R., Millward, G. E. & Gómez-Gesteira, M. Transient oceanic and tidal contributions to water exchange and residence times in a coastal upwelling system in the NE Atlantic: the Pontevedra Ria, Galicia. Marine Pollution Bulletin. *Submitted.*

Publications: Non-peer reviewed

- Prego, R. & **Dale, A. W.** (2002). The Chupa Arctic estuary (White Sea) during the dry season: nutrient and oxygen budgets. In: *Estuarine systems of the Latin American region and estuarine systems of the Arctic region: carbon, nitrogen and phosphorus fluxes* (Camacho-Ibar V., Dupra V., Wulff F. Smith S.V., Marshall J.I. & Crossland C.J., eds.). LOICZ Reports and Studies **23**: 72-76, 93-95.
- **Dale, A. W.** & Prego, R. 2002 Net autotrophy and heterotrophy in the Pontevedra Ria (NW Spain): nitrate and phosphate cycling and fluxes. XI Iberian Seminary on Marine Chemistry, Faro (Portugal), 2-4 April 2002. *In Press.*
- Prego, R & **Dale, A. W.** 2001 Coastal systems to the north of Portugal: biogeochemical view of eutrophication in the Spanish Rias Bajas. In *Estuaries and the Coastal Zone of Northern Portugal: State of the Art.* Estuarine and Coastal Sciences Association (ECSA), Porto, 15-17 June 2001. *In press.*

Conferences and presentations

- Oral Presentation:
  Dale, A. W. *Hydrography and biogeochemistry of the Pontevedra Ria upwelling system (NW Spain): approaches and considerations for modelling.* Department of Geochemistry, University of Utrecht, Holland, 5 December 2002.
- Oral Presentation:
  Dale, A. W., Prego, R. & Millward, G. E. *Coupling Between Net Ecosystem Metabolism and Nitrification-Denitrification in an Upwelling System on the NW Iberian Coast.* ECSA Symposium 34: Estuaries and other Brackish Areas – Pollution Barriers or Sources to the Sea? Gdańsk-Sopot, Poland, 15-20 September 2002.
- Poster Presentation:
  Dale, A. W., Prego, R. & Millward, G. E. *Spring-Cleaning the Iberian Coastal Margin: The Role of Upwelling-Induced Benthic Ammonium Effluxes to the Nitrogen Cycle in the Pontevedra Ria (NW Spain).* The Challenger Society for Marine Science, Centenary conference: Marine Science 2002, Plymouth (UK), 9-13 September 2002.
- Poster Presentation:
  Dale, A. W. & Prego, R. *Net autotrophy and heterotrophy in the Pontevedra Ria (NW Spain): nitrate and phosphate cycling and fluxes.* XI Iberian Seminar on Marine Chemistry, Faro (Portugal), 2-4 April 2002.
- Oral Presentation:
  Dale, A. W. & Prego, R *Tidal and Seasonal Nutrient Dynamics and Budget in the Chupa Estuary, White Sea (Russia): Preliminary Results.* XIV International Conference on Marine Geology, Shirshov Institute of Oceanology, Moscow, 24-29 October 2001.
- Oral Presentation:
  Dale, A. W. *Water Residence Times in Estuaries and Rias: Quantification and Influence on Contamination Processes.* Institute of Civil Maritime Studies, University of Oviedo, Spain, 11 July 2001.
- Poster Presentation:
  Dale, A. W. & Prego, R. *Terrestrial and oceanic contributions of nitrate and phosphate to the Pontevedra Ria. Autotrophy versus heterotrophy?* Oceanus III Millennium. International Conference of Science and Marine Technology, Pontevedra, Spain, 24-27 April 2001.
- Oral Presentation:
  Dale, A. W. *Coastal Upwelling: Hydrography, Chemistry and Biology.* Norwegian Fisheries Institute, University of Tromsø, Norway, 12 April 2001.

Seminars and courses attended

- RYA Level 2 Powerboat Handling, 17-18 October 2002
- COZONE Coastal Waters Network. First Meeting, Kings College, London, 25 June 2002
- Sea-bird Oceanographic Instruments: CTD maintenance, data retrieval, filtering and manipulation. Institute of Marine Research, Vigo, Spain, 16-17 October 2000

Contents

5. Hydrodynamic modelling of the Pontevedra Ria with ECoS

6. Conclusions

References

List of Figures

List of Tables

Glossary of terms used throughout the text

Parameter or variable	Unit	Description
Area	m^2	Cross-sectional area
Bathy	m	Bathymetry at any point
Bn	$mg\ m^{-2}\ h^{-1}$	Rate of benthic nutrient efflux
BSi	$\mu mol\ l^{-1}$	Biogenic silica
C	Ocktas	Cloud cover
Chl a	$mg\ m^{-3}$	Chlorophyll a
Depth	m	Water depth
D_{net}	$mg\ m^{-2}\ h^{-1}$	Net denitrification in the sediment
Dropout	$mg\ m^{-2}\ h^{-1}$	The process of sedimentation of particulate matter
DIN, DIP	$\mu mol\ l^{-1}$	Dissolved inorganic nitrogen / phosphate
DOM	$\mu mol\ l^{-1}$	Dissolved organic matter
ENACW	-	East North Atlantic Central Water
$\varepsilon_S,\ \varepsilon_T$	-, °C	Analytical error of CTD salinity and temperature measurements
$\varepsilon_{Nu},\ \varepsilon_{\Delta Nu}$	$\mu mol\ l^{-1},\ \mu mol\ s^{-1}$	Analytical error of nutrient concentration and nutrient budget
$\varepsilon_Q,\ \varepsilon_V,$	$m^3\ s^{-1}$.	Analytical error of horizontal and vertical advective fluxes
$\varepsilon_Z,\ \varepsilon_{Vo}$	$m^3\ s^{-1};\ m^3$	Analytical error of residual freshwater flow and water volume
ε_τ	d	Analytical error of freshwater residence time
$\overline{E}_{Vc},\ \overline{E}_{Vi}$	$m^3\ s^{-1}$	Mean diffusive vertical salt flux between two consecutive surveys
f	-	Fraction of freshwater
f_W	-	Dimensionless weighting factor
Friction	s^{-1}	Momentum loss due to bed friction
FFW	-	Fraction of freshwater method for residence time evaluation
g	$m\ s^{-2}$	Acceleration due to gravity
GPP	$mg\ C\ m^{-2}\ h^{-1}$	Gross primary production
H	$W\ m^{-2}$	Net heat exchange across the water surface
H_1	$W\ m^{-2}$	Long-wave radiation heat gain from atmospheric water vapour
H_2	$W\ m^{-2}$	Radiation heat loss
H_E	$W\ m^{-2}$	Heat loss due to evaporation
H_S	$W\ m^{-2}$	Sensible heat loss
H_{SW}	$W\ m^{-2}$	Heat gain from short-wave radiation
I_W	$m^3\ s^{-1}\ km^{-1}$	Upwelling index
K_O	m^{-1}	Wave number
K_X	$m^2\ s^{-1}$	Longitudinal dispersion coefficient
MX	$kg\ m^2\ s^{-1}$	ECoS modelled momentum
n	$s\ m^{-2/3}$	Manning coefficient
N	min^{-1}	Brunt-Väisälä stability frequency
NCP	$mg\ C\ m^{-2}\ h^{-1}$	Net community production
$NCP_N,\ NCP_P$	$\mu mol\ l^{-1}$	Net community production based on ΔDIN, ΔDIP
NH_4^+	$\mu mol\ l^{-1}$	Ammonium
NO_3^-	$\mu mol\ l^{-1}$	Nitrate
NO_2^-	$\mu mol\ l^{-1}$	Nitrite
$NO_{3/2}^-$	$\mu mol\ l^{-1}$	The sum of nitrate plus nitrite
Nu	-	Dissolved inorganic nutrient (DIN, DIP, $Si(OH)_4$)
$(Nu{:}Nu)_{P,D,F}$	-	Nutrient ratio in the particulate, dissolved phase and efflux.
ΔNu	$mol\ s^{-1}$	Non-steady state nutrient budget between two consecutive surveys
ΔN	$mg\ m^{-2}\ h^{-1}$	Dissolved inorganic nitrogen anomaly
$N_{storgae},\ Si_{storgae}$	$mg\ m^{-2}\ h^{-1}$	Temporary PON and BSi storage in sediments
$O_2,\ O_{2SAT}$	$\mu mol\ l^{-1},\ \%$	Dissolved oxygen and dissolved oxygen saturation
POM, POC, PON	$\mu mol\ l^{-1}$	Particulate organic matter / carbon / nitrogen
Q_L	$m^3\ s^{-1}$	Box model incoming advective flux

Symbol	Units	Description
Q_{L-T}	m^3 s^{-1}	Box model exchange flux due to tides
Q_{L-M}	m^3 s^{-1}	Box model advection and mixing flux
$\overline{Q_U \times S_U}$, $\overline{Q_L \times S_L}$	kg m^{-3} s^{-1}	Mean surface and bottom advective salt fluxes at the model boundaries between two consecutive surveys
$\overline{Q}_U$, $\overline{Q}_L$	m^3 s^{-1}	Mean surface and bottom advective water fluxes at the model boundaries between two consecutive surveys
$\overline{Q}_Z$	m^3 s^{-1}	Mean residual inflow to the ria between two consecutive surveys
$\overline{Q}_R$	m^3 s^{-1}	Mean river inflow to the ria between two consecutive surveys
$\overline{Q}_P$	m^3 s^{-1}	Mean precipitation to the ria between two consecutive surveys
$\overline{Q}_E$	m^3 s^{-1}	Mean evaporation from the ria between two consecutive surveys
$\overline{Q}_{EFF}$	m^3 s^{-1}	Mean effluent flux to the ria between two consecutive surveys
$\overline{Q}_{Vc}$, $\overline{Q}_{Vi}$	m^3 s^{-1}	Mean advective vertical salt flux between two consecutive surveys
$(Q_U)_S$	m^3 s^{-1}	Surface horizontal flux derived from the salt budget
$(Q_U)_T$	m^3 s^{-1}	Surface horizontal flux derived from the heat budget
Q_{UW}	m^3 s^{-1}	S and T weighted advective horizontal flux
$Respn$	mg C m^{-2} h^{-1}	Aerobic respiration of organic matter
$Resus$	mg m^{-2} h^{-1}	The process of benthic nutrient efflux
ρ_0	m	Theoretical level of the pycnocline
ρ_{ria}	kg m^3	Water density
S	PSU	Salinity
$\overline{S}_U$, $\overline{S}_B$	-	Mean upper and lower layer salinity at the model boundaries between two consecutive surveys
$\Delta S/\Delta t$, $\Delta V/\Delta t$	s^{-1}, m^3 s^{-1}	Change in salt content and volume between two consecutive surveys
$SALINITY$	PSU	ECoS modelled salinity
$S{:}D$	s	Number of seconds per day
SH	J l^{-1} °C	Specific heat of water
$Slope$	kg m^2 s^{-1}	Momentum gain due to water surface slope
$Si(OH)_4$	µmol l^{-1}	Dissolved reactive silicate
SPM	µmol l^{-1}	Suspended particulate matter
$(ST)_U$	PSU, °C	Salinity or temperature in the upper layer at any boundary
$(ST)_L$	PSU, °C	Salinity or temperature in the lower layer at any boundary
$\Delta(ST)_{LAT}$	-, °C	Error in S or T due to lateral inhomogeneity
$\Delta(ST)_{LON}$	-, °C	Error in S or T due to longitudinal inhomogeneity
$\Delta(ST)\rho_0$	-, °C	Error in S or T due to variability in the pycnocline level
$\Delta(ST)_{LON}$	-, °C	Error in S or T due to longitudinal inhomogeneity
$\Delta(ST)_{INT}$	-, °C	Error in S or T due to numerical cross sectional integration
$\Delta(ST)_U$	-, °C	Total error in S or T in the upper layer at any boundary
$\Delta(ST)_L$	-, °C	Total error in S or T in the lower layer at any boundary
σ_θ	kg m^{-3}	Potential density
θ	°C	Potential temperature
t	s	Time
T	°C	Temperature
τ	d	Freshwater residence time
$TEMP$	°C	ECoS modelled temperature
TPA	m	Tidal amplitude
TPF	°	Tidal frequency
TPP	°	Tidal phase
TK	°K	Absolute temperature of water
U	m s^{-1}	Water velocity in the X direction
V	m^3	Water volume of central or internal ria
W_L	m s^{-1}	Local winds resolved along the NE-SW ria axis

Chapter 1

1. Introduction

1.1. ESTUARINE CHEMICAL REACTIVITY

Rivers provide a major pathway for the passage of natural and anthropogenic constituents from the terrestrial compartment to the oceans. The fate and flux of organic material carried therein are modified to a large extent by the sharp gradient in estuarine master variables (salinity, temperature, pH, dissolved oxygen and turbidity), particle-water interactions and, further downstream, by primary productivity. The quantification of annual nutrient fluxes to the coastal zone is notoriously difficult due to the erratic variability in freshwater discharge, complex concentration/flow relationships and modification of fluxes by non-conservative processes. These factors contribute to departure from the theoretical mixing between seawater and freshwater mixing [Fig. 1.1].
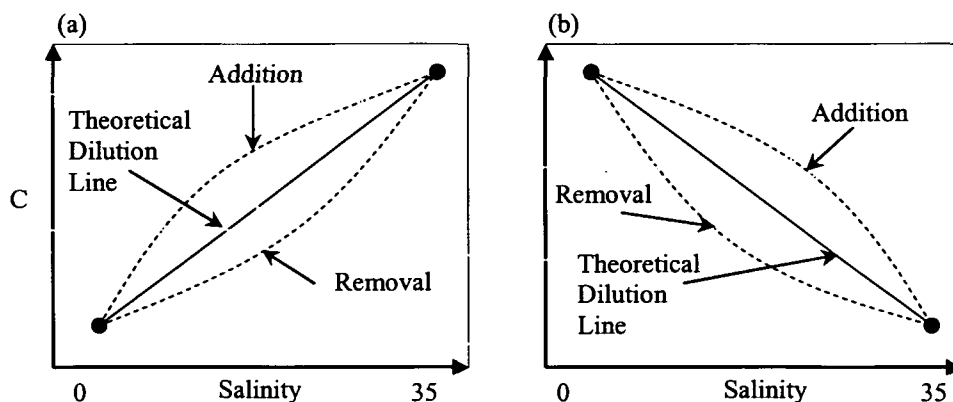
Fig. 1.1. The mixing behaviour of dissolved constituents in estuaries; (a) constituent concentration (C) is greater in seawater than river water e.g. boron, and (b) constituent concentration is greater in river water than seawater e.g. iron, nitrogen.

Pioneering and relevant works on this subject can be found in *Boyle et al.* [1974], *Loder and Reichard* [1981] and [*Ciffuentes et al.*, 1990]. *Morris* [1990] takes a detailed theoretical approach to discuss how conservative mixing of dissolved nutrients is a function of estuarine flushing, and *Balls* [1994] and *Lebo et al.* [1994] provide experimental evidence in support the theory. The complexity of estuarine biogeochemistry has been decisively summarised by *Morris et al.* [1985], whereby "chemical distributions must be perceived as the net outcome of both biological uptake/regeneration

processes and homogeneous/heterogeneous chemical transformations and interpreted accordingly."

The uniqueness of the study area in this thesis is beyond dispute, certainly from a European standpoint, and arguably globally as well. A detailed geographical description is given below. The system under investigation is a wide and deep estuary, or more specifically, ria. The biogeochemistry is strongly cyclic in time and dependant on the oceanic and terrestrial aquatic regimes, although successively. The ria is regarded as highly productive at all trophic levels, and the management of water quality is a local and European long-term objective [e.g. *GESAMP*, 1991]. Generalised conclusions of the physico-chemical properties of the system are complicated by the convergence of two very different spatially and temporally variable biogeochemical signals. Consequently, biogeochemical mixing curves are typically incoherent. Hydrographical and biogeochemical state-of-the-art is provided in detail within the corresponding chapters of this thesis, and at this stage it is worthwhile to briefly discuss literature evidence regarding other coastal systems to put the present work into context.

Salinity, temperature, pH, dissolved oxygen and turbidity determine the extent to which bioreactive elements are exported from the land to the sea. The horizontal gradient of these variables is low in the system studied here. The Humber Estuary (UK) is a large coastal system and was the focus of a concerted multidisciplinary investigation as part of the LOIS programme in the 1990s [e.g. *Huntley et al.*, 2001]. In contrast to the present study, an important variable for biogeochemistry in the Humber is turbidity, and suspended particulate matter concentrations may reach 25 g l⁻¹ in the turbidity maximum zone [*Uncles et al.*, 1998a]. Consequently, phytoplankton production is low, and aerobic nitrifying bacteria attached to suspended particles are instrumental in nutrient biogeochemistry. The upshot is a pronounced nitrate peak at mid-salinities [*Uncles et al.*, 1998b], and low oxygen and ammonia concentrations, especially in summer. Numerical modelling studies have successfully reproduced these observations [*Tappin et al.*, 2003]. A mid-estuarine nitrate peak appears to be an inherent feature of turbid systems [*Owens*, 1986].

As a second example, it is insightful to consider longitudinal spatiality in biogeochemical modification. The longitudinal variability in water residence time is probably the most important determining factor for the extent to which chemical processes, such as nitrification in the Humber, can be observed. The importance of very low salinity regions, particularly for phosphate and particulate-metal exchange, has been recognised for some time [*Morris et al.*, 1978]. Similarly, certain metals such as manganese and zinc [*Ackroyd et al.*, 1986], show pronounced mid-estuarine reactivity, depending on the system residence time. Most deviation from the theoretical flushing curve [Fig. 1.1.] takes place at salinities between 10 and 25 when competition from seawater ions is greatest [*Morris et al.*, 1981, 1982a]. Typically, freshwater residence time increases exponentially between salinity 25-35 and chemical reactivity tends toward more conservative behaviour [*Balls*, 1994]. The data in the present study are generally restricted to this narrow salinity, although as will be shown, chemical reactivity is far from conservative. In summary, the ability of scientists to conceptualise, integrate and generalise scientific knowledge must be formulated on a typological framework [*Regnier et al.*, 2002]. Inter-estuarine comparison is a fundamental stage of this process.

1.2. ESTUARY-RIA INTERCOMPARISONS

The interactions of estuarine topography with river discharge and tides result in a plethora of estuarine classifications [Dyer, 1997]. In addition, this may be compounded by considerable longitudinal variation of stratification. In extreme cases, for instance in the Amazon, mixing of river and seawater takes place up to 200 km from the coastline in the Atlantic Ocean [Edmond et al., 1981]. Estuarine classification has thus been defined, and redefined, several times in recent years [Hansen and Rattray, 1966; Fairbridge, 1980; Dyer, 1997], and still remains a subject of debate [Elliot and McLusky, 2002].

To the wider scientific community, rias are generally accepted as estuarine systems, typically drowned river valleys in a submerged coast of moderate relief [Fairbridge, 1980]. Within Europe, rias are mainly concentrated along the western Iberian Peninsula, the former Yugoslavia, SW England and SW Ireland. The upwelling area of Galicia, NW Spain, is the focus of this study [Fig. 1.2].
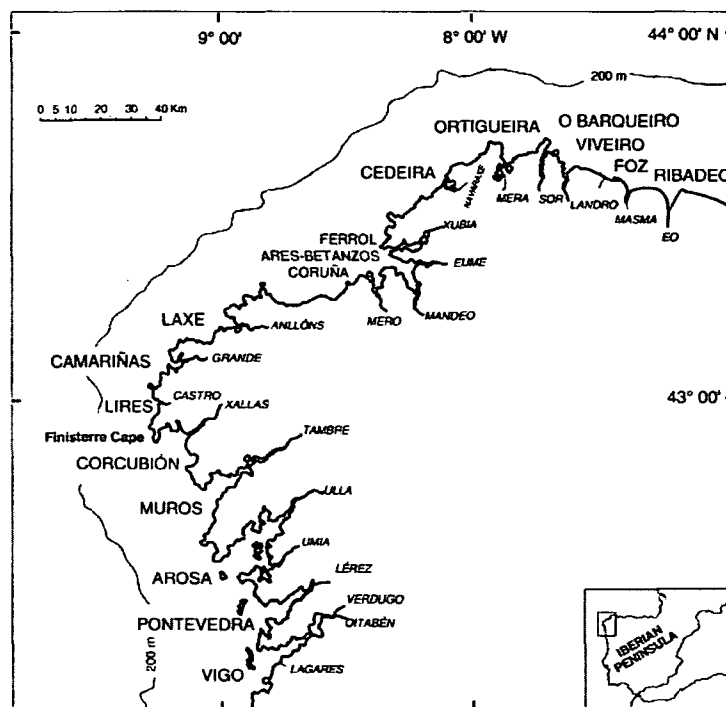
Fig. 1.2. The distribution of the Galician rias to the north and south of Finisterre Cape. Ria names are given on the seaward side in large font, and head rivers on the landward side in small font.

Rias form the connection between estuaries and oceans. Consequently, Prego and Fraga [1992] and Álvarez-Salgado et al. [2000] argue that the Galician rias possess unique characteristics and only the innermost part may strictly be considered as an estuary. However, the definition of the estuary-ria and ria-ocean interface may not be obvious. For example, the Galician rias exhibit an estuarine zone where a river-ria interchange takes place and a wide, deep (~40 m) interface zone where ria-ocean exchange takes place [Prego and Fraga, 1992], similar to Bantry Bay and adjacent embayments in southwest Ireland [Edwards et al., 1996]. The Aveiro Ria in Portugal, on the other hand, is a long, narrow shallow lagoon (mean depth

1.5 m) situated on the west coast of Portugal and is linked to the sea by an narrow artificial channel [*Cortéz et al.*, 1993; *Pereira et al.*, 1998]. The Aveiro Ria thus bears no geomorphological resemblance to the Galician rias.

The hydrographical definition of rias is more ambiguous. For example, Galician rias have been broadly summarised as partially mixed estuaries with positive estuarine circulation [*Otto*, 1975; *Prego and Fraga*, 1992]. However, during the summer months net evaporation may exceed net precipitation, leading to negative residual circulation. It is during such periods that the rias are topographically classified as rias even though hydrographical classification is unsuitable. Consequently, rias cannot be considered as simple estuaries.

1.3. UPWELLING

Upwelling areas are prevalent in the Pacific and Atlantic oceanic margins, notably the Northwest African and Iberian upwelling [Canary Current (12°-25° N)], the Benguela upwelling off south-western Africa [Benguela Current (15°-35° S)], the Peruvian upwelling off southwestern America [northern Humboldt Current (4°-14° S)] and the California upwelling system [California Current (28°-43° N)]. Upwelling is highly seasonal in temperate latitudes with a peak in spring-summer, but is generally continuous in the tropics.

The common feature of the above upwelling systems is their location on the eastern boundaries of the oceans. These areas are characterised by high-pressure atmospheric systems and equator-ward winds blowing parallel to the coastline. Wind stress generates a deformation of the sea surface causing a current to flow. The Coriolis force acts perpendicular to the wind direction, and thus the net water flux is displaced to the right of the wind direction in the northern hemisphere and the left in the southern hemisphere. This phenomenon is known as Ekman transport [Fig. 1.3.]. The offshore water flux results in upwelling of deeper oceanic waters to compensate for the displaced water [*Wooster et al.*, 1976].
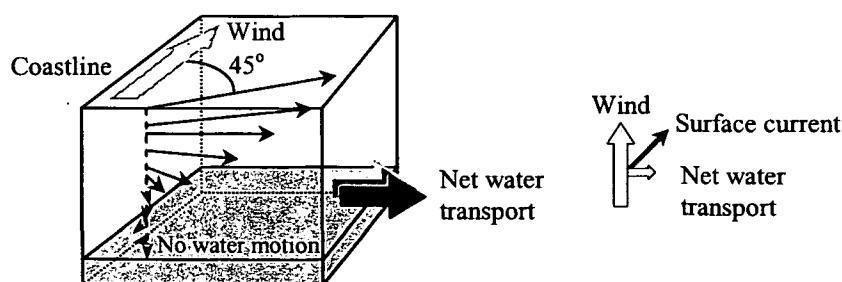
Fig. 1.3.. Schematic of wind-induced Ekman transport. Adapted from *Brown et al.* [1989].

1.3.1. THE IBERIAN UPWELLING: HYDROGRAPHY

The Iberian upwelling is the most northerly extension of the Northwest African upwelling. In Galicia, the wind regimes are dominated by two pressure cells: the Azores anticyclone, which moves over Europe in summer, and the Icelandic depression, which is most prominent in winter.

Upwelling normally occurs from April to September when the two pressure systems drift apart resulting in northerly winds and offshore Ekman transport [*Wooster et al.*, 1976]. Conversely, from October to March, southerly winds are predominant and may provoke downwelling and a reversal of water circulation in the rias [*Figueiras et al.*, 1994]. The spring transition from the downwelling to the upwelling season occurs in February to April, whereas the autumn transition from upwelling to downwelling generally occurs in October.

The Galician rias are directly affected by the seasonal upwelling and downwelling cycles. Upwelling intensity, however, is not consistent. *Bao et al.* [1997] described the segregation of the upwelling into three well defined zones on the basis of silica distribution in the bed sediments; (1) a region of intense and persistent upwelling around the western shelf of Finisterre Cape, (2) a region of upwelling and coastal outwelling south of Finisterre Cape in close proximity to the coastline, and (3) a discontinuous and distinct upwelling to the north of the Coruña Ria close to the edge of the continental shelf [Fig. 1.2]. Silica concentrations in the sediments of zone (2) were comparable to those of the upwelling region of Peru, thus indicative of high pelagic productivity. Conversely, the discontinuous upwelling on the northern shelf in zone (3) was reflected by patchy silica distribution. The low productivity of this area is due to the presence of nutrient-poor coastal waters which impedes upwelling [*Prego et al.*, 1999]. Local shelf topography and the geomorphology of the coastline are also important [*Blanton et al.*, 1984; *Varela et al.*, 2001].

The contrast in productivity between the areas south and north of Finisterre Cape conveniently coincides with the local nomenclature. The term "Rias Bajas" or "low rias" (42° 10' - 42° 50' N) refers to the ria systems in the south, whereas "Rias Altas" or "high rias" (42° 50' N - 43° 40' N) defines the systems to the north [Fig. 1.2]. The four Rias Bajas (Vigo, Pontevedra, Muros and Arosa) are the largest in area and depth and account for 75% of the freshwater input to the Galician coastal zone [*Prego et al.*, 1999]. In addition, upwelling of nutrient-rich waters inside the Rias Bajas has provided the motive for many physical, chemical and biological oceanographic studies. This study focuses on the Pontevedra Ria, the second-largest of Rias Bajas in terms of water volume. A summary of the geomorphological characteristics of the Rias Bajas is presented in Table 1.1.

Fraga et al. [1982] suggested that the intense upwelling in the area around Finisterre Cape [Fig. 1.2] is due to convergence of Bay of Biscay Central Water (BBCW) from the east and North Atlantic Central Water (NACW) from the west. Subsequently, *Ríos et al.* [1992] redefined the NACW in this area as two branches of East North Atlantic Central Water (ENACW), one of sub polar origin (ENACW$_p$, θ=8.56, S=35.23) and the other of sub tropical origin (ENACW$_t$, θ=14.86, S=36.12). ENACW$_t$ lies a few tens of km offshore from the Rias Bajas [*Fraga*, 1981; *Fiúza et al.*, 1998] and during the upwelling period occupies the layer between 60 and 450 m. ENACW$_p$ and ENACW$_t$ are associated with upwelling in the Rias Altas and Rias Bajas, respectively. During downwelling conditions in winter, the shelf water is warmer due to the transport of waters advected from the south (~39-47 °N) by the Portuguese Coastal Counter Current (PCCC) [*Frouin et al.*, 1990; *Pingree et al.*, 1999]. This warm (θ=14.5-16.5 °C) and saline (35.9-36.1) poleward flow has been characterised by *Frouin et al* [1990], and is located between 150-200 m depth on the shelf-slope break. The thermal difference between the water masses during the upwelling and downwelling season is readily traceable by satellite imagery [Fig. 1.4]. The figure shows how

ENACW$_t$ upwells perpendicular to the shelf, penetrates the surface and extends seaward in offshore filaments [*Joint et al.*, 2001]. The coastal water is consequently cooled by up to 5.5 °C with respect to mid-Atlantic Ocean temperatures [*Wooster et al.*, 1976].

Table 1.1. Dimensions of the Rias Bajas and mean annual contributions of principal head rivers.

	Water content (km^3)	Surface area (km^2)	Length (km)	Mouth width^a (km)	Mouth depth^a (m)	Head river	River flow (m^3 s^{-1})
Muros	2.74	125	17	6.1	45	Tambre^b	54.1
Arosa	4.34	230	25	4.6 (3.7)	55 (15)	Ulla^b-Umia	79.3-16.3
Pontevedra	3.45	141	22	7.3 (3.6)	60 (15)	Lérez	25.6
Vigo	3.12	156	31	5.1 (2.8)	45 (25)	Oitaben^b-Lagares	17.0-3.4
Total	13.65	652	-	-	-		195.7
Mean	3.41	163	24	5.8	50		48.9

^{a} Secondary mouth in parentheses
^{b} Estimated flow. River flow modified by a dam in its course

Upwelling   Downwelling
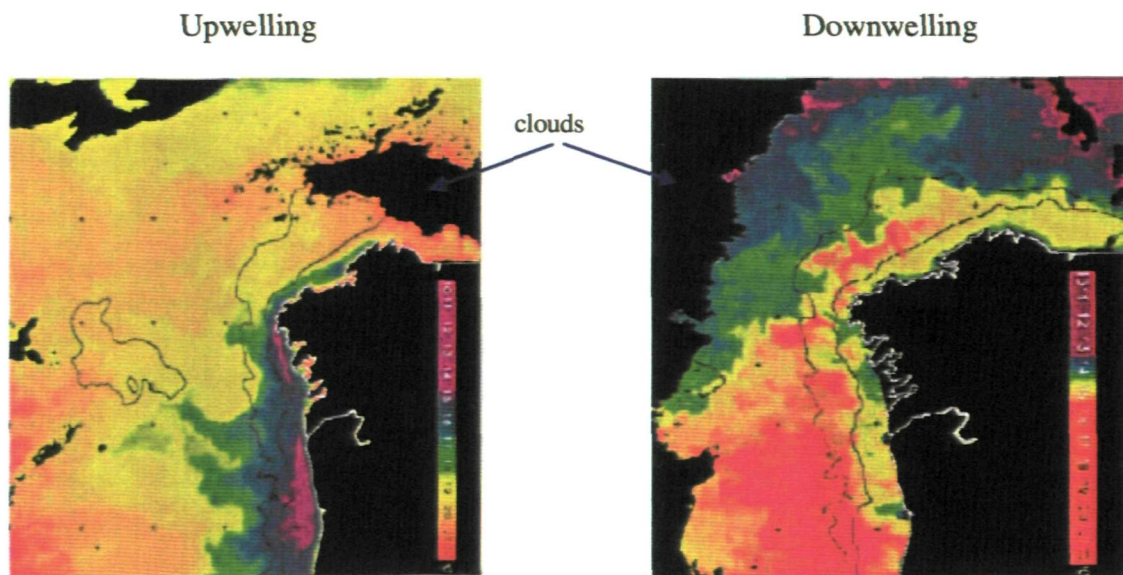
Fig 1.4. AVHRR sea surface temperature images of the NW Iberian Peninsula during upwelling (3 August 1998) and downwelling (21 January 1998). Warmest temperatures are in red, and coolest in purple. From Figueiras et al. [2002].

The sub-surface elevation of ENACW$_t$ depends on the intensity and persistence of northerly winds over the shelf. With sufficient wind intensity, ENACW$_t$ penetrates the Rias Bajas [*Fraga*, 1981]. Accordingly, in this thesis the upwelling water mass is considered to be ENACW$_t$, and hereon defined as ENACW. Upwelling into the rias was first recorded by *Margalef and Andreu* [1958]. *Blanton et al.* [1987] adapted the Norwegian fjord studies of *Klinck et al.* [1981] and proposed that offshore Ekman transport lowers the

sea level at the mouth of the Rias Bajas. The resulting seaward pressure gradient forces the water above the pycnocline out of the ria. The pycnocline becomes shallower and oceanic water is upwelled onto the continental shelf and driven into the rias below the pycnocline. Conversely, during downwelling, water piles up at the mouth, causing the sea surface to rise and the pycnocline inside the ria to deepen. The surface water is then pushed landward by onshore Ekman transport. This cycle occurs on a 14±4 day time scale [*Blanton et al.*, 1987; *Álvarez-Salgado et al.*, 1993], although the frequency is clearly wind-dependent.

1.3.2. THE IBERIAN UPWELLING: BIOGEOCHEMISTRY

Upwelling systems are extreme examples of unstable environments where the physical, chemical and biological system components are highly dynamic. Regular injection of nitrate-rich waters to the photic zone [*Barber and Smith*, 1981] ensures that upwelling ecosystems are extremely productive and associated with high rates of new production (primary productivity sustained by nitrate) compared to regenerated production (primary productivity sustained by ammonium). The mean primary productivity of upwelling areas is ~300 g C m^{-2} y^{-1} [*Murray*, 1992] and compares to the continental shelf mean of 160 g C m^{-2} y^{-1} [*Smith and Hollibaugh*, 1993]. Put into context, 30 % fish landings occur in upwelling areas, despite occupying only 0.2 % of the ocean surface.

In contrast to estuaries, the ria-ocean interchange may contribute a significant source of new and regenerated nutrients in the Rias Bajas [*Prego*, 1993a,b; *Alvarez-Salgado et al.*, 1996a,b]. ENACW upwelling into the Rias Bajas [*Fraga*, 1981] injects nutrient-rich water to the photic zone [*Prego*, 1993a; *Álvarez-Salgado et al.*, 1996a]. The upshot is high primary productivity and sustainability of the largest mussel raft cultivation industry in the world [*Tenore et al.*, 1982]. Mussels are harvested in the Rias Bajas from a total of 3337 rafts [*Figueiras et al.*, 2002]. Each mussel raft (500 m^2, 500 hanging ropes of 12 m length) produces approximately 75 ×10^3 kg y^{-1}. Mussel growth is a function of food availability and supply [*Pérez-Camacho et al.*, 1995; *Fernández-Reiriz et al.*, 1996], which are favoured by upwelling. The upwelling response of mussel production was semi-quantified by *Blanton et al.* [1987] who observed a positive correlation between mussel meat and upwelling.

The majority of biogeochemical modification of active elements along the Galician coast takes place within the Rias Bajas [e.g. *Prego*, 1993a; *Álvarez-Salgado et al.*, 1996a]. Upwelling reinforces the positive residual circulation of the Rias Bajas, transporting seaward the organic material excreted by the mussels and phytoplanktonic material. The biogenic material settles to the seabed over the shelf thus leading to organic and opaline-rich sediments [*López-Jamar et al.*, 1992; *Bao et al.*, 1997; *Prego et al.*, 1995]. Remineralisation of organic matter close to the seabed is responsible for modification of nutrient ratios in the upwelled water [*Álvarez-Salgado et al.*, 1997]. Export of dissolved organic matter (DOM) in the outwelling waters favours phytoplankton growth over the shelf, which further increases the sedimentation of biogenic material [*Doval et al.*, 1997]. The biological pump is ultimately completed such that CO_2 and nutrients are returned to the surface layer of the ocean through physical mixing and upwelling [*Gago et al.*, 2003]. Therefore, this ria-platform coupling acts as a large nutrient trap, whereby organic matter is formed inside the ria, exported, sedimented,

and finally remineralised and upwelled back inside the rias. Consequently, hydrographical and biogeochemical studies of the Galician rias must consider the hydrodynamics on the adjacent continental shelf.

Primary productivity is high in the Rias Bajas [800-1500 mg C m^{-2} d^{-1}; *Fraga*, 1976; *Prego*, 1993a, *Álvarez-Salgado et al.*, 1996a; *Moncoiffé et al.*, 2000]. Mean gross primary productivity *(GPP)* is usually highest during the upwelling period [~1.4 g C m^{-2} d^{-1}; *Fraga*, 1976; *Álvarez-Salgado et al.*, 1996a; *Tilstone et al.*, 1999], despite that spring and dry season transitions are associated with higher chlorophyll *a* (Chl *a*) concentrations. Consequently, high Chl *a*-normalised primary production has been observed [*Tilstone et al.* 1999]. Phytoplankton species are dominated by large diatoms during the first spring upwelling events, giving way to smaller diatoms in summer. Potential red tide species, usually dinoflagellates, may occur at the transition from upwelling to downwelling at the end of summer when circulation reversal is established [*Figueiras and Niell*, 1987; *Prego*, 1992; *Figuerias et al.*, 1994; *Tilstone et al.*, 1994; *Fermín et al.*, 1996].

1.4. THE PONTEVEDRA RIA

1.4.1. GEOGRAPHICAL ASPECTS

The Pontevedra Ria [Table 1.1] extends 23 km from its head at the Lérez river in the east to the islands of Ons and Onza in the west [Fig. 1.5]. The river provides the main freshwater input to the ria (see Chapter 2 for more details). In common with the other Rias Bajas it has a "V" formation and gradually widens seaward toward the islands, whereupon it divides into two channels. The southern channel is deeper (60 m) than the northern channel (14 m), and thus provides the main entrance to the ria.

The City of Pontevedra is the principal commercial and urban centre in the area and infringes upon the Lérez estuary and the ria. Owing to its outstanding natural beauty, the Pontevedra Ria has a thriving tourism industry and the regional population (140,000) doubles during summer [*Ibarra and Prego*, 1997]. Effluents containing elevated concentrations of dissolved metals and organic material are discharged directly to the ria from a paper mill and an electrochemical plant situated in the inner ria near the town of Marín [*Figueiras et al.*, 1985].

1.4.2. HYDROGRAPHY AND BIOGEOCHEMISTRY

Although considerable effort has been devoted to the study of the Rias Bajas during recent years, the hydrography is only partially understood, with little known about the Pontevedra Ria. Available data are mainly complementary to more focused studies [*Jiménez et al.*, 1992; *Tilstone et al.*, 1994], or from specific upwelling investigations [*Álvarez-Salgado et al.*, 1993; *Castro* et al., 1994; *Rosón et al.*, 1997]. Moreover, even less biogeochemical data is available for the Pontevedra Ria. Nevertheless, a general resemblance in the biogeochemical characteristics between the Ria Bajas is evident [*Tilstone et al.*, 1994; *Prego et al.*, 1999]. Substantially more biogeochemical references relevant to this thesis were restricted to the grey literature. This data was judged on the analytical quality of the methods and supporting statistical information, and only used when analytical methods and sampling logistics

were reported in a reproducible form. Before this work was undertaken, a detailed description of the annual variability in hydrography and biogeochemistry of the Rias Bajas was unavailable to the international scientific community.
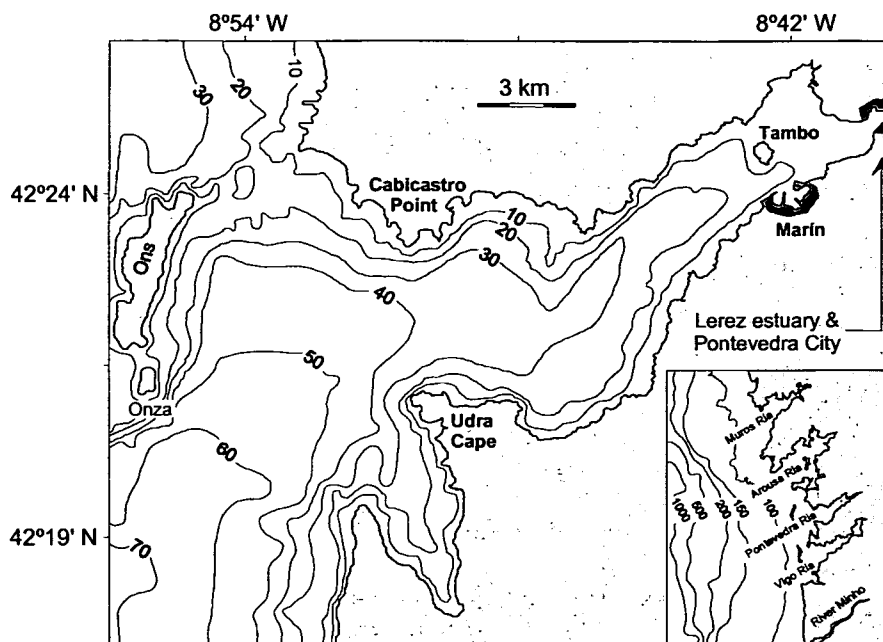
Fig. 1.5. Map of the Pontevedra Ria on a local and regional scale. The City of Pontevedra and river Lérez are located at the ria head in the east.

The principal published hydrographical references for the Pontevedra Ria were founded on the same data set used in this thesis [deCastro et al., 2000; Prego et al., 2001; Ruiz-Villarreal et al., 2002; Gómez-Gesteira et al., 2002; Álvarez et al., In press]. The work by Prego et al. [2001] describes in detail the hydrography of the Pontevedra Ria and forms Chapter 3 in this thesis. Therefore, only a brief description of ria hydrography is required here. With regard to biogeochemistry, supporting data from the same data set has either been published [Dale and Prego, 2002] or submitted for publication [Dale and Prego, In revision].

The hydrography of the rias is a function of (i) tides, (ii) runoff, (iii) local winds, and (iv) upwelling. Stratification is important in in innermost part of the ria close to the Lérez estuary and decreases towards the ria mouth [Figueiras et al., 1985; Prego and Fraga, 1992]. Periodic upwelling events of cold oceanic waters form a sharp thermocline which may extend along the total length of the ria [Doval et al., 1998]. Conversely, downwelling provokes a homogenisation of the water column.

Evidence from the Vigo Ria suggests that the Pontevedra Ria may behave as a partially mixed estuary with residual positive circulation [Taboada et al., 1998]. In partially stratified estuaries, mixing between the two layers is mainly by turbulent diffusion, both being spatially and temporally variable [Dyer, 1997]. Lateral circulation may also be important in wider areas [Bowden, 1980] such as the outer ria, as confirmed by numerical models [Taboada et al., 1998]. In the Arosa Ria, river water approaches the northern coast on leaving the estuary [Rosón et al., 1997]. The seaward flow

presumably increases with mixing of salt across the density gradient whilst simultaneously provoking an increase in the volume of the landward flow [*Bowden*, 1980]. In the Vigo Ria in the absence of upwelling, the seaward mixing flow is the main parameter controlling residual circulation [*Taboada et al.*, 1998]; a finding complemented by previous box-model applications to the ria by *Prego and Fraga* [1992], and estuarine circulation in general [*Pritchard*, 1989].

1.5. RESEARCH OBJECTIVES

The difficulties involved in drawing a qualitative distinction between natural and anthropogenic nutrient concentrations of Galician waters is complicated by the fact that chemical monitoring began almost simultaneously with the onset of the anthropogenic chemical impact. At present, more attention is being devoted to the scientific study of the Galician rias due to an increasing awareness of their global economical importance and impact by ENACW upwelling, which itself is very susceptible to climate change. These studies are becoming more quantitative and multidisciplinary. However, hitherto there have been no systematic studies of the nutrient dynamics occurring within the Pontevedra Ria and reliable data on the biogeochemical cycles are notably lacking. Consequently, a detailed study of the nutrient distributions and dynamics together with a quantification of ocean-ria exchange and fluvial inputs is required to optimise the commercial potential of the ria.

The implementation of effective management schemes, which embrace conflicting socio-economical and ecological arguments, is of utmost urgency to industrially and biologically dynamic regions such as the Pontevedra Ria. Therefore, based on a comprehensive systematic survey, this work aims for the first time to take the first steps towards sustainable management of the Pontevedra Ria by examining in detail the hydrography and biogeochemistry.

In summary, the project goals are addressed below:

• Describe the inter-annual hydrography of the Pontevedra Ria, with reference to runoff, tides, and upwelling/downwelling and their influence on flushing time.

• Quantify the spatial and temporal features of dissolved inorganic nutrients on the basis of first-order box-model fluxes between the river-ria-ocean. Benthic nutrient fluxes will be quantified and coupled to the pelagic nutrient dynamics.

• Assess the suitability of salt and salt-heat box models to the Rias Bajas under conditions of high and low runoff.

• Construct, parameterise and calibrate a 1-D numerical physical and biogeochemical model of the Pontevedra Ria using the commercially-available simulation package ECoS. Compare the box-model nutrient results with numerically-derived model outputs. Is the model suitable for addressing critical management issues arising from global climate change and land use?

Chapter 2

2. Data acquisition, materials and methods

2.1. SAMPLING STRATEGY

The sampling regime in the Pontevedra Ria was conducted between October 1997-1998 under the project "CICYT-MAR96-1782: The hydrodynamics and biogeochemical cycle of silicate in the Pontevedra Ria", funded by CICYT (Comisión Interministerial de Ciencia y Tecnología). The cruise plan was designed to investigate the main physico-biogeochemical processes controlling the annual nutrient behaviour. In this section, the main spatial and temporal aspects of the cruise plan are outlined. Analytical details of the determination of hydrographical and biogeochemical data are detailed here. The sampling stations in the Pontevedra Ria and Lérez estuary are shown in Fig. 2.1. Table 2.1 summarises the cruise dates and details of the data collected and equipment deployed.

2.1.1. SPATIAL VARIABILITY

Due to the abrupt geomorphological variations in the coastline of the Rias Bajas, several authors have alluded to the distinct hydrographical and biogeochemical domains within the rias [e.g. *Prego and Fraga*, 1992; *Álvarez-Salgado et al.*, 1996a,b]. Accordingly, owing to the extent of freshwater mixing and river flow [*Rio and Rodriguez*, 1982], the Pontevedra Ria can be defined hydrographically in terms of the external (73 km²), central (46 km²) and internal (22 km²) ria [Fig. 2.1]. The external ria is influenced by the Atlantic Ocean for the most part of the year, whereas the internal ria is generally dominated by the river. The central ria shows intermediate characteristics depending on the discharge from the river Lérez and the upwelling intensity. The water column and benthic chemical analyses adequately covered all three sections of the ria.

Hydrographic and water column variables. Water samples for biogeochemical analysis were taken from eight stations along the longitudinal axis of the ria on board the *RV Mytilus* [Fig. 2.1]. Samples were

collected in General Oceanic Niskin-type bottles from 6-7 depths including a surface and bottom sample. Vertical conductivity-temperature-depth (CTD) profiles were sampled at 19 stations in total. In addition, surface and bottom samples were taken at 7 stations in the Lérez estuary from a small boat between February and October 1998 concomitant with the ria survey [Table 2.1], from which the salinity, temperature and nutrient content were determined. The freshwater of the river Lérez at the limit of tidal influence was sampled 2-3 times a week for dissolved inorganic nutrients. Regular water samples for chemical analysis were also taken from a wastewater outflow from a sewage treatment plant close to the Lérez estuary [Fig. 2.1].
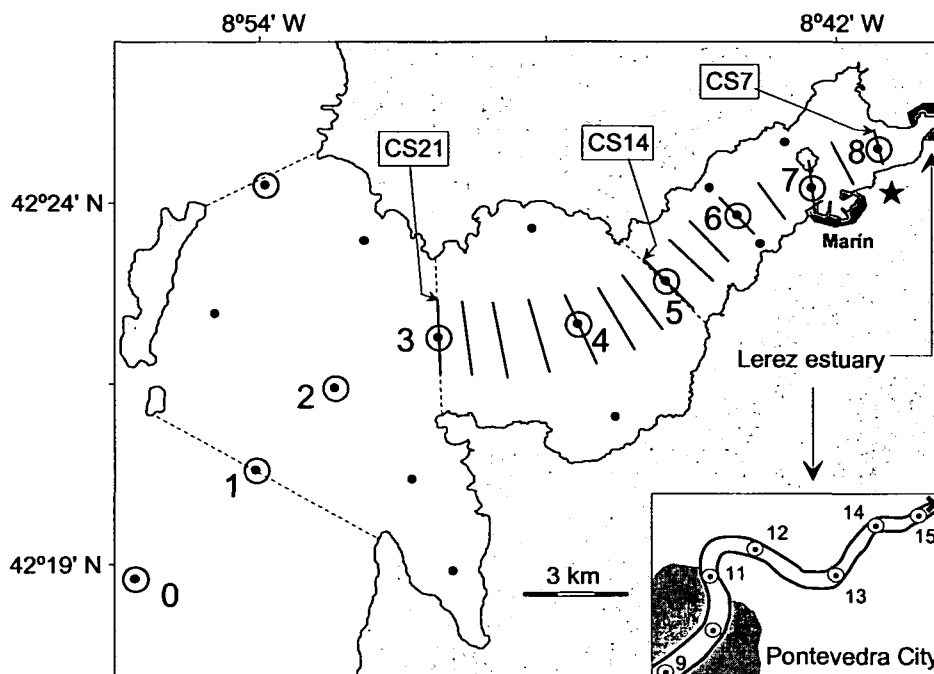
Fig. 2.1. Sampling stations in the Pontevedra Ria and Lérez estuary visited during the investigation (October 1997-1998). Stations at which CTD profiles were recorded and water samples taken for biogeochemical analysis are represented by the concentric circles (⊚). Stations which employed a CTD dip only are represented by closed circles (•). The dashed lines show the division of the ria into internal, central and external zones. The location of the effluent input in the internal ria is denoted by the star. The division along the longitudinal axis of the ria represents kilometres from the limit of tidal influence (cross in estuary). The cross-sections at 21 km (CS21), 14 km (CS14) and 7 km (CS7) are labelled.

Particulate material. An important aspect of the project was to investigate the importance of benthic-pelagic coupling of biogeochemical elements in the ria. On one occasion, sediment samples of the surface oxic layer were taken from evenly distributed sites in the ria and analysed for biogeochemical elements (see below). Water column particulate material was collected over a period of 2-3 d with a sediment trap system anchored to the seafloor at three sites in the ria (Sts. 0, 4 and 6). Trap deployment was intended to span the whole survey period although logistical problems limited the collection period to February-July 1998. The final aspect of benthic-pelagic coupling was achieved via nutrient flux assays from sediment core incubations at Sts. 4, 6 and 8. Analytical details of these experiments are detailed below.

Table 2.1. Cruise dates, reference code, analytical parameters measured in the ria and Lérez estuary and supplementary information for the Pontevedra Ria campaigns.

d	m	y	cruise ref.	ria nutrients	O$_2$	sediment traps *	Chl a *	river Lérez nutrients	O$_2$	flux assays **	anchor station ***
15	X	1997	10a	X	X						
29	X	1997	10b	X	X						
13	XI	1997	11a	X	X						
26	XI	1997	11b	X	X						
17	XII	1997	12a	X	X						
29	XII	1997	12b	X	X						
14	I	1998	1a	X	X						
27	I	1998	1b	X	X						
10	II	1998	2a	X	X	X	X	X	X		X
24	II	1998	2b	X	X	X	X	X	X	X	X
10	III	1998	3a	X	X	X	X	X	X	X	X
24	III	1998	3b	X	X	X	X	X	X	X	X
13	IV	1998	4a	X	X	X	X	X	X	X	X
27	IV	1998	4b	X	X	X	X	X	X	X	X
12	V	1998	5a	X	X	X	X	X	X	X	X
26	V	1998	5b	X	X	X	X	X	X	X	X
9	VI	1998	6a	X	X	X	X	X	X	X	X
23	VI	1998	6b	X	X	X	X	X	X	X	X
7	VII	1998	7a	X	X	X	X	X	X	X	X
21	VII	1998	7b	X	X		X	X	X	X	X
3	VIII	1998	8	X	X		X	X	X	X	X
1	IX	1998	9	X	X		X	X	X	X	X
7	X	1998	10c	X	X		X	X	X	X	X

*   Sts. 0, 4 and 6
**   Sts. 4, 6 and 8
***   Sta. 6

2.1.2. TEMPORAL VARIABILITY

The Rias Bajas display a wide range of short-term hydrographical phenomena which are mostly induced by upwelling and downwelling [*Blanton et al.*, 1984; *Álvarez-Salgado et al.*, 1993]. These authors defined the frequency of upwelling to be 14±4 d, although this depends on the strength and duration of upwelling favourable winds. With this in mind, the sampling plan was designed to adequately capture the more sustained upwelling events whilst simultaneously describing the annual change in hydrographical and biogeochemical characteristics. The Pontevedra Ria campaign consisted of fortnightly cruises, with the exception of August and September 1998 when logistical constraints of ship time restricted the sampling to once a month. Each transect was completed within eight hours following a repetitive sampling regime. Consistency and reproducibility of estuarine sampling is necessary, since the error introduced by the short-interval spatial heterogeneity is presumably greater than the analytical error. Estuarine surveys reported in the literature are often conducted as a landward cruise in order to reach the freshwater sample at the time of high water [e.g. *Morris et al.*, 1982b]. This approach has the advantage of working at a time when tidal velocities are low, thus minimising journey

time and suspended solids concentrations. However, this strategy was not adopted when sampling the Lérez estuary since a low bridge prevented passage of the boat except at low tides. Estuarine sampling thus commenced at the limit of tidal influence at low tide and moved seaward against the tide. With regard to the ria, sampling was not tidally systematic. This was unlikely to have an important effect on spatial and temporal constituent distributions, since tidal excursion of the Galician Rias is short [*Otto*, 1975] and suspended solid concentrations are low.

The discussion of temporal variability in thermohaline properties in this thesis is based on data collected at Sta. 0, located on the adjacent shelf; Sta. 1, located at the main entrance to the ria where the ria exchanges water with the shelf; and Sta. 6, located inside the ria [Fig. 2.1]. The discussion of nutrients centres on Sta. 3, situated at the interface between the external and central ria. A similar interface zone is also observed in the adjacent Vigo and Arosa rias [e.g. *Prego and Fraga*, 1992; *Rosón et al.*, 1997], and box model analyses in the Rias Bajas are consistently designed with a boundary at this location [*Prego and Fraga*, 1992, *Rosón et al.*, 1997; *Álvarez-Salgado et al.*, 2001].

The semi-diurnal temporal variability in hydrographic variables and water velocity is discussed using data collected at Sta. 6 in the internal ria. Sta. 6 (24 m depth) is under the greatest influence of river discharge and tidal effects and therefore provides a suitable reference point for the study of the main currents in the ria and the hydrographic response of the system to changes in external factors, such as wind, tide, and river discharge. From February-October 1998, Sta. 6 was occupied for a complete tidal cycle (13 h). The vessel was stabilised with four anchors and CTD and current meters were deployed every 30 min. Analytical details of the CTD profiler are given below. Current speed was measured at 6 depths with a Valeport 808 electromagnetic current meter, accurate to within ± 0.01 m s^{-1}.

2.2. MODEL VARIABLES

For the estimation of nutrient fluxes using box and numerical models, a concise inventory of freshwater and heat inputs is necessary. Moreover, in view of recent findings [*Nogueira et al.*, 1997a,b, 1998], upwelling into the rias and surface wind stress are likely to be important issues for the Pontevedra Ria. This section describes the collection and process of this supporting data.

2.2.1. UPWELLING INDEX

The magnitude of wind-induced offshore Ekman transport is considered an indicator of the amount of water upwelled in the bottom layer. The upwelling flux (m^3 s^{-1} (km coast)$^{-1}$) can be represented by an upwelling index, I_w [*Bakun*, 1973, *Wooster et al.*, 1976; *Lavín et al.*, 1991] obtained from the wind stress. The upwelling index is the ubiquitous base reference for describing the influence of upwelling on hydrographical and biogeochemical parameters in Galician coastal waters. Positive or negative I_w indicates favourable (northerly winds, offshore Ekman transport) or unfavourable upwelling conditions (southerly winds, onshore Ekman

transport), respectively. The upwelling period is generally from April to September and downwelling during October to March.

I_w for this study was calculated from atmospheric pressure fields and wind stress at the point 43° N 11° W, approximately 150 km west of the Rias Bajas [*Lavín et al.*, 1991], and provided by the Spanish Oceanographic Institute (Vigo City). This location is considered representative of the meteorological conditions for the western Galician coast. I_w is derived from:

> *Wind velocity.* An approximation of the actual wind speed was made with the geostrophic wind velocity, which was derived from atmospheric pressure anomaly. The Ekman transport parallel and perpendicular to the coast was estimated by integrating the pressure differences over a defined area.

> *Wind stress.* Wind stress was calculated from the wind velocity. However, wind stress on the surface is subject to frictional effects, and therefore the derived geostrophic winds were multiplied by a factor of 0.7 [*Lavín et al.*, 1991]. Following *Bakun* [1973], wind stress on the sea surface parallel (τ_y) and perpendicular (τ_x) to the coast was calculated as:

$$\tau_{x,y} = \rho_a\, C_d |V|\, V_{x,y} \qquad [2.1]$$

where ρ_a is the mean density of air (1.22 kg m^{-3}), C_d is an empirical drag coefficient [1.3x10^{-3}], and $V_{x,y}$ is the vector corresponding to the estimated wind speed on the sea surface, with magnitude $|V|$ (m s^{-1}).

Finally, the cross-shore ($-q_x$) and along-shore Ekman transport (q_y) were obtained by calculating the water flux across a 1 m^2 area in the plane x (or y), z. Taking 0 m to be the depth at which the velocity with respect to the surface is zero, integrating between 0 and z gave the total water mass transported by the wind induced current. The cross-shore and along-shore components were rotated 20° anti-clockwise to make them perpendicular and parallel to the ria longitudinal axis, respectively. Consequently, from *Bakun* [1973], offshore Ekman transport I_w (equal to $-q_x$) was calculated as τ_x [Eq. 2.1] divided by the Coriolis parameter, f (9.946x10^{-5} s^{-1}), and the density of seawater, ρ_w (~1025 kg m^{-3}):

$$I_W = \frac{\rho_a C_d |V| V_x}{f \rho_w} \qquad [2.2]$$

Daily values of I_w over the survey period are shown in Fig. 2.2a. The clear seasonality in I_w reflects the North Atlantic climatology, specifically the strength and position of the Azores High and Iceland Low atmospheric cells.

2.2.2. LOCAL WINDS

The transfer of momentum to the surface waters by wind stress and modification of estuarine circulation is well recognised [*Hansen and Rattray*, 1966, *van de Kreeke and Robaczewska*, 1989]. Local winds in the Rias Bajas are mostly dominated by orographic funnelling effects due to the surrounding mountainous topography [*Chase*, 1975]. Furthermore, *deCastro et al.* [2000] reported that the surface layer circulation in the inner Pontevedra Ria were modified by wind speeds > 3-4 m s^{-1}, while bottom

waters were dominated by tides. Salinity variations in the surface waters of the Vigo Ria have been reported to be mainly due to wind stress [Nogueira et al., 1997b]. Wind data supplied by the Spanish National Meteorological Institute were recorded daily at a meteorological observatory (Pontevedra-Mourente, Spanish Meteorological Network Observatory No. 484, location 42° 26.24' N, 8° 36.59' W). Fig. 2.2b shows the local wind velocities resolved along the NE-SW axis parallel to the ria, and the marked similarity between I_W and W_L during upwelling and downwelling periods.
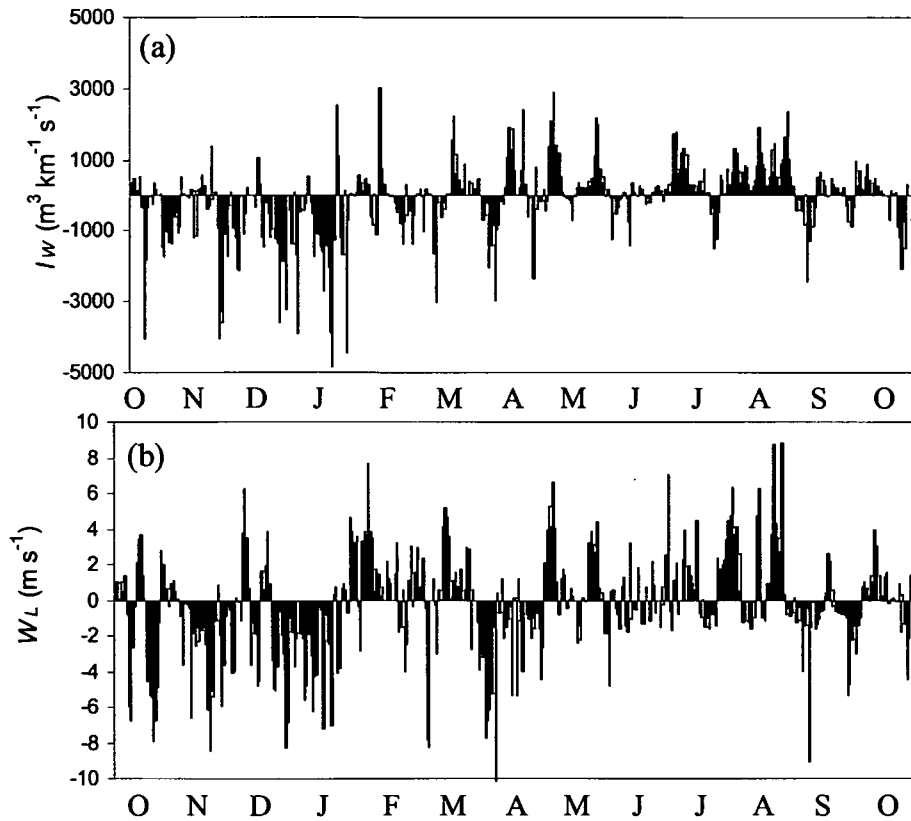
Fig. 2.2. (a) Daily values of upwelling index (I_W, m³ s⁻¹ km⁻¹) derived at the point 43° N, 11° W, (b) Local wind velocity (W_L, m s⁻¹) recorded daily at a weather observatory (42° 26.24' N, 8° 36.59' W), and resolved along the ria NE-SW axis over the survey period (October 1997-1998).

2.2.3. WATER COLUMN STABILITY

The Brunt-Väisälä (or buoyancy) frequency, N (s⁻¹) [Millard et al., 1990], is given by:

$$N = \sqrt{\frac{g}{\sigma_t} \times \frac{d\sigma_t}{dDEPTH}}$$ [2.3]

where g is the acceleration due to gravity (m s⁻²), σ_t is the density, and DEPTH is water depth (m). Density is calculated from salinity data (see below). N is a useful parameter in nearshore oceanography as it provides a measure of water column density stratification. High values of N are normally encountered near to the pycnocline where the density gradient is greatest. A parcel of water displaced from its position at the pycnocline

would rapidly return to its original position, whereas where N is low the water parcel shows less tendency to return.

2.2.4. IRRADIANCE AND LIGHT ATTENUATION

The intensity of irradiation at the water surface is a function of cloud cover, latitude and the angle of the sun to the horizon. Cloud cover (C) is normally measured by eye in ocktas, or eighths of sky coverage from 0 (cloudless) to 8 (overcast). Therefore, if C is known, the short-wave irradiation (H_{SW}, W m^{-2}) can be reasonably well predicted using a theoretical sinusoidal formula. H_{SW} data for the Pontevedra Ria survey were determined in this way using a series of equations [R. Uncles, Pers. Comm.]. Fig. 2.3a shows H_{SW} for C=0 and C=8 as well as pyranometer H_{SW} data supplied by the Mourente observatory. No direct H_{SW} were available for the period 20 July to 18 August 1997. Therefore, these data were determined theoretically using C=6.5. This value of C was obtained by minimising the standard deviation of the observed H_{SW} data with respect to C.
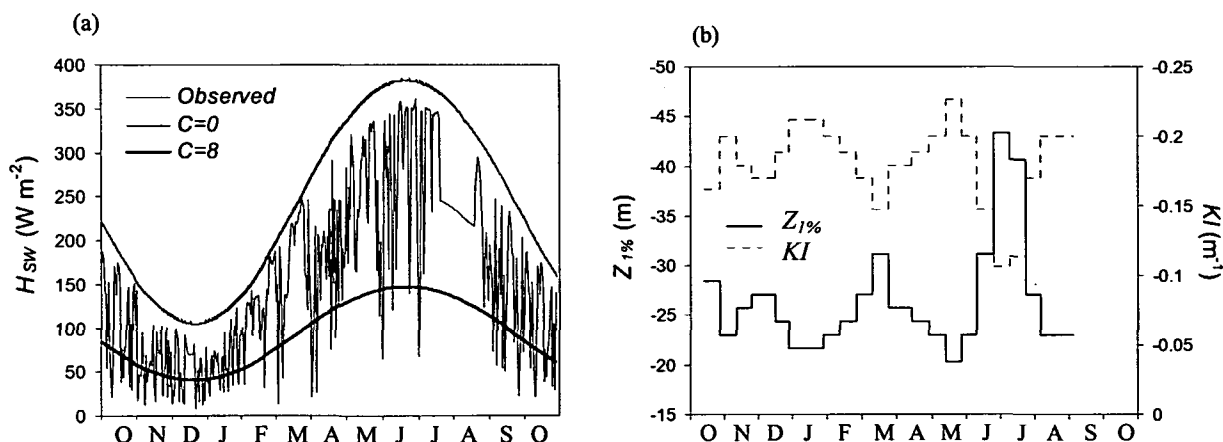
Fig. 2.3. (a) Observed and theoretical values of incoming short-wave radiation, H_{SW} (W m^{-2}) for maximum (C=8) and minimum (C=0) cloud cover (eighths of sky coverage), (b) The variation in mean 1% light level ($Z_{1\%}$, m) and mean water light attenuation coefficient (KI, m^{-1}) at Sta. 3 between two consecutive surveys over the survey period (October 1997-1998).

Water clarity was measured with a Secchi disc, which is a proxy for suspended particulate matter (SPM) concentration. The Secchi disc is a simple instrument consisting of a white disc 30 cm in diameter, which is lowered into the water until it disappears from view. The depth of disappearance is inversely proportional to the amount of suspended particulate matter in the water column, from which the 1 % light level (i.e. the depth where phytoplankton production equals respiration) is derived. The accuracy of the Secchi disc greatly depends on the environmental circumstances of the observation and the abilities of the observer. The vertical attenuation coefficient of water (KI, m^{-1}) can be estimated from the Secchi depth, Se (m), as [Figueiras and Niell, 1986]:

$$KI = \frac{a}{Se}$$
[2.4]

where a is equal to 1.7. From *Otto* [1975], the 1% light level, $Z_{1\%}$ (m) is equal to:

$$Z_{1\%} = \frac{1}{KI} \times ln \frac{I_0}{I_{1\%}}$$ [2.5]

where I_0 and $I_{1\%}$ are the irradiance at the surface and at $Z_{1\%}$. The variation in the mean $Z_{1\%}$ and KI at Sta. 3 between two consecutive surveys is shown in Fig. 2.3b.

2.3. FRESHWATER INPUT TO THE RIA

The Pontevedra Ria receives on average 69.5 km^3 y^{-1} of fresh water, the majority from the river Lérez [Fig. 2.1]. The Lérez is 57 km in length with a drainage basin of 450 km^2 [*Ibarra and Prego*, 1997]. The flow regime of Galician rivers can be represented as a function of river runoff. The wet season comprises November-February when runoff is highest and the dry season covers June-September. Spring and October are transitional periods. Monthly averaged river flow ranges between 80 m^3 s^{-1} in February to 2 m^3 s^{-1} in September, with an annual mean flow of 21.2 m^3 s^{-1} [*Ibarra and Prego*, 1997]. Ranges and means of master variables and constituent concentrations in the river Lérez are presented in Table 2.2. Nutrient concentrations in the river Lérez decrease logarithmically as a function of flow due to dilution [*Vergara and Prego*, 1997], and so the river may be considered pristine [*Meybeck*, 1982]. Deviation from this behaviour in some Galician rivers is partly due to damming [*Vergara and Prego*, 1997], which may also modify nutrient inputs to the coastal zone [*Jickells*, 1998]. The Lérez river flow at the limit of tidal influence (Q_R, m^3 s^{-1}) was measured daily with a stage-discharge curve. No fluvial flow data were available for October 1997, and therefore these data were interpolated using a regression between precipitation (Q_P, m^3 s^{-1}) in the Lérez basin and Q_R from November 1997 – October 1998 [$Q_R=(0.82 \times Q_P)+5.2$, r^2=0.62, n=340, p<0.001].
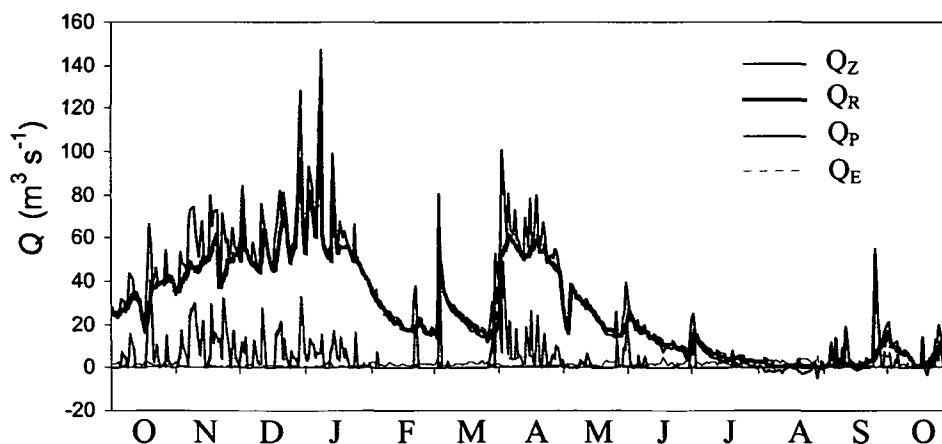
Fig. 2.4. Daily values of fluvial freshwater input (Q_R, m^3 s^{-1}), precipitation (Q_P, m^3 s^{-1}), evaporation (Q_E, m^3 s^{-1}), and residual freshwater inflow (Q_Z, m^3 s^{-1}) to the Pontevedra Ria over the survey period (October 1997-1998). The effluent flux Q_{EFF} (not shown) varies between 0.2-0.4 m^3 s^{-1}.

Table 2.2. Analytical parameters for the Lérez river recorded upstream from the City of Pontevedra during winter. Data from *Ibarra and Prego* [1997].

Parameter	Maximum	Minimum	Mean	Unit
Temperature	22	7.5	14	°C
O_2 saturation	117	62	101	%
pH	7.2	6.0	6.7	-
Redox potential	228	169	203	mV
SPM	84	0	23	mg l^{-1}
Nitrate	70	5	26	$\mu M\ NO_3^-$
Nitrite	1.2	0	0.2	$\mu M\ NO_2^-$
Ammonium	79	0	10	$\mu M\ NH_4^+$
Silicate	102	75	85	$\mu M\ Si(OH)_4$
Phosphate	3.6	0	0.4	$\mu M\ HPO_4^{2-}$

Freshwater inputs from precipitation are important in the Pontevedra Ria due to its large surface area and low flow in the dry season. Mean annual rainfall in the Lérez basin is 2100 mm [*Rio and Rodriguez*, 1982]. Conversely, evaporative flux (Q_E, m³ s⁻¹) is important during summer and may even exceed net freshwater inflow [*Otto*, 1975]. Q_P and Q_E recorded daily at the Mourente observatory were supplied by the Spanish National Meteorological Institute. Effluent discharge (Q_{EFF}, m³ s⁻¹) from the wastewater treatment station in the internal ria [Fig. 2.1] ranged from 0.2-0.4 m³ s⁻¹ [EDAR Aguagest and Degremont Water Authority, Pontevedra]. The sum of the water fluxes to the ria is equal to the residual freshwater flux (Q_Z, m³ s⁻¹):

$$Q_Z = Q_R + Q_{EFF} + Q_P - Q_E \qquad [2.6]$$

Daily Q_R, Q_P, Q_E and Q_Z are shown graphically in Fig. 2.4.
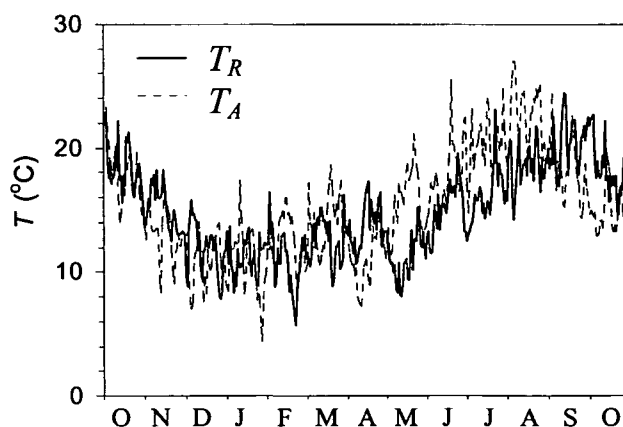
Fig. 2.5. Air (T_A) and river Lérez water (T_R) temperature (°C) over the survey period (October 1997-1998).

The water temperature of the river Lérez (T_R, °C) was recorded during the estuarine surveys [Table 2.1]. On the days where no temperature data were available, a robust correlation was derived between air temperature (T_A, °C)

and freshwater temperature [$T_R=(0.83 \times T_A)+2.01$, $r^2=0.70$, $n=15$, $p<0.001$], from which the remaining data were interpolated. The temperature of Q_P was assumed to be equal to T_A. Daily T_R and T_A are shown in Fig. 2.5.

2.4. HYDROGRAPHIC VARIABLES

2.4.1. SALINITY, TEMPERATURE AND DENSITY

Hydrographic data were collected in the Pontevedra Ria with a CTD profiler in accordance with *UNESCO* [1988] protocols. The Lérez estuary was too shallow to deploy the CTD, and surface and bottom salinity and temperature were measured with a portable salinometer (WTW Multiline P4), calibrated for conductivity with a 0.01 mol KCl solution at 25 °C. The precision and accuracy of the salinity measurements were ±0.01 and ±0.1, respectively, and ±0.1 °C and ±0.1 °C for temperature.

The CTD measures conductivity, temperature and water pressure, from which depth is derived. These variables are the most accurate means of characterising the salinity and density of ocean water on a routine and systematic basis. Highly spatially resolved and accurate CTD data are important for the construction of salt and heat budgets in the Rias Bajas, where the longitudinal thermohaline gradients are low. However, despite the relative ease and rapidity at which this data can be collected, accurate data are only obtainable when measurement and computational errors are identified and minimised.

CTD calibration. The CTD profilers deployed in the Pontevedra Ria were manufactured by Sea-bird Electronics Incorporated, Washington, USA. Owing to the high frequency of data measurement of the Sea-bird CTD, a pump is often employed in conjunction with a temperature-conductivity duct (T-C duct). The T-C duct forces the temperature and conductivity measurements to be made on the same parcel of water, leading to improved spatial co-ordination of the sampled volume and a reduction in salinity spiking. Salinity spikes can be minimised by correcting the mismatch in time-response of the temperature and conductivity sensor. Corrections are only possible in practice if the sensor time responses are constant, a condition met by pumped conductivity sensors. Variable profiling speeds caused by ship-coupled motion inevitably affects the time responses of free-flushing sensors. The hydrographic data for this study were collected with either a free-flushing unpumped (T-C duct absent) CTD (model SBE19) or a pumped CTD (model SBE25).

The manufacturers specifications for the SBE19 are shown in Table 2.3. Calibration of the SBE19 was carried out at Sea-bird Electronics Laboratory in March 1993. In 2000, two years after the sampling campaign, the sensors on the SBE19 were again verified. The CTD was compared both statically (under laboratory conditions) and dynamically (at sea) with a calibrated SBE19. The temperature sensor was verified against an ultrastable digital oceanographic thermometer (model number SBE38) within the temperature range 14-25 °C. The drift in the temperature and conductivity sensors was low and within the expected range. The SBE25 had been fully calibrated at EMS Laboratories (Barcelona) prior to the campaign and was thus operating at manufacturers specifications [Table 2.4].

Table 2.3. SBE19 specifications

	Measurement Range	Initial Accuracy	Resolution
Conductivity (S m^{-1})	0-7	0.0001	0.0001
Temperature (°C)	-5 to +35	0.01	0.001
Pressure	0-350 metres	0.25% of full range	0.005% of full range

Table 2.4. SBE25 specifications

	Measurement Range	Initial Accuracy	Resolution
Conductivity (S m^{-1})	0-7	0.0003	0.00004
Temperature (°C)	-5 to +35	0.002	0.0003
Pressure	0-700 metres	0.1% of full range	0.002% of full range

Optimisation of data quality. Table 2.5 shows a typical data processing sequence for the SBE19 using SEASOFT software. Also shown are the manufacturers recommendations for each process. Fig. 2.6 is an example of salinity spiking in the data set (S±0.1). Several CTD profiles were sent to Sea-bird Electronics (USA) for diagnostic analysis of sensor misalignment. Sea-bird [*R. Baumann, Sea-bird Electronics,* Pers. Comm.] concluded that salinity spikes observed at the thermocline resulted from a temporal misalignment of the conductivity and temperature sensors, possibly due to variable profiling speeds from yawning of the research vessel. These were minimised, but not totally eliminated, by advancing the temperature channel with respect to pressure and conductivity with respect to temperature [Table 2.5]. The SBE25 was fitted with a pump and T-C duct, which directs water over the sensors at a constant rate during profiling. Therefore, no advance of temperature relative to pressure was necessary due to fast time response of temperature sensor.

Sea-bird recommend a minimum profiling speed greater than 0.7 m s^{-1} with free flushing conductivity sensors to avoid thermal contamination of the conductivity measurement. This criterion was employed when processing the data, and drop speeds lower than this threshold were removed using *LOOP EDIT* [Table 2.5]. During rough weather the profiling speed was increased to reduce the dynamic spiking errors caused by rapidly changing CTD descent/ascent rate (yo-yo effect). The submersible pump on the SBE25 and greater sampling frequency (8 Hz) permits slower decent rates and greater vertical resolution in the data than the unpumped SBE19, especially during calm conditions. For all cruises, the down cast data was used in this thesis [*R. Baumann, Sea-bird Electronics,* Pers. Comm.]. Additional steps to enhance the quality of the data included (i) thermal equilibration of the CTD in the surface layer for approximately 1 minute before profiling, and (ii) sensor cleansing after deployment with a non-ionic detergent to remove fouling, and posterior storage in distilled water.

Density, depth, and salinity were calculated from pressure, temperature, and conductivity data using *DERIVE* [Table 2.5]. The formulas used by *DERIVE* were obtained from UNESCO [1981]. In this thesis, the following protocol was employed for reporting thermohaline data, treating the ocean surface as 0.0 db:

Table 2.5. Data processing sequence for the Sea-bird CTDs.

Programme	Function	Sea-bird Recommendations	Constants Employed for Data
DATA CONVERSION	Convert raw data into engineering units. Converted data includes pressure (depth), temperature, and conductivity.	N/A	N/A
WILD EDIT	Marks wild points *bad* in the data. *WILD EDIT's* algorithm requires two passes through the data: Pass I obtains an accurate estimate of the data's true standard deviation and marks *bad* scans lying outside this deviation. Pass II re-computes the standard deviations.	*SBE 19:* Default set-up of 2 standard deviations for the Pass I and 20 standard deviations for Pass II. *SBE 25:* Default set-up of 2 standard deviations for the Pass I and 20 standard deviations for Pass II.	*SBE 19:* As default. *SBE 25:* As default.
FILTER	Runs a low-pass filter on columns of data to smooth high frequency (rapidly changing) data. Typically, only conductivity and pressure data are filtered. Two time constants can be specified allowing conductivity and pressure to be filtered simultaneously.	*SBE 19:* Conductivity filter of approximately 0.5 s to force conductivity to have same response as temperature. 2 s pressure filter to increase pressure resolution for *LOOP EDIT*. *SBE 25:* 0.5 s pressure filter to increase pressure resolution for *LOOP EDIT*.	*SBE 19:* Conductivity filter by 0.5 s [Rick Baumann, Sea-bird Electronics Inc., *Pers. Comm.*]. Pressure filter of 2 s. *SBE 25:* 0.5 s pressure filter
ALIGN CTD	Aligns parameter data (typically temperature and conductivity) in time, relative to pressure. This ensures that calculations of salinity, dissolved oxygen concentration, and other parameters are made using measurements from the same parcel of water.	*SBE 19:* Advance temperature relative to pressure approximately +0.5 s. Conductivity advances relative to temperature range from 0 s (0.75 m s^{-1} drop speed) to -0.6 s (2 m s^{-1}). *SBE 25:* No advance in temperature necessary. With a standard 2000 rpm pump, typical advance of conductivity relative to temperature is +0.1 s.	*SBE 19:* Temperature advanced relative to pressure by +0.4-0.6 s [Rick Baumann, Sea-bird Electronics Inc., *Pers. Comm.*). Conductivity advanced relative to temperature where possible (0.3-0.5 s). *SBE 25:* Temperature advanced relative to pressure by 0 s. Conductivity advanced relative to temperature by +0.1 s.
CELL THERMAL MASS	Uses a recursive filter to remove conductivity cell thermal mass effects from the measured conductivity.	*SBE 19:* Dependent on sharpness of thermocline *SBE 25:* Dependent on sharpness of thermocline	*SBE 19:* None [Rick Baumann, Sea-bird Electronics Inc., *Pers. Comm.*]. *SBE 25:* None
LOOP EDIT	Marks *bad* scans that have pressure slowdowns or reversals due to ship motion.	*SBE 19 & 25:* Judge parameter profile with descent rate to ascertain whether editing is necessary. Minimum velocity 0.7 m s^{-1} for free flushing sensors.	*SBE 19:* Minimum velocity 0.7 m s^{-1} *SBE 25:* Minimum velocity 0.7 m s^{-1}
BIN AVERAGE	Average data into desired pressure or depth bins.	N/A	N/A
DERIVE	Compute salinity, potential temperature, density (σ_t, σ_θ) and other parameters.	N/A	N/A

Temperature. Temperature (°C) is reported as potential temperature θ (s,t,p), which is the temperature an element of seawater would have if raised adiabatically to a reference pressure with no change in salinity.

Salinity. Salinity is equal to the Practical Salinity Scale 1978.

Density. Density (kg m^{-3}) is calculated based on the EOS80 Equation of State for Seawater [*UNESCO*, 1981] and reported as $\sigma_\theta = \rho(s,\theta(s,t,p,0),0) - 1000$.

It is worth noting that the contribution of each measured variable to the salinity error cannot be expressed by a single number, due to conductivity, temperature, and pressure variability in the ocean. To a first approximation, the salinity error implicit in a temperature error of 0.005 °C or a conductivity error of 0.0005 S m^{-1} is about 0.005 in salinity; the error from pressure is of order 0.0005 in salinity per dbar pressure error [*K. Lawson, Sea-bird Electronics*, Pers. Comm.].
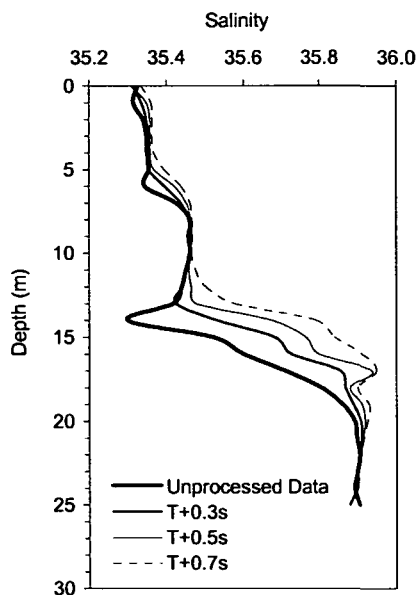
Fig. 2.6. Typical salinity-depth profile from the Pontevedra Ria using the unpumped SBE19, showing the minimisation of the spike by advancing temperature relative to pressure.

2.5. BIOGEOCHEMICAL VARIABLES

The biogeochemical aspects of the campaign focussed on dissolved and particulate carbon, nitrogen, phosphorus and silicon. Dissolved oxygen and chlorophyll *a* measurements were also routinely measured. In this section the corresponding analytical methods are described.

2.5.1. SEDIMENT ANALYSIS

Benthic. On one occasion, 33 benthic sediment samples (evenly spatially distributed over the ria) of the oxic layer (top 0-1 cm) were collected with a Shipek grab and dried in an oven below 40°C. Dried sediments were size-fractionated into mud, sand and gravel with 63 μm and 2000 μm sieves.

Pelagic. The sediment trap system [*Knauer et al.*, 1979] for water column particulate material consisted of four bound Plexiglass tubes (6 cm diameter). NaCl (35g) was added to each tube to raise the density and prevent particle loss. Particulate material was filtered through Whatman GF/F filters on board and stored frozen until further processing in the laboratory.

Particulate organic matter (POM). Total carbon and total nitrogen from the benthic and pelagic samples were determined with a Carlo Erba CHNS-O 1108 elemental analyser by the Research Support Service at the University of La Coruña. Inorganic nitrogen was assumed negligible. Organic and inorganic carbon were determined by differential thermal analysis, whereby organic carbon was determined by weight loss by ignition over the range 550-975°C, and inorganic carbon as the difference between the organic and total measurement. The possible overestimation [~20%, *Mook and Hoskin*, 1982] of organic carbon due to loss of structural water in particulates is acknowledged. However, according to the findings of *Gibbs* [1977], this overestimation may be balanced by an equal (~25%) underestimation of organic carbon due to incomplete combustion.

Silica. Siliceous phytoplankton use dissolved silicate from the water column to construct biogenic siliceous tests. The chemical structure of the phytoplanktonic tests is amorphous, and commonly defined as opal. In this thesis, pelagic and benthic opal is defined as BSi. Determination of BSi followed the alkaline digestion method described by *Mortlock and Froelich* [1989]. In addition, crystalline lithogenic silica in filtered (0.45 µm) water column samples was determined by stronger digestion following the methodology of *Ragueneau and Tréguer* [1994].

2.5.2. NUTRIENT FLUX INCUBATION EXPERIMENTS

Sediment cores were regularly sampled from Sts. 4 (35m depth), 6 (25m) and 8 (9m) for incubation experiments. Triplicate samples were extracted at each site. Cores (6-8 cm) of undisturbed sediment and approximately 200 ml of the overlying water were taken with a Rouvillois box-corer fitted with Plexiglass tubes (length 25 cm, diameter 5.4 cm) [Fig. 2.7]. The tubes were sealed at the bottom with a rubber stopper, inspected for trapped air pockets and verified that the collection process had not artificially disturbed the sediment structure. A fourth control consisted of seawater only, transferred from the three other tubes. The cores were immediately incubated on-board at *in situ* temperature and in darkness. A loose fitting lid was placed on each tube permitting gas exchange with the atmosphere, and the supernatant water was continually circulated by means of a peristaltic pump operating at 4 ml min^{-1}. At intervals of 0, 1, 2, 3, 4, 5, 6 and 12 hr, 10 ml aliquots were taken from each core for analysis of dissolved nitrate, nitrite, ammonium and silicate following the methodology described below. Corrections were made for the decrease in water volume with removal of aliquots over the incubation period, and the fluxes were corrected against the control when necessary. The mean flux of the triplicate cores was calculated from the efflux rate curves. Those displaying random fluxes were not considered. The correlation coefficients of the nutrient efflux rates in the sediment and control cores were greater than $r^2=0.70$ (n=8) for >90% of the incubations.
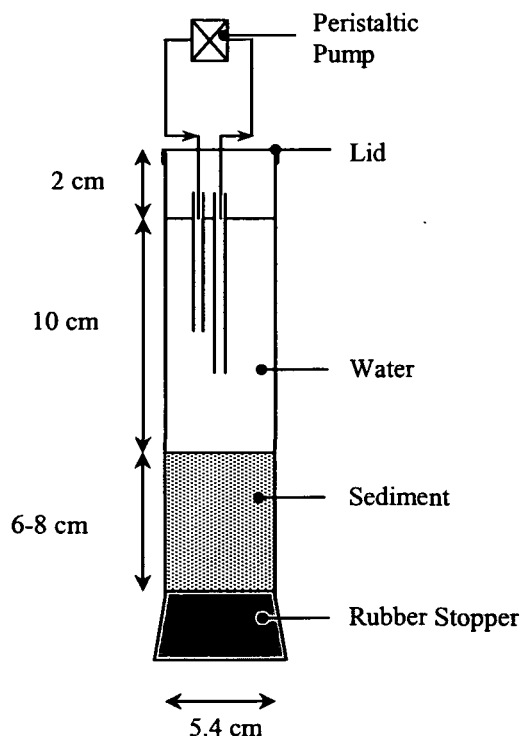
Fig. 2.7. Experimental incubation design. Triplicate sediment cores and a control of water only were used for nutrient flux assessment. All cores were maintained in a water bath at *in situ* temperature in darkness. Water was continually circulated via the peristaltic pump.

2.5.3. DISSOLVED OXYGEN

Water samples for determination of dissolved oxygen concentration were fixed on board in 130 ml glass bottles with 1 ml each of $MnCl_2$ and KI and stored in the dark until analysis the following day. Oxygen was determined by the Winkler titration with visual endpoint detection using a starch solution indicator, following well-established methods [*Grasshoff et al.*, 1983; *Aminot*, 1983]. Concentrations were transformed to percentage saturation using standard conversion tables [*UNESCO*, 1986]. The concentration of dissolved oxygen is a non-conservative parameter of a water body. Therefore, deviations in oxygen concentration from the theoretical saturation for a given salinity and temperature is an indication of aerobic biological activity. Oxygen concentration in this thesis is reported as percentage saturation (O_{2SAT}) and µmol l^{-1}, based on the molar volume of ideal gases at standard temperature and pressure (22.413 l mol^{-1}). The precision of the analysis was 0.5 µmol l^{-1}.

2.5.4. CHLOROPHYLL A

The procedure for sampling and processing of samples for Chl a analysis followed the methods of *Bode and Varela* [1998] and *Varela et al.* [2001]. Analytical methods followed JGOFS protocols [*UNESCO*, 1994]. Briefly, water samples (250 ml) were filtered through Whatman GF/F filters, and the Chl a extracted with 90% acetone. Chl a concentration was determined by fluorimetry following the methods of *Parsons et al.* [1984] and *Yentsch and Menzel* [1963]. Chl a data were provided by Dr. Manuel Varela (Spanish Oceanographic Institute, La Coruña, Spain), and were available for Sts. 0, 4 and 6 from February-October 1998 [Table 2.1]. The precision of the analysis was 0.03 mg Chl a m^{-3}.

2.5.5. DISSOLVED INORGANIC NUTRIENTS

Water samples collected from the ria, estuary, river and effluent were separated into 50 ml HDPE bottles, placed in a refrigerator at 4 °C until analysis (within 24 h). Occasionally, samples were stored frozen. Samples were not filtered due to the low SPM concentrations in the ria, thereby reducing the possibility of introducing error via analytical artefacts. Furthermore, there is considerable controversy over what traditional filtration through a 0.45 μM filter actually measures [*McKelvie et al.*, 1995]. No preservatives were added to the samples prior to analysis in view of contradictory reports associated with preservatives [*Maher and Woo*, 1998; *Kattner*, 1999].

Nutrients analysed in this work are therefore operationally defined as "total reactive nutrients" [*Robards et al.*, 1994]. This fraction contains soluble species such as the major inorganic ions (e.g. orthophosphate, HPO_4^{2-}; nitrate NO_3^-), hydrolysable labile and organic nutrients and reactive particulate species. Therefore, there may be an over estimation of the dissolved inorganic nutrient concentrations. However, given that the SPM concentrations in the Rias Bajas are close to typical seawater values [1-5 mg l^{-1}, *R. Prego*, Pers. Comm.] and the dissolved nutrients (orthophosphate, HPO_4^{2-}; nitrite, NO_2^-; nitrate NO_3^-; ammonium NH_4^+; and silicate $Si(OH)_4$) constitute the major part of the species present, references to the analytes in this thesis correspond to the dissolved inorganic fraction. Unless otherwise stated, the dissolved nutrients are reported as phosphate = DIP, inorganic nitrogen ($NO_2^-+NO_3^-+NH_4^+$) = DIN, and dissolved reactive inorganic silicate = $Si(OH)_4$. This definition permits ease of measurement and predictive power with respect to biological and environmental effects, e.g. bioavailability estimates and nutrient budget calculations [*Robards et al.*, 1994; *McKelvie et al.*, 1995].

Preparation of standards. For calibration, primary standards were made from AnalR grade materials, which were diluted to make secondary standards. The corresponding standard materials for nitrate, nitrite, ammonium, phosphate and silicate were KNO_3, $NaNO_2$, NH_4Cl, KH_2PO_4 and Na_2SiF_6, respectively. The solids were dried in a vacuum over silica gel for 24 h, weighed on an analytical balance (± 100 μg) and dissolved in MilliQ water. Three primary standards were made for each N species, and K_2HPO_4 and Na_2SiF_6 were present in all three. Low nutrient seawater (LNSW) was used to make the secondary standards. LNSW was made by prolonged daylight exposure of a carboy of seawater taken from outside the Pontevedra Ria, thus allowing micro-organisms to consume the nutrients. LNSW was filtered (0.45 μm) before use. Secondary standards were made by 1:100 dilution of the primary standards, which gave a final nutrient concentration of the same order as the maximum values found in the Rias Bajas (2 μmol l^{-1} NO_2^-, 15 μmol l^{-1} NO_3^-, 6 μmol l^{-1} NH_4^+, 1 μmol l^{-1} HPO_4^{2-}, 15 μmol l^{-1} $Si(OH)_4$. When one or more of the secondary standards was exhausted, new standards were prepared in order that the same LNSW was used in all cases. Nutrient concentrations in this thesis are expressed as molar quantities.

Nutrient analysis. The determination of nutrient salts is based upon automated colorimetric analysis [*Grasshoff et al.*, 1983]. Nutrient

concentrations were measured (20 samples per hour) using a Technicon AutoAnalyser II with regular calibration and baseline checks. Colour development of the sample is carried out in mixing coils, after which the sample passes through a photo-tube colorimeter. The automated analyses can be summarised as follows:

> *Phosphate.* The automated determination of phosphate was based on the single solution procedure developed by *Murphy and Riley* [1962]. Acidic molybdate reacts with orthophosphate to form a phosphomolybdate heteropoly acid, which when reduced forms a strongly coloured phosphomolybdenum blue species. Ascorbic acid is used as a reductant with a potassium antimonyl tartrate catalyst. Measurement is made at 880 nm and at pH 0.8-1.0. Interferences from $Cu(II)$, $Fe(III)$, silicate and arsenate were likely to be negligible [*Grasshoff et al.*, 1983].

> *Nitrite.* Under acidic conditions the nitrite ion reacts with sulphanilamide to yield a diazo compound, which is coupled with N-1-napthyl ethylenediamine dihydrochloride (NED) to form a soluble azo dye. Measurement of the azo-dye is made at 540 nm.

> *Nitrate.* The method for nitrate involves the initial reduction of nitrate to nitrite in a heterogeneous reaction in a Cu-Cd reductor. The determination follows that above for nitrite with a slight alteration from the *Grasshoff et al.* [1983] method by employing a citric acid-citrate buffer in place of NH_4Cl to avoid contamination of the ammonium analyses and maintain pH between 5.3-5.7 [*Mouriño and Fraga*, 1985]. An active cadmium surface is maintained with the disodium salt ethylenediamine tetra-acetic acid (EDTA).

> *Ammonium.* In aquatic environments ammonium exists in equilibrium with ammonia. Under typical conditions of pH and temperature found in seawater the total ammonium is much greater than the ammonia fraction [*Clegg and Whitfield*, 1995]. In basic medium (pH 8-11.5), ammonium reacts with hypochlorite to form a monochloroamine. In the presence of excess hypochorite (oxidant) and nitroprusside (catalyst), the amine reacts with phenol to produce indophenol blue. Measurement is made at 625 nm. The final pH should be below 10.8 to avoid the oxidation of the indophenol species.

> *Silicate.* Dissolved orthosilicate, $Si(OH)_4$, is the most abundant form of dissolved silicate in the sea [*Isshiki et al.*, 1991]. The automated determination of orthosilicate in seawater is based on the formation of a siliciomolybdic acid and its partial reduction to an intense blue heteropoly acid. Oxalic acid is added to prevent interferences from phosphate. Measurement is made at 660 nm.

Data validation: the nutrient blank. Systematic errors during the automated colorimetric determination of nutrient salts arise from the change in the refractive index when saline water is used as the analyte rather than freshwater. In addition, optical variations in the glass flow cells within the instrument tend to give greater absorbance than those obtained by manual procedures due to light dispersion. Moreover, LNSW will also lead to erroneously high concentrations if the nutrient concentration therein is not accurately quantified.

A straightforward method to measure the refractive index for an individual nutrient sample is based on the phosphate blank description

given by *Álvarez-Salgado et al.* [1992]. For each nutrient, an aliquot of deionised water was mixed with all the necessary reagents required to bring about complex formation except one. Replacing the deionised water with LNSW leads to an increase in absorbance due to the refractive index of the sample only, since no colourimetric reaction occurred [Peaks A_C in Fig. 2.8]. The missing reagent is then included, leading to an absorbance peak, which is a measure of both the refractive index and the nutrient concentration in the LNSW sample [Peaks B_C in Fig. 2.8]. The nutrient concentration in the LNSW is proportional to the difference between the absorbance peaks (B_C-A_C). Analysis of standard solutions in LNSW gave absorbance peaks C_C. The reagent nutrient concentration was assumed to be zero. *Álvarez-Salgado et al.* [1992] reported the reagent concentration of phosphate to be 1.5% of the concentration of C_C.

If the signal of a water sample is S_C [Fig. 2.8], the nutrient concentration of S_C is:

$$[S_C] = (S_C - A_C) \times \frac{[C_C]}{C_C}$$

[2.7]

where $[C_C]$ is the nutrient concentration (P, N, Si, μmol l^{-1}) of the standard prepared in LNSW. During the course of the analysis, spiked seawater samples and LNSW were analysed regularly so that any drift in seawater and standard signal could be determined. The nutrient concentrations in LNSW, determined regularly over 1997-2000, were: nitrate (0.00-0.36 μM), nitrite (0.01-0.09 μM), ammonium (0.10-0.22 μM), phosphate (0.05-0.17 μM) and silicate (0.10-0.63 μM).

The precision of the data was made at seawater salinity. The nutrient concentrations in freshwater are usually substantially greater than in seawater which reduces the importance of the error in this case.
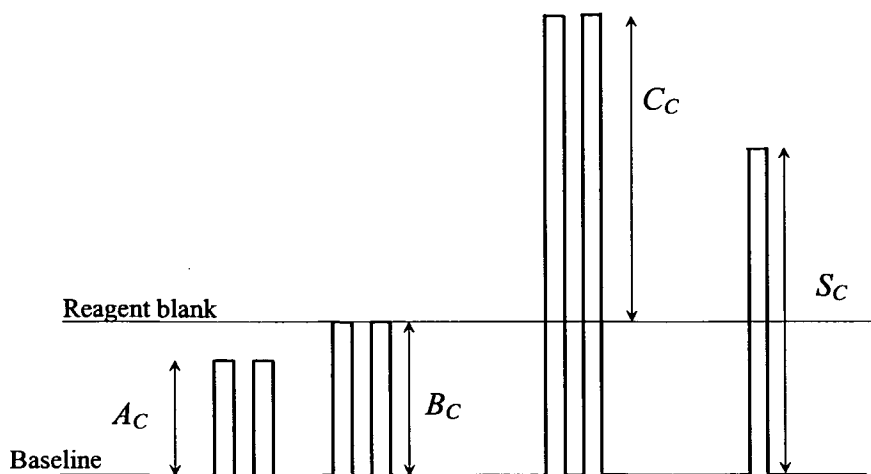
Fig. 2.8. Example of a chart recorder readout to quantify the nutrient concentration in LNSW and marine samples. Each aliquot was analysed twice. Peaks A_C correspond to the absorbance due to the refractive index and B_C to the refractive index plus the nutrient concentration in LNSW. Analysis of standard solutions prepared in LNSW is represented by peaks C_C. The sample corresponds to peaks S_C.

Critical data analysis. The final data were systematically screened for random errors. To evaluate the reproducibility of the analysis, a standard solution of known concentration for each nutrient was analysed 10 times, from which the mean, standard deviation (±☐) and relative standard deviation (RSD) were calculated [Table 2.6].

The detection limit of the analysis is equal to three times the standard deviation of the blank. Blank samples of LNSW, which contain a small amount of dissolved nutrient were analysed on a regular basis intermittent with the seawater samples. From the peaks, the standard deviations and detection limit were calculated [Table 2.6].

Table 2.6. Mean, ±σ, relative standard deviation (RSD) and detection limit (d.l.) of the nutrient analyses (μmol l^{-1}).

	Standard			LNSW Blank		
	Mean	±σ	RSD (%)	Mean	±σ	d.l.
[†]NO_3^-	10	0.01	0.1	0.32	0.063	0.189
NO_2^-	2	0.01	0.5	0.027	0.005	0.015
NH_4^+	2	0.02	1	0.0253	0.007	0.021
HPO_4^{2-}	2	0.03	1	0.031	0.031	0.093
$Si(OH)_4$	6.45	0.01	0.02	0.63	0.022	0.066

[†] Data based on the precision reported by *Prego* [1994].

Chapter 3

Glossary of terms used in Chapter 3

Parameter or variable	Unit	Description
ε_Q, ε_V,	$m^3\ s^{-1}$	Analytical error of horizontal and vertical advective fluxes
ε_Z, ε_{Vo}	$m^3\ s^{-1}$; m^3	Analytical error of residual freshwater flow and water volume
ε_S	-	Analytical error of CTD salinity measurement
ε_τ	d	Analytical error of freshwater residence time
$ENACW$	-	East North Atlantic Central Water
$\overline{E}_{Vc}$, $\overline{E}_{Vi}$	$kg\ m^{-2}\ s^{-1}$	Mean diffusive vertical salt flux between two consecutive surveys
FFW	-	Fraction of freshwater method for residence time evaluation
f	-	Fraction of freshwater
$\overline{I}_w$	$m^3\ s^{-1}\ km^{-1}$	Mean upwelling index between two consecutive surveys
N	min^{-1}	Brunt-Väisälä stability frequency
$\Delta S/\Delta t$, $\Delta V/\Delta t$	s^{-1}, $m^3\ s^{-1}$	Change in salt content and volume between two consecutive surveys
$\overline{Q_U \times S_U}$, $\overline{Q_L \times S_L}$	$kg\ m^{-3}\ s^{-1}$	Mean surface and bottom advective salt fluxes at the model boundaries between two consecutive surveys
$\overline{Q}_U$, $\overline{Q}_L$	$m^3\ s^{-1}$	Mean surface and bottom advective water fluxes at the model boundaries between two consecutive surveys
$\overline{Q}_Z$	$m^3\ s^{-1}$	Mean residual inflow to the ria between two consecutive surveys
$\overline{Q}_R$	$m^3\ s^{-1}$	Mean river inflow to the ria between two consecutive surveys
$\overline{Q}_P$	$m^3\ s^{-1}$	Mean precipitation to the ria between two consecutive surveys
$\overline{Q}_E$	$m^3\ s^{-1}$	Mean evaporation from the ria between two consecutive surveys
$\overline{Q}_{EFF}$	$m^3\ s^{-1}$	Mean effluent flux to the ria between two consecutive surveys
$\overline{Q}_{Vc}$, $\overline{Q}_{Vi}$	$m^3\ s^{-1}$	Mean advective vertical salt flux between two consecutive surveys
S	-	Salinity
$\overline{S}_U$, $\overline{S}_B$	-	Mean upper and lower layer salinity at the model boundaries between two consecutive surveys
σ_θ	$kg\ m^{-3}$	Potential density
θ	°C	Potential temperature
t	s	Time
T	°C	Temperature
τ	d	Freshwater residence time
V	m^3	Water volume of central or internal ria
W_L	$m\ s^{-1}$	Local winds resolved along the NE-SW ria axis

3. Hydrography of the Pontevedra Ria

An assessment of the physico-hydrodynamical characteristics ought to be one of the first steps in any ecosystem analysis. Understanding the hydrographical trends allows for the superimposition and interpretation of biogeochemical parameters, thus leading to practical coastal zone management. In areas where socio-economic demands are high, such as the Pontevedra Ria, this approach becomes all the more important.

3.1. INTRA-ANNUAL SPATIAL AND TEMPORAL TRENDS

The Galician rias display hydrographical characteristics strongly dependent on river discharge and seasonal oceanic upwelling events. The annual spatial and temporal hydrographical trends in the Pontevedra Ria can therefore be inferred from the salinity, temperature, and current profiles taken throughout the sampling period.

3.1.1. ANNUAL TEMPORAL CHANGES

Three key stations along the ria axis were chosen for the development of an accurate hydrographical description of the temporal changes in the ria. These were: Sta. 0, located on the adjacent shelf (oceanic); Sta. 1, located at the main entrance to the ria (ria-shelf interface); and Sta. 6, located inside the ria (ria-river interchange) [Fig. 2.1].

Salinity was closely related to the river Lérez discharge, particularly during river floods, and increased progressively seaward from the river mouth [Fig. 3.1]. In the wet season, the ria received on average between 40 and 60 m^3 s^{-1}, reflected by the salinity decrease at Sta. 6 which affected the whole water column. Buoyant freshwater inputs were important during high-runoff events such as in January. River discharges of ~100 m^3 s^{-1} were followed by a notable salinity decrease to 30 near the surface [Fig. 3.1] and almost 34 near the bottom, thus evidence of competing freshwater-induced buoyancy stratification and downward mixing of fresh water. Bottom

salinity at Sta. 0 at this time was 35.9. Wet season mixing in the Pontevedra Ria was a function of continual terrestrial runoff and partial retention of the water inside the ria by winds of a southwesterly component, in other words, unfavourable upwelling conditions [Fig. 3.2]. Nevertheless, the Brunt Väisälä stability parameter, N (min^{-1}), shows that low surface density of $\sigma_\theta = 21.0$ kg m^{-3} creates a stable water column, of up to 0.5 min^{-1} in the upper water layers [Fig. 3.3]. Vertical stability increased towards the ria head (data not shown) where the waters are shallower [Otto, 1975].
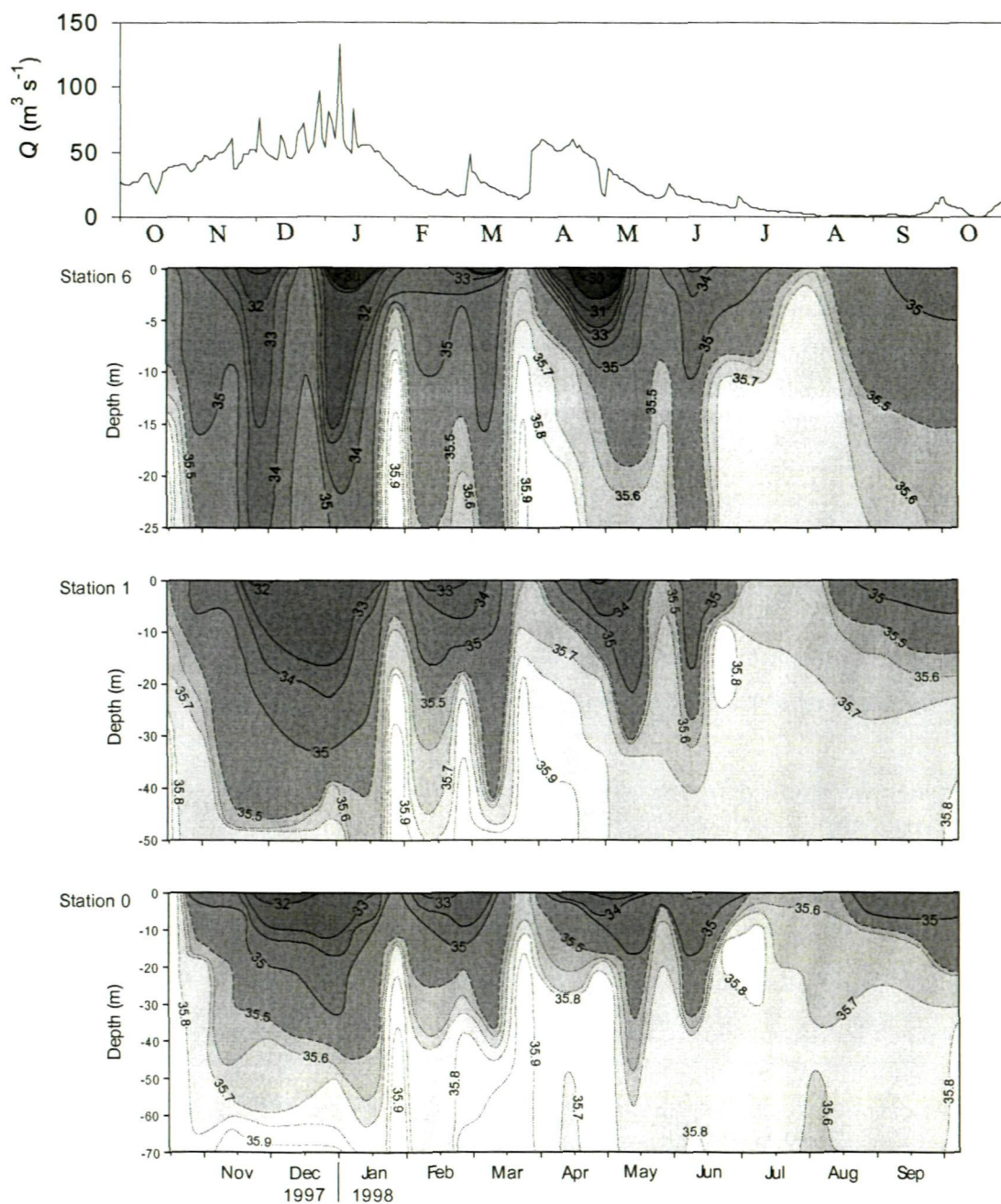
Fig. 3.1. Lérez river discharge (Q m^3 s^{-1}) and water column salinity at Sta. 6 (internal), Sta. 1 (principal mouth), and Sta. 0 (offshore) over the study period (October 1997 to September 1998).

31
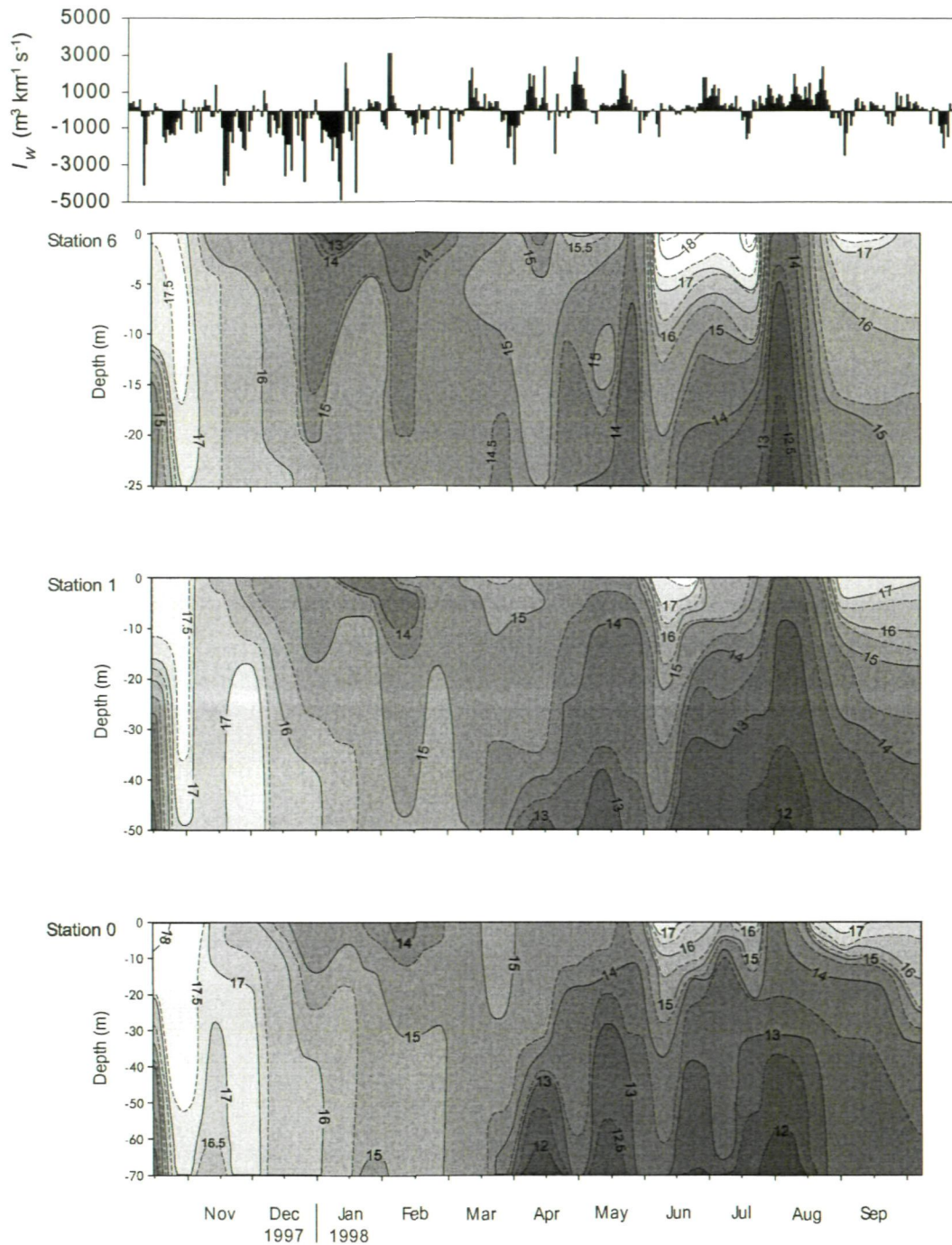
Fig. 3.2. Upwelling index (I_W) and water column temperature at Sta. 6 (internal), Sta. 1 (principal mouth), and Sta. 0 (offshore) over the study period (October 1997 to September 1998).

When the winds veered northeasterly in late January, early February, and March [Fig. 3.2], an intrusion of more saline water occurred and was clearly observable at Sta. 6 as a series of "pulses" [Fig. 3.1]. These additional meteorological conditions are not normally associated with the rainy season in the river basin, and they enhanced the salinisation of the ria. The opposite situation was observed toward the end of April. In this case, the discharge from the river Lérez was high and the mixing layer was far more superficial since fresh water outflow was not hindered by winds,

32

and I_W was small and negative [Fig. 3.2]. Accordingly, it is possible to detect a salinity of 35 at 10 m depth with low salinity water at the surface. The overall effect was an increase in water column stability [Fig. 3.3]. This trend was also evident at the ria mouth [Sta. 1] and offshore at Sta. 0 [Fig. 3.1], where the salinity gradient was lower. The isohalines were more spatially and temporally relaxed in the surface layers at the mouth, indicating longer freshwater mixing times than in the inner ria, whereas in the lower layers water of oceanic salinity (35.5) was always observed at times of offshore water intrusions. Therefore the combined effects of shelf winds (I_W) and fluvial flow can be traced with salinity, and it is clear that the observed trends were generally maintained from the inner to the outer ria. This ria-shelf interaction has not been described previously and, despite the lack of data relative to the other Rias Bajas, it seems reasonable to infer that the haline pattern in the neighboring systems is similar to the Pontevedra Ria.
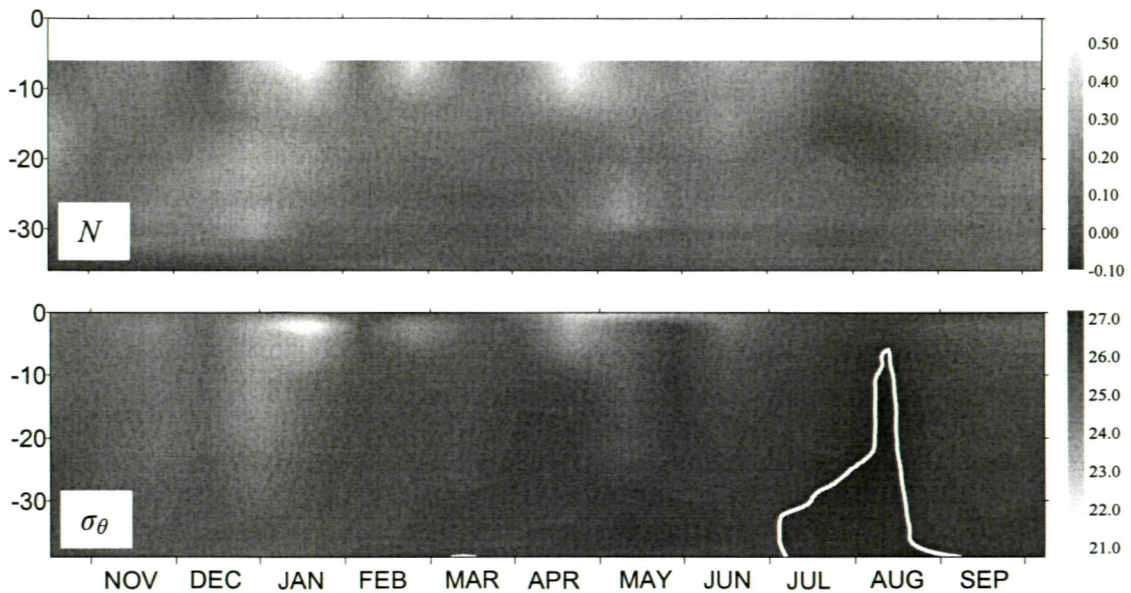
Fig. 3.3. Brunt Väisälä frequency (N, min^{-1}; upper panel) and density (σ_θ, kg m^{-3}; lower panel) at Sta. 3 in the Pontevedra Ria during October 1997-1998. The upper limit of ENACW is traced with the white line representing the σ_θ=27.0 kg m^{-3} isopycnal.

The summer-autumn trends were more adequately described with temperature rather than salinity, since the vertical salinity gradient inside the ria was small, 34.0 to 35.7 [Fig. 3.1] and minimal outside, 35.0 to 35.8. The tendency toward saline homogeneity was due to low runoff and regular upwelling events of ENACW during the dry season engendered by offshore Ekman transport and northerly winds [Fig. 3.2]. The sea level at the mouth of the ria was lowered by the wind-induced flow, setting up a seaward pressure gradient inside the ria which ultimately forced the water seaward above the pycnocline in response [*Blanton et al.*, 1987]. ENACW was subsequently driven into the ria by the outward flow and increased the overall density of the water inside the ria [Fig. 3.3]. This pattern was readily traced with water temperature. The upwelling phenomenon, usually observed from April to October [*Wooster et al.*, 1976; *McClain at al.*, 1986]

on the Galician coast [*Fraga*, 1981; *Prego and Bao*, 1997], was identified by the 13 °C isotherm on the ria-shelf interface during April and May and from mid-June until the end of August [Fig. 3.2]. With a positive I_W in spring the upwelled water arrived at the ria mouth but did not, however, penetrate the internal ria. The I_W increased in May in both duration and intensity and upwelled water reached Sta. 6, where the temperature fell to 14 °C at 7 m depth. This process further intensified in July whereby upwelled water was mixed with existing ria water, and lowered the surface water temperatures at Sta. 6 to 14 °C and those at 25 m depth to 12 °C, in spite of high air temperatures (35 °C maximum) and solar irradiation. In addition, the Brunt Väisälä parameter [Fig. 3.3] shows that water column stability was decreased by intense upwelling in August [*Rosón et al.*, 1995]. Core ENACW is traceable by the $\sigma_\theta = 27.0$ kg m^{-3} isopycnal during July and August [Fig. 3.3]. Upwelling was especially evident in the Pontevedra Ria since its mouth is the deepest of the Rias Bajas [Table 1.1] and thus provides relatively unobstructed entry to incoming ENACW. Nevertheless, it should be noted that there is considerable interannual variation in upwelling strength on the continental shelf [*Lavin et al.*, 1991].

September was characterised by low positive and negative I_W [Fig. 3.2]. Favourable upwelling conditions ceased, and water temperatures increased despite the decrease in solar irradiation with the close of the dry season. This anomaly presumably resulted from the absence of upwelling-induced circulation, low river runoff with slight freshwater-induced buoyancy, and diminishing, but sustained, solar heating [Fig. 2.3]. The combination of the above factors favoured thermal stability of the surface layers until autumn mixing, and higher fluvial inputs lowered temperatures until the winter thermal inversion, as seen in the previous winter [Fig. 3.2]. This phenomenon was believed to be due to atmospheric conditions only, but increasing cold river discharge also played a key role in this process and produced a longitudinal temperature gradient in the surface layers inside the ria [Fig. 3.2]. Accordingly, surface cooling decreased from the ria head to the ria mouth, with a 3 °C vertical gradient of temperature inversion at Sta. 6, compared with only 1 °C at Sta. 0.

3.1.2. ANNUAL CYCLE OF WATER MASSES

The interchange between water masses in the ria can be studied more closely by means of a temperature-salinity (TS) diagram. The subsuperficial inputs of offshore water mainly occur through the deeper southern mouth, and therefore salinity and temperature data measured at 50 m depth at Sta. 1 were used to describe the water exchanges over the sampling period [Fig. 3.4].

From April to September the water mass in the ria was correlated to ENACW of subtropical origin [*Fiuza et al.*, 1998]. Salinity values ranged from 35.67 to 35.83 [Fig. 3.1] and temperature from 11.8 to 13.5 °C [Fig. 3.2], depending on the upwelling intensity and mixing of existing bottom water in the ria. This was further evident in the dense incoming waters in Fig. 3.3. During spring and summer the upwelling may relax, as in the cruise 6a in Fig. 3.4 [see Table 2.1 for cruise date]. This situation was observed only once during the campaign, although it may be much more frequent depending on atmospheric conditions [*Lavin et al.*, 1991] and the sampling frequency. At the end of the upwelling season in 1997, ENACW gave way to a warmer and saltier water mass (cruise 10a). Within less than

a fortnight, between cruises 10a and 10b, the abrupt change in thermohaline properties of the water were attributed to further inputs of warm [15.5 to 17.5 °C, Fig. 3.2] fresher subsuperficial shelf seawater which predominated during the autumn and most of the wet season up to mid-January (cruise 1a). Thereafter, the autumnal water mass was replaced by a distinct water body [Fig. 3.4] on a timescale similar to the previous interchange, which persisted from late January to early March (cruises 1b to 3a). In this case, the substitute water mass was transported by the poleward current, a warm (14.5-16.5 °C) and saline (35.9-36.1) wind-induced current flowing poleward at 0.2-0.3 m s^{-1} along the Iberian Peninsula shelf-slope break at a depth and width of 150-200 m and 25-35 km, respectively [*Frouin et al.*, 1990].
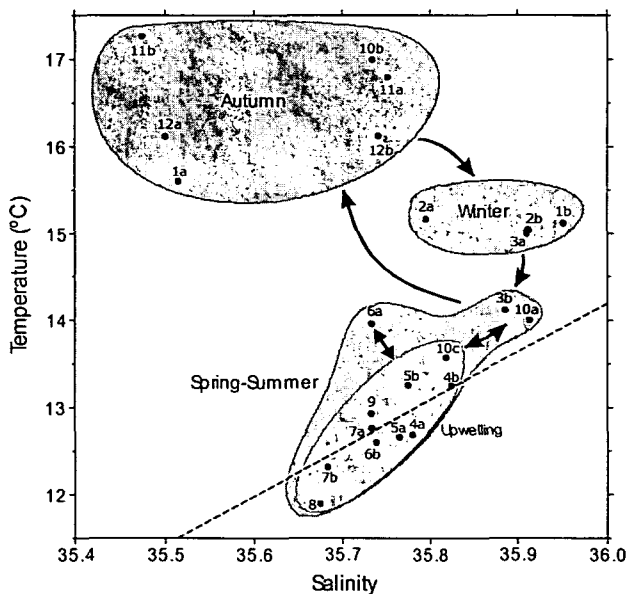
Fig. 3.4. Temperature-salinity diagram of incoming seawater at ria Sta. 1 (50-m depth) over an annual cycle. Numbers refer to the calendar month (October 1997 to September 1998), and letters "a" and "b" refer to the first and second fortnightly cruises, respectively, except 10c, which corresponds to the cruise on 7 October 1998 [Table 2.1]. The dashed line represents the TS range for ENACW.

Intrusion of the poleward current caused a further widening of the temperature difference of the surface and bottom waters inside the ria from January to March [Fig. 3.2]. The same water mass was detected earlier on the shelf [Sta. 0] in November and was correlated to a temperature minimum [16.5 °C; Fig. 3.2] and a salinity maximum of 35.9 [Fig. 3.1] in the near-bed water layers but was not of sufficient strength to advect inside the ria. However, in January, along with unanticipated favourable upwelling conditions, this water was observed at the mouth of the ria down to 15 m, as well as inside the ria down to 20 m, and persisted during February and March. The presence of this water body has previously been detected on the continental shelf [*R. Prego et al.*, unpublished data, 1996] but not inside the rias, and consequently, ria intrusion has not been related to winter upwelling conditions. Therefore it appears that there could be two separate upwelling events that share the same mechanism but introduce different water masses inside the ria depending on the season, to wit, intermittent water driven by the poleward current from November to March and ENACW typically from May to September [Fig. 3.4]. Moreover, in view of the fact that the poleward-directed water mass was readily upwelled into the rias after discontinuous periods of positive I_w [Fig. 3.2], or possibly with relaxation of unfavourable upwelling conditions, it can be surmised that the current lies

within close proximity to the ria mouth and is not confined to the upper slope-shelf break as *Frouin et al.* [1990] have postulated. Owing to the paucity of hydrographic studies in the Rias Bajas, for example, measurements of low spatial and temporal resolution [*Mouriño et al.*, 1985], long-term thermohaline studies from a single station [*Nogueira et al.*, 1997a], and late spring and summer investigations [*Rosón et al.*, 1995, 1997], it is unknown whether this exchange occurs in the neighbouring systems. However, the similar topography suggests that the trends reported here are emblematic of all the Rias Bajas.

Consequently, it is possible to define four different water bodies that penetrate the Pontevedra Ria, each with a different TS signal. TS data for Sts. 0 and 2 are shown in Fig. 3.5. The profile of the autumnal water (cruise 11b) is consistent with an almost straight line both inside the ria and on the shelf, a pattern typical of mixing fresh water with superficial coastal water. The same was observed in winter (cruise 1b), when mixing with the water transported by the poleward current occurs (salinity 35.97 and 15.2 °C), and in May to September (cruise 6a), when the upwelling relaxes (S=35.55, θ=12.5 °C). The fourth water body is ENACW (cruise 8) whose TS characteristics are well known [*Fraga*, 1981].
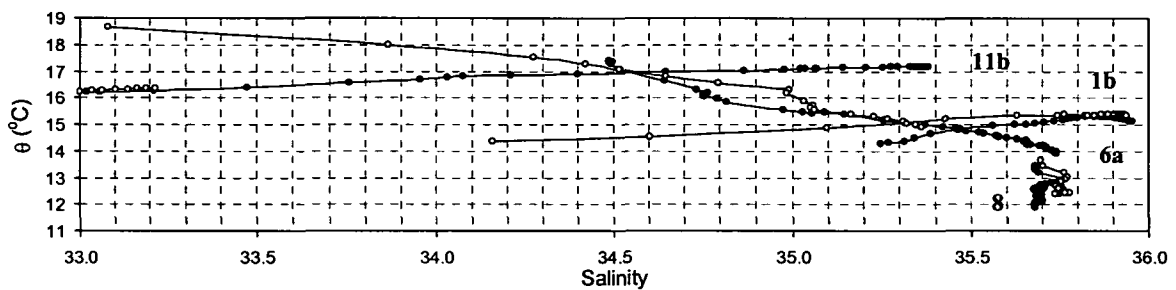
Fig. 3.5. TS diagram corresponding to the four different seawater bodies shown in Fig. 3.3 entering the Pontevedra Ria at Sta. 2 (open circles) and Sta. 6 (closed circles). Cruise 11b is representative of autumn conditions, 1b of poleward current water, 6a of dry season non-upwelling and cruise 8 of ENACW upwelling.

3.1.3. SPATIAL CHANGES INSIDE THE RIA

The spatial trends within the ria have been highlighted in Figs. 3.1 and 3.2, with two driving forces of residual circulation: the river Lérez and upwelling from the continental shelf. In addition, the tidal role should be not be disregarded and will be explored below. Figs. 3.1 and 3.2 further reveal three classic situations which exemplify the fluvial and upwelling patterns in the ria: cruise 11b in winter, when dominant winds were southwesterly i.e. negative I_W and high river flow; cruise 4b in spring with light winds and moderate river flow; and cruise 8 in summer characterised by strong upwelling conditions and limited freshwater inputs.

In order to describe the spatiality incurred by the distinct meteorological settings, the discussion focuses on water density. Tracking the density elucidates the sinking and rising of seawater at different areas inside the ria and hence aids the qualitative description and importance of each driving force inside the ria. Accordingly, three two-stage diagrams were employed

36

[Fig. 3.6 and 3.7], separated into upper and lower parts consisting of the following:

1. Isopycnal contours in the upper part of the figures depicting a two-dimensional map of the ria at the depth of separation between the incoming and outgoing layers. Based upon results obtained in the Vigo Ria [*Prego and Fraga*, 1992; *Taboada et al.*, 1998], this depth has been approximated to 10 m.

2. An isopycnal three-dimensional surface diagram is shown in the lower part of the figures where the density gradients reflect the advection and mixing of the water bodies in the ria. According to literature data [*Fraga*, 1996; *Castro et al.*, 1998], the isopycnal σ_θ=24.0 kg m^{-3} is assumed to label the influence of fluvial and seawater mixing, and σ_θ=27.0 kg m^{-3} denotes the upwelling ENACW water mass. The primary advantage of isopycnal surfaces is their usefulness as "hydrodynamic tracers," which is not possible with salinity or temperature data alone. Representations of the type presented here are clearly useful tools when visualisations of the combined effects of water advection and mixing of distinct water masses are required.

3.1.3.1. FLUVIAL PREVALENCE

Toward the end of November 1997 [cruise 11b, Fig. 3.6a] when river runoff was high [60 m^3 s^{-1}; Fig. 3.1] and I_w negative [Fig. 3.2, -1500 m^3 s^{-1} km^{-1}], the longitudinal and horizontal density gradient at 10 m depth was low and varied between σ_θ=24.0- 24.2 kg m^{-3} over the whole ria. This corresponded to an almost homogeneous water structure below 10 m. Above this depth, the density was slightly higher near the southern mouth of the ria, and the σ_θ=24.0 kg m^{-3} isopycnal surface was 4 m below this level in the northern mouth. The isopycnal surface on the lower part of the upper figure was also deeper along the northern coast of the ria indicating a tendency for fresher water to exit via this coast, as expected by the Coriolis effect. Reiterating previous findings, the water was partially retained along the northern coast owing to atmospheric conditions: moderate winds of a westerly component inside the ria and southerly offshore winds.

During cruise 4b in April 1998 a river runoff of 46 m^3 s^{-1} [Fig. 3.1] and I_w close to zero [Fig. 3.2] forced the water to leave the ria via both the northern and southern mouth [Fig. 3.6b]. The quasi-planar isopycnal surface in spring illustrates the contrast to winter conditions, and the higher density of σ_θ=26.0 kg m^{-3} is indicative of reduced freshwater retention. Unhindered passage of freshwater flow out of the ria has been mentioned previously and was mainly due to switching meteorological conditions, as the I_w suggest, and emphasises the important role of winds in water circulation both inside the ria and on the adjacent shelf. The hydrographic differences between periods of negative and small I_w were elucidated in more detail on cruises 11b and 4b. When onshore Ekman transport was strong (cruise 11b), there was a deepening of the pycnocline as water piled up at the ria mouth, thus confirming the hypothesis put forward by *Blanton et al.* [1987]. Conversely, in the absence of onshore winds, the pycnocline became shallower with unopposed density-driven circulation. A total retention of ria water, similar to the one reported for Vigo Ria by *Prego and Fraga* [1992] and for Pontevedra by *Fraga and Prego* [1989], was not observed owing to the high river discharge, which favoured the water to exit mainly via the northern mouth.

Two further consequences can be inferred from the isopycnals. The first is the low-density water observed close to Ons Island [Fig. 1.5] on cruise 4b (σ_θ=25.8 kg m^{-3}). This may be interpreted as water exiting the ria via both the north and the south mouth, with relatively less dense water trapped against Ons Island. This phenomenon presumably plays a dominant role in the interchange of waters between the continental shelf and the ria and in the accumulation of mud in this area, as shown by sediment maps [*Vilas et al.*, 1996]. The second inference is that the Aldan hydrography [Fig. 3.1] was dominated by the ocean and partially isolated from the rest of the ria, as has been previously predicted with a three-dimensional model [*Taboada et al.*, 2000]. In addition, taking into account the low freshwater input at Aldan, it would be more acceptable to consider this region as an inlet rather than a small ria, as is commonly believed.

(a)

(b)
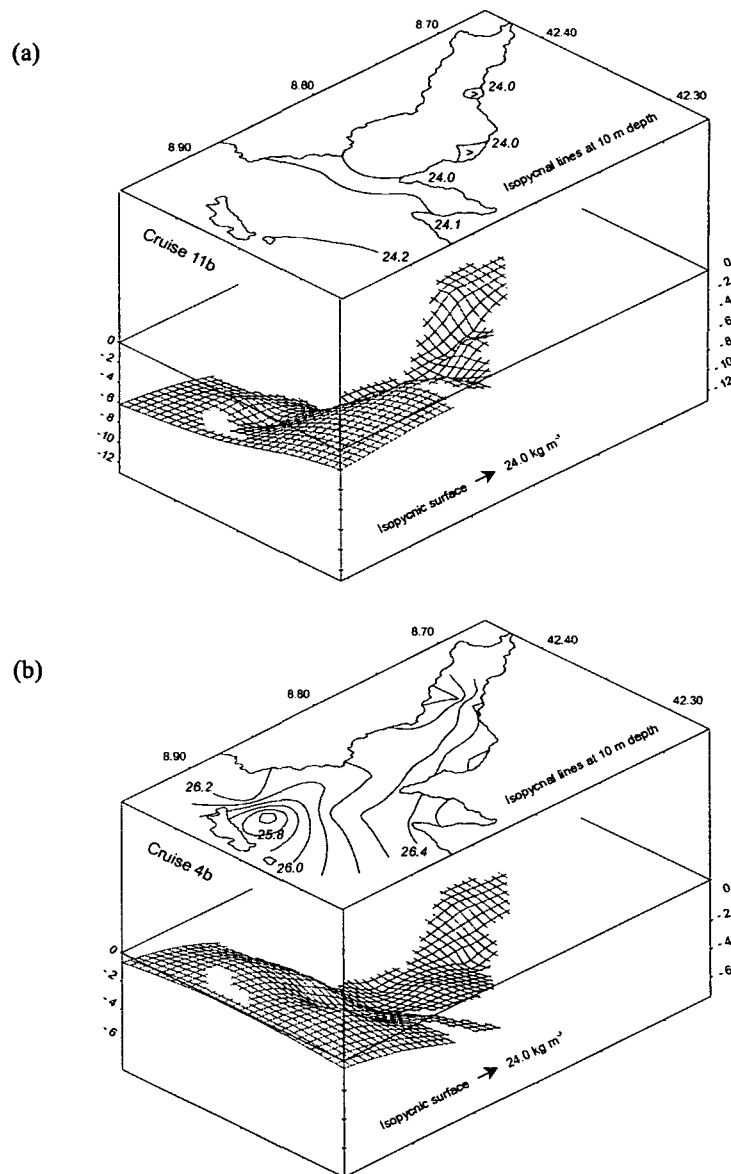
Fig. 3.6. Two-dimensional isopycnal contour plot of density (σ_θ) in the Pontevedra Ria at 10 m depth (upper part) and three-dimensional isopycnal surface (σ_θ=24.0 kg m^{-3}, lower part) in two opposite cases under fluvial prevalence: (a) negative l_W (cruise 11b) and (b) small l_W (cruise 4b).

3.1.3.2. UPWELLING PREVALENCE

In accordance with the data in Fig. 3.2, the temperature minimum in August 1998 is a good indictor of summer upwelling conditions, which in this investigation was more intense than previous upwelling events in the neighbouring rias [*Prego and Fraga*, 1992; *Rosón et al.*, 1995]. Upwelling is traced by the σ_θ=27.0 kg m^{-3} isopycnal in Fig. 3.7. The upwelled water was ENACW, as reflected by the TS diagram [Fig. 3.5], and affected the entire ria and shelf [Fig. 3.2 and 3.7] cooling the water inside [Fig. 3.2]. ENACW had a higher density than ria water and thus penetrated the ria above the seabed at the southern mouth as a deep flow, rising to 16 m below the surface [Fig. 3.7]. The low river flow of 2 m^3 s^{-1} further aided ENACW intrusion, which may otherwise impede landward advection [*Johns et al.*, 1993]. Furthermore, the σ_θ=27.0 kg m^{-3} surface shows that in cases of intense upwelling, the exit of seaward flowing ria water by the northern mouth was impeded by the presence of ENACW upwelling over the shallow sill [Fig. 3.7, upper]. Coupled with the topographic effects of the adjacent coastal margin, this is a region of notable upwelling, and consequently, upwelling was most intense near the northern mouth and surface water only outwelled via the southern exit, the opposite of fluvial dominance [Fig. 3.6]. The coastal upwelling effect can also be readily observed inside the ria on the southern margin where the isopycnal surface rises [Fig. 3.7, lower]. It can therefore be assumed that oceanic shelf water tends to penetrate the ria via this margin, given that the same upwelling trends occur under fluvial prevalence. This hypothesis can be extended to the Vigo and Arosa Rias, which also have islands situated in the ria mouth.
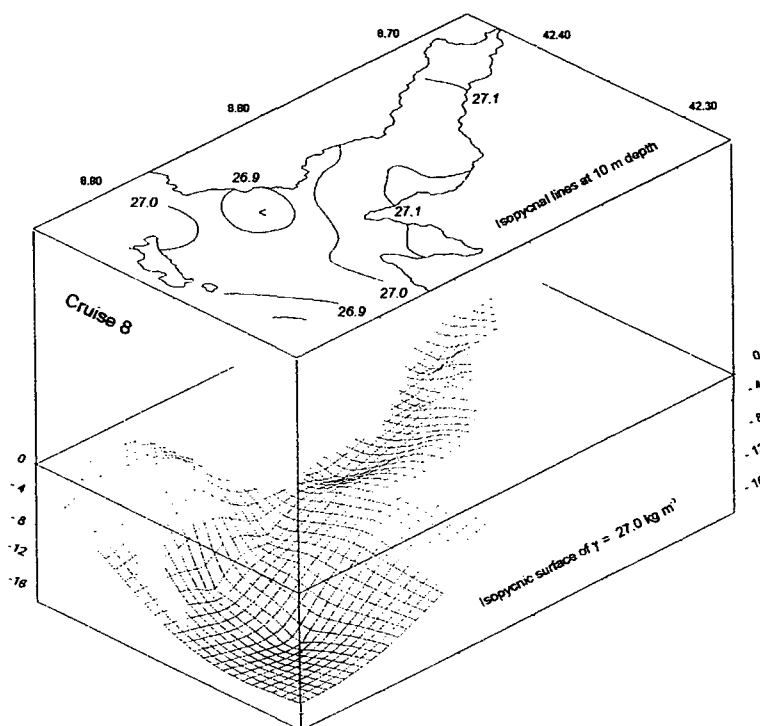
Fig. 3.7. Two-dimensional isopycnal contour plot of density (σ_θ) in the Pontevedra Ria at 10 m depth (upper part) and three-dimensional isopycnic surface (σ_θ=27.0 kg m^{-3}, lower part) under upwelling conditions (positive I_W) on cruise 8.

3.1.3.3. TIDAL INFLUENCE

The Rias Bajas are mesotidal with short tidal excursions. The tidal excursion calculated for Sta. 3, using the methodology of *Head* [1985] and current measurements of *Ruiz Mateo* [1983], works out to be less than 0.8 km. However, despite this seemingly small tidal influence, measurements were made at the anchored Sta. 6 [Fig. 3.1] situated in the inner part of the ria over 11 separate tidal cycles in order to qualitatively determine the tidal role with more accuracy. Sta. 6 was under the greatest influence of river discharge and tidal effects and therefore provided a suitable reference point for the study of the main currents in the ria and the hydrographic response of the system to changes in external factors, such as wind, tide, and river discharge. It is recognised that both the speed and direction residual flows and tidal pumping of salt are influenced by channel topography [*Uncles et al.*, 1985a], and therefore the discussion is restricted to the deeper part of the section.

An overall analysis of the data at the semidiurnal station has shown that maximum currents corresponded to the upper 5 m of the surface layer during February to July 1998, when highest surface velocities oscillated around 22 cm s^{-1} and around 14 cm s^{-1} below 5 m, with a tidal range of 3.2 m. Therefore the Pontevedra Ria may be compared with hypersynchronous estuaries [*Dyer*, 1997], where convergence exceeds friction and tidal currents increase toward the head of the estuary. Accordingly, it is postulated that tidal forcing in the Pontevedra Ria was only important in the innermost part of the ria landward of Sta. 6, since the ria widens seaward and both gravitational circulation and tidal currents were presumably reduced, increasing the importance of transverse shear dispersion of salt [*Uncles et al.*, 1985b].
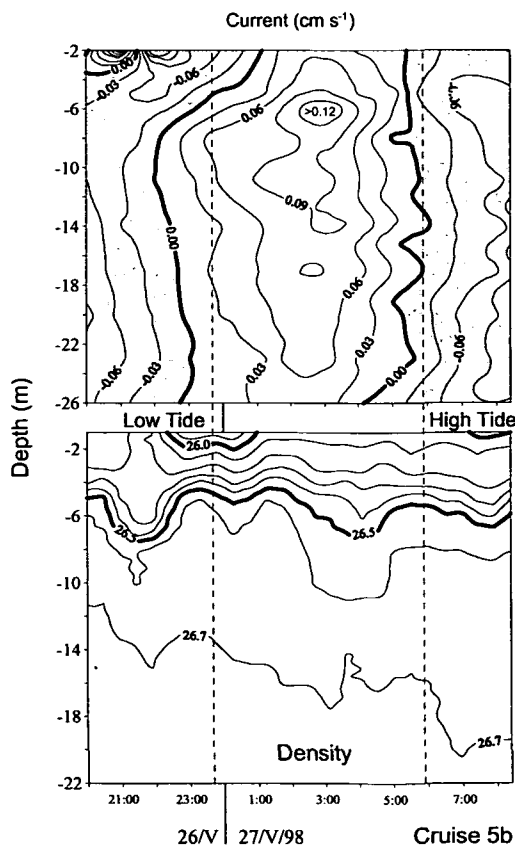
Fig. 3.8. Current and density (σ_θ) contour plots in the inner zone of the Pontevedra Ria without wind influence (cruise 5b). The data were collected over a tidal cycle at Sta. 6 (anchored) with a tidal range of 3.2 m on May 26-27, 1998.

Current velocities over a typical tidal cycle (i.e., negligible wind influence) were exemplified by those obtained in cruise 5b [Fig. 3.8], when winds measured on board the boat were of an east-southeasterly component with an average velocity of 1 to 3.5 m s^{-1}. At the surface and bottom the water left the ria on the ebb and entered on the flood whereby the whole water column shifts back and forth on the same time scale. At high and low tide, the velocities at all levels were practically zero. Maximum velocities (0.12 m s^{-1}) were measured at approximately 6 m depth on the incoming flow. Near the bottom, velocities decreased due to bed friction. Considerable vertical shear dispersion was observed in the water column around low tide, where the surface layers continued to ebb for up to 2 hours while the lower layers were on the flood. At high tide the effect was less important. This inertia of the water column was similar to what is commonly known as tidal straining [*Simpson et al.*, 1990], which describes the inertia of the surface layers to move with the bottom layers at the start of the ebb. In view of the fact that the transverse component of the current was practically negligible in comparison with the longitudinal flow, the currents in Fig. 3.8 only depict the latter.
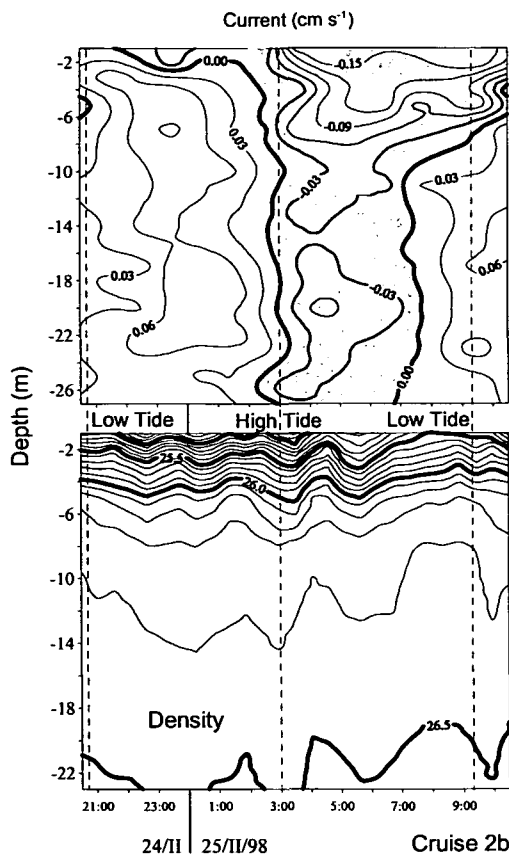
Fig. 3.9. Current and density (σ_θ) contour plots in the inner zone of the Pontevedra Ria under wind influence (cruise 2b). The data were collected over a tidal cycle at Sta. 6 (anchored) with a tidal range of 3.0 m on February 24-25, 1998.

The circulation pattern described above may have been altered when winds in the ria were greater than 4 m s^{-1}, which appears to be the velocity threshold for wind-induced circulation in the surface layers [*deCastro et al.*, 2000]. This was the case in February [cruise 2b; Fig. 3.9], when the wind measured on the boat was of an easterly component with a velocity of 5 to 7 m s^{-1}. The asymmetry of the tidal cycle in both time and space was clearly visible in the water column. Essentially, there was a weak gravitational circulation on approach to high tide with the incoming tidal flow tending to

circulate below the surface layer with a velocity below 8 cm s^{-1}, while the seaward flow remained at the surface for most of the tidal cycle with velocities reaching 15 cm s^{-1}. Therefore the flow at depth may move in the contrary direction to the wind as a result of the barotropic pressure gradient established by the wind. The water flows out of the ria regardless of the tidal state and results in an ebb of 4 hours and a longer flood of 8 hours to compensate for the indirect wind influence on the bottom waters.

Density did not present any large intratidal cycle contrasts, although it did show vertical oscillations of the isopycnals at tidal frequencies [Figs. 3.8 and 3.9]. The lowest density on cruise 5b was recorded on the ebb (25.9 kg m^{-3}) when a pocket of lower-density water passed the boat. The internal waves on both cruises were in phase throughout the water column with greater amplitude in the bottom layers than at the surface. An interesting feature between these structures was the higher wave amplitude in the upper water column on cruise 5b under low wind influence, which was suppressed on cruise 2b. The marked superficial stratification in both figures reflects the thermal gradient characteristic of May and modification by river discharge and tide at the surface layers (uppermost 7 m).

In February, the buoyancy of freshwater mainly controlled water column stratification, and density ranged from 24.4 kg m^{-3} in the surface layers up to 26.2 kg m^{-3} at 5 m depth over a complete tidal cycle. Contrary to what might be expected from the typical setting, there was a surface density minimum during the flood. The rationale could lie with the continual decreasing May fluvial runoff [Fig. 3.1] or, as is more likely, a freshwater discharge near Sta. 7 from a paper pulp factory before high tide. Aside from the paper factory, effluents from a wastewater treatment plant for the city and Marín Harbour are focused in the internal ria in the zone of Marín [Fig. 3.1]. The upshot of the contamination has been studied previously on various occasions [*Figueiras et al.*, 1985; *Mora et al.*, 1989], observing isolated pockets of low-salinity water at low tide. Presumably, therefore, the water in this area was advected in agreement with the circulation pattern previously described.

In contrast to estuaries [*Dyer*, 1997], tides in the Pontevedra Ria only played a significant role in the innermost part of the ria. Given the similar physical and topographical features of the Rias Bajas [Table 2.1], this finding further clarifies the complex hydrodynamics and highlights the physical contrast between general estuarine systems and the Galician Rias Bajas.

3.2. WATER EXCHANGE AND RESIDENCE TIMES

The hydrographic flushing or residence time, τ, is a fundamental auxiliary of aquatic research which must be determined accurately. In situ chemical reactivity, including biogeochemical uptake or production processes, must be referred to τ if coastal zone management policies are to be sustainable in the long term [e.g. *Morris*, 1990; *Shaw et al.*, 1998]. The residence time can be defined as the average lifetime of a constituent within the boundaries of a defined reservoir. Statistically, τ can be shown to be equal to the time taken for the constituent to fall to $1/e$ or 37% of its original concentration assuming no additional constituent supply. Accordingly, dye dispersion techniques have proved popular for determining τ due to their independence of steady state assumptions [*Adams et al.*, 1998; *Vallino and Hopkinson*, 1998]. Alternative approaches include box model analyses [*Guo and Lordi*,

2000; *Hagy et al.*, 2000], sophisticated hydrodynamic models [*Signell and Butman*, 1992] and estuarine morphological parameterisation of water exchange [*Rasmussen and Josefson*, 2002]. Each method has its associated uncertainty, although the relative degree of accuracy can be assessed by a comparison of results from two or more different approaches.

In this section, τ was estimated with the fraction of freshwater (*FFW*) method [*Dyer*, 1997], which requires salinity and freshwater input data. The budget calculations paralleled the modelling guidelines recommended by IGBP-LOICZ (International Geosphere-Biosphere Program-Land Ocean Interactions in the Coastal Zone) [*Gordon et al.*, 1996]. Water exchange fluxes and influences from wind and upwelling on residence times were examined. Finally, the implications of residence times on biogeochemistry and the suitability of the *FFW* method to the Pontevedra Ria were considered.

3.2.1. WATER BUDGET FRAMEWORK

3.2.1.1. BOX MODEL APPROACH

Box models have proved to be useful tools for rapid exploratory analysis of the biogeochemical reactivity of coastal systems [*Smith et al.*, 1991; *Prego*, 1993a; *Pérez et al.*, 2000]. A box model considerably simplifies estuarine hydrodynamics, principally in terms of the definition of finite sections or boxes [*Officer*, 1981]. Advective exchange coefficients are derived directly from the spatial and temporal variability of a conservative and measurable tracer, usually salinity. Despite their drawbacks, box models permit an association of the variability of an observed quantity with other measurable changes, for example, river flow, salt intrusion or effluent input.

The salt-budget approach with regard to near shore oceanography usually consists of a single or series of spatially defined boxes of one or two layers separated form their surroundings or from each other by spatial boundaries. The boundaries are usually, although not implicitly, defined as a low salinity up-estuary boundary with a freshwater input and a seaward boundary sited along the mixing zone, with as many additional intermediate boundaries as desired. The coastline between the upper and lower limiting boundaries generally, but again not implicitly, forms convenient lateral spatial limits. The location of the seaward boundary is often a compromise between spatial resolution and accuracy, particularly when the working salinity range is small.

The Pontevedra Ria, along with the neighbouring Rias Bajas, may be considered as partially mixed [*Prego and Fraga*, 1992]. Moreover, in their work on the Arosa Ria, *Álvarez-Salgado et al.* [1996a,b] concluded that the central and internal ria present distinct hydrographical and biogeochemical characteristics. These findings justify vertical two-dimensionality of the box model for the Pontevedra Ria, in terms of an upper seaward-moving and a lower landward-moving layer, and also the need for treating the central and internal rias separately. The box model representation of the Pontevedra Ria is shown in Fig. 3.10. The approach for investigating the residence times and biogeochemical fluxes in this thesis begins by treating the Pontevedra Ria as stratified system, separated into central and internal sections. A stratified approach may better represent the pycnocline separation of the upper and lower layers often observed during upwelling and downwelling events [e.g. *Rosón et al.* 1997]. The data can then be compared and

interpreted in the context of current awareness of the hydrography of the Rias Bajas.
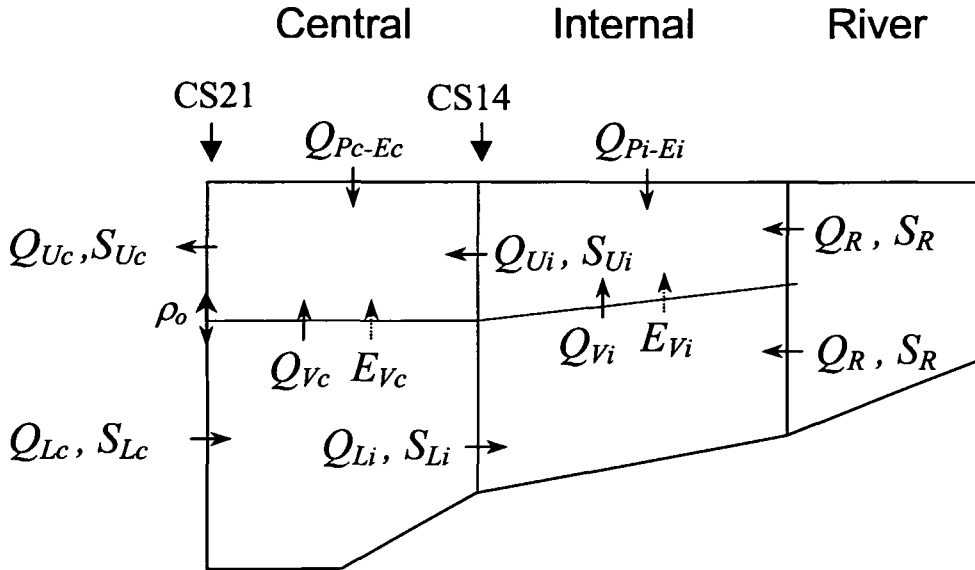
Fig. 3.10. Box model representation of the Pontevedra Ria. The seaward boundary corresponds to CS21 [Fig. 2.1], the boundary between the central and internal ria to CS14, and the landward boundary to the limit of tidal influence. Surface and bottom layer horizontal advective fluxes are denoted by Q_U and Q_L, respectively, with subscript c or i denoting the central or internal ria. Vertical advective and non-advective fluxes are Q_V and E_V, respectively. Net precipitation minus evaporation is Q_{P-E}, the river flux is Q_R of salinity S_R (=0). The separation between the incoming and outgoing flows at the seaward boundary is indicated by the pycnocline level, ρ_0.

The landward boundary of Pontevedra Ria is defined as the river Lérez mouth at the limit of tidal influence and the seaward boundary is situated 21 km downstream [CS21, Fig. 2.1]. An additional boundary is placed at 14 km (CS14) which conveniently delimits the internal and central sections of the ria [Fig. 3.10]. The morphology of the coastline makes CS21 a natural front between the ria and ocean and a crucial location for water and, by implication, nutrient exchange. In addition, the ria narrows at this point thus strengthening tidal currents perpendicular to the axis [*Taboada et al.*, 1998; *Ruiz-Villarreal et al.*, 2002], thus reducing errors arising from topographic effects and cross-channel flow [*Kjerfve et al.*, 1981]. This is an important consideration to bear in mind when lateral flows must be considered [*Ruiz-Villareal et al.*, 2002].

The derivation of advective and vertical fluxes for each boundary is presented in Box 1 [Eqs. 3.1-3.11]. Salt fluxes were budgeted at CS21 and CS14 where conditions of volume and salt conservation were conserved. The mean upper, S_U, and lower salinity, S_L, of each layer was calculated by numerical integration of CTD salinity profiles data over the cross sectional area bearing in mind the geometric characteristic of each layer. Additionally, S_L and S_U were tidally averaged to the mean tidal height at the mouth (2.5 m). The theoretical equivalent of the pycnocline level was assumed to coincide with the depth of mean density at each boundary, and defines the separation of the upper and lower layers [*Rosón et al.*, 1997].

The pycnocline was favoured over the halocline [*Prego and Fraga*, 1992] and thermocline [*Otto*, 1975] since temperature exerts the main control on density when runoff is low.

3.2.1.2. RESIDENCE TIME

Álvarez-Salgado et al. [2000] and *Rosón et al.* [1997] noted the importance of sampling in the Rias Bajas to a time resolution that adequately captures the variability engendered by offshore upwelling events. Consequently, the upwelling frequency implies that the minimum time scale of data resolution required for accurate calculation of residual fluxes may be as low as 3 days [*McClain et al.*, 1986; *Rosón et al.*, 1997]. Where such data is available, *Álvarez-Salgado et al.* [2000] proposed the non-steady form of Eq. 3.7 in Box 1 for deriving Q_U:

$$\overline{Q}_U = \frac{(\overline{Q}_Z \times \overline{S}_L) \times \left(V \times \frac{\Delta S}{\Delta t}\right)}{\overline{S}_L - \overline{S}_U} \qquad [3.12]$$

However, since the data is fortnightly resolved, an approach is required which corrects and transforms the data from steady state to non-steady state conditions. The ideas by the above authors can be extended by suggesting that the residence time is the minimum time at which sampling ought to be performed. Accordingly, a method is presented below for optimising the advected flows to the mean system residence time.

The fraction of freshwater method (*FFW*) is based on the salinity difference between a spatially defined body of water and its adjacent water body, and defines τ as the time required to replace the existing freshwater in the estuary at a rate equal to the net freshwater input [*Dyer*, 1997]. The residence time for the central or internal ria can be quantified as:

$$Q_Z \times \tau = V \left(\frac{S_L - S_U}{S_L}\right) \qquad [3.13]$$

where S_U is the mean salinity of the box under study. The term in parenthesis in Eq. 3.13 is equal to the fraction of freshwater, f. In view of the fact that ria water is diluted with freshwater by Q_Z in the same proportion as the freshwater is diluted with sea water by Q_L, it can be shown that for either box:

$$Q_L = \frac{Q_Z}{f} \qquad [3.14]$$

$$\tau = \frac{V}{Q_L + Q_Z} \qquad [3.15]$$

BOX 1. Derivation of box model fluxes

The steady-state water and salt fluxes for any layer or section in Fig. 3.10 can be developed from freshwater input and salinity data, and the box or section volume. The central and internal rias are considered to have constant volume, V_c (1.15 km³) and V_i (0.34 km³), with freshwater inputs from the Lérez river, Q_R, effluent, Q_{EFF}, direct precipitation, Q_P, and water losses via evaporation, Q_E [Fig. 2.4]. The net residual flow up to any boundary, Q_Z, (m³ s⁻¹), is thus the balance of the individual fluxes for that box, which will be negative if flow is out of the ria:

$$\frac{dV}{dT} = Q_R + Q_{EFF} + Q_P + Q_E + Q_Z = 0 \qquad [3.1]$$

The salinity of these flows is assumed to be zero. The daily values for upper outgoing, S_U, and lower incoming salinity, S_L [Fig. 3.10] are incorporated into the salt budget. *Álvarez-Salgado et al.* [2000] defined the average surface layer water, $\overline{Q}_U$, and salt fluxes, $\overline{Q_U \times S_U}$, at each boundary between two consecutive surveys (t_1 to t_2) as:

$$\overline{Q}_U = \frac{\int_{t_1}^{t_2} Q_U(t)dt}{t_2 - t_1} \qquad [3.2]$$

$$\overline{Q_U S_U} = \frac{\int_{t_1}^{t_2} Q_U(t)S_U(t)dt}{t_2 - t_1} \qquad [3.3]$$

Identical equations can be written for the horizontal advection and mixing exchange flux [*Gordon et al.* 1996], $\overline{Q}_L$, and salt flux, $\overline{Q_L \times S_L}$, in the lower layer. Conservation of water and salt for the central or internal ria is expressed by Eqs. 3.4 and 3.5:

$$\frac{dV}{dt} = \overline{Q}_Z - \overline{Q}_U + \overline{Q}_L = 0 \qquad [3.4]$$

$$V\frac{dS}{dt} = \overline{Q_L \times S_L} - \overline{Q_U \times S_U} = 0 \qquad [3.5]$$

Eq. 3.5 can be solved to give $\overline{Q}_U$ if the following assumption can be upheld:

$$\overline{Q_{L,U} \times S_{L,U}} \approx \overline{Q}_{L,U} \times \overline{S}_{L,U} \qquad [3.6]$$

Therefore, by substitution and rearrangement of Eqs. 3.4 and 3.5:

$$\overline{Q}_U = \frac{(\overline{Q}_Z \times \overline{S}_L)}{\overline{S}_L - \overline{S}_U} \qquad [3.7]$$

From *Officer* [1981], the vertical advective flow in the central, $\overline{Q}_{Vc}$, and internal ria, $\overline{Q}_{Vi}$, can be quantified by difference from the horizontal advective flows and the residual freshwater input:

$$\overline{Q}_{Vc} = \overline{Q}_{Uc} - \overline{Q}_{Ui} - \overline{Q}_{Pc-Ec} \qquad [3.8]$$

$$\overline{Q}_{Vi} = \overline{Q}_{Ui} - 0.5 \times \overline{Q}_{Zi4} \qquad [3.9]$$

From the balance of salt fluxes in the upper box of each section, the vertical non-advective flow in the central, $\overline{E}_{Vc}$, and internal ria, $\overline{E}_{Vi}$, can be quantified as:

$$\overline{E}_{Vc} = \frac{(\overline{Q}_{Ui} \times \overline{S}_{Ui}) + (\overline{Q}_{Vc} \times \overline{S}_{Lc}) - (\overline{Q}_{Uc} \times \overline{S}_{Uc})}{\overline{S}_{Uc} - \overline{S}_{Lc}} \qquad [3.10]$$

$$\overline{E}_{Vi} = \frac{(\overline{Q}_{Vi} \times \overline{S}_{Li}) - (\overline{Q}_{Ui} \times \overline{S}_{Ui})}{\overline{S}_{Ui} - \overline{S}_{Li}} \qquad [3.11]$$

E_V is the turbulent mixing and entrainment flux required to restore the salt balance. In the text, the overbar denoting the mean value between two consecutive surveys is removed from the parameters.

Typically, $\tau > 1$ day in the Rias Bajas [e.g. *Prego and Fraga*, 1992], and thus daily variability in Q_Z will introduce non-steadiness in the calculations due to the natural delay in seaward freshwater mixing. To circumvent this problem, τ was determined by iteration with Q_Z, which averages Q_Z to the time that the water spends in the ria [*Kaul and Froelich* 1984; *Moran et al.*, 1999]. Individual Q_Z were inserted into Eq. 3.13 to obtain a residence time τ_1. Subsequently, Q_Z data τ_1 days previous to the cruise were then meaned to obtain a new value of residual flow Q_{Z2}, and hence τ_2. Substitutions were repeated until the number of days over which the residual flow was averaged, Q_{Zj}, equalled the residence time of the water in the ria, τ_j. *Hilton et al.* [1998] tackled a similar problem by using an exponential filter on Q_Z. The iterative method filters non-steady state spikes due to daily fluctuations in Q_Z, and thus provides a method by which the upper and lower advective flows for each box can be determined under quasi-steady state conditions. On three cruises, however, data for the central ria [cruises 7b, 8 and 9; Table 2.1] were rejected since low values of S_L-S_U during summer [Eq. 3.7] led to numerical instability of the calculation and anomalously high water fluxes. This is a recognised problem of salt budgets, when S_L-S_U becomes small and close to the analytical noise of the salinity data [*Smith and Hollibaugh*, 1997]. For similar reasons, the data on cruises 8 and 9 were rejected for the internal ria.

The daily fraction of ria water, and thus contamination, exchange (d_{ex}) for the central or internal ria can be estimated as:

$$d_{ex} = \left[\frac{Q_L + Q_Z}{V}\right] \times 8.64 \times 10^4 \times 100 \qquad [3.16]$$

The intra-annual variability of the horizontal advective flows, Q_U and Q_L, and vertical advective and non-advective flows, Q_V and E_V, between two surveys are shown in Fig. 3.11. Fig. 3.12 shows the iterative results for Q_Z, τ, d_{ex} and effect of the iterative procedure on τ for the central an internal ria.

3.2.1.3. DATA QUALITY ASSURANCE

The accuracy of a biogeochemical budget model relies on the ability of the box model to represent the local hydrographical characteristics. Failure of the budget to do so, or equally, choosing the wrong type of box representation for the system of interest, may lead to potentially serious inaccuracy in the final result [*Webster et al.*, 2000].

The error in the advective fluxes of the Pontevedra Ria can be estimated by examining the analytical error of the measured variables. In the steady-state form, the error of Q_U (ε_{Qu}) in Eq. 3.7 takes the form:

$$\varepsilon_{Qu} = Q_U\left[\frac{\varepsilon_Z}{Q_Z} + \left(\frac{\varepsilon_S}{S_L}\right)^{1/2} + \left(\frac{2 \times \varepsilon_S}{S_L - S_U}\right)\right] \qquad [3.17]$$

where ε_S is the analytical error of S_U or S_L (± 0.005), and ε_Z is the analytical error of Q_Z, assumed to be ~10% [*Álvarez-Salgado et al.*, 2000].

Similarly, for the vertical advective fluxes, Q_{Vc} [Eq. 3.8] and Q_{Vi} [Eq. 3.9], the corresponding analytical errors are:

47

$$\varepsilon_{Vc} = \varepsilon_{Quc} + \varepsilon_{Qui} + \varepsilon_{Z21} \qquad\qquad [3.18]$$

$$\varepsilon_{Vi} = \varepsilon_{Qui} + 0.5 \times \varepsilon_{Z14} \qquad\qquad [3.19]$$

ε_Q and ε_V are shown on the corresponding diagrams in Fig. 3.11. Mean±SD for ε_{Qu} is 14±3% and 91±341% for ε_{Vc}. However, *Álvarez-Salgado et al.* [2000] reported that these errors must be considered the maximum expected errors. They conclude with the assumption of *Matsukawa and Suzuki* [1985], in that the actual error is probably much lower because of the averaging effect of all the calculation terms.

Based on the tidal variability in water volume of the ria (see Chapter 4), the error in volume, ε_{Vo}, is taken as 8%. From Eq. 3.15, the error in τ calculated by iteration (ε_τ) for the central and internal ria is thus:

$$\varepsilon_\tau = \tau\left[\left(\frac{\varepsilon_{Vo}}{V}\right)^2 + \left(\frac{\varepsilon_{Qu}}{Q_U}\right)^2\right]^{1/2} \qquad\qquad [3.20]$$

The mean±SD for ε_τ based on the analytical quality of the data is 17±3%.

Despite the low analytical error for salinity (±0.005), this uncertainty was probably a minor source of inaccuracy in τ. Departure from ideal conditions (steady-state and well mixed) and corresponding lateral and longitudinal inconsistencies in the salinity field are probably more important. For the moment, inherent lateral inconsistencies in salinity were assumed to be reduced by the salinity integration over each box [*Rosón et al.*, 1997; *Álvarez-Salgado et al.*, 2000]. The validity of this assumption is dealt with in more detail in Chapter 4, and for the moment, the standard protocol for treatment of box model errors in the Rias Bajas was followed [*Álvarez-Salgado et al.*, 2000].

3.2.2. INTRA-ANNUAL VARIABILITY OF WATER FLUXES AND RESIDENCE TIMES

Q_L represents the incoming mixing flux across the ria boundaries and hence provides a useful parameter for assessing the relative magnitude of upwelling. Q_{Lc} and Q_{Li} show irregular evolution over the study period, with notable peaks on more than 3000 m^3 s^{-1} in January and April [Fig. 3.11]. Further high influx events of Q_{Lc} were observed during May an early July, and attributable to upwelling, as evidenced by the 13.0 °C isotherm at Sta. 0 in Fig. 3.2. *Prego and Fraga* [1992] suggested that upwelling triggered up to a three-fold increase of incoming bottom currents in the adjacent Vigo Ria. Mean incoming lower layer water flux in the central Arosa Ria was estimated by *Rosón et al.* [1997] using a combined salt-heat box model to be between 1200 and 2500 m^3 s^{-1}. During strongest upwelling, a residual flux of 5035 m^3 s^{-1} was observed. In addition, a regression of Q_L against I_W by these authors showed that upwelling accounted for 47% of the incoming water flux. *Álvarez-Salgado et al.* [2000] found a strong correlation between Q_U and I_W (r=0.86), although no significance of this correlation was given. Using a reduced major axis regression [*Sokal and Rohlf*, 1995], correlation of I_W and Q_{Lc} in this work was weakly-significant (p<0.05, r=0.12). In contrast to *Álvarez-Salgado et al.* [2000], a marked reduction in significance resulted from inclusion of Q_R as an independent variable.
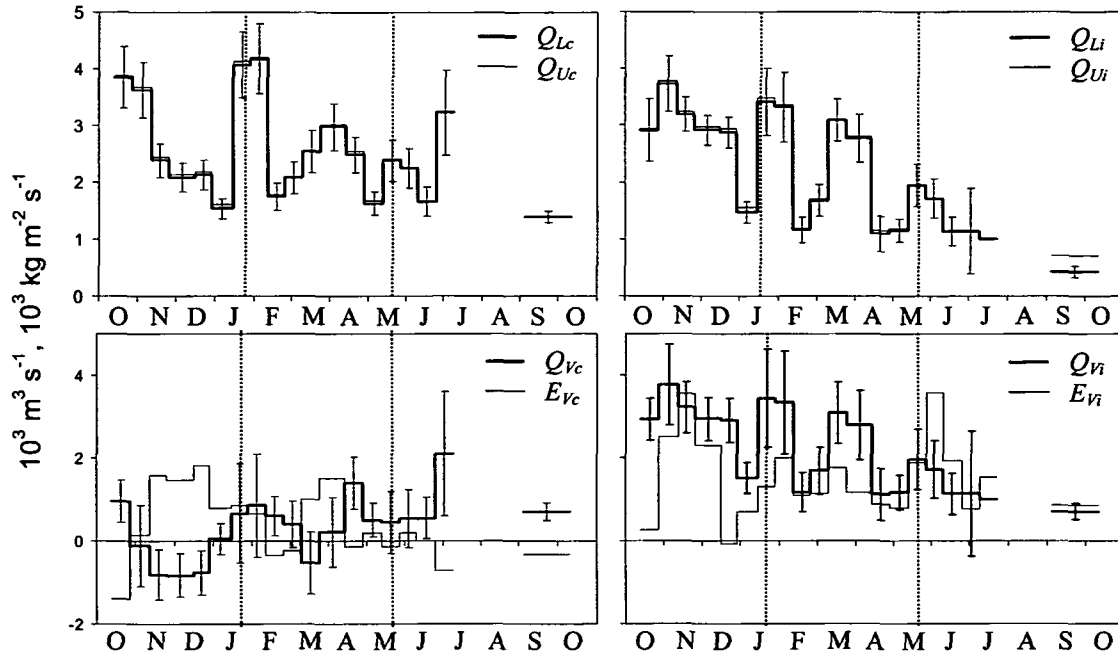
Fig. 3.11. Box model-derived advective (Q, 10^3 m^3 s^{-1}) and non-advective water fluxes (E, 10^3 kg m^2 s^{-1}) in the Pontevedra Ria between two consecutive surveys over the period October 1997-1998. Water fluxes correspond to the schematic in Fig. 3.10. The wet, spring and dry seasons are separated by the vertical dashed lines.

Rosón et al. [1997] and *Álvarez-Salgado et al.* [2000] recorded negative surface layer horizontal fluxes of up to -12000 m^3 s^{-1} during the downwelling season in the Arosa and Vigo rias, implying a reversal of water circulation. Negative horizontal fluxes were not predicted here, presumably because of more refined thermohaline variability in their equations arising from the combined S and T fluxes. However, negative Q_{Vc} may be indicative of downwelling conditions [Fig. 3.11]. During November to December, downwelling fluxes in the central ria of up to -1130 m^3 s^{-1} were predicted. In view of the fact that Q_{Uc} and Q_{Ui} were positive, the data suggests water entering the surface layer in the central ria from the internal ria was forced to the lower layer at a downwelling front located in the central ria, and then re-advected landward in the lower layer. This description would agree with *Pardo et al.* [2001] who observed a downwelling front during a simultaneous campaign in the Pontevedra Ria. However, during these apparent downwelling periods, Q_{Lc} were lower than Q_{Li} as a result of the salinity integration over CS21 and CS14 which, by nature of the derivation, implies that Q_{Vc} must be negative. In Chapter 4, these box model artefacts are explored in more detail. It is worth mentioning at this stage that aside from box model interpretations, very little is known about the mechanism of downwelling in the Galician Rias Bajas and thus the significance of negative Q_V.

The data strongly suggest that high Q_{Vc} of 1500-2000 m^3 s^{-1} in the Pontevedra Ria were due to upwelling. This hypothesis corresponds with the ENACW signal noted throughput the ria [Fig. 3.2]. A stronger coupling between horizontal and vertical advective fluxes was noted in the internal ria, whereby negative Q_{Vi} were not predicted due to freshwater-induced

buoyancy. The abrupt change in bathymetry in this area may also be partly responsible [Rosón et al., 1997]. High vertical fluxes in the central and internal ria during January-February were associated with low water column stability and stratification [Fig. 3.1 and 3.3]. At these times, up to 34% of incoming water was advected to the surface layer. During upwelling in early July, this value increases to 65%, similar to the Arosa Ria [Álvarez-Salgado et al., 1996a]. Therefore, the possible existence of a front appears to have an important effect on the rate and direction of the advective flow.
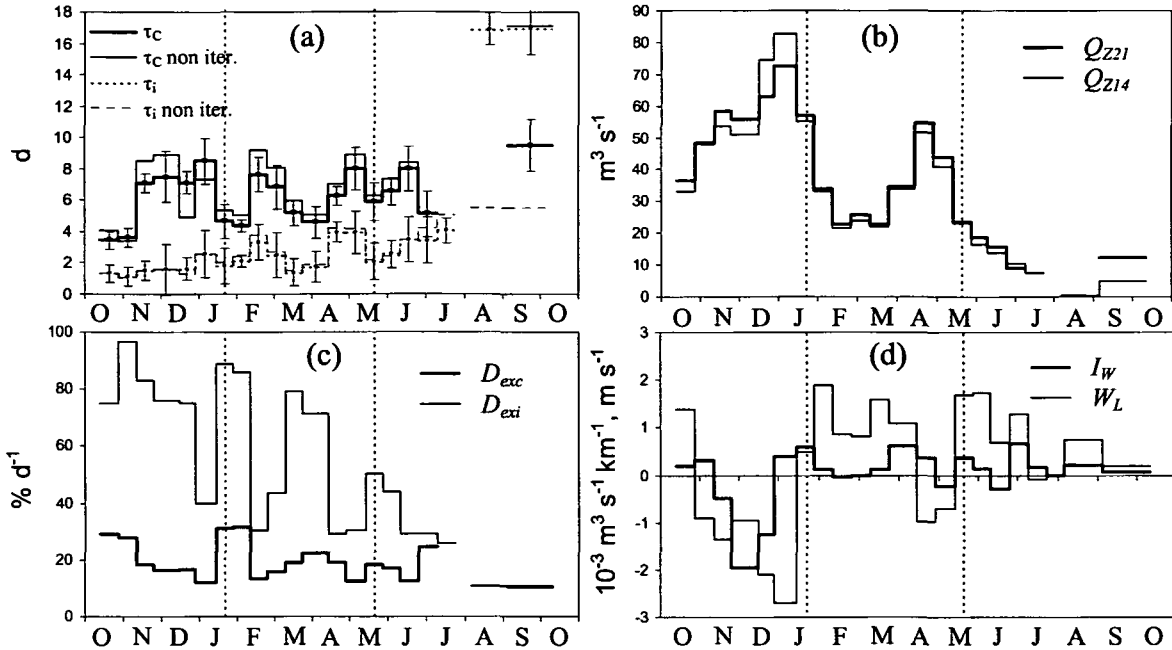
Fig. 3.12. (a) Residence time (τ, days) for the central (τ_c) and internal ria (τ_i) calculated with and without iteration; (b) Net residual flow (Q_Z, m^3 s^{-1}) up to CS21 and CS14; (c) Daily water exchange rate (d_{ex}, % d^{-1}) for the central (d_{exc}) and internal ria (d_{exi}), and (d) Upwelling index (I_W, 10^3 m^3 s^{-1} km^{-1}) and local wind velocity (W_L, m s^{-1}) resolved along the NE-SW ria axis during the sampling campaign. Favourable upwelling conditions are denoted by positive I_W (N winds) and W_L (NE winds). The wet, spring and dry seasons are separated by the vertical dashed lines.

The interpretation of E_V is more complicated. E_{Vc} appeared to be inversely correlated to Q_{Vc}, and compensated the salt flux for the upwelling or downwelling between the layers. In the internal ria, E_{Vi} and Q_{Vi} were positively correlated, probably due to the input of freshwater to the lower layer at the ria head. Rosón et al. [1997] stated that weaker non-advective fluxes were associated with more stratification caused by isolation and/or runoff since the pycnocline acts as a physical barrier between both layers. However, the authors also reported that high values of vertical mixing may also be observed under strong upwelling or downwelling conditions. These statements appear to be contradictory, and it can therefore be concluded that a finely resolved salt-budget is required to adequately describe the variability in E_V.

3.2.3. FLUSHING ANALYSIS

The freshwater residence time is a good indicator of the ability of a system to disperse pollutants. A well-flushed system will naturally have a lower residence time than one with sluggish circulation and poor mixing. Typically, residence time data is graphically presented in the literature by an exponential plot of residence time versus river flow where high river flows generally lead to lower flushing times [e.g. *Alber and Sheldon*, 1999; *Hagy et al.*, 2000]. However, contrary to this argument, a cursory inspection of Fig. 3.12 reveals a distinct lack of correlation between τ and Q_z. The stochastic nature of the relationship may be attributed to the variability at the mouth of the ria, primarily engendered by upwelling intrusions inside the ria [*Prego et al.*, 2001]. Consequently, using the information below, any effect by upwelling or local winds on τ can be qualitatively described:

(i) *Upwelling*: Offshore Ekman transport per kilometre of coast is represented by the upwelling index, I_W (m^3 s^{-1} km^{-1}), derived from Eq. 2.2. The mean positive (upwelling favourable) and negative I_W (downwelling favourable) calculated from a 23 year data set [*Lavín et al.*, 1991] are 341 m^3 s^{-1} km^{-1} and -271 m^3 s^{-1} km^{-1}, respectively. The response time of upwelling after the onset of northerly winds is approximately 3 days owing to water column inertia [*McClain et al.*, 1986]. Accordingly, daily I_W data processed with a 3 d moving average filter were averaged τ d before each cruise, where τ is data in Fig. 3.12. Accordingly, the mean I_W between two consecutive surveys processed in this way is shown in Fig. 3.12.

(ii) *Surface winds* (W_L): *deCastro et al.* [2000] reported that the surface layer circulation in the inner Pontevedra Ria over a tidal cycle may be modified by wind speeds W_L > 3-4 m s^{-1}, while bottom waters were dominated by tides. Daily local wind data [Fig. 2.2] were filtered 48 h prior to each cruise and processed as for I_W [Fig. 3.12]. This time period was assumed adequate to characterise the response of currents to short-term wind-induced circulation [*Wang and Elliot*, 1978; *Kiley and Welch*, 1989].

Water flushing in the Pontevedra Ria was a function of surface wind stress, upwelling and downwelling and tidal mixing. The tidal mixing contribution can be accurately quantified with a tidal model of the ria, and is discussed further in Chapter 5. The role of upwelling and winds is harder to quantify. The TS plots in Fig. 3.13 show that cruises 1b and 3b [Table 2.1] were influenced by ENACW upwelling at the time of sampling. Low τ for these cruises of 4.6 and 5.2 d, respectively, in the central ria and 1.8 and 1.4 d in the internal ria shows that upwelling affected the whole ria at these periods. Moreover, cruises 1b and 3b corresponded to positive I_W of 120 and 600 m^3 s^{-1} km^{-1} [Fig. 3.12], when up to 31 and 19% of water was renewed in the central ria [d_{ex}, Fig. 3.12]. *Rosón et al.* [1997] estimated an average summer residence time of 9 d for the Arosa Ria, falling to < 2 d during upwelling. For a similar volume of the Vigo Ria, upwelling values for τ were typically 3 d [*Álvarez-Salgado et al.*, 2000]. This rapid rate of water removal is important in supplying phytoplankton with inorganic nutrient substrate from the nutrient rich ENACW [e.g. *Pérez et al.*, 2000], with further contributions from sediment efflux and enhanced resuspension of bed sediment [*Dale and Prego*, 2002]. However, water exchange rates during intense upwelling may be too rapid to permit any significant build up of phytoplankton biomass. Accordingly, *Doval et al.* [1997] observed an increase in chlorophyll *a* on the upwelling relaxation phase when the water dwell time became longer than the phytoplankton doubling time. Efficient

water exchange during summer and offshore nutrient input raises the mussel carrying capacity of the Rias Bajas [*Álvarez-Salgado et al.*, 1996a], which is an important consideration for the sustainability of commercial shellfish management [*Raillard and Menesguen*, 1994; *Brooks et al.*, 1999].
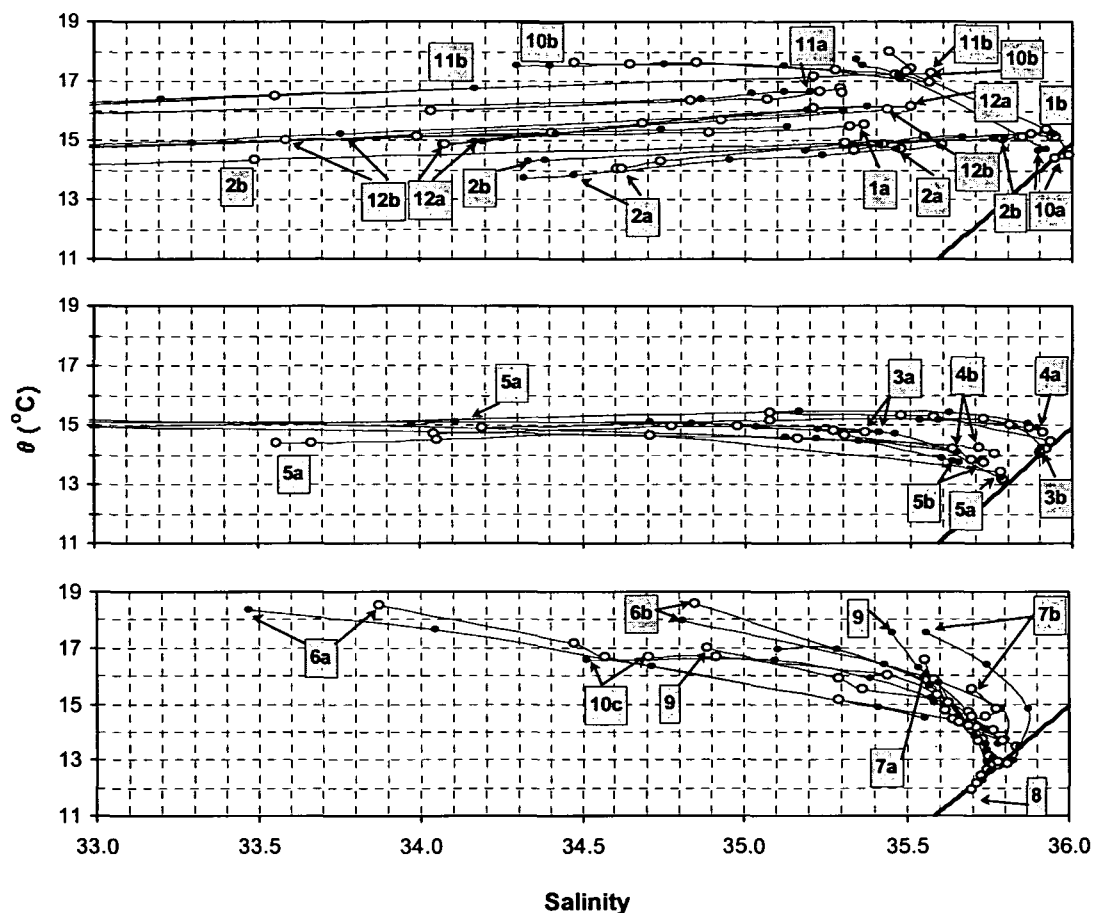
Fig. 3.13. Temperature (θ) - salinity plots for St. 3 (open circles) and St. 5 (full circles) between October 1997-1998. Refer to Fig. 2.1 for locations. Data recorded at various depths during mid-October 1997 to February 1998 (top panel), March to May (centre panel) and June to September (lower panel). Each cruise is denoted numerically by its calendar month and "a" or "b" referring to the first and second fortnight of the month respectively [Table 2.1]. October 1998 is indicated by "10c". The heavy black line represents the TS characteristics of ENACW.

By contrast, long τ encountered on cruises 11b, 12b and 5a, associated with downwelling conditions and onshore winds [Fig. 3.12], are suggestive of freshwater retention by suppression of the barotropic gradient and horizontal gravitational circulation [*Geyer*, 1997; *Valle-Levinson et al.*, 1998]. Prolonged τ of 9.5 and 17 d in the central and internal ria, respectively, were also noted during September and October when runoff and I_W were low. Restricted circulation in the water at the end of the upwelling season is suspected of being a key factor in the formation of red tide events [*Prego*, 1992; *Tilstone et al.*, 1994].

However, while some of the observations above can be generally corroborated with literature findings, the correlations are tentative, and the τ data show inconsistencies between the central and internal rias. For

example, on cruise 2b, ENACW appears to be present in the lower waters throughout the ria, but the residence time was relatively high at 9.2 d in the central ria [Fig. 3.12] and showed little coherence with the I_W data. This may due to a relaxation in upwelling. In general, τ was poorly correlated with I_W and W_L, and showed a weak correlation (r=0.17, p<0.1). This suggests that more consistent investigation of the upwelling process is required, in particular for studies parameterising upwelling with I_W. Calibration against ADCP or current meter measurements would be advantageous. Accurate parameterisation was complicated by local topographic effects [Blanton et al., 1984] and complex water circulation on the continental shelf [Pérez et al., 2001]. Despite difficulties in separating local wind effects on water exchange, this work and previous findings suggest that winds may also be important [deCastro et al., 2000]. Long-term data sets, such as those advocated by Nogueira et al. [1997a,b] will prove invaluable in expressing τ as a function of upwelling and winds.

3.2.4. THE USE OF QUASI-STATIONARY STATE BALANCES IN RESIDENCE TIME EVALUATION

Under normal estuarine conditions $\Delta V/\Delta t$ and $\Delta S/\Delta t$ vary, otherwise residence times would be constant. Non-steady state conditions in the Rias Bajas are primarily engendered by offshore water inputs. In fact, it has been suggested that non-steadiness may account for up to 95% of the water flux [Álvarez-Salgado et al., 2000]. On the assumption that residence time can be adequately described as a function of incoming salinity, S_L, the fact that S_L varies over short time scales in the Pontevedra Ria leads to the conclusion that the system was in a transient state. How, therefore, can the data presented here be regarded as accurate?

Alber and Sheldon [1999] presented τ data for five estuarine systems of the east coast of North America. They were able to justify a steady state assumption since the absence of external oceanic inputs provided a more or less constant salinity seaward boundary condition. In addition, their variability in Q_Z was ameliorated by employing long-term mean water flows. In the Rias Bajas, however, the short-term variability of salinity at the mouth introduces a second source of non-steadiness via S_{LC}. For example, short-term upwelling stress [McClain et al., 1986] or, perhaps, downwelling [Álvarez-Salgado et al., 2000] can rapidly result in an imbalance of salt and freshwater in the ria. This question has been noted [Rosón et al., 1997] and sampling campaigns redesigned accordingly [Álvarez-Salgado et al., 2000]. In this work, the problem was avoided by calculating τ and Q_Z iteratively. A more robust method, although constrained by sampling logistics, would involve averaging Q_L by iteration as described for Q_Z. The upshot of not averaging Q_L iteratively will be an exaggeration of the effects of upwelling stress or relaxation. In addition, with fortnightly sampling, the box model was able to calculate residual fluxes, but was unable to elucidate whether the flux corresponded to the stress or relaxation of an upwelling event. From both a scientific and socio-economic point of view, it is of interest to quantify the total residual water and nutrient over an upwelling cycle. A sampling resolution of 2-3 days has been suggested as the minimum requirement for applying water-salt budgets can be applied to the Rias Bajas with a higher degree of confidence in the results [Rosón et al., 1997; Álvarez-Salgado et al., 2000]. However, given the salinity variability at the

mouth of the Pontevedra Ria [*Prego et al.*, 2001], even at this time scale it is unlikely that the salinity field persists towards steady state. For example, a change in S_L of 0.1 d^{-1} was sufficient to change f typically by 0.5%, which is equivalent to 0.5-4 flushing days for the whole ria. The Pontevedra Ria, therefore, was constantly labouring toward steady state conditions, where upwelling and runoff may either work synergistically or antagonistically against the salt balance.

Chapter 4

Glossary of additional terms used in Chapter 4 [see also Chapter 3 glossary]

Symbol	Unit	Description
Bn	mg m^{-2} h^{-1}	Rate of benthic nutrient efflux
BSi	μmol l^{-1}	Biogenic silica
C	Ocktas	Cloud cover
Chl a	mg m^{-3}	Chlorophyll a
D_{net}	mg m^{-2} h^{-1}	Net denitrification in the sediment
Dropout	mg m^{-2} h^{-1}	The process of sedimentation of particulate matter
DIN, DIP	μmol l^{-1}	Dissolved inorganic nitrogen / phosphate
DOM	μmol l^{-1}	Dissolved organic matter
$ENACW$	-	East North Atlantic Central Water
$\varepsilon_S, \varepsilon_T$	-, °C	Analytical error of CTD salinity and temperature measurements
$\varepsilon_{Nu}, \varepsilon_{\Delta Nu}$	μmol l^{-1}, μmol s^{-1}	Analytical error of nutrient concentration and nutrient budget
f_W	-	Dimensionless weighting factor
GPP	mg C m^{-2} h^{-1}	Gross primary production
H	W m^{-2}	Net heat exchange across the water surface
H_1	W m^{-2}	Long-wave radiation heat gain from atmospheric water vapour
H_2	W m^{-2}	Radiation heat loss
H_E	W m^{-2}	Heat loss due to evaporation
H_S	W m^{-2}	Sensible heat loss
H_{SW}	W m^{-2}	Heat gain from short-wave radiation
I_W	m^3 s^{-1} km^{-1}	Upwelling index
NCP	mg C m^{-2} h^{-1}	Net community production
NCP_N, NCP_P	μmol l^{-1}	Net community production based on $\Delta DIN, \Delta DIP$
NH_4^+	μmol l^{-1}	Ammonium
NO_3^-	μmol l^{-1}	Nitrate
NO_2^-	μmol l^{-1}	Nitrite
$NO_{3/2}^-$	μmol l^{-1}	The sum of nitrate plus nitrite
Nu	-	Dissolved inorganic nutrient (DIN, DIP, Si(OH)$_4$)
$(Nu{:}Nu)_{P,D,F}$	-	Nutrient ratio in the particulate, dissolved phase and efflux.
ΔNu	mol s^{-1}	Non-steady state nutrient budget between two consecutive surveys
ΔN	mg m^{-2} h^{-1}	Dissolved inorganic nitrogen anomaly
$N_{storage}, Si_{storage}$	mg m^{-2} h^{-1}	Temporary PON and BSi storage in sediments
O_2, O_{2SAT}	μmol l^{-1}, %	Dissolved oxygen and dissolved oxygen saturation
POM, POC, PON	μmol l^{-1}	Particulate organic matter / carbon / nitrogen
$(Q_U)_S$	m^3 s^{-1}	Surface horizontal flux derived from the salt budget
$(Q_U)_T$	m^3 s^{-1}	Surface horizontal flux derived from the heat budget
Q_{UW}	m^3 s^{-1}	S and T weighted advective horizontal flux
$Respn$	mg C m^{-2} h^{-1}	Aerobic respiration of organic matter
$Resus$	mg m^{-2} h^{-1}	The process of benthic nutrient efflux
ρ_0	m	Theoretical level of the pycnocline
Si(OH)$_4$	μmol l^{-1}	Dissolved reactive silicate
SPM	μmol l^{-1}	Suspended particulate matter
$(ST)_U$	PSU , °C	Salinity or temperature in the upper layer at any boundary
$(ST)_L$	PSU , °C	Salinity or temperature in the lower layer at any boundary
$\Delta(ST)_{LAT}$	-, °C	Error in S or T due to lateral inhomogeneity
$\Delta(ST)_{LON}$	-, °C	Error in S or T due to longitudinal inhomogeneity
$\Delta(ST)_{\rho_0}$	-, °C	Error in S or T due to variability in the pycnocline level
$\Delta(ST)_{LON}$	-, °C	Error in S or T due to longitudinal inhomogeneity
$\Delta(ST)_{INT}$	-, °C	Error in S or T due to numerical cross sectional integration
$\Delta(ST)_U$	-, °C	Total error in S or T in the upper layer at any boundary
$\Delta(ST)_L$	-, °C	Total error in S or T in the lower layer at any boundary
W_L	m s^{-1}	Local wind speed resolved along the ria longitudinal axis

4. Chemical Oceanography of the Pontevedra Ria

4.1 DESCRIPTIVE CHEMICAL OCEANOGRAPHY

Recent biogeochemical studies in the Galician rias have focussed on the development of nutrient budgets based on salt and heat fluxes [e.g. *Prego*, 1993a,b, 1994; *Álvarez-Salgado et al.*, 1996a; *Rosón et al.*, 1997, 1999]. To date, no budget of the Pontevedra Ria has been undertaken. This chapter explores the pelagic and benthic nutrient biogeochemical cycles and budgets of the Pontevedra Ria and questions the suitability of first-order budgets in quantifying the nutrient flux in the Rias Bajas.

The results in Section 4.1 are discussed according to the seasonal variability in freshwater runoff and subsurface oceanic inputs as described in the hydrography section. To facilitate the discussion of the data, the "downwelling" or wet season encompassed the months of November to February, and the "upwelling" season from May to September.

4.1.1. TEMPORAL ANALYSIS OF NUTRIENT DISTRIBUTIONS

Fig. 4.1 presents annual depth-time distributions of nutrients, dissolved oxygen, chlorophyll a and 1 % isolume at Sta. 3 in the Pontevedra Ria. Salinity, temperature, density and Brunt Väisälä temporal distributions have been discussed in Section 3.1.1. The fluvial dominance of nutrient inputs to the ria was clearly observable during November-February where nutrient-rich waters from the river mixed with nutrient-poor waters within the ria. NO_3^- and $Si(OH)_4$ showed a strong coupling in the surface layers, with maximum NO_3^- (24.6 μmol l^{-1}), NO_2^- (1.0 μmol l^{-1}) and $Si(OH)_4$ (33.8 μmol l^{-1}) concentrations recorded at the surface. DIP concentrations were generally low (0.2 μmol l^{-1}) and not significantly correlated to freshwater inputs.
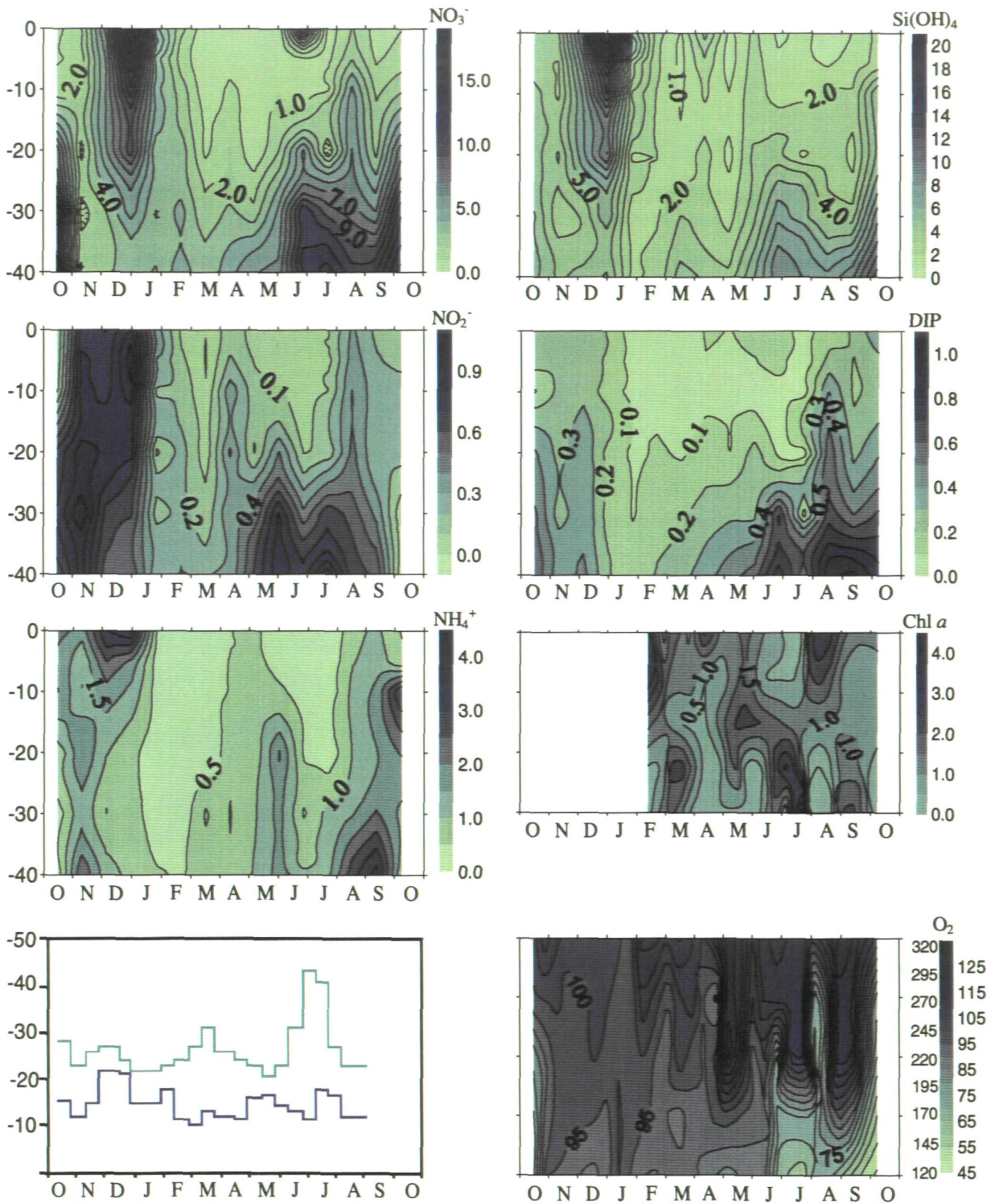
Fig. 4.1. Annual depth time-series distributions of nutrients (µmol l^{-1}), Chl a (µg l^{-1}), dissolved oxygen (µmol l^{-1}, left scale; %O$_{2SAT}$, right scale), and the depth of the 1% isolume and the pycnocline (ρ_0) at Sta. 3 in the Pontevedra Ria during October 1997-1998.

Ammonium concentrations of up to 4.2 µmol l⁻¹ were noted at Sta. 3. These concentrations were similar to the other Rias Bajas [*Álvarez-Salgado et al.*, 1996a; *Doval et al.*, 1998] although they were lower than other European estuarine systems [*Middelburg and Nieuwenhuize*, 2001]. Urban and industrial effluent from the City of Pontevedra is directed to a nitrification plant in Placeres [Fig. 2.1], which has reduced NH_4^+ inputs to the ria in recent years [*Ibarra and Prego*, 1997]. Diffuse sources of NH_4^+ from land runoff are low, and point source inputs are mainly confined to the ria itself.

A clear paucity of nutrient salts in the upper water layers was recorded in the months of February through late July. The sharp decline in nutrients coincided with a simultaneous increase in O_2 and Chl a concentrations, indicative of biological activity. February 1998 was notably mild with long sunshine hours which resulted in favourable conditions for phytoplankton growth. Consequently, a "mini-bloom" was observed in early February with 4 µg Chl a l⁻¹ below the surface [Fig. 4.1]. Other workers described similar findings as a "false start" [*Owens et al.*, 1986]. Thereafter, biological activity was depressed by low irradiance [Fig. 2.3] and nutrients until April when a second phytoplankton bloom occurred. High O_2 saturation was again noted and Chl a concentrations of 1.3 µg l⁻¹ extended to 10 m at the approximate depth of the 1% isolume. DIN and DIP were often depleted below detection limits at the surface during this period, ultimately leading to a decrease in Chl a. In addition, nutrient supply to the upper water layers by upward nutrient diffusion from the lower levels was probably reduced by thermohaline stratification [Fig. 3.1].

From May onwards a combination of low nutrient supply and high nutrient demand limited phytoplankton production until the deep water layers became enriched with upwelled nutrients. The sloping up of the 6-8 µmol l⁻¹ NO_3^- and $Si(OH)_4$ isopleths, 0.6 µmol l⁻¹ DIP isopleth and decrease in bottom water O_2 concentrations were characteristic of ENACW upwelling from the continental margin [*Fiúza et al.*, 1998; Figs. 3.1 and 3.2]. Enrichment of the water column by upwelling has been shown to provoke phytoplankton blooms in marine systems [*Stolte et al.*, 1994; *Stolte and Riegman*, 1996]. Recently *Lomas and Gilbert* [1999] observed an inverse relationship between phytoplankton NO_3^- uptake and temperature for diatom dominated populations. Accordingly, Chl a and O_2 concentrations increased shortly afterwards in parallel with nutrient enrichment to 2.4 µg Chl a l⁻¹ and >300 µmol l⁻¹ (125% O_{2SAT}) and remained high down to the 1% isolume [Fig. 4.1]. Employing more temporally resolved data, *Doval et al.* [1998] have described the tight coupling between parallel increases in Chl a and O_2 concentrations in the Vigo Ria of up to 6-7 µg l⁻¹ and 330 µmol O_2 l⁻¹ in the surface layers during upwelling relaxation. DOM accumulation in surface water may also become prominent after the Chl a bloom [*Álvarez-Salgado et al.*, 1999]. Chl a concentrations offshore on the shelf break during upwelling are in the range 2-5 µg l⁻¹ [*Teira et al.*, 2001]. Low Ekman transport rates following upwelling allow sufficient dwell time for phytoplankton biomass to increase, mainly as diatomic species [*Tilstone et al.*, 2000]. Intense biological activity has been observed by other workers [*Prego et al.*, 1995; *Álvarez-Salgado et al.*, 1996a,b]. Without a high sampling resolution, Chl a data are difficult to interpret due to their patchy nature and the hydrodynamic control of spatial and temporal distributions [*Cloern*, 1991; *Figueiras and Pazos*, 1991; *Vezina et al.*, 1995].

Between upwelling pulses, high NH_4^+ effluxes have been observed from the sediments [*Álvarez-Salgado et al.*, 1996a], a feature also clearly observable in

the data with ~5 μmol l⁻¹ close to the ria bed in late August. Remineralised NH₄⁺ may account for 26% of net community production (gross primary production minus respiration) in the Arosa Ria [Álvarez-Salgado et al., 1996a]. High rates of organic matter remineralisation are normally observed at the end of the upwelling season in October, when a seasonal change in wind patterns on the shelf from northerly to southerly bring about the onset of downwelling conditions [e.g. Álvarez-Salgado et al., 1993; Fig. 2.3]. Thereafter, a combination of increased residence time [Fig. 3.12] and wind-induced mixing and advection processes in October and November resulted in vertical homogeneity of thermohaline properties [Fig. 3.1 and 3.2] and nutrients [Fig. 4.1].

4.1.2. SPATIAL ANALYSIS OF NUTRIENT DISTRIBUTIONS

The range, mean and standard deviation of concentrations of nutrients, dissolved oxygen, chlorophyll a, salinity and temperature in the ria and river are presented in Table 4.1. To a greater or lesser extent, nutrient concentrations were influenced by runoff throughout the ria, as observed previously at Sta. 3. The large standard deviations were due to variable river inputs. NO_3^- and $Si(OH)_4$ surface layer distributions in the wet season were strongly influenced by freshwater runoff, as confirmed by the near-conservative mixing diagrams in Fig. 4.2 and the high correlation between NO_3^- and $Si(OH)_4$ ($p<0.001$, $n=86$). Mixing curves for other nutrients are not shown since they display highly irregular behaviour at high salinities and have low freshwater end member concentrations.
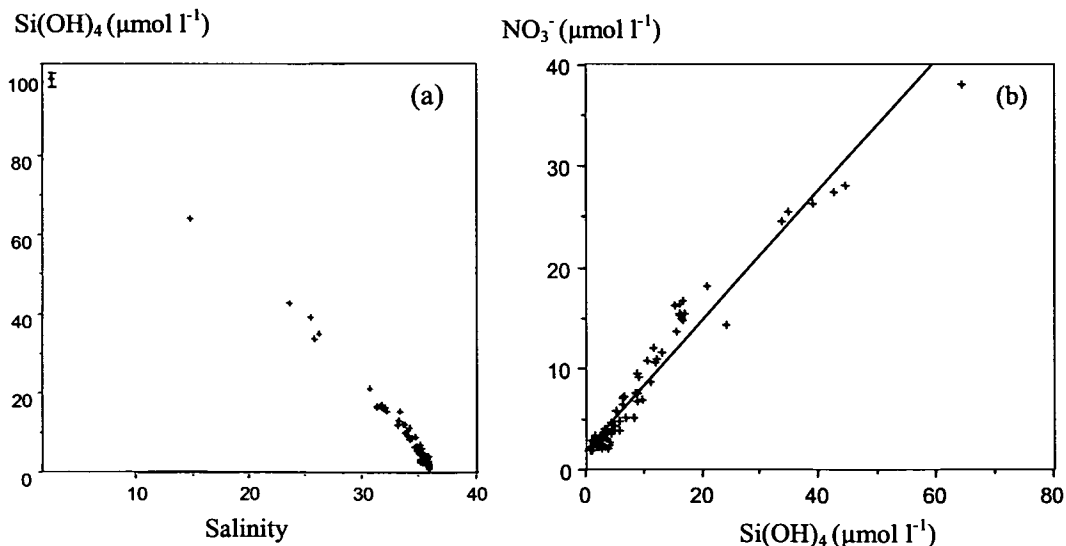
Fig. 4.2. (a) $Si(OH)_4$ (±SD for freshwater end member) salinity mixing curve and (b) NO_3^--$Si(OH)_4$ plot in the Pontevedra Ria using wet season data 1997-1998. The NO_3^--$Si(OH)_4$ relationship is significant at the 99.9 % level ($p<0.001$), $r^2 = 0.95$, $n=86$.

Higher concentrations of NO_2^-, DIP and NH₄⁺ in the internal ria compared to the river imply that the internal ria was a source for these nutrients. This behaviour is shown in more detail in the 2-dimensional nutrient profiles recorded on 14 January 1998 [Fig. 4.3]. There was an indication of relatively

higher levels of these nutrients close to the ria bed at Sts. 7 and 8. Maximum surface layer concentrations at Sta. 8 for NO_2^-, NH_4^+ and DIP were 1.1 μmol l^{-1}, 2.3 μmol l^{-1} and 0.4 μmol l^{-1}, respectively. DIP concentrations were agreeable with recent observations in the Arosa Ria [*Rosón et al.*, 1995]. Maximum NO_3^- (38.0 μmol l^{-1}) and $Si(OH)_4$ (64.4 μmol l^{-1}) were noted near the ria head, with up to 12 μmol l^{-1} at Sta. 2 near the ria mouth. NO_2^- accounted for less than 5 % of total nitrogen concentration, as found in other Rias Bajas [e.g. *Álvarez-Salgado et al.*, 1996a].
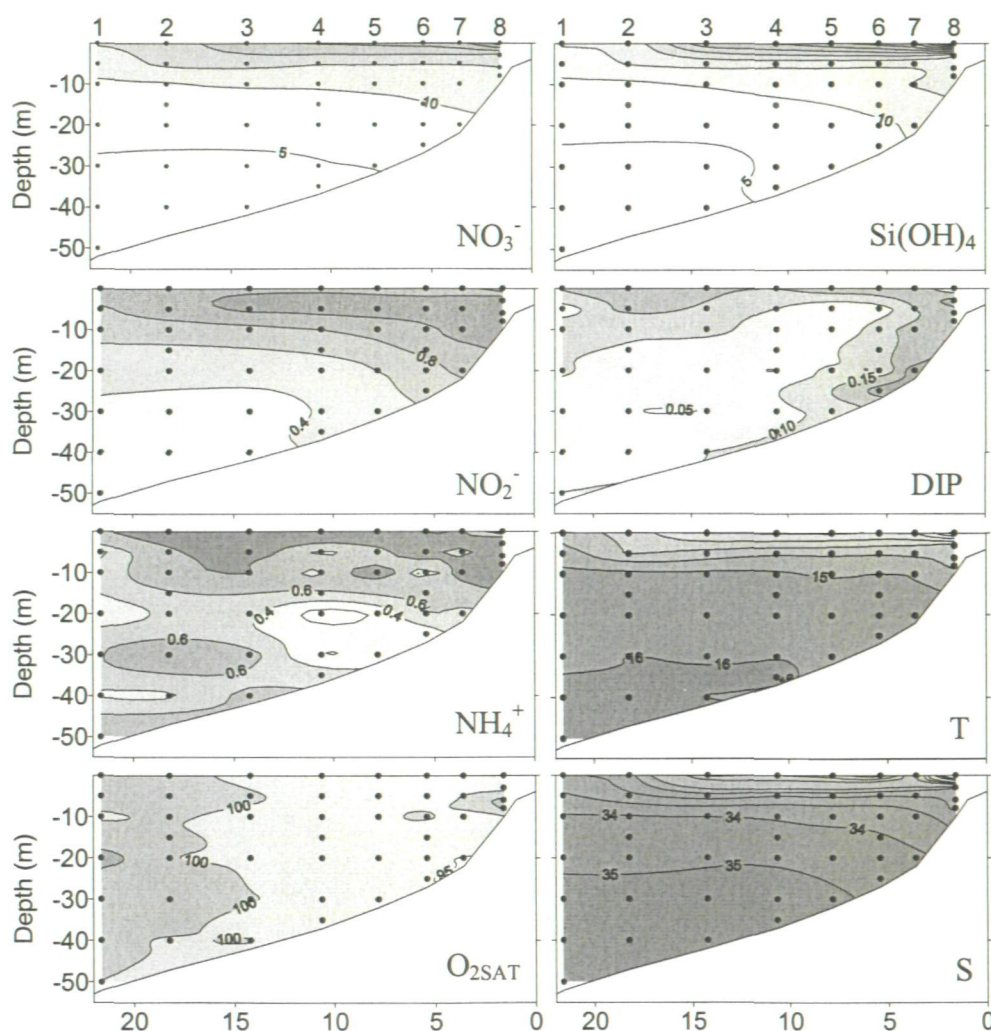
Fig. 4.3. Isopleths of nutrients (μmol l^{-1}) NO_3^-, NO_2^-, NH_4^+, $Si(OH)_4$, DIP, O_{2SAT} (%), salinity isohalines and temperature (θ, °C) isotherms along the main axis of the Pontevedra Ria during 1998 in the wet season (14 January 1998). Sts. 1 to 8 [Fig. 2.1] are indicated on the top horizontal axes. The mouth of the river Lérez is located upstream of Sta. 8. Sampling depths are shown by the vertical black points.

The spring concentrations of NO_3^-, NO_2^- and NH_4^+ [Table 4.1] were of the same order as those reported for the Arosa and Vigo rias [*Prego*, 1994; *Rosón et al.*, 1995; *Álvarez-Salgado et al.*, 1996a; *Doval et al.*, 1998]. Chl a ranged from 1.10±0.62 μg l^{-1} in the external ria to 1.48±0.82 μg l^{-1} in the internal ria. The longitudinal nutrient profiles recorded shortly after the phytoplankton bloom [Fig. 4.4] showed nutrient depletion in the upper water layers, although still maintaining high levels near the Lérez mouth (Sts. 6-8).

Table 4.1. Ranges, means and standard deviations of the seasonal nutrient concentrations, chlorophyll a, dissolved oxygen, salinity and temperature data recorded in the three sections of the Pontevedra Ria and the Lérez river over the period November 1997-September 1998. The number of samples used for the analyses are given. <d.l. = below detection limit.

Parameter		External Ria			Central Ria			Internal Ria			River Lérez		
		No.	Concentration		No.	Concentration		No.	Concentration		No.	Concentration	
			Range	Mean±1 s.d		Range	Mean±1 s.d		Range	Mean±1 s.d		Range	Mean±1 s.d
NO_3^-	Wet	96	<dl -16.46	4.34±3.58	96	0.6-25.57	5.42±4.71	140	<dl-38.01	8.14±6.75	31	17.41-36.42	29.61±5.25
(μmol l^{-1})	Spring	78	<dl-9.64	2.32±2.63	70	<dl-6.38	1.64±2.04	111	<dl-16.27	2.56±3.25	26	15.50-35.31	25.65±4.18
	Dry	78	<dl-18.35	4.83±4.70	66	<dl-12.67	3.82±4.26	108	<dl-11.60	2.72±3.41	28	10.99-30.40	25.28±5.67
NO_2^-	Wet	96	<dl-0.92	0.44±0.28	96	<dl -1.30	0.59±0.35	140	0.06-1.61	0.79±0.33	32	0.09-0.13	0.10±0.03
(μmol l^{-1})	Spring	78	<dl-0.87	0.21±0.21	70	<dl-1.02	0.22±0.24	111	<dl-0.75	0.23±0.18	18	0.03-0.13	0.06±0.03
	Dry	65	0.04-1.11	0.37±0.28	55	<dl-1.14	0.32±0.28	90	<dl-1.21	0.24±0.27	28	0.04-0.19	0.11±0.03
NH_4^+	Wet	96	0.05-19.95	0.75±2.09	84	0.08-4.20	0.96±0.93	122	0.12-12.79	1.69±2.05	18	<dl-0.59	0.10±0.20
(μmol l^{-1})	Spring	78	<dl-1.00	0.59±0.57	70	0.18-2.07	0.71±0.47	111	0.14-5.87	1.20±1.16	26	<dl-1.41	0.20±0.31
	Dry	78	<dl-5.76	0.76±0.96	66	<dl-6.54	1.05±1.24	108	<dl-7.1	1.25±1.08	28	0.04-2.00	0.42±0.43
DIP	Wet	95	<dl -2.05	0.19±0.22	96	<dl -0.76	0.20±0.14	136	0.05-1.14	0.33±0.19	32	0.07-0.20	0.12±0.04
(μmol l^{-1})	Spring	52	<dl -0.63	0.19±0.18	47	<dl -0.46	0.16±0.12	77	<dl -1.25	0.25±0.20	18	<dl-0.25	0.08±0.07
	Dry	78	<dl -1.04	0.32±0.27	66	<dl-1.24	0.35±0.41	108	<dl -1.13	0.41±0.33	28	<dl-0.16	0.06±0.03
$Si(OH)_4$	Wet	96	0.14-16.35	4.58±3.90	96	0.97-35.08	6.41±6.07	140	2.01-64.36	10.85±10.8	32	89.86-107.65	101.03±6.14
(μmol l^{-1})	Spring	78	0.21-5.30	2.08±1.38	70	<dl-7.63	2.09±1.59	111	<dl-46.85	4.99±8.20	26	65.00-115.00	93.75±20.97
	Dry	77	<dl-8.39	2.97±2.29	66	0.14-10.99	3.13±2.71	108	<dl-15.96	3.18±3.18	28	100.00-160.00	114.38±19.72
O_{2SAT}	Wet	90	89-165	101±9	96	86-116	98±6	140	74-106	93±7	-	-	-
(%)	Spring	78	79-131	102±13	66	84-136	104±14	103	73-140	101±17	-	-	-
	Dry	78	63-127	99±19	66	57-140	101±22	108	57-148	104±23	-	-	-
Salinity	Wet	102	31.74-35.95	34.64±1.25	96	25.57-35.95	34.20±2.06	140	14.78-35.94	33.38±2.95	-	-	-
	Spring	78	32.30-36.02	35.28±0.79	70	31.25-35.92	35.04±1.16	112	20.61-35.91	34.33±2.51	-	-	-
	Dry	78	34.05-35.84	35.54±0.39	66	33.45-35.89	35.49±0.48	108	32.47-35.93	35.33±0.65	-	-	-
Chl a	Wet	10	0.46-3.05	1.90±0.84	10	0.30-3.92	1.71±1.27	10	0.33-2.50	1.45±0.62	-	-	-
(μg l^{-1})	Spring	30	0.13-2.35	1.10±0.62	30	0.30-2.61	1.19±0.66	30	0.13-3.27	1.48±0.82	-	-	-
	Dry	30	0.17-4.84	1.49±1.11	30	0.13-4.25	1.17±0.98	30	0.13-2.40	1.14±0.74	-	-	-
Temperature	Wet	102	13.8-17.3	15.4±0.9	96	12.9-17.3	15.2±0.9	140	11.8-16.7	15.1±1.0	-	-	-
(°C)	Spring	78	12.7-15.6	14.4±0.7	70	13.2-15.5	14.6±0.5	112	13.7-16.2	14.9±0.6	-	-	-
	Dry	78	12.3-18.2	14.3±1.6	66	11.9-18.6	14.7±1.7	108	12.3-19.4	15.6±1.9	-	-	-
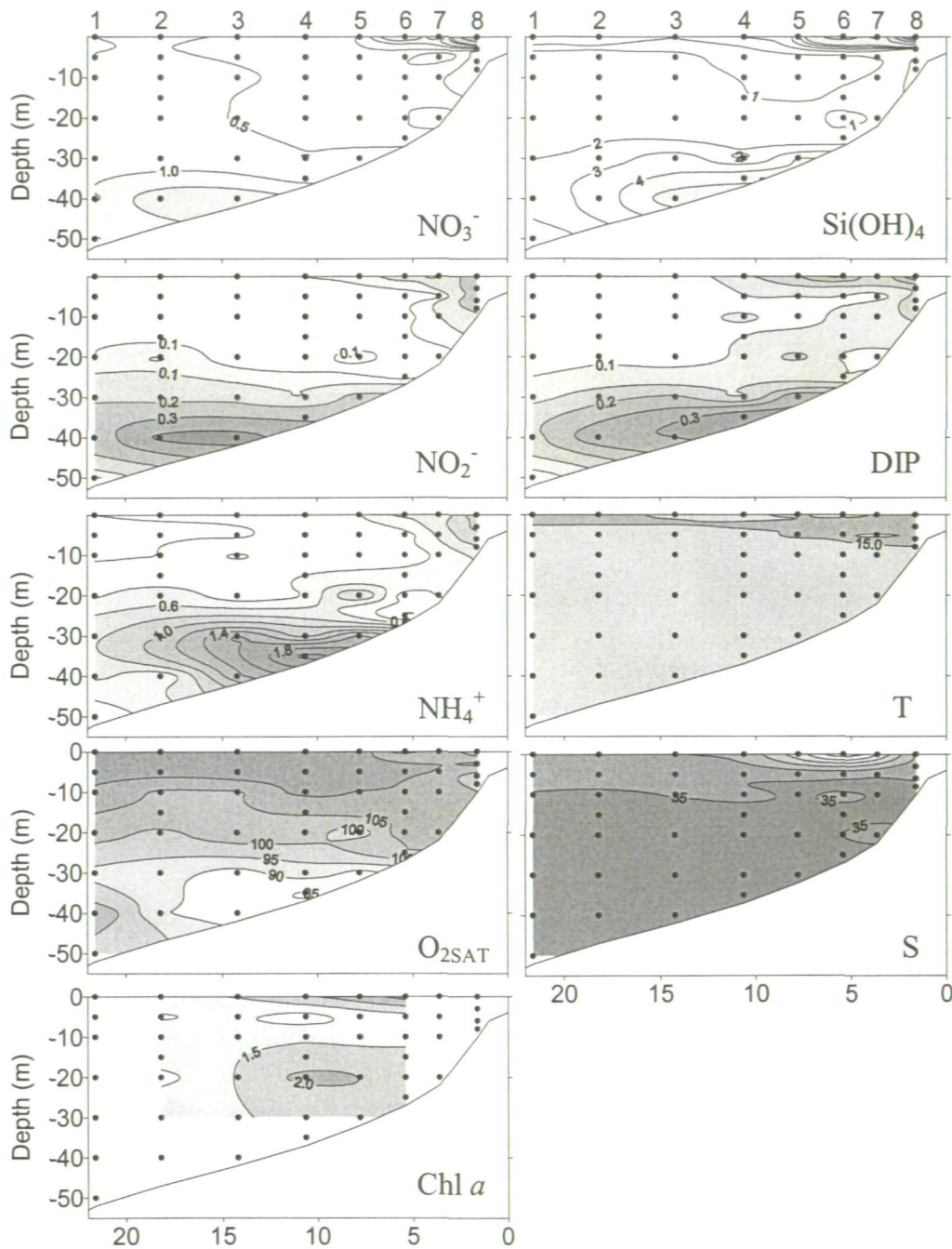
Fig. 4.4. Isopleths of nutrients (μmol l^{-1}) NO_3^-, NO_2^-, NH_4^+, $Si(OH)_4$, DIP, O_{2SAT} (%), Chl a (μg l^{-1}), salinity isohalines and temperature (θ, $^\circ$C) isotherms along the main axis of the Pontevedra Ria during 1998 in spring (10 March 1998). Sts. 1 to 8 [Fig. 2.1] are indicated on the top horizontal axes. The mouth of the river Lérez is located upstream of Sta. 8. Sampling depths are shown by the vertical black points.

Dissolved oxygen supersaturation at the surface was noted at every station, indicative of the post-bloom situation described previously. Sediment effluxes of all nutrients in the central-internal ria are clearly observable. Phytodetrital aggregates are degraded and remineralised by bacteria, and subsequent tidal- or upwelling-induced resuspension of the phytodetritus could explain the observations. However, residual incoming velocity to the

ria [Fig. 3.11] was 1-2 cm s^{-1} and, furthermore, the negative vertical flux, Q_v, was suggestive of downwelling conditions and extended residence times. Therefore, in the same way as at the end of the upwelling season, downwelling conditions throughout the year may provoke remineralisation of organic material on the seabed. NH_4^+ was nitrified in situ, which caused a decrease in ambient O_2 concentrations. Growth restriction from oxygen depletion was more severe for NO_2^- oxidisers than for NH_4^+ oxidisers [*Helder and de Vries*, 1983], resulting in augmented near-bed NO_2^- and NH_4^+ concentrations with respect to NO_3^-.
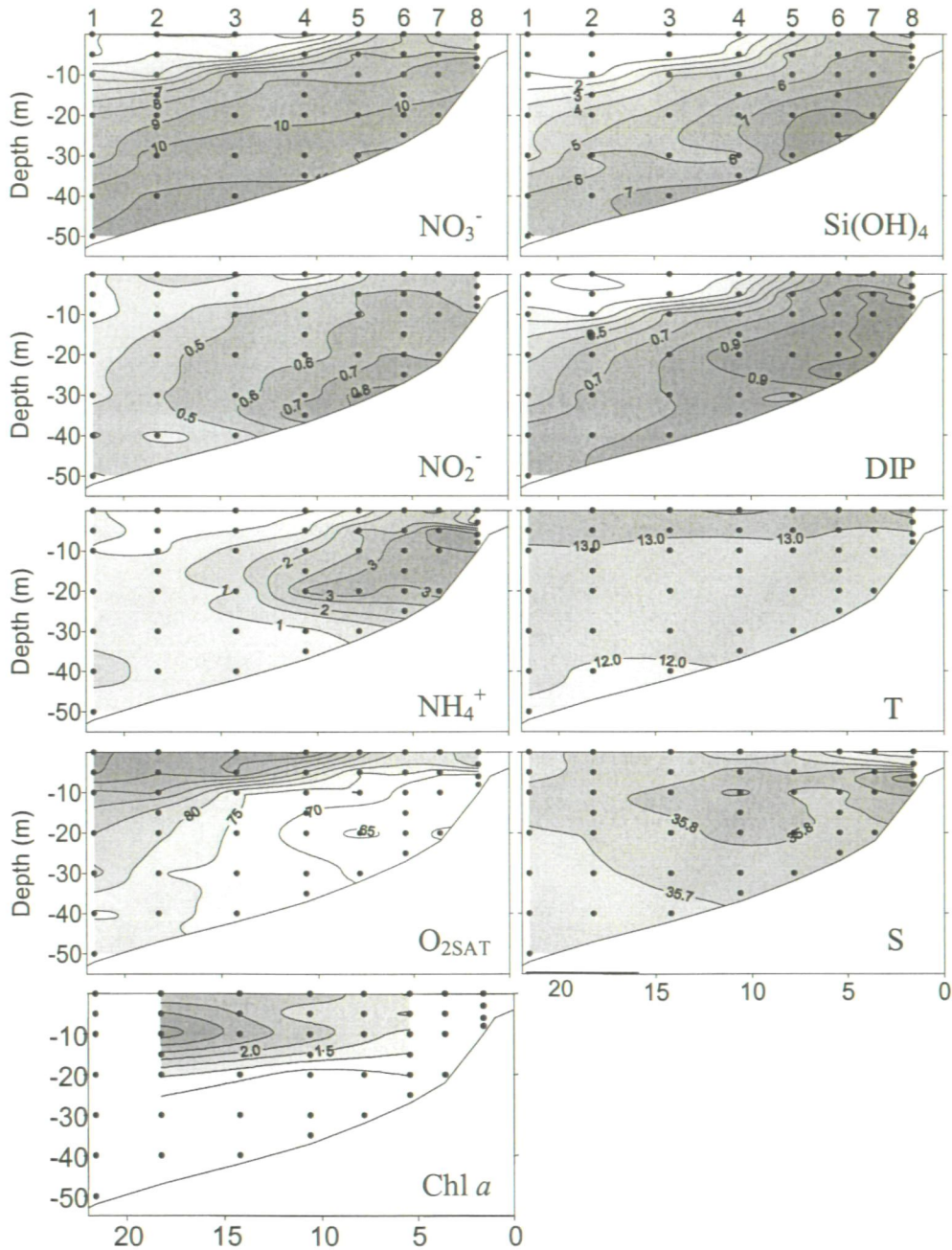
Fig. 4.5. Isopleths of nutrients (μmol l^{-1}) NO_3^-, NO_2^-, NH_4^+, Si(OH)$_4$, DIP, O_{2SAT} (%), Chl a (μg l^{-1}), salinity isohalines and temperature (θ, $^{\circ}$C) isotherms along the main axis of the Pontevedra Ria during 1998 in the dry season (3 August 1998). Sts. 1 to 8 [Fig. 2.1] are indicated on the top horizontal axes. The mouth of the river Lérez is located upstream of Sta. 8. Sampling depths are shown by the vertical black points.

In August, ENACW upwelling [Fig. 3.2] rapidly increased nutrient concentrations to 5.0 μmol l^{-1} NO$_3^-$, 0.5 μmol l^{-1} NO$_2^-$, 1.2 μmol l^{-1} NH$_4^+$, 0.6 μmol l^{-1} DIP and 3.2 μmol l^{-1} Si(OH)$_4$ in the superficial waters of the internal ria [Fig. 4.5]. Prior to upwelling the presence of a marked pycnocline [Fig. 3.4] caused the reduction of nutrient concentrations to almost undetectable levels in the photic zone [data not shown]. High nutrient assimilation by phytoplankton triggered a fourfold increase of Chl a concentrations to 3.8 μg l^{-1} in the external ria [Fig. 4.5]. Pre-upwelling Chl a concentrations of the order of 2 μg l^{-1} have been reported in the Pontevedra Ria by *Mouriño et al.* [1985] which generally agree with those at the nutricline from this survey.

Nutrient concentrations were highest towards the shallow ria head and showed seaward dispersal in the upper layers. Due to low runoff, high nutrient concentrations in the internal ria were likely to be due to remineralisation of biogenic material and subsequent depression of O$_2$ concentrations [*Lebo*, 1990; *Seitzinger and Sanders*, 1997]. Industrial and urban inputs containing high amounts of DOM and POM contribute a greater proportion of the freshwater inputs to the ria [*Figueiras and Niell*, 1986; *Figueiras et al.*, 1986; *Ibarra and Prego*, 1997]. From spring to the dry season the zone of maximum remineralisation had moved further into the internal ria, possibly due to landward transport of fluff over the upwelling period. In agreement with the present findings, *Prego et al.* [1999] noted a zone of DIP remineralisation in the internal zone of the Vigo Ria, with concentrations of up to 1 μmol l^{-1} emanating from the sediments. Pore water infusions of DIP, as with other regenerated nutrients, will be favoured in the internal ria since the sediments in this zone are comprised of fine mud [*Vilas et al.*, 1996] and are anoxic in the innermost sections [*Arbones et al.*, 1992]. Therefore, remineralisation of nutrients from the benthos combined with upwelling recycles a proportion of the nutrient salts exported during the winter and consumed by the phytoplankton in spring, and creates the potential for high primary productivity.

4.2. PHYSICO-BIOGEOCHEMICAL CONTROLS ON BENTHIC-PELAGIC NUTRIENT COUPLING

4.2.1. BENTHIC BIOGEOCHEMICAL DISTRIBUTIONS AND FLUXES

Benthic remineralisation processes strongly influence the functioning of coastal systems [*Boynton et al.* 1995]. Contributions of 30-80% of the phytoplanktonic nitrogen requirement in shallow (5-50 m) coastal environments have been reported to originate from the sediments [*Nixon*, 1981; *Blackburn and Henriksen*, 1983, *Boynton and Kemp*, 1985]. Equally, deposition of algal phytodetritus provokes sediment nutrient exchange by microbial remineralisation and gradient-driven diffusion. Whilst these findings are valuable to coastal resource managers, relatively few workers have considered the potential hydrodynamical role on sediment nutrient processing [*Floderus and Håkanson*, 1989; *Vorosmarty and Loder*, 1994; *Nielsen et al.*, 1995, *Sloth et al.*, 1996]. Laboratory studies by *Christiansen et al.* [1997] showed that resuspension modifies nutrient effluxes and oxygen consumption. Similarly, resuspension may give rise to profound modification of the water column nutrient characteristics [*Morris et al.*, 1985]. In the absence of resuspension, *Li et al.* [1997] discussed the influence of the rate of mass transfer across the sediment-water interface on constituent efflux.

Changes in river flow may also affect sediment accumulation and redistribution [Bale et al., 1985]. Therefore, strictly speaking, the majority of microcosm experiments should be interpreted semi-quantitatively. This section employs data for water column chemistry, bed sediment analysis, suspended particulate matter, and nutrient flux incubation cores.

Benthic BSi, POC and PON distribution. The percentage BSi, POC and PON and the sediment sorting in the upper 1 cm of the sediment in the Pontevedra Ria are presented in Fig. 4.6. Table 4.2 provides further data of the size-fractionated sediment.

Table 4.2. Sediment characteristics for the three sites investigated with incubation microcosms. Total sediment represents the oxic layer in the upper 1 cm. All values other than particulate molar C:N ratios are given as percentage dry weight.

Sta.	Description	Total Sediment			Fraction < 63µm			Fraction > 63µm		
		BSi	POC	PON	POC	PON	C:N	POC	PON	C:N
4	Mud/ Sand	1.91	2.16	0.24	3.74	0.40	10:1	1.87	0.22	9:1
6	Mud	2.73	4.02	0.53	5.27	0.55	10:1	3.41	0.52	7:1
8	Sand	1.34	7.42	0.66	6.28	0.55	11:1	8.11	0.72	12:1
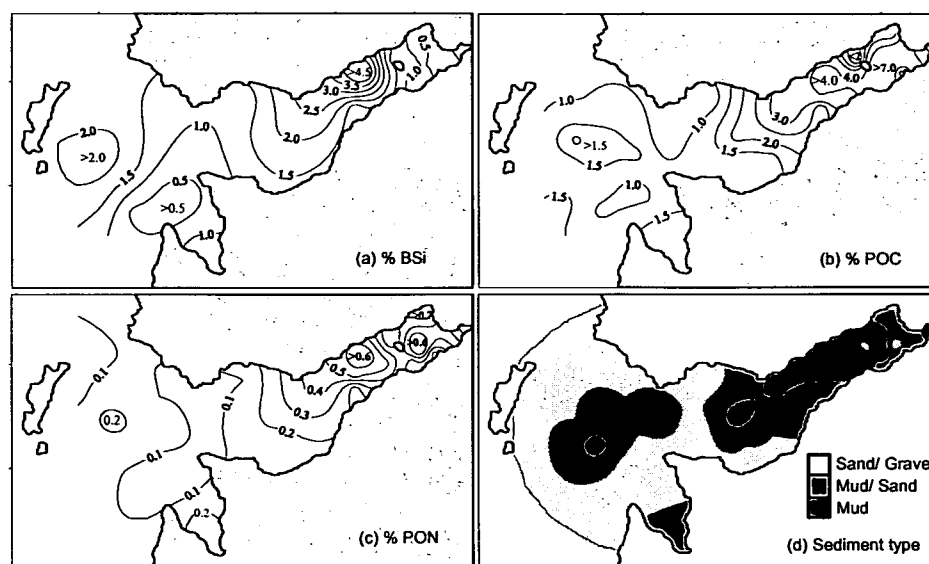
Fig. 4.6. Total fractions (%) of BSi (a), POC (b), PON (c) and the superficial sediment structure (d) in the Pontevedra Ria. Samples were taken from the uppermost oxic layer (0-1 cm).

The highest percentage of BSi in the Pontevedra Ria sediments (5.0%) was found in the internal ria adjacent to the northern coast, concentrated behind Tambo Island [Fig. 4.6a]. At the ria head, coarse terrestrial material dominated the sediment structure and the BSi fraction decreased below 0.5%. At Sta. 4 the BSi content was ~2.0%, a value representative of the adjacent continental shelf [Prego and Bao, 1997]. Total POC and PON showed a similar geographical distribution with the highest fractions (4.8 and 0.7% respectively) close to the northern coast in the internal ria [Fig.

4.6b,c]. Total organic material in the inner ria may be as high as 10% [*López-Jamar et al.*, 1992], and enhanced by sedimentation of faecal material from the intensive aquaculture of the mussel *Mytilus edulis* in this area. In contrast to BSi, a second zone of high POC (7.4%) and PON (0.7%) was located behind Tambo Island close to the mouth of Marín Harbour. The area was likely to be impacted by discharges of particulate organic material from a nearby paper mill [*Mora et al.*, 1989, Arbones *et al.* 1992] and urban wastewater from the Pontevedra urbanisation. The upshot is maximum POC and PON fractions in the coarse and fine sediments at Sta. 8 [Table 1].

Suspended and bed sediment pools are closely coupled in dynamic coastal systems. The material caught in the sediment trap apparatus at the sediment surface can be used to gauge the extent of the coupling between the two reservoirs. The temporal variability in the elemental PON:BSi and POC:PON molar ratio of particulate material (hereafter $(N:Si)_P$ and $(C:N)_P$) collected in traps at Sts. 4 and 6 is shown in Fig. 4.7, respectively, together with the mean sedimentation rates of BSi and PON at Sts. 4 and 6. A decrease in $(C:N)_P$ was observed to coincide with an increase in PON sedimentation, and similar trends can be seen with regards to $(N:Si)_P$ and BSi sedimentation rate. This suggests that high sedimentation occurs with fresh biogenic material, such as bloom deposition.
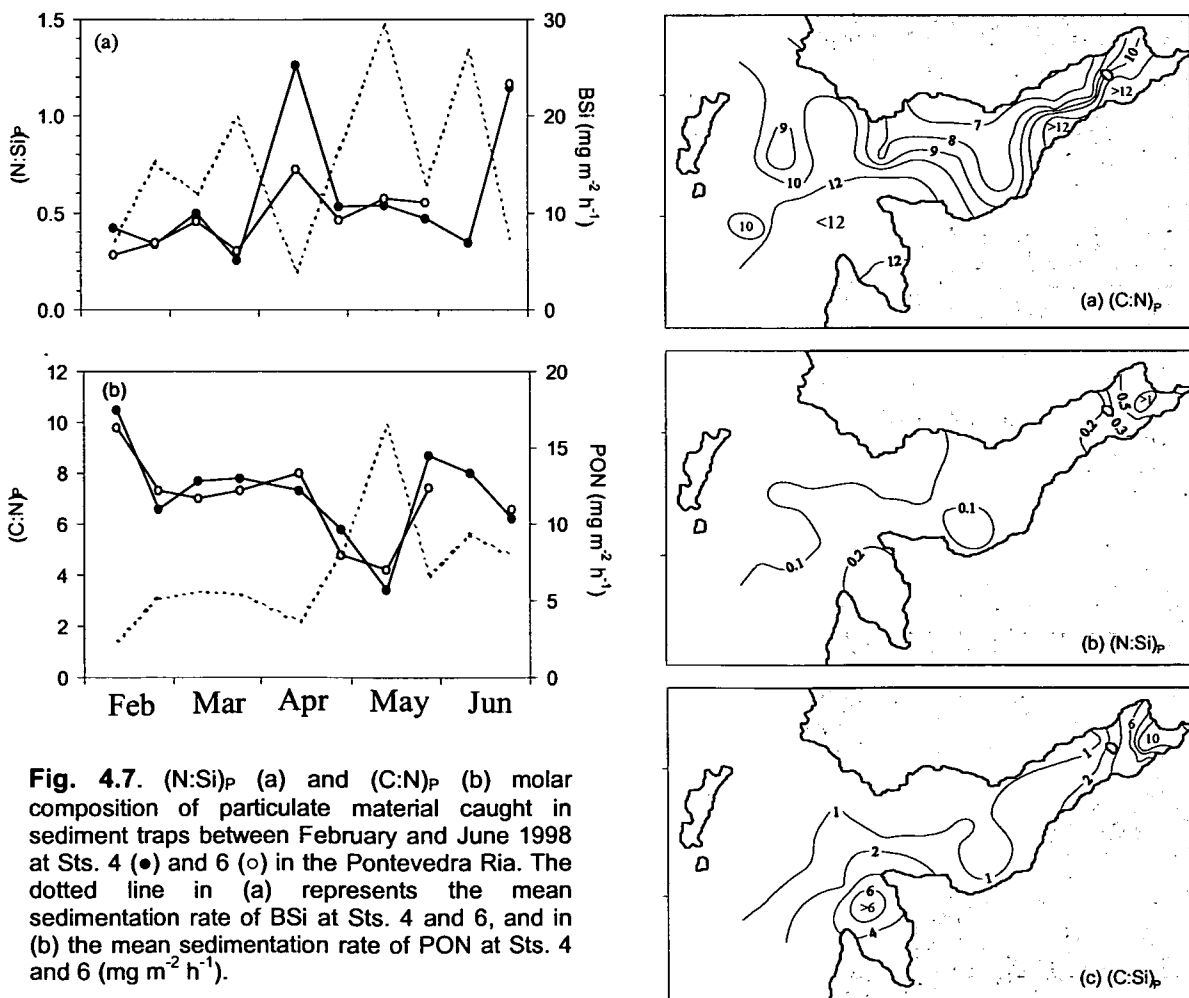
Fig. 4.7. $(N:Si)_P$ (a) and $(C:N)_P$ (b) molar composition of particulate material caught in sediment traps between February and June 1998 at Sts. 4 (•) and 6 (o) in the Pontevedra Ria. The dotted line in (a) represents the mean sedimentation rate of BSi at Sts. 4 and 6, and in (b) the mean sedimentation rate of PON at Sts. 4 and 6 (mg m^{-2} h^{-1}).

Fig. 4.8. Nutrient elemental molar ratios in the oxic upper 1 cm of the sediment in the Pontevedra Ria collected on one occasion at the start of the sampling campaign (October 1997).

The (N:Si)$_P$ composition of the captured sediment was consistently below the diatom (N:Si)$_P$ composition of ~1 [*Nelson et al.*, 1995], and averaged 0.56. The (C:N)$_P$ ratio [Fig. 4.7b] of local phytoplankton has been determined to be 6-7 by *Rios et al.*, [1998]. This is consistent with the sediment trap data, with notable deviations in early February, (C:N)$_P$~10, and in April and May, (C:N)$_P$~4-5. The sediment maps in Fig. 4.8 show further evidence for PON loss throughout the ria. The (C:N)$_P$ ratios were notably higher along the southern margins of the internal ria [Fig. 4.8a], and increased toward the inner ria, (C:N)$_P$~12. On the northern coast (C:N)$_P$ was more comparable to the local phytoplanktonic composition [*Rios et al.*, 1998]. The (N:Si)$_P$ ratio in the sediment surface was ~0.2 over the ria, except in the industrial areas of the inner ria [Fig. 4.8b]. (C:Si)$_P$ ratios were consistently lower than in the phytoplankton (7-8), and increases to >10 at the ria head [Fig. 4.8c].

Sediment fluxes. The seasonal variation in the benthic Si(OH)$_4$, NH$_4^+$, NO$_3^-$ and NO$_2^-$ fluxes calculated from the mesocosm experiments are shown in Fig. 4.9, and follow the general trend of Si(OH)$_4$ > NH$_4^+$ > NO$_3^-$ > NO$_2^-$. Si(OH)$_4$ was always released from the sediment, and the mean effluxes were four-fold higher at Sts. 4 and 6 than at Sta. 8, with rates of 4.2, 3.8 and 1.0 mg Si m^{-2} h^{-1} (respectively). NH$_4^+$ effluxed the sediment at Sts. 4 and 6, but NH$_4^+$ was occasionally taken up at Sta. 8. The NH$_4^+$ efflux reached a maximum on May 26 at Sta. 6, at almost 3.5 mg N m^{-2} h^{-1}. The direction of the NO$_3^-$ and NO$_2^-$ fluxes was variable. Net NO$_3^-$ fluxes were small and directed into the sediment during spring at a rate of 0.01 mg N m^{-2} h^{-1}. In the dry season maximum NO$_3^-$ and NO$_2^-$ efflux rates were 0.7 mg N m^{-2} h^{-1} and 0.05 mg N m^{-2} h^{-1} at Sta. 4, respectively, and 0.28 mg N m^{-2} h^{-1} and 0.14 mg N m^{-2} h^{-1} at Sta. 6.
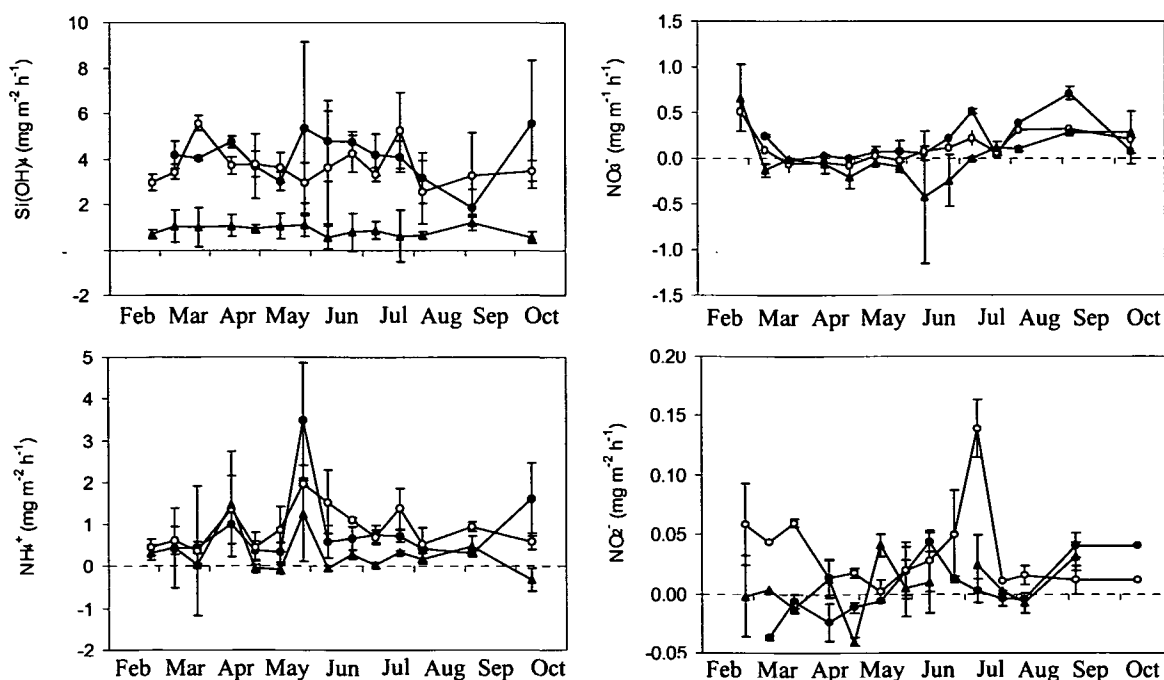
Fig. 4.9. Seasonal variation in the fluxes (mg m^{-2} h^{-1}) of Si(OH)$_4$, NH$_4^+$, NO$_3^-$ and NO$_2^-$ across the sediment-water interface at Sts. 4 (•), 6 (o) and 8 (▲). Each flux is the mean of triplicate analyses (±SD, n=3). Positive fluxes indicate release to the water column and negative fluxes indicate sediment nutrient uptake.

4.2.2. HYDROGRAPHICAL INFLUENCE ON BENTHIC-PELAGIC COUPLING

Offshore water input creates friction on the seabed and determines the flushing time, both of which indirectly regulate ria ventilation, phytoplankton nutrient availability and, therefore, the particulate organic material deposited and resuspended from the sediments. Accordingly, it is hypothesised that hydrodynamical processes ultimately dominate the sediment biogeochemistry in the Pontevedra Ria.

One important aspect of the hydrodynamical influence on sediment composition is highlighted in Fig. 4.6, where high BSi, PON and PON fractions were observed seaward of Tambo Island and along the northern coast. A 3D hydrodynamical model of the Pontevedra Ria [Taboada et al., 2000] revealed that seaward flowing surface water currents were deflected behind Tambo Island, weakened, downwelled and advected landwards. This circulation was thus presumably partly responsible for the size-distribution of particulates [Fig. 4.6d] and the spatial variability of BSi, POC and PON in the sediment [Fig. 4.6] [Table 1]. Similar trends have been observed in the adjacent Vigo and Arosa rias [Barciela et al., 2000; Torres López et al., 2001].

Given the hydrographical importance of offshore inputs of cold, nutrient-rich ENACW in the Pontevedra Ria [Prego et al. 2001] it is reasonable to assume that upwelling also plays an important role in the sediment biogeochemistry. However, little is known about the impact of upwelling stress and relaxation cycles on sediment regimes. The upwelling index [I_w, Fig. 2.2] can be used to assess the relative magnitude of landward water flux in the Pontevedra Ria. In spring, it can be seen that the NH_4^+ effluxes on April 13 and May 26 in Fig. 4.9 were concomitant with discrete upwelling events [Fig. 2.2], with up to 3.5 mg N m^{-2} h^{-1} at Sta. 4. $Si(OH)_4$ showed a similar efflux increase on May 26 at Sta. 4 close to the ria mouth. Benthic nutrient inputs have been observed previously in the data [Figs. 4.3 and 4.6], and a notable peak in bed sediment efflux of NH_4^+ and NO_2^- was noted at Sta. 3 in May [Fig. 4.1] coincident with the experimental flux result. Since NH_4^+ is absent in ENACW [Castro et al., 1998] and other aged shelf waters [Minas et al., 1982], the source alludes to remineralisation of organic matter from the spring bloom [Prego, 1994] with subsequent stirring by upwelling. Other workers have also described similar seasonal trends of organic matter oxidation along upwelling margins [e.g. Friedrich and Codispoti, 1981].

Literature evidence [Hansen and Blackburn, 1992; Conley and Johnstone, 1995; Sloth et al., 1995] suggests that these observations of NH_4^+ efflux in April and May possibly result from two separate detrital deposition events. Delayed remineralisation of the spring phytoplankton blooms is also conceivable, since NH_4^+ fluxes may take up to 15 days to return to steady state levels [Hansen and Blackburn, 1992]. However, SCUBA divers working in the narrow inner zone of the Rias Bajas have observed resuspension of bed sediment. The idea of decaying biological fluff of low settling velocity held in suspension above the sediment surface in response to tidal currents has been discussed as part of the recent North Sea Sediment Resuspension Experiment (SERE) [Jago and Jones, 1998; Millward et al., 1998]. Furthermore, the mineralisation of algal material results in increased porewater NH_4^+ concentration [Conley and Johnstone, 1995], which may be effluxed by advective flushing [Owens et al., 1986; Asmus et al., 1998; Uncles et al., 1998b]. The results of these workers prompt the hypothesis that the incoming water flux plays an important role in generating the large NH_4^+

effluxes throughout the ria by stirring of bottom waters. In support of this theory, the tongue of water characterised by oxygen undersaturation and near-bed emanation of NH_4^+ in March [Fig. 4.3] resembles remineralisation of quasi-benthic neutrally buoyant phytodetritus immediately above the sediment surface. This biological fluff is an important niche for microbial processes and was almost certainly incorporated in the sediment core extractions. Furthermore, *Doval et al.* [1997] noted high DOM concentrations and resuspension of carbon-rich POM in bottom waters of the Vigo Ria due to degradation of organic matter. There may also be an issue of pelagic or benthic nitrification [*Codispoti*, 1983; *Prego et al.*, 1999], possibly via bacteria adsorbed on SPM [*Owens*, 1986]. These intriguing observations highlight the need for more process-related investigation into how upwelling modifies benthic nutrient dynamics in the Pontevedra Ria.

In summer, the lower NH_4^+ and higher NO_3^- effluxes [Fig. 4.9] and the NH_4^+ and NO_2^- isoplots [Fig. 4.5] were evidence of benthic nitrification, and contrast other areas where summer was characteristically a period of low sediment nitrification potential, mainly due to depressed O_2 concentrations or high oxygen consumption [*Seitzinger et al.*, 1983; *Jenkins and Kemp*, 1984]. The prominent oxygen decrease [Fig. 4.5] and high Chl a concentration above the bed sediment [3.5 µg l^{-1}, Fig. 4.1] lend further support to this premise. An important feature of the data was a decrease in NH_4^+ efflux [Fig. 4.9] despite positive I_W [Fig. 3.2] and sediment loading of fresh biogenic material [Fig. 4.1]. An explanation for low NH_4^+ efflux may be found based on the laboratory resuspension experiments of *Sloth et al.* [1996], who highlighted the importance of the natural frequency of resuspension. In other words, regular summer upwelling in the Pontevedra Ria may impede accumulation of NH_4^+ at the benthic boundary layer by continual reworking of the sediment and fluff. Essentially, a similar sequence of events has been discussed by *Álvarez-Salgado et al.* [1996a] regarding rapid dispersal of NH_4^+ at the benthic boundary during upwelling in the Arosa Ria, and also by *Christensen et al.* [2000] who observed a "wash out" of sedimentary organic material by water bottom currents. Consequently, it is likely that resuspension was a likely fate of PON in summer, when high rates of PON export have also been observed in the adjacent Arosa and Vigo rias [*Prego*, 1994, *Álvarez-Salgado et al.*, 1996a].

4.2.3. SEDIMENT NUTRIENT PROCESSING

The rate of benthic nutrient processing can be assessed by first considering the $DIN:Si(OH)_4$ ratio of the nutrient efflux [hereafter $(N:Si)_F$] at Sts. 4, 6 and 8 during the spring and summer [Fig. 4.10], where DIN is the sum of the NO_3^-, NO_2^- and NH_4^+ fractions. An increase in $(N:Si)_F$ was noted at all stations, with positive upwelling stress in April and May, mainly due to the NH_4^+ efflux [Fig. 4.10]. The sediment flux data on the dates of sediment trap deployment [February–July; Fig. 4.7], reveal that the mean $(N:Si)_F$ at Sts. 4 (0.46) and 6 (0.57) were higher than those of the bed sediment particulate material (0.13 Sta. 4, 0.19 Sta. 6) but similar to the composition of the particulate material caught in the sediment traps (0.58 Sta. 4, 0.54 Sta. 6). This suggests that the majority of material remineralised and effluxed from the sediments was recently deposited algal matter. Low $(N:Si)_P$ in the bed sediment commonly arises from *in situ* oxidation of labile POC and PON in the water column and sediments, which increases the proportion of BSi and refractive material in the particulate matter [*Westrich and Berner*, 1984]. BSi

appears to be more resistant to microbial attack than POC and PON, since dissolution is partially impeded by the organic matrix surrounding diatom tests [*Bidle and Azam*, 1999]. Furthermore, as the porewaters become saturated with $Si(OH)_4$, further BSi dissolution is inhibited [*Hurd*, 1983], ultimately leading to sediment BSi preservation and burial and low particulate and $(N:Si)_F$ ratios [Fig. 4.10].

The amount of a particular nutrient (Nu) sequestered by the sediments is a function of the nutrient sedimentation rate $(dDropout /dt)$ and the net nutrient efflux rate $(dResus /dt)$ across the sediment-water interface. The sequestered nutrient was considered to be temporally buried or stored $(Nu_{storage})$. In addition, particulate detrital algal fluff may be resuspended. Direct measurements of resuspension were unavailable and, crucially, the data have shown that this was an important process in the Pontevedra Ria. Resuspension would lead to an overestimation of PON sedimentation. Consequently, assuming that 50% of the sedimented nutrient was resuspended, apparent $Nu_{storage}$ was quantified using the following mass balance, and shown graphically in Fig. 4.11:

$$Nu_{storage} = \left[0.5 \times \frac{dDropout}{dt} \right] - \frac{dResus}{dt} \qquad [4.1]$$
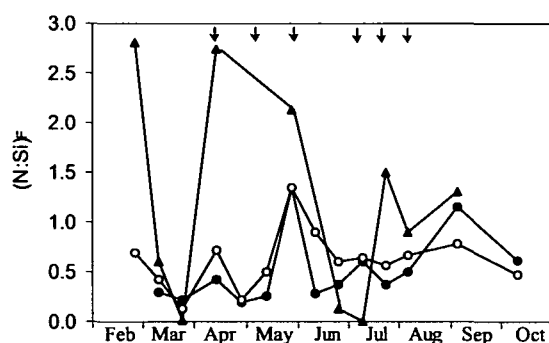
Fig. 4.10 (above). $(N:Si)_F$ molar ratio of the effluxed nutrients between February and October 1998 at Sts. 4 (●), 6 (o) and 8 (▲). The arrows represent periods of high water influx into the ria.
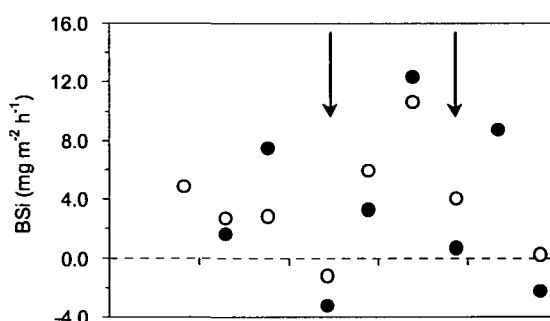
Fig. 4.11 (right). Apparent sediment storage of PON and BSi (mg m^{-2} h^{-1}) in the Pontevedra Ria at Sta. 4 (●) and Sta. 6 (o) between February and June 1998 calculated with [Eq. 4.1]. The arrows represent periods of high water influx into the ria.
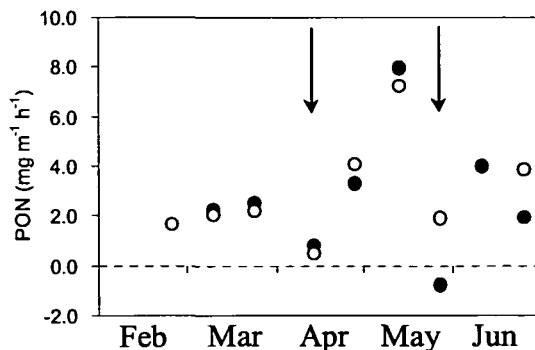
Steady state in bacterial biomass is assumed for Eq. 4.1 over the study period, despite the possibility of some nitrogen storage within this pool. With isolated upwelling (April 13 and May 26), both $N_{storage}$ and $Si_{storage}$ were low, and occasionally negative, indicating a sediment net nutrient loss. The bottom sediments sequestered Si and N throughout the sampling period, with mean rates of 3.5 (Sta. 4) and 3.6 mg Si m^{-2} h^{-1} (Sta. 6), and 2.7 (Sta. 4) and 2.9 mg N m^{-2} h^{-1} (Sta. 6). Employing the whole data set, there was a linear relationship between $N_{storage}$ and $Si_{storage}$ (reduced major axis regression

[*Sokal and Rohlf,* 1995]: $N_{storage}$ = 0.40 $Si_{storage}$ + 1.4; r^2 = 0.69, p<0.01). The sediment N:Si sequestration ratio was equal to 1.55 at Sta. 4 and 1.58 at Sta. 6 and, therefore, there appears to be a greater capacity for N removal compared to Si if the particulate material is considered phytoplanktonic, $(N:Si)_P = 1$.

Clearly then, additional N must have been lost from the sediments in order to preserve the surface sediment $(N:Si)_P$ ratio of ~0.1-0.2 [Fig. 4.8]. Organic N reaching the sediment will be buried, resuspended, remineralised and either effluxed or denitrified. The sediments at Sts. 4 and 6 were located below the 1% light level throughout the experiment and so benthic algal nutrient assimilation was presumed negligible. Burial was also ignored as this takes place over very long time scales. Resuspension is included in Eq. 4.1, and so assuming that denitrification was the remaining dominant process in the benthic nitrogen cycle, a first order estimate of net denitrification (D_{net}) can be calculated with a constituent flux balance across the benthic boundary [*Kamp-Nielsen,* 1992]. The sedimentation rate inferred from the sediment trap deployment is used, together with BSi and PON fractions in bed and suspended sediment and the net flux of N and Si across the benthic boundary layer. Assuming apparent $Si_{storage}$ was equal to true $Si_{storage}$;

$$D_{net} = \text{Apparent } N_{storage} - \text{True } N_{storage} \qquad [4.2]$$

$$\text{True } N_{storage} = \text{Sediment } (N:Si)_P \times \text{Apparent } Si_{storage} \qquad [4.3]$$

Sediment $(N:Si)_P$ in Eq. 4.3 was calculated from the particulate material contained in the top 0-1 cm of sediment, representing many years of sedimentation. The mean $(N:Si)_P$ of the sediment trap material (0.56) was substantially higher than the uppermost 0-1 cm of bed sediment (0.13-0.19) and implies that this sediment horizon was well degraded, although the possibility that a small amount of fresh organic material was included is acknowledged, which will tend to increase the D_{net} estimate.
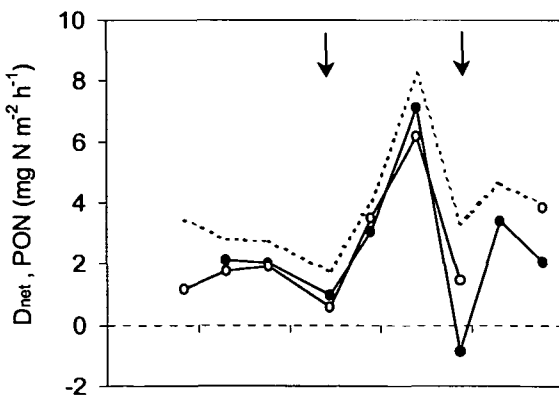
Fig. 4.12. Time-series net denitrification (mg N m^{-2} h^{-1}) at Sts. 4 (●) and 6 (○). The dotted line is the mean rate of PON flux (mg N m^{-2} h^{-1}) to the sediment at Sts. 4 and 6. The arrows represent periods of high water influx into the ria.

The time-series results for D_{net} and PON deposition at Sts. 4 and 6 are shown in Fig. 4.12. In view of the uncertainty in resuspension term, the error in D_{net} is ±50%. The negative value during late may was due to large NH_4^+ efflux from the sediments compared to sedimentation. After examining many combinations, there was no significant correlation between D_{net} and other physical (temperature, Brunt-Väisälä water column stability) or chemical (water column NO_3^-, NH_4^+ and O_2) parameters. An interesting

feature of Fig. 4.12 is the notable decrease in PON sedimentation and D_{net} when upwelling stress was high [arrows in Fig. 4.12]. Between upwelling, D_{net} showed a five-fold increase from 1.4 mg N m^{-2} h^{-1} in early April to 7.0 mg N m^{-2} h^{-1} in May. Mean D_{net} values were 2.5 mg N m^{-2} h^{-1} at Sts. 4 and 6. Regional denitrification estimates include 0.16 mg N m^{-2} h^{-1} for North Sea sediments [Lohse et al., 1996] and 9.8 mg N m^{-2} h^{-1} for the North Atlantic continental shelf [Seitzinger and Giblin, 1996]. Higher rates are generally observed in estuaries, with up to 140 mg N m^{-2} h^{-1} in the muddy reaches of the Thames Estuary, UK [Trimmer et al., 2000]. A more conservative range for temperate coastal sediments frequently quoted in the literature is 0.7-3.5 mg N m^{-2} h^{-1} [Seitzinger, 1988], and the Pontevedra Ria D_{net} falls well within this range.
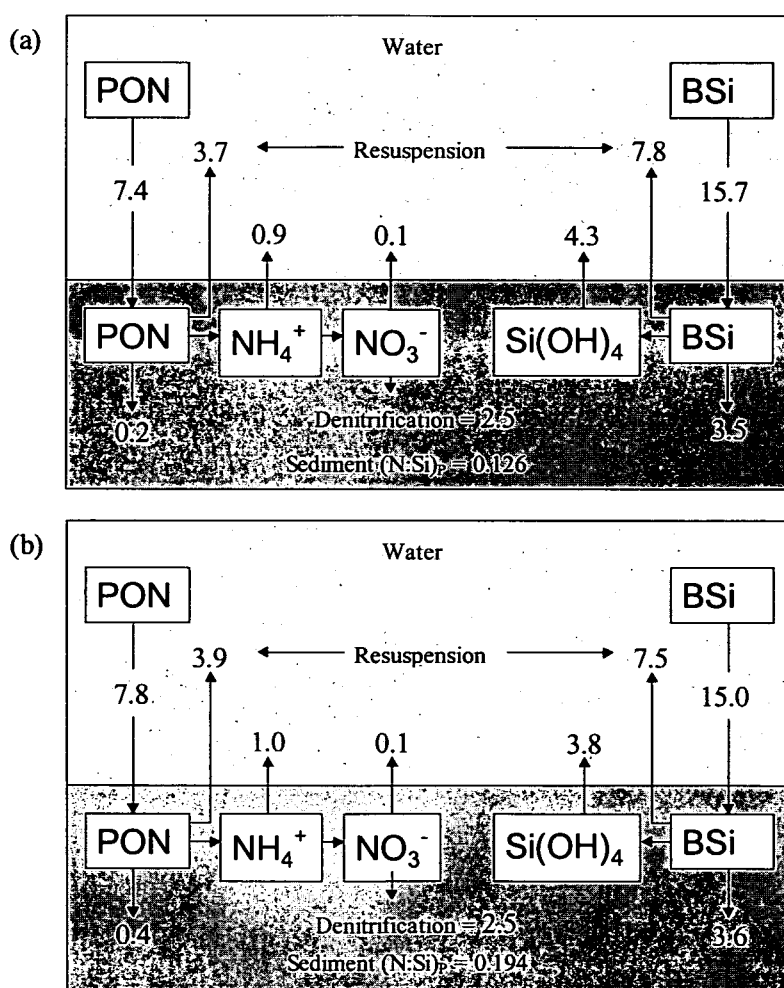
Fig. 4.13. Conceptual diagram for N and Si benthic-pelagic coupling in the Pontevedra Ria during spring 1998 at (a) Sta. 4 and (b) Sta. 6. Denitrification is estimated to be correct within ±50 % (see text). Units mg m^{-2} h^{-1}.

The conceptual balance in Fig. 4.13 summarises the benthic N cycling in the Pontevedra Ria during spring 1998. The imbalance between D_{net} and DIN efflux demonstrates that the sediments were a sink for N and consumed 34% of the sedimented PON at Sta. 4 and 33% PON at Sta. 6. Elsewhere, denitrification from NO_3^- diffusing into the sediments (commonly termed D_w) may act as a buffering mechanism for high NO_3^- loading from rivers [Trimmer

et al., 1998]. In the Pontevedra Ria, the small positive spring NO_3^- fluxes (0.1 mg N m^{-2} h^{-1}) suggest tight coupling of nitrification and denitrification and sedimentary NO_3^- buffering [*Jenkins and Kemp,* 1984]. It must be noted, however, that Eq. 4.1 overlooks several uncertainties, including denitrification outside the period of mass balance application, bioturbation [*Aller,* 1988], effluxes of DOM [*Enoksonn,* 1993] and possible anaerobic conditions during microcosm incubations. For example, *Rowden et al.* [1998a] estimated that bioturbation by the mud shrimp *Callianassa subterranea* turns over ~11 (kg dry sediment) m^{-2} y^{-1} in the North Sea, which also increases the porewater content of the sediment *Rowden et al.* [1998b]. A mass-balance more finely synchronised to the variability of upwelling would also be desirable [*Álvarez-Salgado et al.,* 1996a]. A sensitivity analysis of the independent terms in Eqs. 4.1-4.3 showed that the greatest uncertainty was the resuspension term, which was arbitrarily proposed as 50% of the sedimented material. It is entirely conceivable, however, that resuspension of algal fluff may provide a larger or smaller sink for PON. Further investigation of this hypothesis is required. For the present, the D_{net} estimate is considered to be a satisfactory agreement with other literature estimates.

4.2.4. UPWELLING ENHANCEMENT OF SEDIMENT BIOGEOCHEMISTRY

First order approximations suggest that the principal fate of benthic PON in the Pontevedra Ria was resuspension and denitrification, both of which appear to be influenced by positive upwelling stress. Water advection over the sediments will have an impact on disturbance and transport of sediment and hence the sediment nutrient source-sink term [*Li et al.,* 1997]. At the outset, upwelling was intermittent and dependent on wind-induced offshore water transport, leading to cycles of high and low primary productivity [*Rosón et al.,* 1999] and thus sedimentation. It seems further probable that a significant quantity of detrital material in the Pontevedra Ria was held in suspension above the bed sediment as neutrally buoyant fluff. The specific role of the quasi-benthic algal fluff in nutrient recycling remains unclear. It is hypothesised that regular organic matter deposition between upwelling cycles and the superficial fluff provide the substrate for coupled nitrification-denitrification across zones of distinct oxygen potential (termed D_n in the literature), in a similar fashion to faecal pellets in the sediment [*Jenkins and Kemp,* 1984]. Many areas of high denitrification are based on high concentrations of NO_3^- in the bottom water [e.g. *Nielsen et al.,* 1995; *Trimmer et al.,* 1998]. However, with low dissolved NO_3^-, such as in the Pontevedra Ria (mean±SD=4.18±0.33 µmol l^{-1}), experiments by *Rysgaard et al.* [1994] have shown that denitrification is favoured by high dissolved O_2 concentrations in the bottom waters. Upwelling maintains oxic conditions in the Pontevedra Ria, which may therefore be an important consideration for further denitrification studies. Moreover, nitrification will be promoted by the ventilating effect of offshore water input [*Jenkins and Kemp,* 1984; *Koike and Sørensen,* 1988; *Kemp et al.,* 1990], and there is further evidence to suggest that water column bacterial activity [*Wainright,* 1987], D_w and D_n increase after resuspension [*Nielsen et al.* 1990; *Sloth et al.,* 1996].

Many recent advances in the field of sediment POC and PON recycling have been reported in the literature. In this thesis, the advantages of considering the hydrodynamical characteristics of the system have been highlighted. This is important since well-defined biological processes such as

denitrification are intricately related to estuarine hydrodynamics via alteration of the dissolved oxygen concentrations by resuspension and, in the case of the Pontevedra Ria, stirring of quasi-benthic biogenic fluff. Benthic-pelagic particulate coupling in the Pontevedra Ria remains to be fully rationalised, although the rate of PON deposition appears to be important. For the reasons outlined in the previous paragraph, the direct effect of water advection on sediment nutrient cycling ought to be considered alongside the more obvious physico-biogeochemical processes which modify nutrient fluxes in the Galician Rias Bajas.

4.3. NET ECOSYSTEM PRODUCTION AND DENITRIFICATION IN THE PONTEVEDRA RIA

4.3.1. BUDGETING STRATEGY

The quantification of water exchange between estuaries and the coastal zone is one of the key research priority areas of the International Geosphere-Biosphere Program - Land Ocean Interaction in the Coast Zone (IGBP-LOICZ). The determination of residual estuarine water fluxes is of global importance for carbon export to the coastal zone [Gordon et al., 1996]. To this end, an online database of budgets for biogeochemical reactive elements is continually being expanded by contributions from researchers worldwide [http://www.nioz.nl/loicz].

Box models have been applied as quantitative investigative tools in the Rias Bajas and elsewhere with realistic results [Smith et al., 1991; Prego, 1993a; Pérez et al., 2000]. Using the advective fluxes derived in Chapter 3 [Box 1] the ria was treated as a stratified system, and separated into central and internal sections as before [Fig. 3.10]. In their work on the Arosa Ria, Álvarez-Salgado et al. [1996a] concluded that the central and internal ria present distinct hydrographical and biogeochemical characteristics, therefore justifying independent investigations.

The flux (mol s^{-1}) of a dissolved nutrient in the Pontevedra Ria is the product of the advective water flux, Q [m^3 s^{-1}, Box 1] and the nutrient concentration, Nu (mol m^{-3}). As for salinity, the mean inorganic nutrient concentrations in the upper and lower layers of each boundary [CS21 and CS14, Fig. 2.1 and 3.10] can be readily calculated by integration of the measured nutrient profile over the section, taking into account the geometric characteristics of the layer. Nutrient concentrations in the river and in the upper and lower layers of the central and internal ria are shown in Fig. 4.14. In this chapter, NO$_3^-$ and NO$_2^-$ concentrations are summed together, and defined as NO$_{3/2}^-$. Nutrient fluxes to the ria from the river Lérez and effluent are shown in Table 4.3, along with fluxes across the mouth of the ria at CS21. Nutrient gains and losses via precipitation and evaporation were assumed negligible compared to terrestrial and oceanic inputs.

The non-steady state biogeochemical budget for a dissolved inorganic nutrient, ΔNu, in a defined box or layer is the sum of the net hydrodynamic accumulation ($V\delta Nu/\delta t$) and the input ($Q_{in}Nu_{in}$) and output fluxes ($Q_{out}Nu_{out}$) across the boundaries of that box:

$$\Delta Nu = V\frac{\partial Nu}{\partial t} + \sum Q_{out} \times Nu_{out} - \sum Q_{in} \times Nu_{in}$$

[4.4]
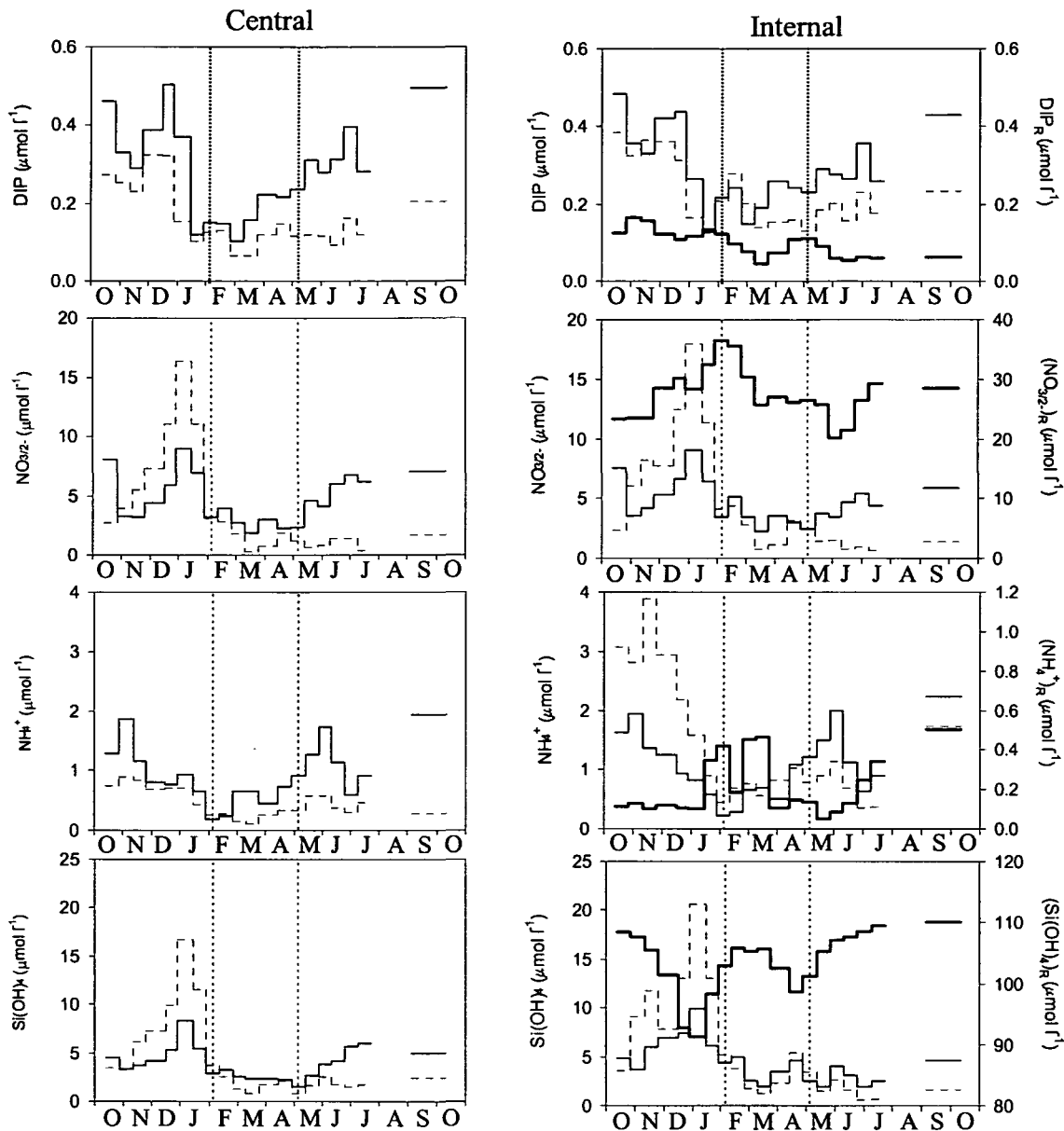
Fig. 4.14. Time series nutrient concentrations (μmol l⁻¹) in the upper (broken line) and lower layer (solid line) between two consecutive for central and internal Pontevedra Ria over the period October 1997-1998. Nutrient concentrations in the river Lérez (Nu_R, heavy line) are plotted on the secondary y-axis on the internal ria plots. The wet, spring and dry seasons are separated by the vertical dashed lines.

For the Pontevedra Ria, fluvial ($Q_R Nu_R$) and effluent ($Q_{EFF} Nu_{EFF}$) inputs must also be considered. Therefore, for the central or internal ria, ΔNu between two consecutive surveys is quantified with Eq. 4.5, where the overbar has been removed from the water flux and concentration terms [see Box 1]:

$$\Delta Nu = V \frac{\partial Nu}{\partial t} + (Q_S \times Nu_S) - (Q_B \times Nu_B) - (Q_R \times Nu_R) - (Q_{EFF} \times Nu_{EFF}) - Bn \qquad [4.5]$$

In view of the fact that the effluent discharges into the internal ria only, $Q_{EFF} \times N_{EFF} = 0$ for the central ria budget. Bn represents the benthic flux (mol s⁻¹), which can be either positive or negative. A negative value of ΔNu implies a net loss of inorganic material inside the ria and therefore net autotrophy,

and a positive value implies net heterotrophy. In the absence of non-conservative biogeochemical reactivity, the nutrient budget would be dependent only on physical mixing and transport processes, and $\Delta Nu = 0$. The seasonal and annual results for ΔNu are shown in Table 4.4, and time series ΔNu in the central and internal ria in Fig. 4.15. Fig. 4.16 shows ΔNu in the upper and lower layer of the central and internal ria. In view of the fact that the area of the central and internal ria are different (46×10^6 and 22×10^6, respectively), ΔNu is reported in area units (mg m^{-2} h^{-1}).

Table 4.3. Seasonal and annual fluvial and sewage nutrient fluxes and marine exchange fluxes across the mouth of the Pontevedra Ria at CS21 [Fig. 2.1] for October 1997-1998 [see Fig. 3.10]. Values in parenthesis correspond to the percentage contributions of each source to the total nutrient flux entering the ria. Units are in mol s^{-1} except values in bold (mmol s^{-1}).

Flux	Season	NO$_{3/2}^-$	(%)	NH$_4^+$	(%)	DIP	(%)	Si(OH)$_4$	(%)
Incoming	Wet season	13.79	(89	2.53	(89)	0.78	(99)	12.51	(69)
Q_{Lc}	Spring	5.91	(80	1.33	(48)	0.41	(98)	5.19	(41)
	Dry season	12.97	(96)	2.68	(54)	0.79	(99)	10.00	(68)
	Mean†	11.82	(92)	2.32	(54)	0.71	(99)	9.61	(58)
Outgoing	Wet season	21.79		1.77		0.58		22.00	
Q_{Uc}	Spring	3.09		0.54		0.24		3.54	
	Dry season	2.59		1.07		0.31		4.30	
	Mean†	10.23		1.22		0.43		11.01	
Fluvial	Wet season	1.63	(11)	**9.88**	(0.3)	**7.56**	(1.0)	5.69	(31)
Q_R	Spring	1.02	(15)	**8.01**	(0.3)	**3.33**	(0.8)	3.77	(30)
	Dry season	0.26	(2)	**1.44**	(0.0)	**0.75**	(0.1)	1.17	(8)
	Mean†	0.94	(7)	**6.32**	(0.1)	**3.80**	(0.5)	3.47	(21)
Effluent	Wet season	**54.02**	(0.3)	0.30	(10)	**3.51**	(0.4)	**29.26**	(0.2)
Q_{EFF}	Spring	**36.09**	(0.5)	0.33	(12)	**4.12**	(1.0)	**40.32**	(0.3)
	Dry season	**28.87**	(0.2)	0.39	(8)	**4.12**	(0.5)	**45.16**	(0.3)
	Mean†	**38.61**	(0.3)	0.35	(8)	**4.12**	(0.6)	**38.96**	(0.2)
Benthic	Wet season								
Bn	Spring	0.08	(1)	1.14	(41)	-		3.63	(29)
	Dry season	0.42	(3)	1.92	(39)	-		3.49	(24)
	Mean†	0.30	(2)	1.64	(38)	-		3.54	(21)

† Mean includes data for October 1997/1998

Pérez et al. [2000] suggested that the error of any nutrient budget ($\varepsilon_{\Delta Nu}$) between two-consecutive surveys (t_2-t_1) in the central or internal ria can be quantified as a linear combination of the error in the terms in Eq. 4.5:

$$\varepsilon_{\Delta Nu} = V \times \frac{2\varepsilon_{Nu}}{t_2 - t_1} + (2\varepsilon_{Nu} \times Q_U) + (Nu_B - Nu_U) \times \varepsilon_{Qu} \qquad [4.6]$$

where ε_{Nu} is the analytical error of the nutrient species [Table 2.6], Q_U is the advective flow across the boundaries CS21 or CS14 [Fig. 3.10], and Nu_B-Nu_U is the average vertical gradient in the central or internal ria. The mean $\varepsilon_{\Delta Nu}$ over the upwelling and downwelling seasons in the Arosa Ria [Pérez et al., 2000] was 3.6 mol s^{-1} for DIN, 0.35 mol s^{-1} for DIP and 2.3 mol s^{-1} for Si(OH)$_4$. For the central Pontevedra Ria, $\varepsilon_{\Delta Nu}$ equals 1.27±1.52mol s^{-1} for NO$_3^-$, 0.16±0.11 mol s^{-1} for NO$_2^-$, 0.27±0.15 mol s^{-1} for NH$_4^+$, 0.15±0.07 mol s^{-1} for DIP and 0.05±1.98 mol s^{-1} for Si(OH)$_4$. The individual $\varepsilon_{\Delta Nu}$ for each cruise in the central and internal ria are shown in Fig. 4.15.

The errors in Eq. 4.6 only considered the error in the boundary flows, and neglected the additional inputs from runoff and the benthos. Nevertheless, even considering the supplementary inputs, the uncertainty in interpolating and integrating the mean nutrient concentration in the upper and lower layers of the ria is dominant. If the integration error in Nu_U and Nu_L is assumed to be, say, 10% of Nu_U and Nu_L, then ε_{Nu} was found to increase by 1-2 orders of magnitude. This "oceanographic error" is propagated through Eq. 4.6 leading to a correspondingly large $\varepsilon_{\Delta Nu}$. Therefore, the actual error of the nutrient budgets must be significantly greater then the analytical error.

Assuming that the loss of inorganic material was due to photosynthesis of organic material, ΔNu can be used to estimate the net community production (NCP), equal to the difference between gross primary production (GPP) and phytoplankton respiration (Respn). Gross uptake and remineralisation cannot be distinguished with the box model approach. NCP was calculated by stoichiometric linkage from DIN (NCP$_N$) or DIP (NCP$_P$) assuming particulate organic material of Redfieldian compositional relationship (C$_{106}$N$_{16}$P) for phytoplankton [Redfield et al., 1963; Gordon et al., 1996]. NCP can be prorated over time and the spatial dimensions of the space layer or box. In this chapter, in agreement with box model formulations [Eq. 4.4], a negative NCP denotes net nutrient uptake (i.e. autotrophy), whilst a positive value denotes net nutrient remineralisation (i.e. heterotrophy).

The importance of nitrogen cycling in the Pontevedra Ria has been discussed in the previous section. In addition to the benthic estimate of D_{net}, a second estimate of net denitrification or net nitrification from the remineralisation of organic matter can be made from ΔNu assuming that DIP uptake by phytoplankton (ΔDIP) was 1/16 of DIN uptake (ΔDIN), i.e. N:P=16. Microbial nitrogen fixation of NO$_3^-$ from dissolved nitrogen gas can be considered negligible compared to nitrification of NH$_4^+$. The nitrogen anomaly, ΔN, for a layer was thus quantified as the difference between the total DIN budget (ΔDIN) calculated from Eq. 4.5 and the expected ΔDIN calculated from stoichiometric linkage of the phosphorus budget:

$$\Delta N = (\Delta DIN)_{observed} - (\Delta DIN)_{expected} \qquad [4.7]$$

$$(\Delta DIN)_{expected} = \Delta DIP \times N : P \qquad [4.8]$$

A positive value for ΔN denotes net remineralisation and a negative values denotes net denitrification. This approach assumes that nutrient uptake was due to phytoplankton uptake only [Smith and Hollibaugh, 1997].

4.3.2. SEASONAL NUTRIENT METABOLISM IN THE PONTEVEDRA RIA

Wet season. The data presented in the tables and figures are comparable to those reported in other studies of the Galician Rias Bajas [*Figueiras et al.*, 1986; *Prego*, 1994; *Prego et al.* 1995; *Rosón et al.*, 1995]. Wet season fluvial $Si(OH)_4$ concentrations [Fig. 4.14] averaged 101 μmol l⁻¹ $Si(OH)_4$, which agrees well with a reported mean concentration of 105 μmol l⁻¹ for the Rias Bajas [*Pérez et al.*, 1992]. $Si(OH)_4$ concentrations in the River Lérez, as with all the rivers in Galicia, [*Vergara and Prego*, 1997], decrease as the river flow increases. Persistently low dissolved DIP concentrations are a feature of Galician rivers [*Vergara and Prego*, 1997] and are likely to be a manifestation of the low use of artificial fertilisers and the low fluvial SPM concentrations [*Ibarra and Prego*, 1997]. Moreover, the river basin is dominated by acidic soils and, therefore, it is conceivable that DIP was not easily leached from the surrounding basin, thus resulting in the low concentrations found in the Lérez river.

Table 4.4. Seasonal and annual nutrient balance in the central and internal Pontevedra Ria for the period October 1997-1998 calculated with Eq. 4.5. Negative values denote a net loss of inorganic nutrients from the ria and positive values denote a net input. Units are in mg m^{-2} h^{-1} and converted to mol s^{-1} by multiplying by 12.78*(molecular mass)⁻¹ for the central ria and 6.11*(molecular mass)⁻¹ for the internal ria. NCP_N and NCP_P are in mg C m^{-2} h^{-1}. The values in parenthesis include the benthic nutrient fluxes, Bn. The area for the central ria is 46×10^6 m^2, and for the internal ria 22×10^6 m^2.

		$\Delta NO_{3/2}^{-}$		ΔNH_4^{+}		ΔDIP	$\Delta Si(OH)_4$		NCP_N		NCP_P
Central											
Wet	Total	-4.47	-	-4.59	-	-0.32	-11.63	-	-51.5	-	-13.0
	Surface	-11.42	-	-5.89	-	-1.22	-33.12	-	-98.3	-	-50.1
	Deep	+6.84	-	+1.12	-	+0.90	+21.21	-	+45.2	-	+36.8
Spring	Total	-1.23	(-1.25)	-1.01	(-1.38)	-0.23	-3.00	(-5.67)	-12.8	(-15.0)	-9.6
	Surface	-2.97	-	-1.39	-	-0.55	-6.40	-	-24.8	-	-22.8
	Deep	+2.62	(+1.72)	+0.48	(+0.11)	+0.36	+4.31	(+1.64)	+13.4	(11.3)	+14.6
Dry	Total	-6.58	(-6.75)	-0.89	(-2.21)	-0.74	-8.25	(-12.86)	-41.9	(-50.9)	-30.3
	Surface	-3.76	-	-1.03	-	-0.54	-3.22	-	-27.2	-	-22.2
	Deep	-2.98	(-3.15)	+0.15	(-1.17)	-0.23	-4.59	(-9.21)	-16.0	(-24.5)	-9.3
Mean†		-3.97	(-4.04)	-2.73	(-3.20)	-0.48	-7.12	(-9.22)	-38.3	(-41.6)	-19.6
Internal											
Wet	Total	+23.22	-	+6.92	-	-0.52	+42.88	-	+171.1	-	-21.3
	Surface	+6.27	-	+2.21	-	-3.29	+11.8	-	+48.2	-	-135.0
	Deep	+17.35	-	+4.66	-	+2.76	+32.87	-	+125.0	-	+113.3
Spring	Total	-7.68	(-7.79)	-0.49	(-1.69)	-0.49	-23.12	(-30.01)	-46.4	(-53.9)	-20.2
	Surface	-14.51	-	-1.06	-	-1.71	-30.67	-	-184.9	-	-135.0
	Deep	+7.47	(+7.36)	+1.87	(+0.67)	+1.24	+9.23	(+1.17)	+53.1	(45.6)	+51.0
Dry	Total	-10.64	(-10.92)	-2.80	(-5.50)	-0.71	-14.99	(-22.74)	-76.3	(-93.2)	-29.0
	Surface	-28.22	-	-9.18	-	-3.47	-37.72	-	-212.4	-	-142.2
	Deep	+17.77	(+17.48)	+6.41	(+3.71)	+2.75	+19.60	(+5.93)	+111.3	(97.7)	+112.9
Mean†		+0.98	(+0.82)	+1.78	(+0.64)	-0.58	+1.54	(-2.94)	+15.7	(17.0)	-24.0

† Mean includes data for October 1997/1998

Despite high nutrient concentrations in the effluent [µmol l⁻¹: 93 NO$_{3/2}$, 912 NH$_4^+$, 10 DIP and 97 Si(OH)$_4$] and river, the flux of nutrients to the ria was dominated by the ocean due to the large incoming flows [Fig. 3.11; Table 4.3]. The river Lérez and effluent discharges were important for Si(OH)$_4$ and NH$_4^+$, respectively, supplying 31% (Si(OH)$_4$) and 10% (NH$_4^+$) of total inputs.
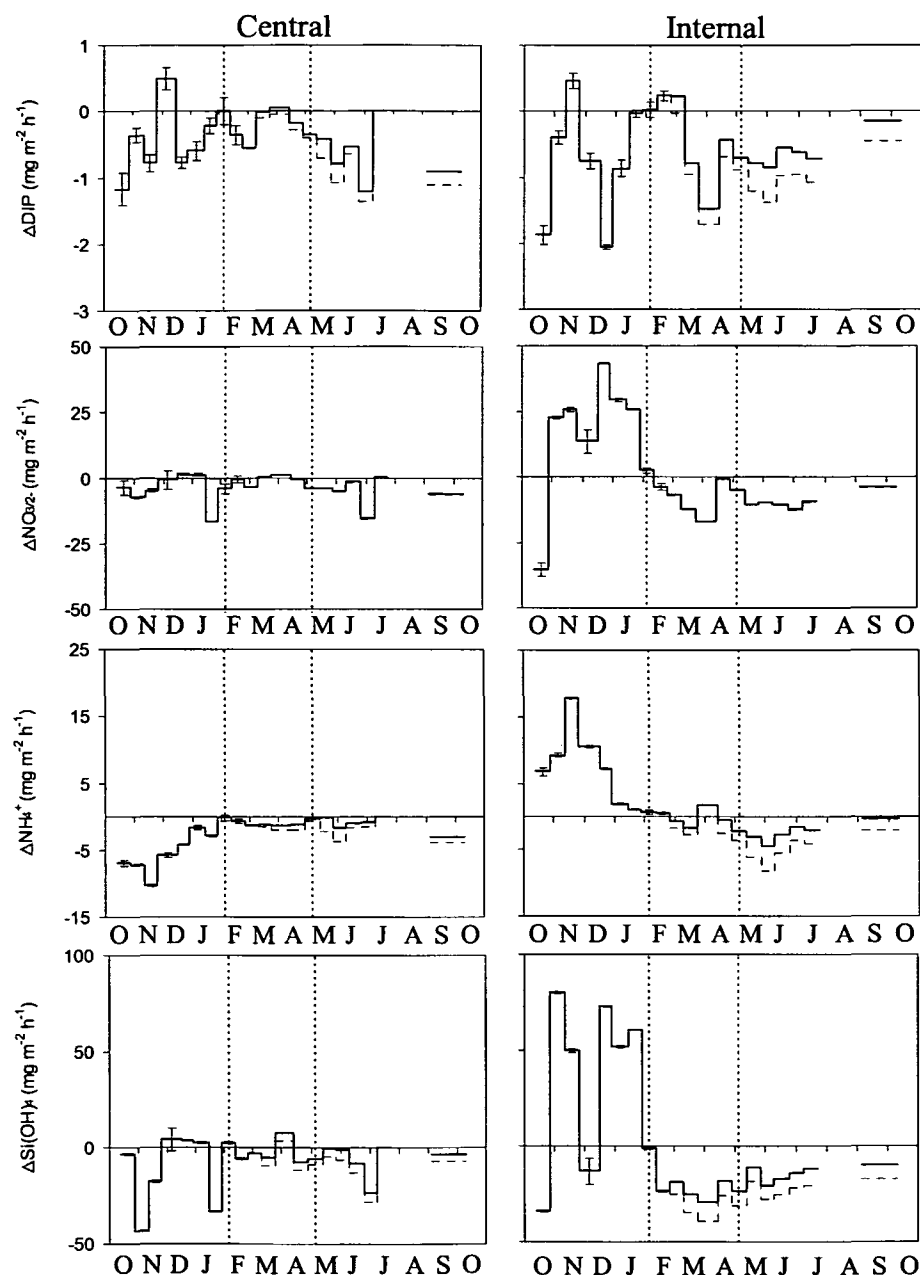
Fig. 4.15. Time series nutrient budgets (ΔNu, mg m⁻² h⁻¹) between two consecutive for the central and internal Pontevedra Ria over the period October 1997-1998. Negative values correspond to net uptake and positive values to net remineralisation. Where data are available, the benthic nutrient input, Bn, has also been included (broken line). The wet, spring and dry seasons are separated by the vertical dashed lines.

Spatial and temporal nutrient concentrations in the ria have been described in detail in the previous section, and here the discussion is restricted to the integrated concentrations in each layer of the box model. The nutrient concentrations measured in the lower incoming layer at CS21

in the central ria [Fig. 4.14] show a distinct bi-modal trend of high fluxes in the wet and dry seasons with lower concentrations in spring. With the exception of DIP and NH$_4^+$, mean upper layer nutrient concentrations in the wet season were almost double those in the lower layer due to runoff. In contrast, in the internal ria NH$_4^+$ showed highest wet season concentrations in the surface layer, reaching almost 4.0 µmol l^{-1} in November 1997. Internal ria surface layer concentrations at CS14 were higher than those at CS21 by 38±36% for DIP, 23±26% for NO$_{3/2}^-$, 208±105% for NH$_4^+$ and 50±56% for Si(OH)$_4$. There was considerably less variability in the lower layer, reflecting runoff-induced short-term variability in the surface layer, and seasonal influence of deep water concentrations [Nogueira et al., 1998].

Nutrient budgets in the central ria were heavily biased toward net uptake [Fig. 4.15], occurring exclusively in the surface layer whereas the lower layer was associated with remineralisation [Fig. 4.16]. In the internal ria the converse appears to be true, particularly for NO$_{3/2}^-$, NH$_4^+$ and Si(OH)$_4$ [Fig. 4.15]. Accordingly, mean wet season budgets [ΔNu, Table 4.4] showed net uptake in the central ria and net remineralisation in the internal ria, with the exception of DIP. The Pontevedra Ria was therefore net heterotrophic for DIN in the wet season, with large positive NCP$_N$ of +171.1 mg C m^{-2} h^{-1}, compared to uptake of -51.5 mg C m^{-2} h^{-1} in the central ria. Negative NCP$_P$ implies net carbon uptake, at rates of -13.0 and -21.3 mg C m^{-2} h^{-1} for the central and internal ria, respectively. Spatially integrated, the Pontevedra Ria was net autotrophic based on NCP$_P$ stoichiometry and net heterotrophic according to NCP$_N$, with uptake in the surface layers and remineralisation in the deep layer.

Spring. Mean spring nutrient concentrations in the Lérez river were not substantially different from those in the wet season [Fig. 4.14]. The lower runoff, however, led to a reduction in the fluvial nutrient flux to 1.02 mol NO$_{3/2}^-$ s^{-1}, 8.0 mmol NH$_4^+$ s^{-1}, 3.3 mmol DIP s^{-1} and 3.77 mol Si(OH)$_4$ s^{-1} [Table 4.3]. As for the wet season, effluent was an important source of NH$_4^+$ (12%). Nevertheless, 41% and 29% of NH$_4^+$ and Si(OH)$_4$ inputs, respectively, were from the benthic sediments, which illustrates the importance of this previously unquantified nutrient input.

From March to May the Pontevedra Ria was in a transitional state between the wet and dry seasons. The salient feature of the nutrient profiles [Fig. 4.14] was a reduction in nutrient concentration in the incoming and outgoing layers both at CS21 and CS14. Thereafter, bottom later concentrations showed a steep increase from mid-spring onward at both CS21 and CS14, coincident with the onset of upwelling [Fig. 3.2; Prego et al., 2001]. The rise in NH$_4^+$ concentration in the lower layer at CS21 [Fig. 4.14] and sustained influx of NH$_4^+$ from the ocean of 1.33 mol s^{-1} [Table 4.3] again alludes to remineralisation of organic matter from the spring bloom [Prego, 1994]. The nutrient enrichment was assimilated by the ria, which became a sink for all nutrients in both the central and internal sections [Table 4.4]. The trend of uptake in the surface layers and remineralisation in the lower layer was conserved [Fig. 4.16, Table 4.4]. Intriguingly, the internal ria in spring became the site of greatest nutrient uptake, with notable difference for NO$_{3/2}^-$ and Si(OH)$_4$ from the wet season to spring [Table 4.4.]. NCP was negative for the central and internal sections in spring with mean NCP$_N$ of -12.8 and -46.4 mg C m^{-2} h^{-1} in the central and internal rias, respectively, and NCP$_P$ of -9.6 and -20.2 mg C m^{-2} h^{-1}, respectively. Including the benthic input, NCP$_N$ in the central and internal ria increases to -15.0 and -53.9 mg C m^{-2} h^{-1}, respectively. Spring bloom production in the Arosa Ria reported by

Tenore et al. [1982] was -42 mg C m⁻² h⁻¹ and spring estimates of -83 mg C m⁻² h⁻¹ have been recorded in open ocean upwelling areas by *Codispoti et al.* [1986]. An increase in daylight hours and increased thermal stability in the upper water layers [*Prego et al.*, 2001] was presumably the reason for the nutrient uptake over the ria.
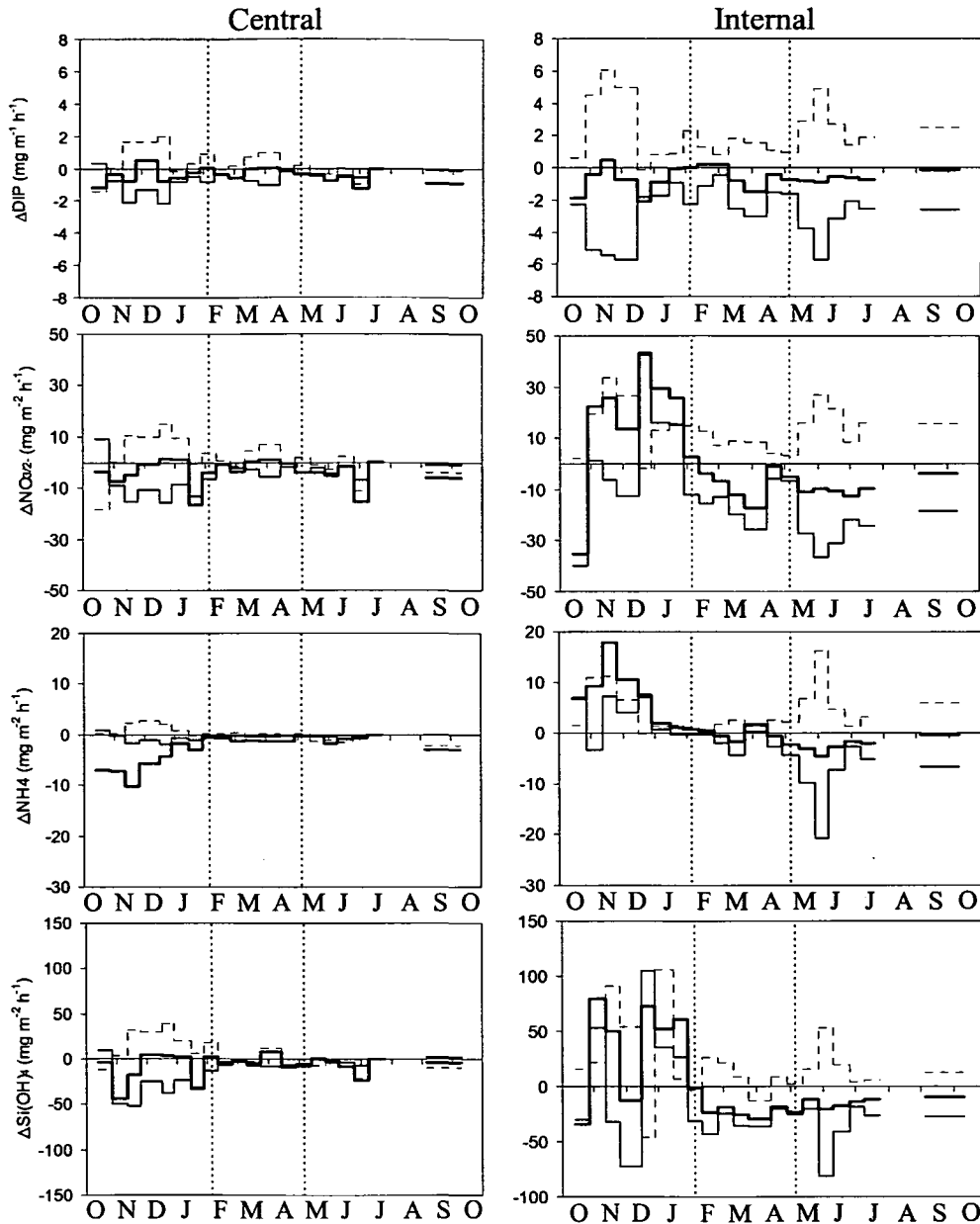
Fig. 4.16. Time series nutrient budgets (mg m⁻² h⁻¹) between two consecutive surveys for the upper (broken line) and lower (solid line) layer of the central and internal Pontevedra Ria over the period October 1997-1998. Negative values correspond to net uptake and positive values to net remineralisation. Lower layer budgets do not include benthic inputs. The mean budget for the central and internal ria from Fig. 4.15 has been reproduced for comparison (heavy line). The wet, spring and dry seasons are separated by the vertical dashed lines.

Dry season. Residual freshwater input decreased <0.5 m³ s⁻¹ in the dry season, with a corresponding decrease in nutrient fluxes [Table 4.3]. Fluvial nutrient inputs in the dry season were probably only of benefit to phytoplankton populations in the most internal parts of the ria.

Concentrations in the lower layer throughout the ria were more than double those in the upper layer due to upwelling and remineralisation [Fig. 4.14], in accordance with observations by $Prego$ [1994] in the Vigo Ria. Typical nutrient concentrations in ENACW situated outside the Rias Bajas were 8.2 μmol NO_3^- l^{-1}, 0.43 μmol DIP l^{-1} and 2.8 $Si(OH)_4$ μmol l^{-1}, respectively, NH_4^+ being absent [$Castro$ et $al.$, 1998]. Therefore, based on the mean nutrient concentrations in Q_{Lc} [Fig. 3.10], over shelf nutrient enrichment equals 50% and 100% of $Si(OH)_4$ and NH_4^+ inputs, respectively. Curiously, NO_3^- was 35% lower than in ENACW, which suggests an over-shelf sink of NO_3^-, possibly by benthic denitrification [Fig. 4.12].

Relatively high dry season surface layer nutrient concentrations at CS21 (mean values in μmol l^{-1}: 0.13 DIP; 1.27 $NO_{3/2}^-$; 0.35 NH_4^+; 1.19 $Si(OH)_4$) compared to, say, the Rias Altas on the northern Galician coast [$Prego$ et $al.$, 1999] suggest that total nutrient depletion by phytoplankton was impeded by regular upwelling events [Fig. 3.2; $Álvarez$-$Salgado$ et $al.$, 1993; $Doval$ et $al.$, 1998]. From Table 4.3, nutrient retention ([1-(output/inputs)*100] in the dry season was always higher than in spring, although never more than 70% for NH_4^+, DIP and $Si(OH)_4$, and 85% for $NO_{3/2}^-$. From Table 4.3, effluent NH_4^+ contributed ~3% of total ria productivity in the internal ria (~2 mg C m^{-2} h^{-1}) and thus constitutes a previously unconsidered [$Prego$, 1994; $Álvarez$-$Salgado$ et $al.$, 1996a] contribution to the overall productivity. Furthermore, including the benthic N input, NCP_N increase by 22% to -93.2 mg C m^{-2} h^{-1}. Thus, sediment nutrient enrichment constitutes almost 25% of nutrient uptake. However, this contribution is probably greater since the microcosms did not fully account for resuspension. Nevertheless, this is an important conclusion, particularly since benthic nitrogen cycling to date has not included in any budget for the Rias Bajas.

ΔNu for all nutrients indicated net uptake, with highest values in the internal ria [Table 4.4]. Spatially integrated NCP_N and NCP_P were -64.6 and -29.9 mg C m^{-2} h^{-1}, respectively, more than double spring values. Higher NCP_N than NCP_P is to be expected as a result of the extensive nitrogen redox chemistry [e.g. $Smith$ et $al.$, 1991], thus confirming the fact that nitrogen is a poor surrogate for carbon for estimating NCP compared to phosphorus [$Gordon$ et $al.$, 1996]. In the internal ria, the deep layer was associated with high rates of remineralisation of +97.7 mg C m^{-2} h^{-1} for NCP_N and +112.9 mg C m^{-2} h^{-1} for NCP_P, which essentially corroborates previous findings of net remineralisation in the lower layer. The NCP of the Pontevedra Ria is compared to other Rias Bajas estimates in Table 4.5. With regard to the Rias Bajas, the present values were well within the range of other workers. The large variability between reported estimates is disconcerting, and undoubtedly arises from methodological and sampling artefacts in addition to and inter-annual upwelling variability in the Rias Bajas [$Prego$, 1993a; $Álvarez$-$Salgado$ et $al.$, 1996a; $Rosón$ et $al.$, 1999]. The NCP_P value compares well to the mean upwelling area NCP of -34 mg C m^{-2} h^{-1} given by $Murray$ [1992], and -25 mg C m^{-2} h^{-1} for the Peruvian upwelling system [$Minas$ et $al.$, 1986]. Based on data from upwelling and non-upwelling areas [$Walsh$, 1988], $Smith$ and $Hollibaugh$ [1993] estimated an average continental shelf GPP of -18 mg C m^{-2} h^{-1} (160 gC m^{-2} y^{-1}). A good agreement was found between the NCP_P estimate and the estuarine average of -22 mg C m^{-2} h^{-1} given by $Boynton$ et $al.$ [1982].

Part of the NCP of the Pontevedra Ria will be assimilated by cultivated mussels. In the Arosa Ria, which contains 70% of total rafts in Galicia, mussels may assimilate up to 12% of the NCP [$Álvarez$-$Salgado$ et $al.$ 1996a].

The Pontevedra Ria contains 346 mussel rafts, or 11% of the total in the Rias Bajas. From the total carbon content of mussel wet weight [~2.5% *Tenore et al.*, 1982] and the mussel production of the Pontevedra Ria [2.61×10^7 kg y^{-1}; *Figueiras et al.*, 2002], the total mussel carbon content in the Pontevedra Ria is 6.53 kg $\times 10^5$ kg C y^{-1}. Taking the surface area of the ria as 145 km^2 and the mean upwelling season *NCP* as -0.72 g C m^{-2} d^{-1} (30 mg C m^{-2} h^{-1}), then the mean *NCP* for the upwelling season is -1.89$\times 10^7$ kg C (assuming 180 day growth period). Therefore, mussels incorporate 3.5% of organic carbon produced in the Pontevedra Ria.

Table 4.5. Literature values of gross primary production (*GPP*) and net community production (*NCP*) in the Rias Bajas (mg C m^{-2} h^{-1}). Where applicable, values were converted from ΔO_2 and ΔDIN using a photosynthetic respiratory quotient of 1.4 (O:C =1.4; characteristic of a system in which nitrate supports net primary productivity: *Laws* [1991]) and C:N = 106:16. Estimates correspond to dry season averages. Negative values correspond to net autotrophy and positive values to heterotrophy.

	Method	*GPP*	*NCP*	Reference
Vigo Ria	Light-dark incubations	-87.5 to -112.5		*Moncoiffé et al.* [2000]
	DOC mass balance		18.4 to -22.5	*Álvarez-Salgado et al.* [2001]
	DIC mass balance		1.3 to -27.7	*Prego* [1993a]
Arosa Ria	DIC mass balance		-34.8±20.1	*Pérez et al.* [2000]
	N mass balance	-58.3	-48.9	*Álvarez-Salgado et al.* [1996a]
	DIC mass balance		-35	*Rosón et al.* [1999]

The mean annual spatially integrated *NCP* in the Pontevedra Ria was -33.6 mg C m^{-2} h^{-1} for *NCP$_N$* and -23.0 mg C m^{-2} h^{-1} for *NCP$_P$*. Thus, the Pontevedra Ria was net autotrophic, although alternating between net heterotrophy in the wet season and autotrophy in the dry season. These findings lend no support to a general tendency towards net heterotrophy in marine systems [*Smith et al.*, 1991], presumably due to low fluvial loading of allocthonous organic material [*Smith and Kemp*, 1995] for which, unfortunately, adequate supporting data is lacking. However, the large differences between *NCP$_N$* and *NCP$_P$* over the sampling period highlight the complexity of ria biogeochemistry. The extent to which short term variability in nutrient fluxes across the ria boundaries influence *NCP* cannot be ascertained from the data set, and highlights the need to investigate more thoroughly the biogeochemistry of the upwelling cycle with regard to export of organic material and remineralisation.

4.3.3. STOICHIOMETRY OF ECOSYSTEM NUTRIENT METABOLISM

The potential limiting nutrient to net production in the Pontevedra Ria can be identified from the molar composition of dissolved inorganic nutrients and the anomaly from the Redfield ratio (DIN:DIP=16:1). Phytoplankton growth

was assumed to be limited by nitrogen if DIN:DIP<16 and DIN:Si(OH)4<1 [hereafter $(N:P)_D$, $(N:Si)_D$]. Conversely, $(N:P)_D>16$ and $(N:Si)_D>1$ denotes phosphorus and silicon limitation with respect to nitrogen, respectively. The ratios are indicative of potential limitation only, since the concentration of the limiting nutrient may be present at saturating levels.

$(N:P)_D$, $(N:Si)_D$ and $(Si:P)_D$ seasonal ratios for the river, effluent and advective flows at CS21 and CS14 are shown in Table 4.6. There was a general trend of DIN limitation with respect to both DIP and $Si(OH)_4$. Phosphate limitation was only observed in the wet season, when runoff of DIP-depleted freshwater was highest. In spring, the surface waters became potentially DIN limiting for phytoplankton growth. This could be partly due to decreased runoff [Fig. 4.15]. Similar seasonal variations in nutrient limitation were made in the Delaware Estuary [*Pennock and Sharp*, 1994] and Chesapeake Bay [*Malone et al.*, 1996], where transformation to DIN limitation roughly coincided with the collapse of the spring bloom. During spring and summer, the ria was more influenced by offshore ENACW inputs. *Levasseur and Therriault* [1987] suggested that the limiting nutrient in the upwelling water mass may be the dominant factor controlling phytoplankton community structure. The $(N:P)_D$ at $CS21_L$ [Table 4.6] during spring and the dry season were considerably lower than the mean $(N:P)_D$ observed at Sta. 0 in the mouth of the ria (26±18), and on the shelf [*Prego et al.*, 1999; *Álvarez-Salgado et al.*, 1997] and is evidence of potential DIN limitation to phytoplankton growth. The $(N:Si)_D$ ratio of ~0.7 in the Pontevedra Ria also suggests DIN limitation, and compares to 2.5-3.5 in ENACW source waters on the shelf [*Álvarez-Salgado et al.*, 1997] and 1.9±1.0 at the mouth of the Pontevedra Ria recorded in this study. Moreover, DIN limitation is further suggested by the dry season budget $\Delta DIN:\Delta Si(OH)_4$ of ~0.7 [Table 4.4]. However, rapid changes in species succession between siliceous diatoms and non-siliceous dinoflagellates [*Tilstone et al.*, 1999; *Figueiras et al.*, 2002] may partially negate the usefulness of $\Delta DIN:\Delta Si(OH)_4$ ratios in this context.

The 9% decrease in $(N:P)_D$ between $CS21_L$ and $CS14_U$ during the dry season alludes to increasing landward DIN limitation. Conversely, $(N:Si)_D$ increased from 0.7 to 0.9, and $Si(OH)_4:DIP$ decreased from 5.7 to 4.2. Rapid DIP recycling compared to DIN would explain the landward decrease in $(N:P)_D$ and $(Si:P)_D$ [*Garber*, 1984]. A reduction in $(N:P)_D$ and $(N:Si)_D$ upon transit through the Arosa Ria was noted by *Pérez et al.* [2000]. *Álvarez-Salgado et al.* [1997] also suggested that similar observations on the shelf were due to in situ $Si(OH)_4$ and DIP recycling rather than DIN removal. Low $(N:Si)_D$ and nitrogen limitation are a feature of upwelling areas elsewhere [*Treguer and Le Corre*, 1979; *White and Dugdale*, 1997]. In spring and the dry season, $(N:P)_D$ and $(N:Si)_D$ showed further decreases by up to 50% as the water was lifted to the surface layer of the internal ria from the deep layer, and $(Si:P)_D$ decreased by 31%. Since the river and effluent remained poor in DIP, there appeared to be prevailing DIN removal from the system in the internal ria, coupled to a more general trend of increasing DIN limitation as water upwelled into the ria. Subsequently, the extent of DIN limitation relaxed towards the central ria and $(N:P)_D$ and $(N:Si)_D$ ratios presented a slight increase.

Fig. 4.17 shows the temporal evolution of net nitrogen anomaly from Redfieldian uptake, ΔN [Eq. 4.6]. The figure shows that net denitrification was predominant in the upper central ria in the wet season with a mean denitrification rate of 8.49 mg N m^{-2} h^{-1}. The upper internal ria, in contrast, displayed high rates of net nitrogen remineralisation in the wet season at 32.3 mg N m^{-2} h^{-1}. Therefore, the majority of nutrient remineralisation in the

Pontevedra Ria appeared to take place in the surface waters, in accordance with the Arosa Ria [Pérez et al., 2000]. A plausible explanation could be remineralisation of river-borne allocthonous material. However, it is unclear why denitrification should be greatest in the surface layer, as presumably denitrification is a predominantly benthic process in pristine coastal systems.

Table 4.6. (N:P)$_D$, (N:Si)$_D$ and (Si:P)$_D$ ratios for the upper (U) and lower (L) boundaries at CS21 and CS14 over the period November 1997-September 1998. Stoichiometric ratios are calculated according to Si$_{16}$N$_{16}$P.

	Season	CS21$_L$	CS21$_U$	CS14$_L$	CS14$_U$	River	Effluent
(N:P)$_D$	Wet season	12.4	23.8	12.3	24.6	123	68
	Spring	9.2	7.0	9.1	8.5	175	45
	Dry season	8.8	5.4	8.0	4.0	275	43
	Mean[†]	9.8	11.7	9.5	12.1	178	51
(N:Si)$_D$	Wet season	0.6	0.6	0.5	0.5	0.1	6.1
	Spring	0.8	0.5	0.8	0.6	0.1	4.7
	Dry season	0.7	0.7	0.9	0.7	0.1	4.1
	Mean[†]	0.7	0.6	0.7	0.6	0.1	4.9
(Si:P)$_D$	Wet season	9.6	22.7	11.7	24.5	405	5.5
	Spring	6.2	6.8	6.5	8.5	670	4.8
	Dry season	5.7	5.1	4.2	2.9	1137	5.0
	Mean[†]	6.8	11.3	7.2	11.5	689	4.9

[†] Mean includes data for October 1997/1998
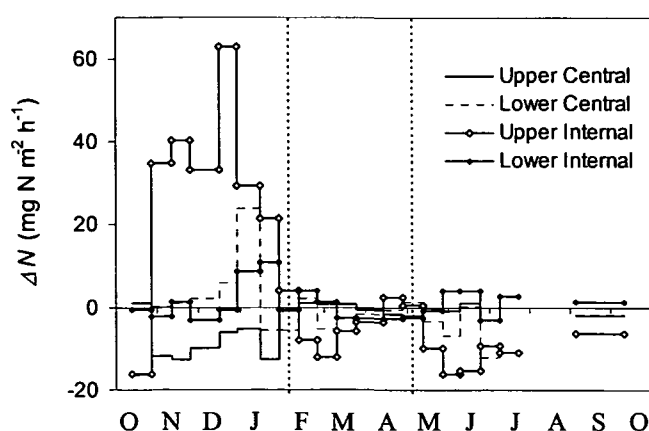
Fig. 4.17. Time series ΔN (mg N m^{-2} h^{-1}; Eq. 4.7) between two consecutive for the upper and lower layer of the central and internal Pontevedra Ria over the period October 1997-1998. Negative values correspond to net denitrification and positive values to net nitrification. Benthic budgets are included in the lower layer data.

The spring and dry season ΔN data include the benthic effluxes. During spring, net denitrification was 0.47 mg N m^{-2} h^{-1} in the central ria and 2.97 mg N m^{-2} h^{-1} in the internal ria. These N losses were equal to 21% and 36% of spring NCP_N, respectively [Table 4.4]. In the dry season, net denitrification

increased to 1.82 mg N m^{-2} h^{-1} and 5.66 mg N m^{-2} h^{-1} for the central and internal ria, respectively, equal to 27% and 42% of dry season NCP_N. Increasing denitrification in the dry season accords with the previous discussion on benthic nutrient remineralisation. These values compare to 2.52 mg N m^{-2} h^{-1} obtained previously by the mass balance at the sediment-water interface and falls within the range denitrification of 0.7-2.8 mg N m^{-2} h^{-1} for coastal marine sediments given by *Seitzinger* [1988], and further examples in a review by *Koike and Sørensen* [1988]. In view of the uncertainties in both budgeting approaches, this is considered to be a good agreement and supportive of the hypothesis that the Pontevedra Ria acts as a sink for DIN in spring and summer.

Apparent denitrification may be partly due to DIP release from sediments if they become oxygen stressed during upwelling relaxation, similar to observations in Chesapeake Bay [*Boynton and Kemp*, 1985]. Further explanations include preferential remineralisation of DIP from sinking particles [*Karl et al.*, 1996], faster recycling of DIP compared to DIN [*Garber*, 1984] and desorption of particulate phosphate upon freshwater and seawater mixing [*Morris et al.*, 1981; *Crosby et al.*, 1984; *Froelich*, 1988; *Fox*, 1989; *Lebo*, 1991]. There is a significant lack of publications dedicated to the biogeochemical phosphorus cycling in the Rias Bajas [*Prego*, 1993a] and the importance of these above processes to the Pontevedra Ria remains unexplained. With regard to the Galician shelf, *Álvarez-Salgado et al.* [1997] ruled out denitrification, on the basis that the observed O_2:DIN remineralisation ratio of 9.5-10.5 in the water column agreed with aerobic degradation of organic matter. Similar conclusions were made by *Pérez et al.* [2000] for the Arosa Ria and *Nogueira et al.* [1997a,b] for the Vigo Ria. However, whilst it is agreed that rapid DIP recycling may form an integral part of nutrient recycling in the landward advected waters, denitrification will reduce the pool of total DIN whilst O_2 concentrations will be unaffected. *Pérez et al.* [2000] calculated ΔDIN:ΔDIP uptake of ~21 for the upwelling season in the Arosa Ria. Thus in their case, denitrification would equal 5 mol s^{-1} for the whole ria, or 1.38 mg N m^{-1} h^{-1}. Moreover, the ΔDIN:ΔDIP remineralisation ratio in the deep layer during spring and the dry season is ~7 [Table 4.4] which is further suggestive of preferential DIN loss in the deep layer. Denitrification has been reported in upwelling systems worldwide [*Friedrich and Codispoti*, 1979; *Codispoti*, 1983; *Codispoti et al.*, 1986; *Braga and Müller*, 1998; *Tyrell and Lucas*, 2002;]. *Tyrell and Law* [1997] have suggested that deviation from Redfield ratios in upwelling areas indicates potential denitrification when oxygen concentration is below saturating. Furthermore, denitrification may occur even in oxygenated waters if a close coupling of nitrification and denitrification exists within detrital aggregates [*Jenkins and Kemp*, 1984]. Therefore, denitrification hypothesis would explain progressively low $(N:P)_D$ ratios in the upwelling water in the Pontevedra Ria and further corroborate the benthic mass balance developed in the previous section.

4.4. COUPLED SALT-HEAT THERMOHALINE MASS BALANCE: APPROACHES AND CONSIDERATIONS FOR MODELLING

Recent studies on the Rias Bajas have focussed on the influence of upwelling and downwelling processes on ria hydrography and biogeochemistry [*Prego*

and Fraga, 1992; Álvarez-Salgado et al., 1993; Castro et al., 1994]. Early investigations applied a stationary state salt budget to the Vigo Ria to quantify the upwelling water flux [Prego and Fraga, 1992] and subsequent nutrient budgets [e.g. Prego, 1993a]. However, shortly afterwards it was realised that steady state models were unsuitable due to the short-term variability in salinity at the mouth of the ria [Álvarez-Salgado et al., 1993]. Accordingly, Rosón et al. [1997] adapted previous ideas of a weighted salt-heat budget [Rahm and Wulff, 1992] to the Arosa Ria in order to circumvent the problem of low salinity variability. In addition, their data were temporally resolved on a scale of 3-4 days to more adequately capture the short-term thermohaline variability. In this work, an iterative method has been developed for calculating advective fluxes. On the basis of box-models, horizontal advective fluxes [Álvarez-Salgado et al., 2000] and net ecosystem production [Pérez et al., 2000] have been parameterised with the upwelling index. Moreover, Gilcoto et al. [2001] applied inverse modelling techniques to data from the Vigo Ria where the results appear to both qualitatively and quantitatively substantiate previous findings using traditional box-modelling techniques. To a first approximation, the results these workers are an encouraging indication of our further understanding as to how the rias function under different oceanographic and meteorological influences.
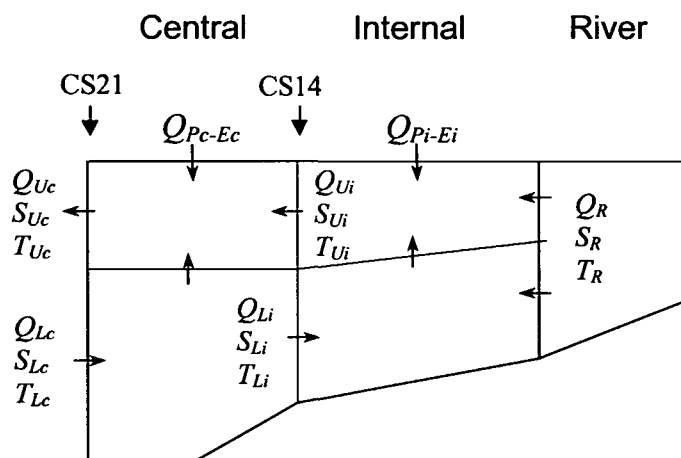
Fig. 4.18. Advective fluxes employed in the salt-heat budget. Boundaries CS21 and CS14 are shown.

Due to the current interest in box-modelling, it was decided to critically evaluate the usefulness of box models to the Galician Rias Bajas, in particular the salt-heat model [Rosón et al., 1997]. Firstly, daily values of S and T at the boundaries CS21 and CS14 [Fig. 4.18] were derived from the original data using multiple regression techniques. Subsequently, daily individual salt and heat fluxes were calculated with a non-steady salt and heat budget. Advective water fluxes were derived from the salt balance following the methodology in Box 1. The additional equations necessary for quantifying the advective flux derived from the heat budget are described in Box 2. These fluxes are subsequently combined in the way advocated by Rosón et al. [1997] and Álvarez-Salgado et al. [2000] to derive the combined non-steady salt-heat weighted budget. Since daily resolved S and T boundary conditions are used, the iterative methodology was substituted for the more traditional non-steady state formulation [Officer, 1981; Box 2]. For meeting the objectives of this section, it was not necessary to quantify the vertical

advective and non-advective mixing fluxes between the upper and lower layers. Finally, the suitability of these methods to the Rias Bajas is addressed by performing a rigorous sensitivity analysis of the model input parameters.

4.4.1. WEIGHTED SALT-HEAT BUDGET

This section describes the derivation of daily S and T data required for calculating advective fluxes [Box 2] in the two layers at the CS21 and CS14 boundaries [Fig. 4.18]. It is now well recognised that accurate water flux estimates for the Rias Bajas depend on a sampling resolution that captures the short-term thermohaline variability [Álvarez-Salgado et al., 2000]. The present data is fortnightly resolved, and therefore the intermediate S and T data in the upper $(ST)_U$ and lower $(ST)_L$ layer at each boundary were interpolated with a stepwise multiple regression analysis. The independent variables for the regression were the upwelling index (I_W, m^3 s^{-1} km^{-1}, 3 d moving average filter), local winds resolved along the ria axis (W_L, m s^{-1}, 2 d moving average filter) and total freshwater input up to the boundary (Q_Z, m^3 s^{-1}). These parameters appear to be instrumental in determining S and T in the Rias Bajas [Nogueira et al., 1997a,b]. For the lower layer, W_L was not considered in the regression. This section is not overly concerned with predicting rigorously accurate thermohaline data with the regression, but rather more concerned with addressing the suitability of the salt-heat box-model approach under what can be considered as typical thermohaline conditions. Consequently, a realistic temporal evolution of $(ST)_U$ and $(ST)_L$ is the objective. The regression equations take the form:

$$S,T = C_1 + (C_2 \times A_1 \times Q_Z) + (C_3 \times A_2 \times I_W) + (C_4 \times A_3 \times W_L) \qquad [4.9]$$

where C_1, C_2, C_3 and C_4 are constants derived directly from the statistical multiple regressions. A_1, A_2 and A_3 are temporally variable constants introduced as maximising factors to prevent unrealistically high or low values of $(ST)_U$ and $(ST)_L$ engendered by extreme values of I_W.

The accuracy of the water fluxes is dependent on the daily variability in the model tracers of water exchange; freshwater (Q_Z) for the salt budget, and Q_Z and T for the heat budget. If the residence time, τ, of the Pontevedra Ria were □1 day daily values of Q_Z and T could be employed with confidence since short-term variability in Q_Z and T would be detected at the mouth of the ria. However, when τ is substantially longer than 1 day the time period over which daily variables are to be averaged before insertion into the model requires careful consideration. Nogueira et al. [1997a] termed this the "system functional autonomy", or the time scale at which coupling between external forcing factors and model parameters can be determined. A measure of how τ and therefore functional autonomy changes under different conditions of runoff and upwelling, forms an essential basis for budgeting. For example, it is futile to use weekly averages of Q_Z and T if τ is typically of the order of a tidal cycle. Equally, inserting daily values for Q_Z and T in the model is inadequate if τ is considerably longer than 1 day. Therefore, the derived $(ST)_U$ and $(ST)_L$ data were processed with a 12 d moving average filter, based on the mean residence time of the ria [~9 d, Fig. 3.12] and literature reports of the 14±4 d upwelling frequency by Álvarez-Salgado et al. [1993] and Blanton et al. [1984]. The same averaging procedure was applied to the

model input parameters [Qz, H, Tz; Box 2] to filter out random runoff and heating events which may otherwise introduce noise into the final result.

BOX 2. Derivation of weighted salt-heat budget

Surface heat exchange

Compared to shelf seas [*Taylor and Stephens*, 1983], temperature changes engendered via advective water flows are important in estuarine systems [*Uncles and Stephens*, 2001]. Therefore, the heat budget must include heat gain and loss processes [*Bunker*, 1976; *Fischer et al.*, 1979] across the water surface. Net heat exchange, H (W m^{-2}), is a balance of heating and cooling processes. Heat gain from short-wave radiation (H_{SW}, W m^{-2}) was determined directly from pyranometer readings [Fig. 2.3]. For comparison, H_{SW} was also determined theoretically at 42° N latitude using a value of 0.76 for atmospheric absorption [*Uncles and Stephens*, 2001].

Sensible (convective) heat loss (H_S) was calculated as:

$$H_S = -\rho_a C_S C_{PA} W_L (T_C - T_A)$$
[4.10]

where ρ_a is the density of air (1.22 kg m^{-3}), C_S is an empirical coefficient [*Bunker*, 1976] typically 1.45×10^{-3}, C_{PA} is the specific heat of air (1.012×10^3 J kg^{-1} °C^{-1}), W_L is the wind speed (m s^{-1}), T_C is the surface water temperature (°C) and T_A is the air temperature (°C).

Long-wave radiation heat gain from atmospheric water vapour (H_1) is quantified with the cloud cover fraction (C):

$$H_1 = 5.18 \times 10^{-13} (1 + 0.17 \times C^2) \times (273 + T_A)^6$$
[4.11]

Radiation heat loss per unit area from the estuary's water surface (H_2):

$$H_2 = -5.23 \times 10^{-8} (273 + T_C)^4$$
[4.12]

Heat loss due to evaporation, H_E, was calculated by from the rate of evaporation (E, mm d^{-1}, Fig. 2.4), the latent heat of evaporation (L_W, typically 2.4×10^6 J kg^{-1}) and the number of seconds per day ($S:D$):

$$H_E = \frac{E}{S:D \times 10^3} \times L_W$$
[4.13]

Finally, the heat budget (H, W m^{-2}) across a representative area of the ria is the sum of the individual heat terms:

$$H = H_{SW} + H_1 + H_2 + H_S + H_E$$
[4.14]

Continued overleaf...

<div style="border:1px solid">

BOX 2. Continued...

Residual fluxes

As for salt flux [Eq. 3.3, Box 1] *Álvarez-Salgado et al.* [2000] defined the average surface layer heat flux, $\overline{Q_U T_U}$, at each boundary between two consecutive surveys (t_1 to t_2) as:

$$\overline{Q_U T_U} = \frac{\int_{t_1}^{t_2} Q_U(t) T_U(t)\, dt}{t_2 - t_1} \qquad [4.15]$$

However, with daily data, the non-steady state form of Eqs. 3.5 and 3.7 [Box 1] can be used to calculate the surface advective flux derived from the salt budget $(\overline{Q_U})_S$:

$$(\overline{Q_U})_S = \frac{(\overline{Q_Z} \times \overline{S_L}) + V \frac{\Delta S}{\Delta t}}{\overline{S_L} - \overline{S_U}} \qquad [4.16]$$

Hence for heat, employing the heat input from the residual freshwater inflow, $\overline{Q_Z T_Z}$, and surface heat exchange, H:

$$(\overline{Q_U})_T = \frac{\overline{Q_Z}(\overline{T_L} - \overline{T_Z}) - H + V \frac{\Delta T}{\Delta t}}{\overline{T_L} - \overline{T_U}} \qquad [4.17]$$

Heat transfers are considered as advected fluxes of temperature, and therefore H (W m^{-2}) is transformed to °C m^3 s^{-1} with the latent heat of water (4.185 kJ kg^{-1}) and extrapolated to the total ria surface area.

Rosón et al. [1997] combined the advective fluxes due to salinity [Eq. 4.16] and temperature [Eq. 4.17] based on the relative contribution of temperature or salinity to the density gradient at each boundary:

$$\overline{Q_{UW}} = (\overline{Q_U})_S \times (1 - \overline{f_W}) + (\overline{Q_U})_T \times \overline{f_W} \qquad [4.18]$$

where f_W is a dimensionless weighting factor derived from weighting factors which minimise the weighted sum of squared residuals of the equations:

$$\overline{f_W} = \frac{(\overline{T_L} - \overline{T_U})^2}{(\overline{T_L} - \overline{T_U})^2 + (\overline{S_L} - \overline{S_U})^2 \times \frac{\sum_{j=1}^{n}(\overline{T_L} - \overline{T_U})^2}{\sum_{j=1}^{n}(\overline{S_L} - \overline{S_U})^2}} \qquad [4.19]$$

In this case, values for f_W vary between 0.0 and 1.0 depending on the contribution of salt and heat to the salt-heat weighted solution Q_{UW}. When the difference between surface and bottom temperature is large, typically during summer [*Prego et al.*, 2001], f_W tends toward 1.0 as temperature makes the largest contribution to density. Conversely, during winter when the salinity gradient is large f_W will tend toward 0.0. A comprehensive discussion on the derivation and variability of f_W is given in *Álvarez-Salgado et al.* [2000] and *Gilcoto et al.* [2001].

In summary, the parameters required to calculate a full salt and heat budget at each boundary of the Pontevedra Ria over the year are S_L, S_U, T_L, T_U, H, Q_Z and T_Z. Daily H and Q_Z were obtained directly, and daily S_L, S_U, T_L, T_U and T_Z were derived empirically. In the text, the overbar is removed from the parameters denoting the mean value between two consecutive surveys.

</div>

4.4.2. DATA QUALITY

Salinity is commonly considered to be a conservative solute, and salinity deviations from the theoretical freshwater mixing curve [Fig. 1.1] result from longitudinal and lateral inconsistencies in circulation and mixing. In fast flowing systems where the estuarine water volume is flushed over a tidal cycle, this is unlikely to be a significant issue for salt-heat flux calculation. However, for the Pontevedra Ria, seemingly small longitudinal and lateral salinity deviations engendered by non-uniform mixing must be accounted for when determining the salt flux at any point in the ria.

Lateral error, $\Delta(ST)_{LAT}$. In the northern hemisphere, the Coriolis force acts to the right of the pressure gradient force. Accordingly, for the westward facing Pontevedra Ria, the salinity of the outflowing waters on the northern shore will tend to be less saline than those to the south, creating lateral variability in the salinity field throughout the ria [*Ruiz-Villareal et al.*, 2002]. Therefore, a single sampling at the centre of the cross section may not be representative of the whole estuarine width. Box models in the literature generally employ a single CTD cast at each boundary whilst making the assumption that the ratio of lateral to longitudinal salinity gradients are small enough to be ignored. The validity of this assumption has been tested by lateral sampling at two locations in the Pontevedra Ria. At CS17 and CS11 [Fig. 2.1] three and two CTD casts were taken over the section, respectively. Cross sectional maps of isohalines and isotherms were then constructed with Surfer® graphics package using a minimum curvature interpolation method. $(ST)_U$ and $(ST)_L$ were integrated to ρ_0 as before. Thus for *CS17*, $(ST)_U$ and $(ST)_L$ obtained from one CTD dip in the central channel, $(ST)_{1DIP}$, can then be compared with the more spatially resolved digitised data, $(ST)_{3DIP}$, to derive a estimate of $\Delta(ST)_{LAT}$ for each layer of each boundary:

$$\Delta(ST)_{LAT} = \left|(ST)_{1DIP} - (ST)_{3DIP}\right| \qquad [4.19]$$

The relative lateral error was subsequently applied to $(ST)_U$ and $(ST)_L$ data at CS21 to provide an estimate of lateral salinity error at the seaward boundary. The same procedure was followed for the boundary at CS14. *Rosón et al.* [1997] conducted a similar exercise for their weighted salt-heat box model of the Arosa Ria.

Longitudinal error $\Delta(ST)_{LON}$. Pockets of freshwater moving seaward due to sporadic runoff events create longitudinal variability in S and T than would be otherwise expected from conservative mixing. Over long time scales, short term non-steadiness will sum to zero, particularly if long term time series data are used [*Nogueira et al.*, 1997a]. However, for large volume systems parcels of freshwater constitute a finite source of non-steady state. In a simple 1-D mixing model under ideal conditions of conservative mixing, the salinity of a parcel of water can be quantified from the salinity of the water at its boundaries. In restricted salinity systems such as the Pontevedra Ria, the model salinity range is $30<S<35$ and the data confirm that for this range the longitudinal increase in salinity is typically linear (data not shown). Therefore, salinity at CS21 and CS14 can be forecast from the salinity at CS17 and CS11, respectively, by correlating the two corresponding sets of measurements for each of the 23 cruises. Consequently, $\Delta(ST)_{LON}$ can be

estimated as the difference between the observed salinity and the salinity expected from the correlation:

$$\Delta S_{LON} = |S_{OBS} - S_{EXP}| \qquad\qquad [4.20]$$

Reduced major axis regressions were used [*Sokal and Rohlf*, 1995] since salinity is subject to non-normal error distributions.

Error in ρ_0, $\Delta(ST)\rho_0$. The error the level of the pycnocline will be reflected in the estimate of $(ST)_U$ and $(ST)_L$. Despite good correlation of empirical estimates of v_0 with 3-D model results [*Taboada et al.*, 1998] the effect of ±1 m vertical variation in ρ_0 at each boundary was used to test the sensitivity of $(ST)_U$ and $(ST)_L$ and thus provide an estimate of $\Delta(ST)\rho_0$.

Integration error $\Delta(ST)_{INT}$. The error in integrating $(ST)_U$ and $(ST)_L$ over the cross-section is a function of the analytical error of the CTD salinity (ε_S, ±0.005) and temperature measurements (ε_T, ±0.005°C) and the uncertainty in the cross sectional area, ΔA. Semi-diurnal tides in the Pontevedra Ria ensure that the cross sectional area at the ria mouth varies sinusoidally concomitantly with tidal elevation. Typically, a polynomial rather than a linear mathematical function more adequately describes the increase in A from the seabed to surface in estuaries. Therefore, in the absence of synoptic sampling at the mouth over a tidal cycle the calculation error must be included. For simplification, the horizontal depth sections at the mouth cross section were assumed to expand and contract uniformly over a tidal cycle. If the mean tidal elevation at the mouth is 2.5 m [*Ruiz-Villarreal et al.*, 2002], or 8% of A for CS21 and CS14, the mean variability in area for each 1m depth slice will also be ±8%. ΔA, ε_S and ε_T for each 1 m section, and hence each layer are quantifiable, independent and combined linearly.

Fig. 4.19 shows the absolute error in observed ΔS and ΔT at CS21 and CS14 for each cruise as a composite of the individual errors $\Delta(ST)_{LAT}$, $\Delta(ST)_{LON}$, $\Delta(ST)\rho_0$ and $\Delta(ST)_{INT}$. Table 4.7 shows the mean individual error for the observed data in each layer. At CS21 and CS14 the individual errors at the surface were greater than their corresponding lower layer errors which tended to present a more consistent variability, particularly for salinity. The surface layer was more influenced by freshwater runoff and surface heat transfer than the bottom layer, which showed considerable inertia to transient heating and runoff events [*Nogueira et al.*, 1997a]. Accordingly, high ΔS_U was observed during winter, whereas the highest ΔT_U mostly occurred in the summer. The longitudinal error was mainly responsible for these trends, which was more pronounced for salinity in winter when runoff is high and more pronounced for temperature in summer when thermal stratification increased. $\Delta(ST)\rho_0$ was greater in the surface layer since the vertical salinity gradient was highest at the water surface. ΔS_{LAT} and ΔT_{LAT}, although relatively low, showed a coupling with the lower layer suggesting effective mixing of surface waters into the lower layer as the water moved seaward. Again, ΔS_{LAT} is greatest in winter when runoff is high, whereas high ΔT_{LAT} was noted in summer when upwelling of cold ENACW entered the ria along the southern coast [*Rosón et al.*, 1997]. Nevertheless, Table 4.7 clearly shows that the dominant error in $(ST)_U$ and $(ST)_L$ is from $\Delta(ST)_{INT}$. The SD of ΔST_{INT} for salinity was low compared to lateral and longitudinal surface errors because ΔS_{INT} was comparatively constant, whereas lateral and longitudinal S and T were more influenced by runoff and heating.

Table 4.7. Mean (±SD) of individual errors in the upper (U) and lower (L) layers of CS21 and CS14.

		Δ_{LAT}	$\pm\Delta_{LAT}$	Δ_{LON}	$\pm\Delta_{LON}$	Δ_{INT}	$\pm\Delta_{INT}$	$\Delta\rho_0$	$\pm\Delta\rho_0$
CS21$_U$	S	0.005	0.113	0.000	0.677	1.308	0.199	0.067	0.093
	T	0.031	0.106	0.000	0.402	0.592	0.102	0.051	0.057
CS21$_L$	S	0.007	0.118	0.000	0.132	1.010	0.091	0.024	0.025
	T	0.029	0.096	0.000	0.243	0.423	0.056	0.030	0.022
CS14$_U$	S	0.012	0.181	-0.001	0.722	1.561	0.252	0.125	0.187
	T	0.032	0.107	0.000	0.309	0.716	0.132	0.058	0.046
CS14$_L$	S	0.013	0.195	0.001	0.180	1.133	0.073	0.028	0.034
	T	0.029	0.097	0.001	0.367	0.479	0.048	0.038	0.031

4.4.3. DAILY RESIDUAL WATER FLUXES

The results for derived $(ST)_U$ and $(ST)_L$ at CS21 and CS14 using the multiple regression model [Eq. 4.9] are shown in Fig. 4.20 with the corresponding error calculated above. The interpolation has successfully reproduced characteristic thermohaline trends typically observed in the Rias Bajas [Nogueira et al., 1997a; Doval et al., 1998; Prego et al., 2001]. An annual cycle in salinity can be discerned, with the surface layer of the ria more sensitive to freshwater runoff than the lower layer. During the winter months surface salinity was depressed and, under sustained periods of high runoff [Q_Z, Fig. 3.12], the bottom layer salinity decreased to below 32. At other times, salinity in the bottom layer showed low variability (mean±SD, 35.52±0.63). Equally, T_U was more influenced by surface heating and cooling processes than T_L. During autumn and winter a temperature inversion developed, whereby $T_L > T_U$ [Prego et al., 2001]. In addition, for the purpose of the discussion, salinity at CS21 as predicted by Eq. 4.9 was always greater than the salinity at CS21. This was done in order to avoid negative fluxes from the box model calculations [Eq. 4.16, Box 2].

Fig. 4.21 shows the results for outgoing flux at CS21 calculated from the salt, $(Q_U)_S$ and heat $(Q_U)_T$ budgets [Eqs. 4.15 and 4.16]. The weighted results, Q_{UW}, are also shown. For clarity, only CS21 is shown, although the discussion is equally applicable to CS14. From a preliminary inspection of Fig. 4.21 two major issues for discussion immediately become apparent. Firstly, for both steady and non-steady S and T budgets, $(Q_U)_{S,T}$ gave the general impression of noisy data, presenting large fluctuations throughout the year with maximum fluxes greater than $\pm10^5$ m^3 s^{-1}. A day-to-day variability of upwelling of this magnitude will have potentially serious implications for quantifying nutrient flux to the coastal zone and managing the sustainability of the mussel industry. Given the inertia of upwelling in response to favourable upwelling winds on the shelf (~3 d), daily variability of this magnitude is probably physically impossible. Moreover, this variability is transferred to the S-T weighted model and Q_{UW}. The largest literature upwelling and downwelling fluxes for a similar boundary in the Rias Bajas were approximately 8000 m^3 s^{-1} and -14000 m^3 s^{-1} [Rosón et al., 1997]. Therefore, it appears that large upwelling and downwelling fluxes may be expected, although perhaps not to the extent of the derived values reported here.

(a)

(b)
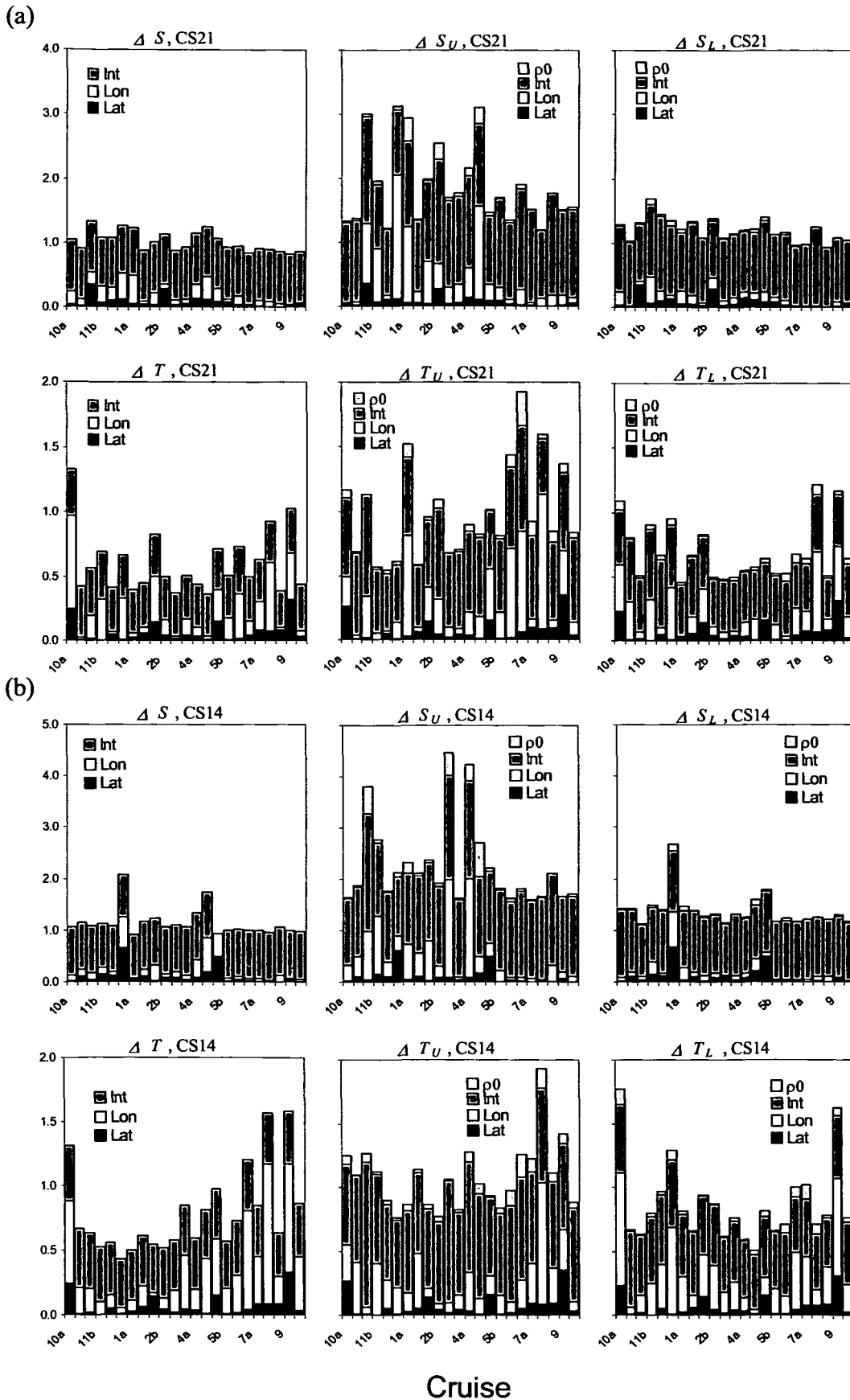
Cruise

Fig. 4.19. Absolute errors for mean cross-section S and T (left column of figures), $(ST)_U$ (middle figures) and $(ST)_L$ (right figures) on each of the 23 cruises in the Pontevedra Ria over October 1997-1998 at CS21 (a) and CS14 (b). Each cruise is denoted numerically by its calendar month and "a" or "b" referring to the first and second fortnight of the month respectively.
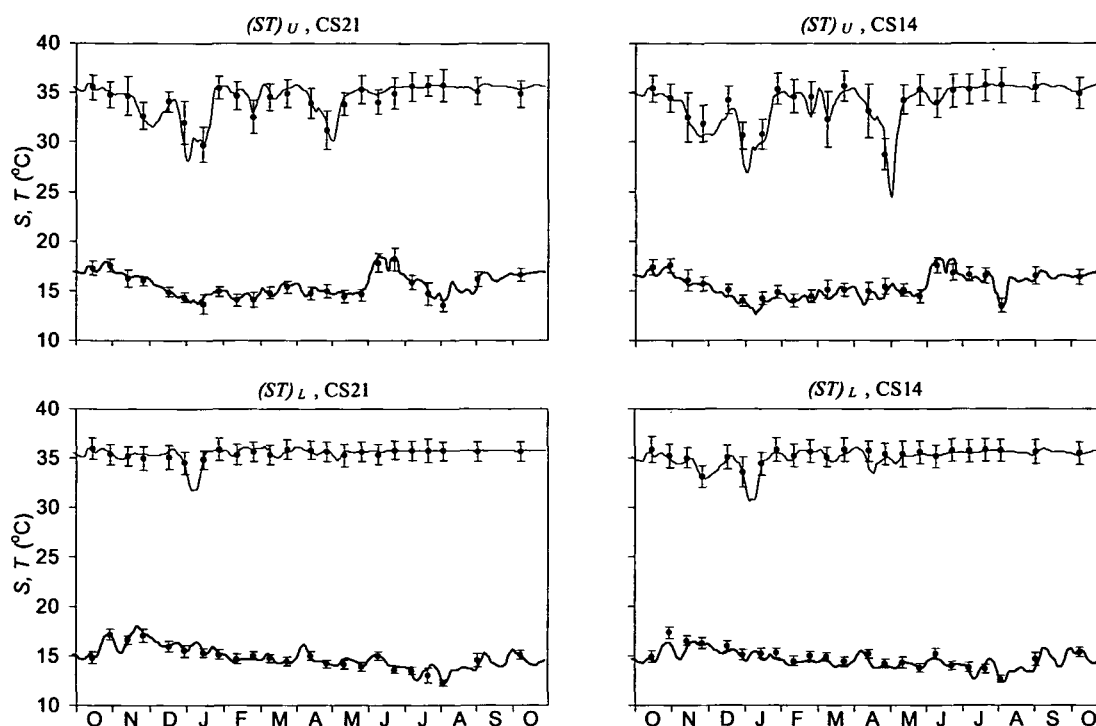
Fig. 4.20. Upper and lower layer salinity (light line) and temperature (°C, heavy line) at CS21 and CS14 in the Pontevedra Ria over the study period derived using multiple regression analysis [Eq. 4.9]. Observed values are shown by the points.

With regard to the second observation, $(Q_U)_S$ and $(Q_U)_T$ did not co-vary and statistical correlations were non-significant. It is remarkable that large upwelling and downwelling fluxes predicted by $(Q_U)_S$ were uncoupled to those predicted by $(Q_U)_T$, for both the steady and non-steady state models. Salt and heat are assumed to be dispersed at a rate equal to water. If S and T were advected conservatively identical results for $(Q_U)_S$ and $(Q_U)_T$ would be expected, or at least residual fluxes of the same sign. Ignoring groundwater and fluvial salt inputs, salinity may be considered as a truly conservative solute at the time scale of the investigation. Heat, however, has a plethora of sources and sinks, of which only heat exchange across the surface is treated in this section, others including heat exchange from intertidal mudflats, thermicity of chemical processes and heat exchange with the seabed. These additional heat transfers were presumably negligible in the Pontevedra Ria since the ria is deep (mean depth 22 m) and mudflats comprise <5% of the total area [*Harrison and Phizacklea*, 1985]. Therefore, the challenge remains as to how the weighted fluxes in Fig. 4.21 are to be interpreted.

4.4.4. MODEL SENSITIVITY ANALYSIS

Thermohaline properties. A large proportion of systems currently being assimilated into the LOICZ database are of Mediterranean- or subtropical-type climate, with corresponding low salinity variability at the mouth and tendency toward hypersalinity in summer. It is therefore of paramount importance to address fundamental quality control issues for such systems where potentially large water fluxes can be routinely inferred from the data.
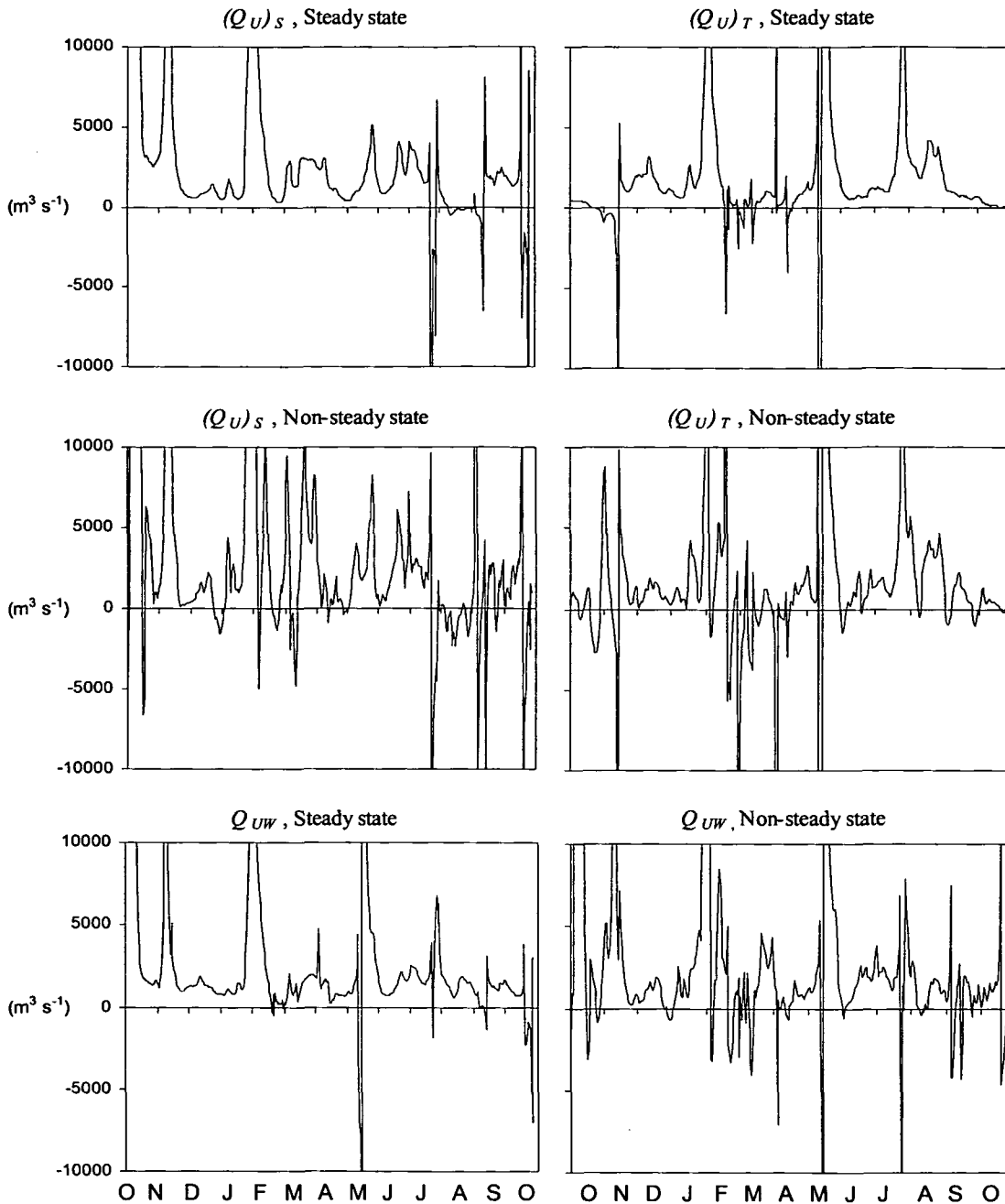
Fig. 4.21. Daily average surface fluxes (m^3 s^{-1}, positive seaward) at CS21 over the study period, October 1997-1998. Fluxes calculated using the salt budget, heat budget and combined salt heat budget for steady and non-steady state scenarios.

Tomales Bay is a coastal lagoon situated in a Mediterranean-type climate on the eastern coast of the USA. This estuary has been the subject of thorough investigation over the years, chiefly by Smith and co-workers [*Smith et al.*, 1989, 1991; *Smith and Hollibaugh*, 1997, 1998], and has provided a template for residual and nutrient flux estimation for LOICZ protocols [*Gordon et al.*, 1996]. Tomales Bay tends toward hypersalinity in summer when net evaporation exceeds precipitation ($Q_P<Q_E$). Similarly, the Pontevedra Ria shows net evaporation in summer, although for a short period only [Fig. 2.4]. The transient seasonal switch between $Q_P>Q_E$ and $Q_P<Q_E$ in Tomales Bay is associated with observed small values of S_L-S_U [Eq.

4.16] during re-establishment of the salinity balance [*Smith and Hollibaugh*, 1997]. Consequently, these authors calculated unrealistically high advective fluxes at these times. In fact, they were forced to eliminate several data from their time-series when S_L-S_U fell below 0.3 during the dry summer months. Their threshold of 0.3 is analytically equivalent to the experimental noise in the model i.e. the detection limit, and becomes important for high salinity systems when S_L-S_U falls within the signal-to-noise ratio. Therefore, a careful investigation of the model detection limit should be carried out in all estuarine budgeting studies.

The detection limit of thermohaline properties in the Pontevedra Ria can be derived from the previously derived errors in S and T. From Fig. 4.19, the mean total error (±SD) in salinity (ΔS_U) and temperature (ΔT_U) at CS21 are 1.46±0.30 and 0.70±0.19 °C, respectively, and 1.02±0.09 for ΔS_L and 0.49±0.11 for ΔT_L, respectively. For CS14, the mean total errors are 1.69±0.41 (ΔS_U), 0.78±0.16 (ΔT_U), 1.16±0.11 ΔS_U and 0.59±0.16 (ΔT_L). These errors were assumed to be equal to the model detection limit, and thus for numerically robust fluxes and conservation of statistical significance S_L-S_U and T_L-T_U must be greater then the sum of their respective errors.
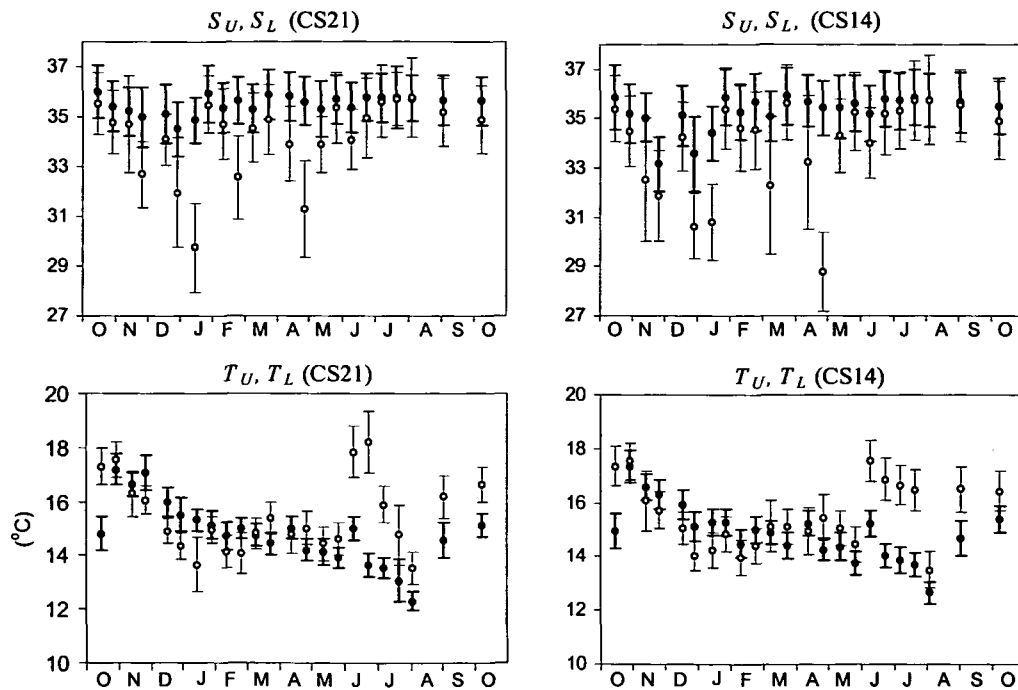
Fig. 4.22. Observed salinity and temperature (°C) at CS21 and CS14 in the Pontevedra Ria. Error bars represent the total error in each datum.

Consequently, applying the detection limit to each thermohaline variable, the observed S and T data have been reproduced in Fig. 4.22, with surface and bottom S and T at each boundary displayed together. The error bars show that salinity and temperature in the upper and lower layers of each boundary are statistically equivalent, with exception of high runoff periods in winter and high irradiation in summer. Furthermore, an Analysis of Variance model (ANOVA) showed that S or T in the upper layer was statistically equivalent to S or T in the lower layer at the 95% confidence

level, for both CS21 and CS14 (p<0.05). Therefore, the robustness of the original data for calculating water fluxes is statistically weak. *Gilcoto et al.* [2001] acknowledged the potential non-analytical error in their data of the Vigo Ria, although their argument in support of the box-model results was questionable. The fact is that horizontal and vertical gradients of salinity and temperature in the Rias Bajas are too small too permit a box-model analysis with confidence. Even though there may well be a cancelling effect of the total uncertainty for each term, at the very least this potential error should be qualified in future studies.
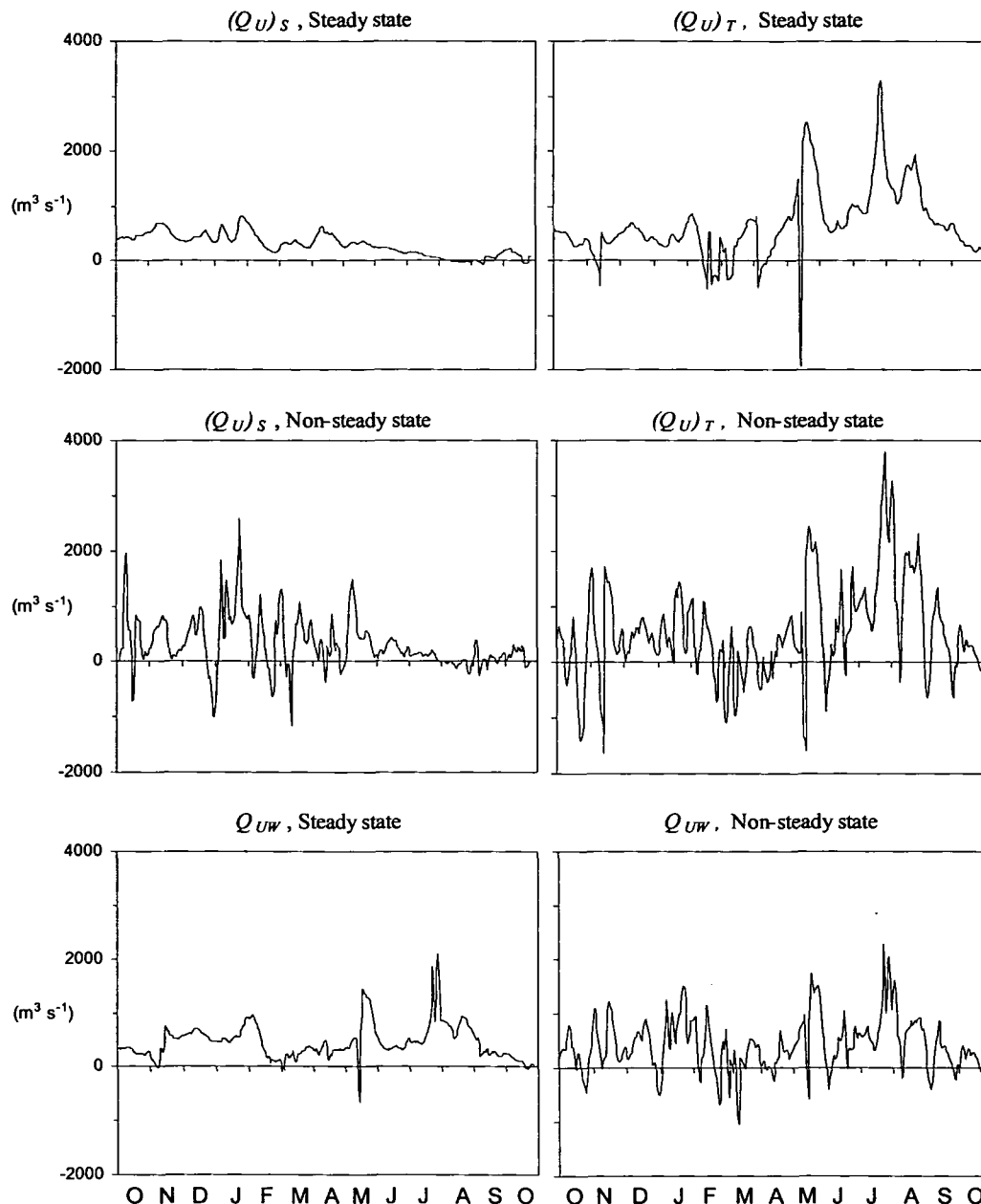
Fig. 4.23. Daily average surface fluxes (m^3 s^{-1}, positive seaward) at CS21 over the study period, October 1997-1998. Fluxes calculated using the salt budget, heat budget and combined salt heat budget for steady and non-steady state scenarios, where the model detection limit has been added to S_L-S_U and T_L-T_U [Eq. 4.16 and 4.17].

As a final example to emphasise the importance of these findings, the derived box model advective fluxes in Fig. 4.21 were recalculated, whilst ensuring that S_L-S_U [Eq. 4.16] and T_L-T_U, [Eq. 4.17] were at least equal to the corresponding S and T detection limit. This was achieved by adding the magnitude of the detection limit to the denominator in each equation. The recalculated fluxes are presented in Fig. 4.23. The reduction in analytical noise in the flux profiles is immediately obvious, particularly for the steady state model. In the dry season, large upwelling fluxes are not predicted with $(Q_U)_S$ as a result of low, or even negative, residual freshwater input in summer, whereas $(Q_U)_T$ fluxes are high. The weighted budget reproduces upwelling events throughout the year. Therefore, in systems such as the Rias Bajas where offshore water inputs are a frequent occurrence, the combined salt-heat budget is probably the most effective approach, provided that the error in S and T can be accurately determined. However, the non-steady model continues to predict a large variability in water fluxes, which may be a model artefact due to the large volume of the system.

Surface heat exchange. Both $(Q_U)_S$ and $(Q_U)_T$ show negligible sensitivity to Q_Z and T_Z. The final term in the budget equations is the net heat exchange across the water surface, H. H is calculated from the individual heat terms [Eq. 4.14] which, with exception of long-wave radiation heat gain from atmospheric water vapour (H_l), are empirically derived from analytically measurable parameters and well-established physical constants. H_l, however, is quantified with the cloud cover fraction raised to the second power [C, Eq. 4.11]. C is subject to considerable interpretative error and daily as well as spatial variability. Moreover, in view of the fact that C is often reported in ocktas (eighths of sky coverage), the accuracy in C is restricted to increments of ±11%. Unsurprisingly, therefore, C is the term associated with the largest error in heat budgets in coastal systems [Smith, 1985].
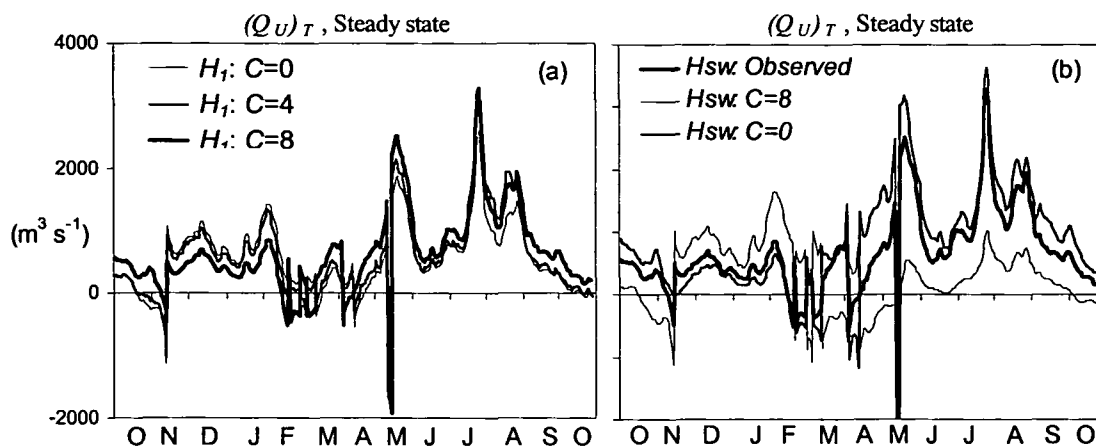
Fig. 4.24. Steady state horizontal advective surface layer fluxes at CS21 calculated from the heat budget, (a) using values of C=0 and C=4 for H_l, and (b) using observed values for H_{SW} and theoretical values for H_{SW} employing C=0 and C=8.

Previously, a value of 0.5 was assumed for C for calculating the advective fluxes in Fig. 4.21. In Fig. 4.24a the surface layer advective flux at CS21, $(Q_U)_T$, is quantified using a values of C=0, C=4 and C=8 for H_l. In Fig. 4.24b fluxes calculated with observed H_{SW} are compared with theoretically

calculated H_{SW} using $C=0$ and $C=8$. The variability of $(Q_U)_T$ is clear, and illustrates the potential for error in Q_U if C shows high daily variability. H_l shows lower sensitivity to C than H_{SW}, whereby mean $(Q_U)_T$ is 535 m³ s⁻¹ for $C=0$, 598 m³ s⁻¹ for $C=4$ and 693 m³ s⁻¹ for $C=8$. Equally, for H_{SW}, mean $(Q_U)_T$ is 816 m³ s⁻¹ when $C=0$ and 278 m³ s⁻¹ when $C=8$. Therefore, considering the daily variability in C, using theoretically calculated H_{SW} would lead to derived values of $(Q_U)_T$ being seriously flawed by error, thus bringing into question the usefulness of heat budgets in water flux estimation.

Chapter 5

Glossary of terms in used for the physical model

Parameter or variable	Unit	Description
Area	m^2	Cross-sectional area
Bathy	m	Bathymetry at any point
C	-	Any model advected constituent
Δt	s	Model time step
Friction	s^{-1}	Momentum loss due to bed friction
g	$m\,s^{-2}$	Acceleration due to gravity
Depth	m	Water depth
HEAT	$J\,l^{-1}$	ECoS modelled heat content of the water
I_W	$m^3\,s^{-1}\,km^{-1}$	Upwelling index
K_O	m^{-1}	Wave number
K_X	$m^2\,s^{-1}$	Longitudinal dispersion coefficient
MX	$kg\,m^2\,s^{-1}$	ECoS modelled momentum
n	$s\,m^{-2/3}$	Manning coefficient
Q_L	$m^3\,s^{-1}$	Box model incoming advective flux
Q_{L-T}	$m^3\,s^{-1}$	Box model exchange flux due to tides
Q_{L-M}	$m^3\,s^{-1}$	Box model advection and mixing flux
Q_Z	$m^3\,s^{-1}$	Residual freshwater input
ρ_{ria}	$kg\,m^3$	Water density
S	PSU	Salinity
SALINITY	PSU	ECoS modelled salinity
S:D	s	Number of seconds per day
SH	$J\,l^{-1}\,°C$	Specific heat of water
Slope	$kg\,m^2\,s^{-1}$	Momentum gain due to water surface slope
T	$°C$	Temperature
TEMP	$°C$	ECoS modelled temperature
TPA	m	Tidal amplitude
TPF	°	Tidal frequency
TPP	°	Tidal phase
TK	$°K$	Absolute temperature of water
U	$m\,s^{-1}$	Water velocity in the X direction
U_{max}	$m\,s^{-1}$	Maximum tidal velocity
U_W	$m\,s^{-1}$	Wave velocity in shallow water
V	$m^2\,s^{-1}$	Kinematic viscosity of water
W_L	$m\,s^{-1}$	Local winds resolved along the NE-SW ria
X	km	Longitudinal spatial component

5. Hydrodynamic modelling of the Pontevedra Ria with ECoS

5.1. MODELLING TIDES, SALINITY AND HEAT

5.1.1. OVERVIEW OF ECoS

In this chapter the tidal exchange fluxes, salt and heat dispersion in the Pontevedra Ria were simulated with the commercially available modelling software package ECoS [Estuarine Contaminant Simulator, *Gorley and Harris*, 1998; *Harris and Gorley*, 1998a,b]. The modelling development built upon previous results to describe the constituents hydrodynamically. The modelling took a logical and structured approach whereby each step was critically evaluated before proceeding with the next.

   ECoS is a user-friendly hydrodynamic simulation environment allowing transfers both in time and 1- or 2-D space. The attraction of ECoS is that it can be readily constructed with a basic understanding of estuarine hydrodynamics. A hierarchical structure permits different constituents to be added in layers or shells of various complexity. Constituents are defined as either dynamic advected (e.g. salinity), functional (e.g. bathymetry) and tidally averaged or tidally resolved. The concentration of a dynamic

constituent is subject to transport within the model boundaries. Transfers between constituents are fully allowed, at user-defined exchange rates, and may be spatially and temporally variable. An example of the ECoS model structure and on-screen format of the model structure is shown in Fig. 5.1. A review of ECoS is given by *Varney* [1992], and a more detailed description is found in *Harris et al.* [2003] and *Tappin et al.* [2003].
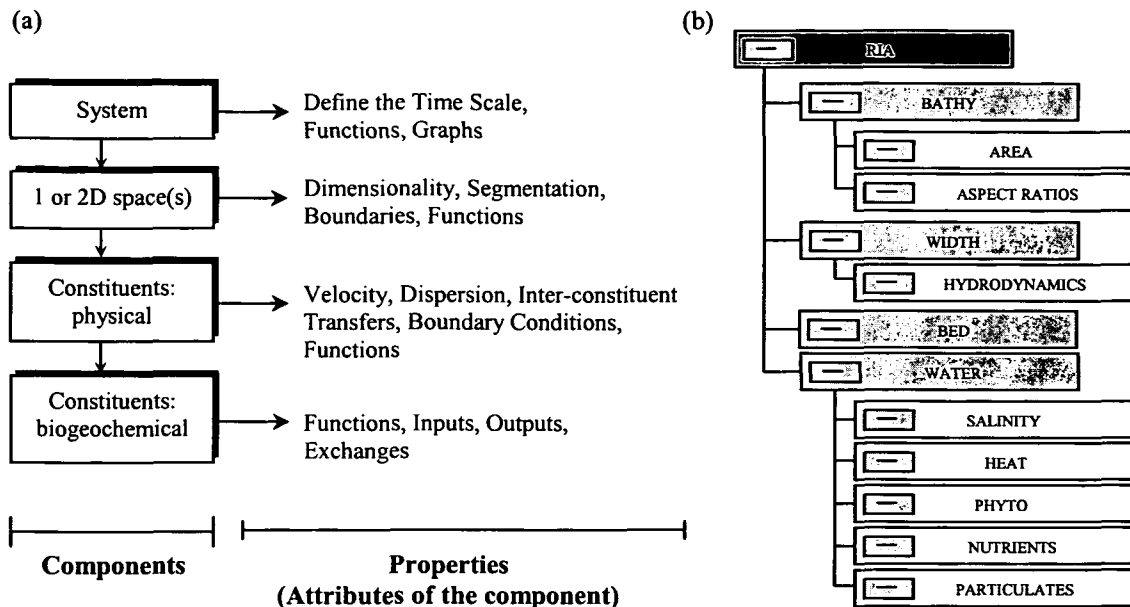
Fig. 5.1. (a) ECoS components and properties, and (b) on-screen hierarchical structure of ECoS.

ECoS has been widely applied to a variety of estuary types in Europe in 1-D along the longitudinal axis with satisfactory results [*Harris et* al., 1984; *Pham et al.*, 1997; *Abreu et al.*, 1998; *Liu et al.*, 1998; *Punt*, 2000; *Steen et al.*, 2002; *Tappin et al.*, 2002]. 1-D implies that constituent concentrations are depth averaged. Water velocity in ECoS is described by cubature, which defines velocity at any point by the cross-sectional area, $Area$ (m^2). Cubature can take either a simple depth-area representation or a more complex definition based on conservation of momentum [e.g. *Punt*, 2000]. The latter may be considered to be the more sensitive option since a parameterisation of momentum transfer is required, which directly affects water velocity and dispersion. For both templates, the distribution of a dissolved or particulate constituent is determined by the dispersion coefficient which, in the above papers, represents the longitudinal dispersion coefficient, K_X. As with other functional parameters in ECoS, dispersion may be fixed, or spatially and temporally variable.

Pham et al. [1997], *Liu et al.* [1998] and *Steen et al.* [2002] used tidally averaged ECoS models. This is convenient if semi-diurnal variability of constituents are not of interest, thus making a considerable saving on model run time. In this chapter, a tidally resolved ECoS model of nutrient dynamics was developed for the Pontevedra Ria, and hydrodynamics defined by conservation of momentum with longitudinal dispersion defined by K_X. Although semi-diurnal fluctuations in nutrient concentrations were

not considered, for reasons explained below, the tidally resolved model was chosen due the inherent dispersion of salt created by tidal dynamics.

5.1.2. TEMPORAL AND SPATIAL DIMENSIONS

Previous chapters in this thesis have emphasised the importance of scaling the sampling resolution to the water exchange time of the system. This also applies in defining the model time unit in ECoS. The field data must be aggregated upon the time and space scales in accordance with the model formulation [Sauchuck and Wulff, 1996]. Non-steady state conditions are engendered by runoff variability, upwelling and tides. Box-model results suggest that a model internal time scale of 2-3 d would be adequate to capture the short-term thermohaline variability [Rosón et al., 1997]. Alternatively, by running ECoS in the tidally resolved mode, a time scale of «1 h could be used. However, nutrients were sampled fortnightly, implying that tidal nutrient variability could not be verified or calibrated. This somewhat limited the scope of the model, and therefore a seasonal evolution of nutrient dynamics was undertaken, thereafter investigating the influence of upwelling and runoff. Consequently, a time interval of 1 d was chosen as the basis for defining constituent inputs and exchange rates.

With regard to spatial boundaries, modelling the Pontevedra Ria and not the Lérez estuary was the object of this study because (i) aquaculture of edible mussel is carried out in the ria rather than the estuary, and (ii) industrial discharges are directed to the internal ria. Therefore, from a socio-economic standpoint, developing a model of the ria is more attractive than a model of the estuary. Secondly, without supporting SPM data, an attempt to model nutrient dynamics of the Lérez estuary would be a futile exercise. There is no published material of SPM concentration in the Lérez estuary or other Rias Bajas "estuaries". However, with a mean depth of approximately 3 m and tidal range of 2-4 m, bed scouring and sediment redistribution effects in the estuary will presumably play a large role in biogeochemistry [Bale et al., 1985; Morris et al., 1985]. When more data becomes available, a hydrodynamic model of the Lérez estuary will make an interesting study, particularly with regard to up-estuary dispersion of industrial effluent discharge and heavy metal pollution [Prego and Cobelo, 2003].

Vertical gradients in salinity, temperature and biogeochemical tracers in the ria were generally greater than horizontal gradients [e.g. Figs. 3.1 and 3.2]. This is also the case in many coastal seas. For example, Sauchuck and Wulff [1996] and Halvorsen et al. [2001] developed horizontally averaged vertical resolved biogeochemical models of the Baltic Sea and Galician shelf, respectively. This approach is unsuitable for the Pontevedra Ria due to relatively high horizontal gradients, compounded by substantial spatial and temporal horizontal variability. Initial modelling was therefore carried out with the 1-D depth-averaged structure. The seaward boundary was located at the same position as for the box model [CS21, Fig. 2.1] in Chapter 3 to allow comparisons between the different model approaches. The limit of tidal influence (CS0) formed the corresponding landward boundary, although for reasons mentioned above the physico-biogeochemical modelling of the Lérez estuary was not considered. Therefore, spatial variability was thus explored longitudinally along the ria axis, assuming lateral homogeneity, extending from the mouth of the Lérez estuary at CS7 to the seaward model boundary at CS21 [Fig. 5.2].

In the 1-D model, the top component of the model, *RIA* [Fig. 5.1] represents the longitudinal axis of the ria, with a distance parameter equal to X (km). At the ria head (CS0) $X=0$ and at the mouth (CS21) $X=21$. Any number of equal length sections or boxes are positioned between these boundaries. The ria was segmented into 10 segments of 2100 m. Segment length is a function of time step, which is discussed in more detail below.
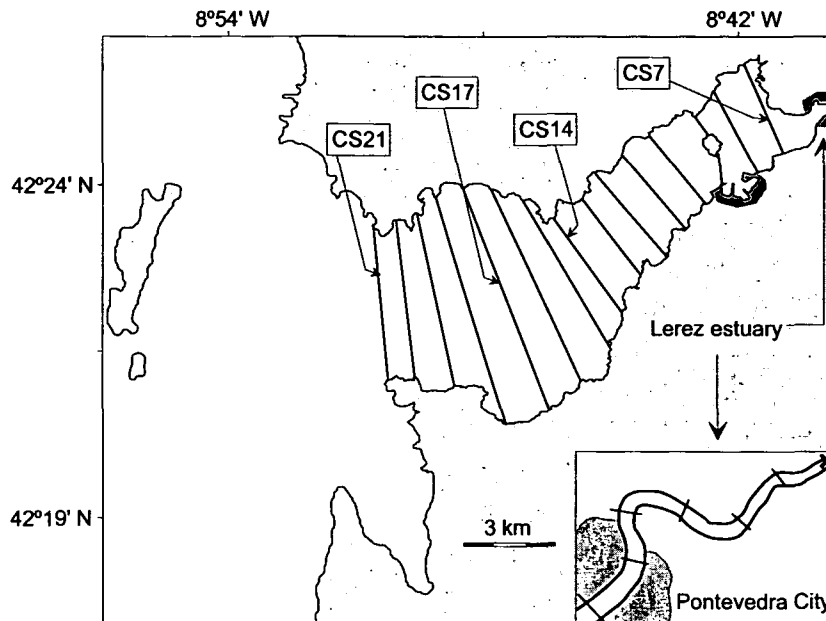
Fig. 5.2. Map of the Pontevedra Ria showing the ria segmentation in 1 km sections from the limit of tidal influence (CS0, cross in estuary) to the ria mouth (CS21). For ECoS modelling, a segment length of 2.1 km was used (i.e. 10 adjacent "boxes").

5.1.3. NUMERICAL TECHNIQUES IN ECoS

5.1.3.1. ENCODING MODEL HYDRODYNAMICS

Water velocity in ECoS is calculated by changes in cross-sectional area, *Area* (m²) along the ria. *Area* is described within the bathymetry constituent, *BATHY*, [Fig. 5.1], which in turn defines how the maximum depth, relative to a fixed datum, varies down the estuary as a function of X. *Area* from CS1 to CS21 were electronically digitised from a hydrographic chart. CS1 to CS6 correspond to the Lérez estuary, CS7 to CS21 to the Pontevedra Ria. Fig. 5.3 graphically displays *Area* from CS7 to CS21. Subsequently, the mean width and depth of each section were calculated from *Area*. The aspect ratio (*W:D*) of each section is then simply the ratio of mean width to depth. Table 5.1 summarises the geomorphological characteristics of the Pontevedra Ria.

Hydrodynamic calculations based on the transport, gains and losses of momentum (*MX*) were used to develop tide- and runoff-induced variations in *Area* along the ria. With the bathymetry encoded into the model, the flux of advected constituents is determined by well-established principals of fluid mechanics. In three dimensions, the advection-dispersion equation for a constituent, *C*, in a fluid takes the form:

Table 5.1. Dimensions of the cross-sections (CS) and corresponding boxes between sections in the Pontevedra Ria required for ECoS [see Fig. 5.2]. *Area* and widths were calculated from digitised 1m depth slices. The aspect ratio (*W:D*) of a section is the ratio of its mean width to mean depth.

CS (km from head)	Area (m^2)	bed area at CS (m^{-1})	mean CS depth (m)	mean box depth (m)	box surface area (km^2)	box volume (km^3)	mean width (m)	W:D
CS7	12904	2901	4.45	2.90	2.41	0.007	2490	560
CS8	15404	2338	6.59	5.40	2.56	0.014	742	113
CS9	38835	2900	13.39	10.35	2.30	0.024	2210	165
CS10	48031	3200	15.01	14.24	2.73	0.039	2324	155
CS11	51557	2923	17.64	16.26	3.03	0.049	2095	119
CS12	60127	3506	17.15	17.37	3.15	0.055	2193	128
CS13	68216	3507	19.45	18.30	3.08	0.056	2275	117
CS14	82154	3603	22.80	21.15	3.51	0.074	2451	107
CS15	133211	6806	19.57	20.69	5.66	0.117	4074	208
CS16	147624	7253	20.35	19.98	7.34	0.147	3995	196
CS17	206038	8002	25.75	23.18	8.40	0.195	5623	218
CS18	195181	6804	28.69	27.10	7.54	0.204	5303	185
CS19	168234	6023	27.93	28.33	7.46	0.211	4352	156
CS20	145585	5200	28.00	27.96	5.12	0.143	3676	131
CS21	168293	5228	32.19	30.10	4.43	0.133	4053	126

$$\frac{\partial C}{\partial t} = -\frac{\partial(UC)}{\partial X} - \frac{\partial(VC)}{\partial Y} - \frac{\partial(WC)}{\partial Z} + \frac{\partial(K_X \partial C / \partial X)}{\partial X} + \frac{\partial(K_Y \partial C / \partial Y)}{\partial Y} + \frac{\partial(K_Z \partial C / \partial Z)}{\partial Z} + f(C) \qquad [5.1]$$

The first three terms on the right-hand-side of Eq. 5.1 are the advection terms in the X, Y and Z directions with respective velocity components U, V and W. The following three terms correspond to diffusion in the X, Y and Z directions, whose magnitude is defined by the dispersion coefficient, $K_{X,Y,Z}$. The final term represents the non-conservative change in concentration which, for salinity, $f(S)=0$. ECoS is encoded with the 1- or 2-D form of the advection-dispersion equation with finite difference integration scheme. In the 1-D model, the combined effects of flow and dispersion can be mathematically described by a differential equation, considering motion in the X direction only:

$$\frac{\partial C}{\partial t} = -\frac{\partial(UC)}{\partial X} + \frac{\partial(K \partial C / \partial X)}{\partial X} + f(C) \qquad [5.2]$$

The concentration of C is integrated over a user-defined time interval or time-step (Δt). If the concentration of C at X is C_X, in which ΔX is defined to have the opposite sign for velocity, then the convention $\Delta a_X = a_{X+\Delta X} - a_X$ can be used for any a. Accordingly, $\partial(UC)/\partial X$ transforms to $\Delta(UC)/\Delta X$ and $\partial(K\partial C/\partial X)/\partial X$ becomes $\Delta(K_X \Delta C_X /\Delta X)/\Delta X$. Therefore, the final concentration of each species provides the initial concentration for the next time step and is solved as [*Gorley and Harris*, 1998]:

$$C - C^\Delta = \left(-\frac{\Delta(UC)_X}{\Delta X}\right) + \left(\frac{\Delta(K_X \Delta C_X /\Delta X)}{\Delta X}\right)\Delta t \qquad [5.3]$$
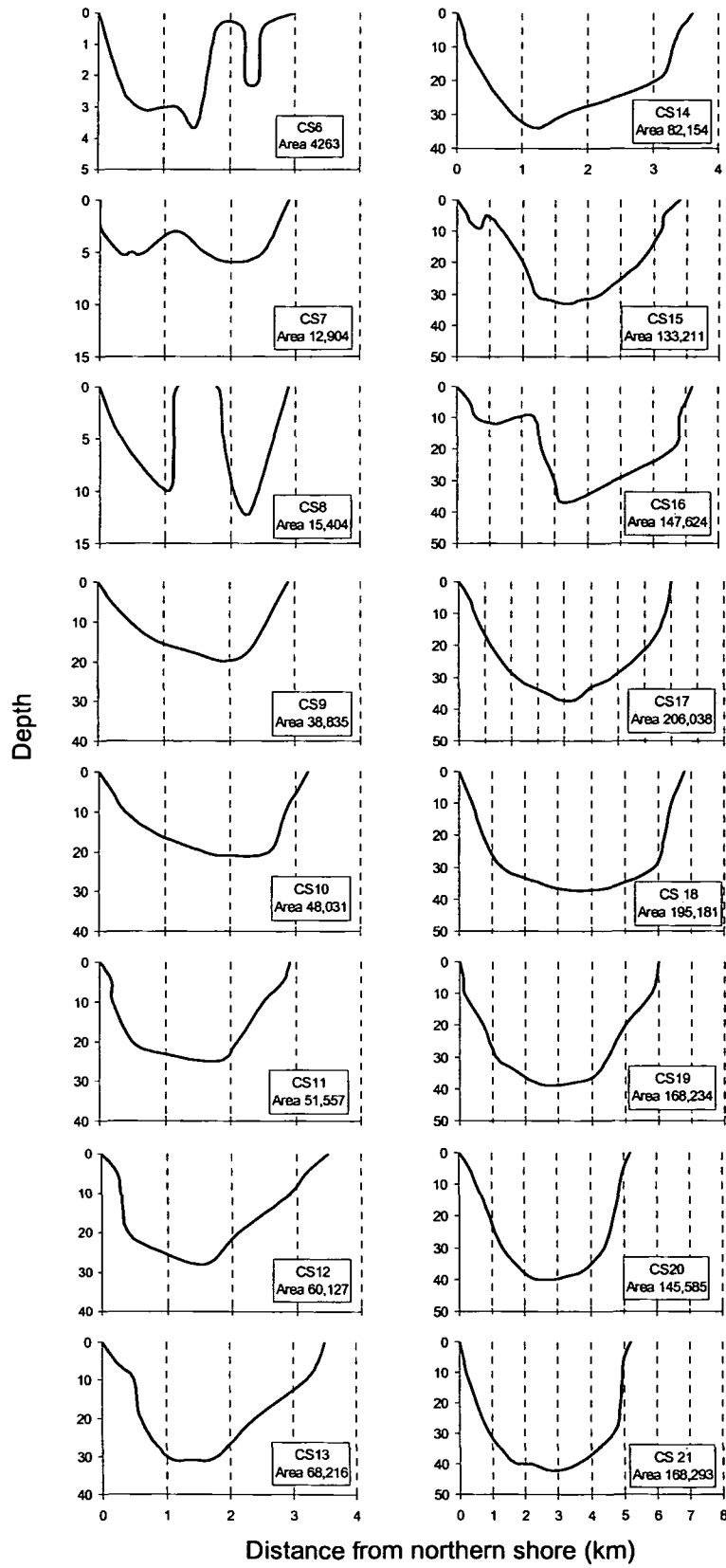
Fig. 5.3. Depth (m) profiles of the cross-sectional areas in the Pontevedra Ria from CS6 to CS21. The cross-sectional area is also shown.

Essentially, this is the fundamental of the finite difference integration scheme. For a more detailed description of the integration scheme within ECoS, and finite difference in general, the reader is referred to *Dyke* [1996], *Harris and Gorley* [1998a] and *Jones* [2002].

Δt determines the rate of successive updates of time variable quantities. Under steady state conditions, Δt should not affect the advection-dispersion equations, but a steady state assumption may not be appropriate under all conditions and can lead to model inaccuracies [*Gorley and Harris*, 1998]. Therefore, an understanding of the real-time evolution of the non-steadiness of the parameters of interest is required for accurate modelling. Deciding on an appropriate value for Δt must satisfy the following condition on segment size to avoid instability:

$$\frac{\Delta X}{\Delta t} > U_W \qquad [5.4]$$

where U_W is the wave velocity in shallow water, given by

$$U_W = \sqrt{g \times Depth} \qquad [5.5]$$

where g is the acceleration due to gravity (9.81 m s^{-2}) and *Depth* is the water depth (m). Therefore, model stability is a function of segment length and Δt, whereby short segment length requires a short time step and correspondingly longer computational time. Instability can be envisaged as the tendency for the model solution to oscillate rather than settle down to an acceptable value [*Dyke*, 1996]. In the Pontevedra Ria, the mean depth is 21.4 m and U_W is therefore 14.5 m s^{-1}, implying a maximum time step of 69 s for a segment length of 1000m. Fig. 5.4 shows how the maximum permitted time step varies with the axial mean depth of the Pontevedra Ria. For accurate modelling of tidal current velocities, a small time step in relation to the semi-diurnal tidal cycle (12.42 h) is required. Accordingly, a compromise between Δt and ΔX for the Pontevedra Ria was met with Δt=140 s and ΔX= 2100 m.
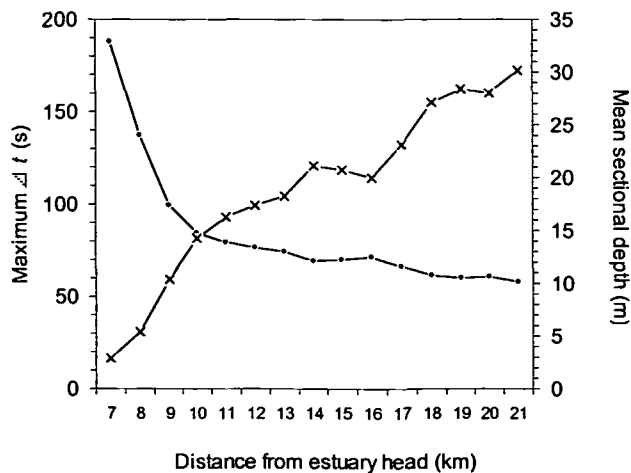
Fig. 5.4. Spatial variation of the maximum permitted time step, Δt (•, s), and mean water depth (×, m) in the Pontevedra Ria. The time step function is based on a model segment length of 1000m.

Momentum, *MX* (kg m^{-2} d^{-1}), is defined as an advective constituent. Momentum is assumed to move with the water. The water velocity, *U* (m d^{-1}) is the ratio of momentum to water density, ρ_{ria} (kg m^{-3}):

$$U = \frac{MX}{\rho_{ria}} \qquad [5.6]$$

Momentum is dispersed by the viscous drag within the water, and its dispersion coefficient is the kinematic viscosity of the water, *V* [100-1000 m^2 s^{-1}; *Harris and Gorley*, 1998b]. Small values of *V* are associated with turbulent flow [*Dyer*, 1973].

The slope of the water surface (*Slope*) provides an input to *MX*:

$$Slope = S : D^2 \times \rho_{ria} \times g \times AREA \times \left[\frac{\delta Depth}{\partial X} - \frac{\delta Bathy}{\partial X} \right] \qquad [5.7]$$

S:D^2 is the square of number of seconds per day to convert *g* to units of m d^{-1}. The surface slope is the difference between the slope of the sea bed (*δBathy/δX*) and the variation in total water depth (*δDepth/δX*).

Water friction on the sea bed (*Friction*) causes a proportionate loss in momentum:

$$Friction = a \times U \times Depth^b \qquad [5.8]$$

where *b* = -1.33 and *a* is determined from the Manning coefficient, *n*:

$$a = g \times n^2 \qquad [5.9]$$

The default *n* is 0.025 s m$^{-2/3}$; a value commonly associated with sandy estuaries [*Wolanski et al.*, 1997]. Increased friction is associated with larger *n* [*Unnikrishnan et al.*, 1997; *Wolanski et al.*, 1997]. In their estuarine study, *McDowell and O'Connor* [1977] reported *n*=0.013 for a depth of 8 m and *n*=0.026 for 3 m depth. Accordingly, large *n* decreases tidal elevation [*Punt*, 2000]. However, bed friction effects are only likely to be important in shallow systems [*Wolanski et al.*, 1997; *Inoue and Wiseman*, 2000]. No data were available for modelling bed friction in the Rias Bajas, and therefore the default value for *n* was used here. The sensitivity of salt intrusion in the ria to *n* is tested below.

5.1.3.2. DETERMINING MODEL RUN-UP TIME

Model stability and stabilisation period, commonly termed the spin-up time, depend on the ratio of system volume to the rate of water exchange, i.e. the flushing time. Essentially, the spin-up phase is equal to the time required for a dissolved solute to reach equilibrium concentrations under conditions of constant water exchange. In a small tidally dominated system such as the Tweed Estuary (UK), the spin-up time is of the order of tidal cycles [*Punt*, 2000]. Fig. 5.5 illustrates how the model mixes salt out of the Pontevedra Ria using varying values for K_X. Logically, steady state (constant salinity) is achieved more rapidly as K_X increases. With lower K_X, equilibrium requires longer run time, and the equilibrium salinity is lower

since a greater build up of freshwater is permitted. Under these test conditions, steady state was reached after approximately 30 d with a dispersion coefficient of 200 m² s⁻¹. It is worth noting salinity equilibrium was reached after 25-30 d for the tidally resolved that with K_X=0 m² s⁻¹. This implies that dispersion introduced by the tide only was equal to 100-200 m² s⁻¹. Tides created dispersion proportionally throughout the ria and gave a better representation of the salinity field, for which reason the tidal model was chosen in favour of the tidally resolved model. It would be interesting to see whether previously tidally-averaged model simulations would be improved by incorporation of tidal dynamics [*Pham et al.*, 1997; *Liu et al.*, 1998; *Steen et al.*, 2002].
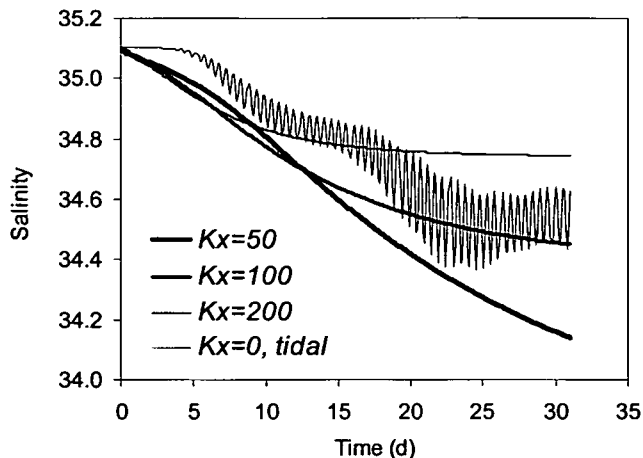
Fig. 5.5. Evaluation of model spin-up time as determined from salinity equilibration under conditions of constant freshwater runoff and variable longitudinal dispersion coefficients, K_X (m² s⁻¹).

5.1.4. MODELLING TIDAL EXCHANGE

Tides provide a finite contribution to water flushing in the Rias Bajas, although perhaps surprisingly their role has received little attention in the literature despite the availability of numerical models [*Taboada et al.*, 1998; *Torres Lopez et al.*, 2001; *Ruiz Villarreal et al.*, 2002]. Consequently, the tidal exchange flux in the Rias Bajas has not yet been quantified.

Quantification of the tidal exchange in the Rias Bajas is important since potential productivity estimates are required by the mussel aquaculture industry located within the rias. Additionally, tidal exchange is the baseline from which additional water exchange fluxes [Chapter 3] should be compared. Box model calculations in the Rias Bajas have not previously considered the state of the tide, although this will ultimately affect the final flux calculation. In this section tidal fluxes are quantified for the first time, and compared with the residual flux results from the *FFW* method.

Tidal exchange varies over the year depending on the relative positions of the sun and the moon. Topographic and frictional effects also introduce asymmetry into the tidal curve [*Dyer*, 1997]. Tides in ECoS are represented by a sine wave with a period of 12.42 h, whose amplitude varies sinusoidally on the 14.76 d spring-neap cycle. Using a six component tide, the tidal elevation at the mouth is given by:

$$TIDES = TPA \times COS((TPP - TPF \times t \times 24) \times \pi/180) \qquad [5.10]$$

TPA, *TPF* and *TPP* are the tidal amplitude (m), tidal frequency (°) and phase (°) for the user-defined harmonic constants. In this work, the M_2, S_2, N_2 and L_2 semi diurnal constants and the K_1 and O_1 diurnal constants were employed. *TPA* and *TPP* were taken from *Ruiz Mateo* [1983] and standard values were used for *TPF*.

Fig. 5.6 shows the calibration of modelled tidal elevation against chart data at the port of Marín in the internal Pontevedra Ria [Fig. 5.2]. October 1997 and April and July 1998 are displayed as examples. Tidal height was probably correct to within ±10% with the number of harmonic constants employed. The form ratio (*F*) of a tide [*Pond and Pickard*, 1983] is equal to the amplitudes of $(K_1+O_1)/(M_2+S_2)$. For the Pontevedra Ria *F*=0.11, characteristic of a semi-diurnal equal tide. Seasonal changes in sea level in the Pontevedra Ria are negligible [*UK Hydrographic Office*, 2001]. Tides at the mouth of the Pontevedra Ria and those at Marín are practically symmetrical [*Ruiz Mateo*, 1983].
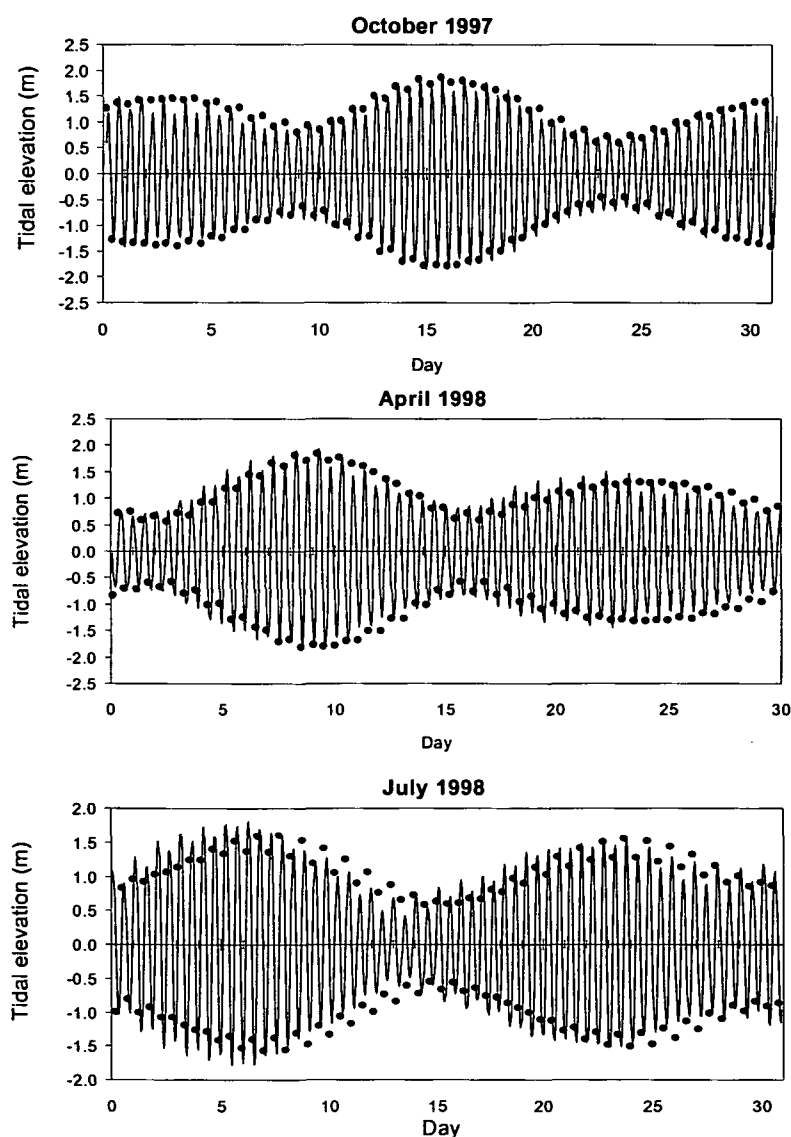
Fig. 5.6. Modelled tidal elevation (m, solid line) at the port of Marín (42° 24'N, 8° 42' W) in the internal Pontevedra Ria (10 km from head) with respect to the mean sea level at that point (1.91 m). The points represent tide table values.

Fig. 5.7 shows the daily residual tidal flux at 3 key areas: ria mouth (CS21), internal ria boundary (CS14) and internal ria (CS10). The model predicts that residual water exchange at the mouth varied from approximately 800 m³ s⁻¹ for the highest spring tides and 400 m³ s⁻¹ during neaps. From *Area* at the mouth [Table 5.1], these fluxes equated to 0.48 cm s⁻¹ and 0.24 cm s⁻¹, respectively. Moreover, tidal exchange decreased by up to 60-80 % in the 7 km between the mouth and the internal ria. This agrees with the low tidal excursion of <1 km reported in Chapter 3.
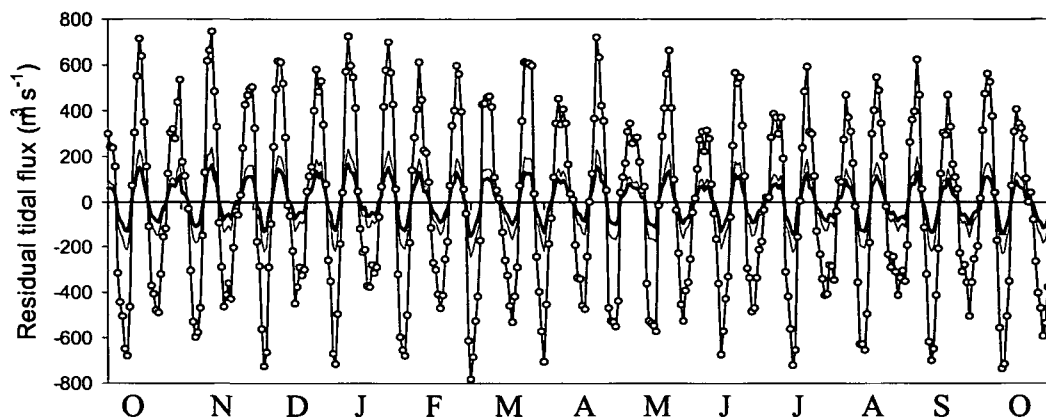
Fig. 5.7. Modelled residual daily water fluxes (m³ s⁻¹) in the Pontevedra Ria due to tidal exchange only at (i) the ria mouth (CS21, dotted line), (ii) at the border between the central and internal ria (CS14, light line), and (iii) in the internal ria (CS10, heavy line).

Instantaneous tidal velocities at CS10 during May 1998 are shown in Fig. 5.8a. Maximum velocities ranged from 5.1 cm s⁻¹ during neap tides to 12.1 cm s⁻¹ during springs. These values were very similar to those derived for the Arosa Ria by *Pascual and Calpena* [1985]. Considering the wind and oceanic forcing in the ria, they also compare favourably to current meter data recorded during 26 May at the same location [Fig. 3.8].

Maximum tidal velocity U_{max} (m s⁻¹) at any point in the ria can be calculated theoretically from the wave number, K_O (m⁻¹) [*Dyer*, 1997]:

$$U_{max} = a_O \times \sqrt{\frac{g}{Depth}} \times \frac{sin(K_O \times L)}{cos(K_O \times L)}$$

[5.11]

$$K_O = \frac{2 \times \pi}{t \times \sqrt{g \times Depth}}$$

[5.12]

where L (m) is the distance from the ria head, *Depth* (m) is the mean depth at that point, t is the wave period (12.42×86400 s), and a_O is the mean tidal amplitude [1.91m, *UK Hydrographic Office*, 2002]. Results for U_{max} are shown in Fig. 5.8b. Theoretical tidal currents in the central and internal ria were 0.18±0.01 m s⁻¹. This value is quite different to observations [Fig. 5.8a] and probably results from the theoretical nature of Eq. 5.11 and 5.12. Nevertheless, for the purpose of this work, the values were sufficiently close

be sure that ECoS was predicting tidal velocities of the correct order of magnitude.
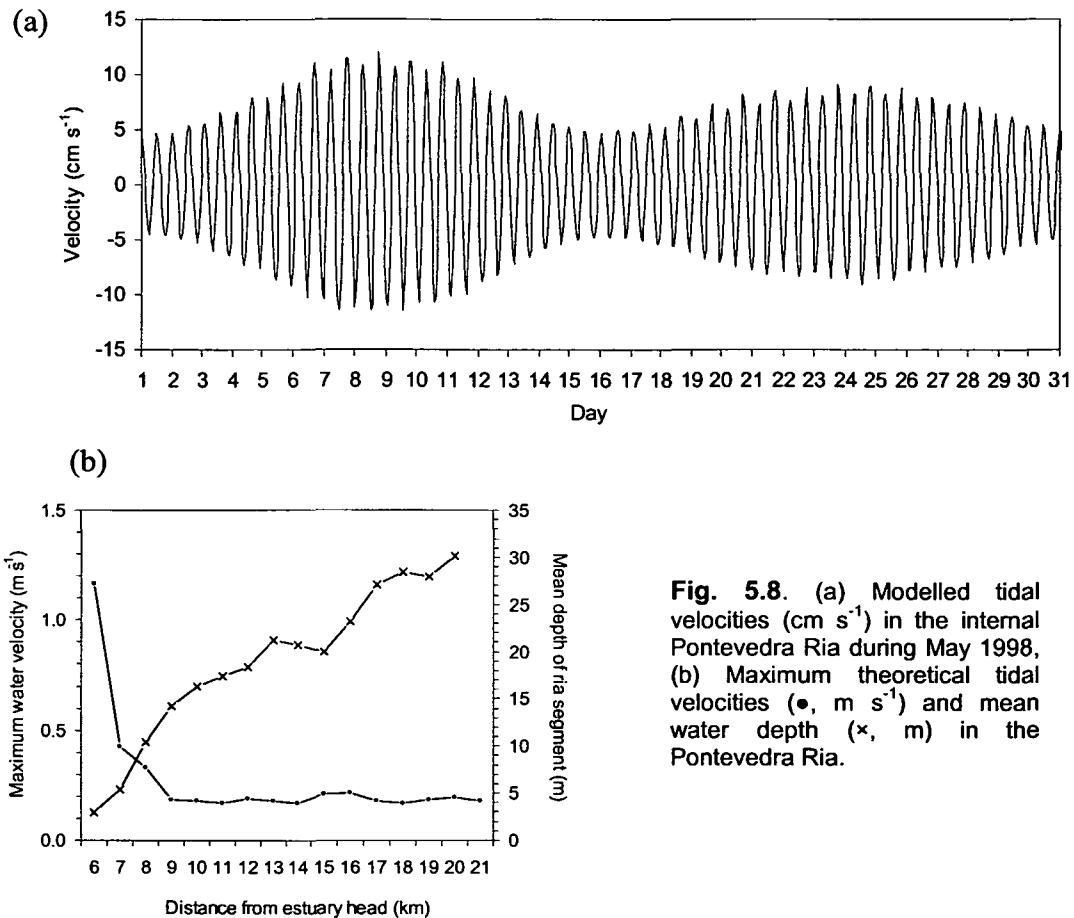
Fig. 5.8. (a) Modelled tidal velocities (cm s^{-1}) in the internal Pontevedra Ria during May 1998, (b) Maximum theoretical tidal velocities (•, m s^{-1}) and mean water depth (×, m) in the Pontevedra Ria.

Water flushing in the Pontevedra Ria is a function of surface wind stress, upwelling, downwelling and tidal mixing. In Chapter 3, the incoming advective flux Q_L [Fig. 3.10 and 3.11] was quantified with the *FFW* method. This exchange flux can be separated into the tidal contribution, Q_{L-t}, and the flux due to advective and turbulent mixing Q_{L-m}. Depending on the strength of upwelling at the mouth, tidal mixing was important for maintaining residual circulation and exchange of salt between the ria and ocean. Fig. 5.9 shows Q_L separated into the Q_{L-t} and Q_{L-m} components. Tides accounted for up to 45% of total water flushing during late December and February on cruises 12b and 2b when τ was long [Fig. 3.12]. At other times, tides were too weak to dominate τ, thus supporting previous speculation of the minor role of tides in determining water flushing [Prego et al., 2001], although this is partly dependent on the time of sampling and the phase of the spring-neap cycle. Based on these results, tides accounted for ~10-25% of water flushing.
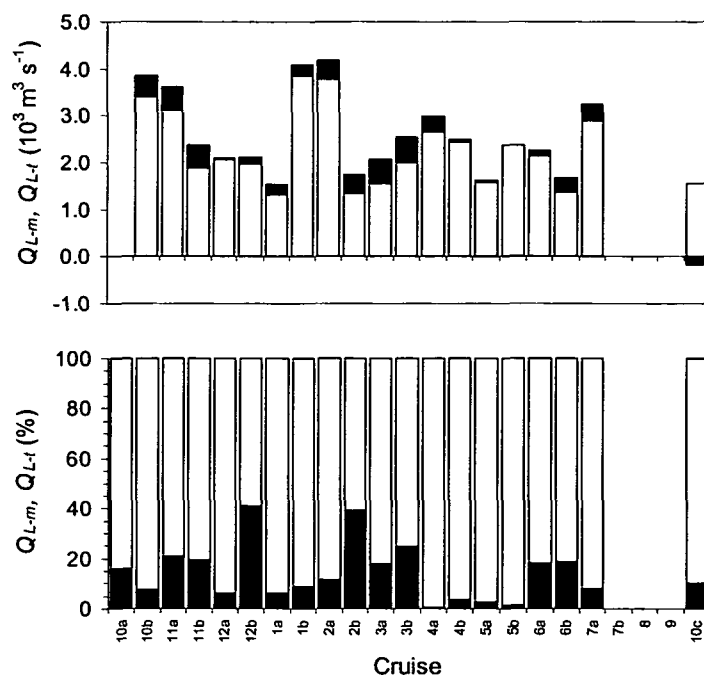
Fig. 5.9. Absolute (top panel, 10^3 m^3 s^{-1}) and relative (lower panel, %) contributions of the tidal (Q_{L-t}) and advective mixing flux (Q_{L-m}) to the total incoming mixing flux (Q_L) in the Pontevedra Ria. Each cruise is denoted numerically by its calendar month and "a" or "b" referring to the first and second fortnight of the month, respectively [Table 2.1]. October 1998 is indicated by "10c".

5.1.5. MODELLING SALINITY AND HEAT

5.1.5.1. SALINITY

Both salinity and heat in the 1-D model were treated as advected constituents, and therefore calibrated with the longitudinal dispersion coefficient, K_X [Eq. 5.2]. In this chapter, salinity and temperature corresponding to the ECoS model state variables are referred to as SALINITY and TEMP, respectively. Dispersion of a solute in water is dependent on the Area over which the substance diffuses and the water velocity, both through its effects on turbulence and on current shear [Lewis, 1997]. Accordingly, assigning a dispersion coefficient for the Pontevedra Ria is problematical, particularly in view of the longitudinal and lateral thermohaline inconsistencies. In addition to tides and runoff, upwelling at the mouth provides a third source of solute dispersion. An accurate assessment of dispersion is crucial for determining flushing times and pollution transport, and sufficient time should be devoted to this stage of modelling. In this work, a single temporally variable dispersion coefficient was used for the whole ria since the relatively small gain in SALINITY accuracy (<0.05 PSU) with a spatially variable K_X did not warrant the extra computational model run time. Improvements in model accuracy were made by calibrating K_X with TEMP as well as SALINITY.

An initial estimate of K_X was made with the following calculation [Dyer, 1973], assuming that salinity gradients reflected an approximate steady state balance of salt and dispersion:

$$K_X = \frac{U \times S}{(\partial S / \partial X)}$$ [5.13]

The net seaward velocity of water, U (m s^{-1}), is equal to the total freshwater input (m^3 s^{-1}) above the *Area* (m^2) at that point. Therefore, to a first approximation, K_X in the Pontevedra Ria varied between 10-400 m^2 s^{-1}. However, the longitudinal variability of K_X showed no clear trends and increased both upstream and downstream, due to the salinity gradient falling within the signal-to-noise ratio. Moreover, negative K_X, a theoretical impossibility, were engendered by pockets of freshwater moving downstream in the wet season or by net evaporation in the dry season. In order to circumvent similar problems, *Steen et al.* [2002] calculated K_X from polynomial functions derived from smoothed salinity profiles. In view of the low signal-to-noise ratio in the present data, K_X was determined by fitting the modelled *SALINITY* to observed salinity as described below.

K_X was estimated with a stepwise multiple regression with independent variables of the upwelling index (I_w, m^3 km^{-1} s^{-1}) freshwater runoff (Q_z, m^3 s^{-1}) and NE-SW local winds (W_L, m s^{-1}) since these variables appear to have most influence over thermohaline variability [*Nogueira et al.*, 1997a,b]. I_w and Q_z were processed with a 3 d moving average filter, equal to the response time of upwelling after the onset of northerly winds [*McClain et al.*, 1986], and W_L with a 2 d moving average filter. The final multiple regression was the following:

$$K_X = 250 + (0.5 \times I_W) + (0.2 \times Q_Z) + (332 \times W_L)$$ [5.14]

Eq. 5.14 provides a means by which K_X is related to upwelling. Dispersion is increased by upwelling, runoff and seaward local winds. During strong downwelling conditions, K_X predicted by Eq. 5.14 was negative. In these cases K_X was set to zero, so that downwelling implies a blockage of water outflow, to agree with observations in Fig. 3.1. The maximum value of K_X was set to 250 m^2 s^{-1} to avoid unrealistically high dispersion. Technically, a linear regression of this type assumes that the system was in steady state despite evidence to the contrary.

5.1.5.2. HEAT

Modelling heat has the advantage that it provides an extra tool for calibrating dispersion with increased confidence. ECoS is encoded with a template for heat, which is adapted for a particular system by defining the seaward *TEMP* boundary condition, and the *TEMP* of the freshwater inputs. However, heat exchange across the water surface is not included in the default template, and therefore ECoS was encoded with the surface exchange heat fluxes based on the empirical equations in Box 2. Heat content of the water (*HEAT*, J l^{-1}) within the model was converted to absolute temperature, *TK*, using the product of its specific heat (*SH*, J l^{-1} °C^{-1}) and its density (ρ_{ria}, g l^{-1}):

$$TK = \frac{HEAT}{SH \times \rho_{ria}}$$ [5.15]

SH and ρ_{ria} were calculated from *SALINITY* and *TEMP* using well established derivations from *Millero et al.* [1973] and the international one-atmosphere equation of state of seawater [*Millero and Poisson*, 1981], respectively.

The depth-averaged mouth boundary condition (*MBC*) for *SALINITY* (S_{MBC}) and *TEMP* (T_{MBC}) were quantified in the same way as outlined in Section 4.4.2. Fig. 5.10 shows S_{MBC} and T_{MBC} over the sampling period and the temporally variable K_x used in the hydrodynamic model and. I_w is also included as a reference.
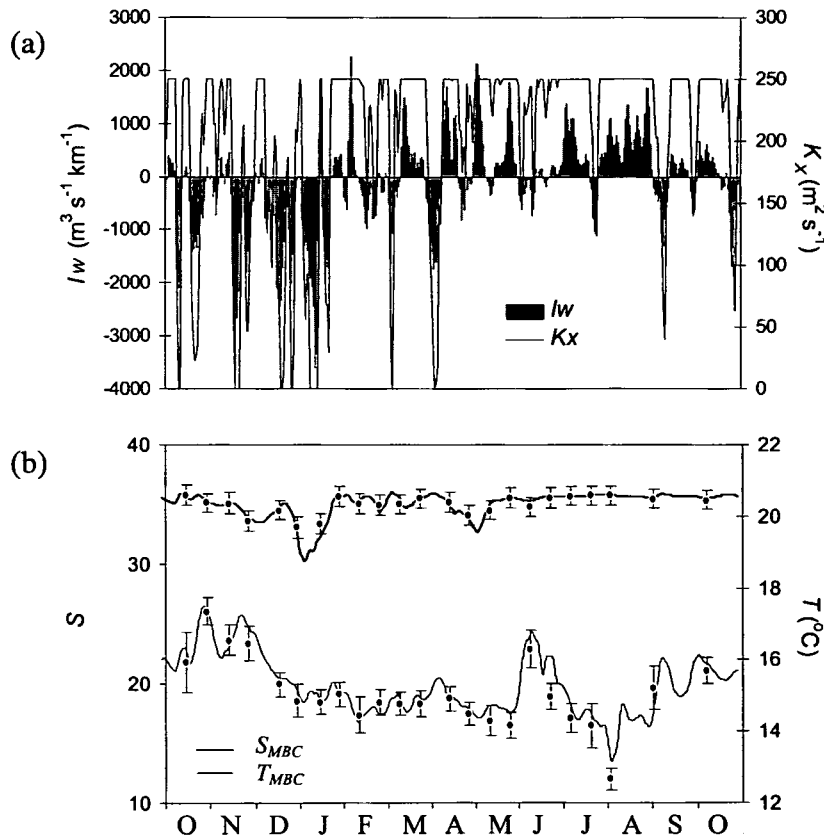
Fig. 5.10. (a) Daily values for upwelling index, I_w (m^3 s^{-1} km^{-1}), and longitudinal dispersion, K_x (m^2 s^{-1}), used for the hydrodynamic model of the Pontevedra Ria, (b) Salinity (S_{MBC}) and temperature (T_{MBC}, °C) mouth boundary conditions derived from observed depth averaged data (•).

5.1.5.3. MODEL SIMULATIONS

The modelled results for *SALINITY* and *TEMP* at CS17, CS14, CS11 and CS8 are shown in Fig. 5.11. The annual variation in simulated *SALINITY* was <6 at CS17 and >10 at CS8. The observed *S* and *T*, calculated in Section 4.4.3, showed good agreement to simulated data. Modelled *SALINITY* was generally within 0.5 of the observed data, which is of the same order or better than other ECoS model simulations [*Punt*, 2000; *Steen et al.*, 2002]. The similarity of the simulated data and the *MBC* suggests that the sailnity in the ria was strongly influenced by water exchange at the mouth, rather than freshwater input [*Pardo et al.*, 2001]. During the highest runoff conditions in January, *SALINITY* at CS8 was only 7-8 less than the S_{MBC}. For *TEMP*, the longitudinal gradients were even smaller, and the difference between *TEMP* and T_{MBC} at CS8 was never more than 0.5 °C. However, the

fit of simulated *TEMP* to observations becomes progressively underestimated during the summer months toward the ria head, suggesting that the dwell time in the internal ria was longer than predicted by the model.
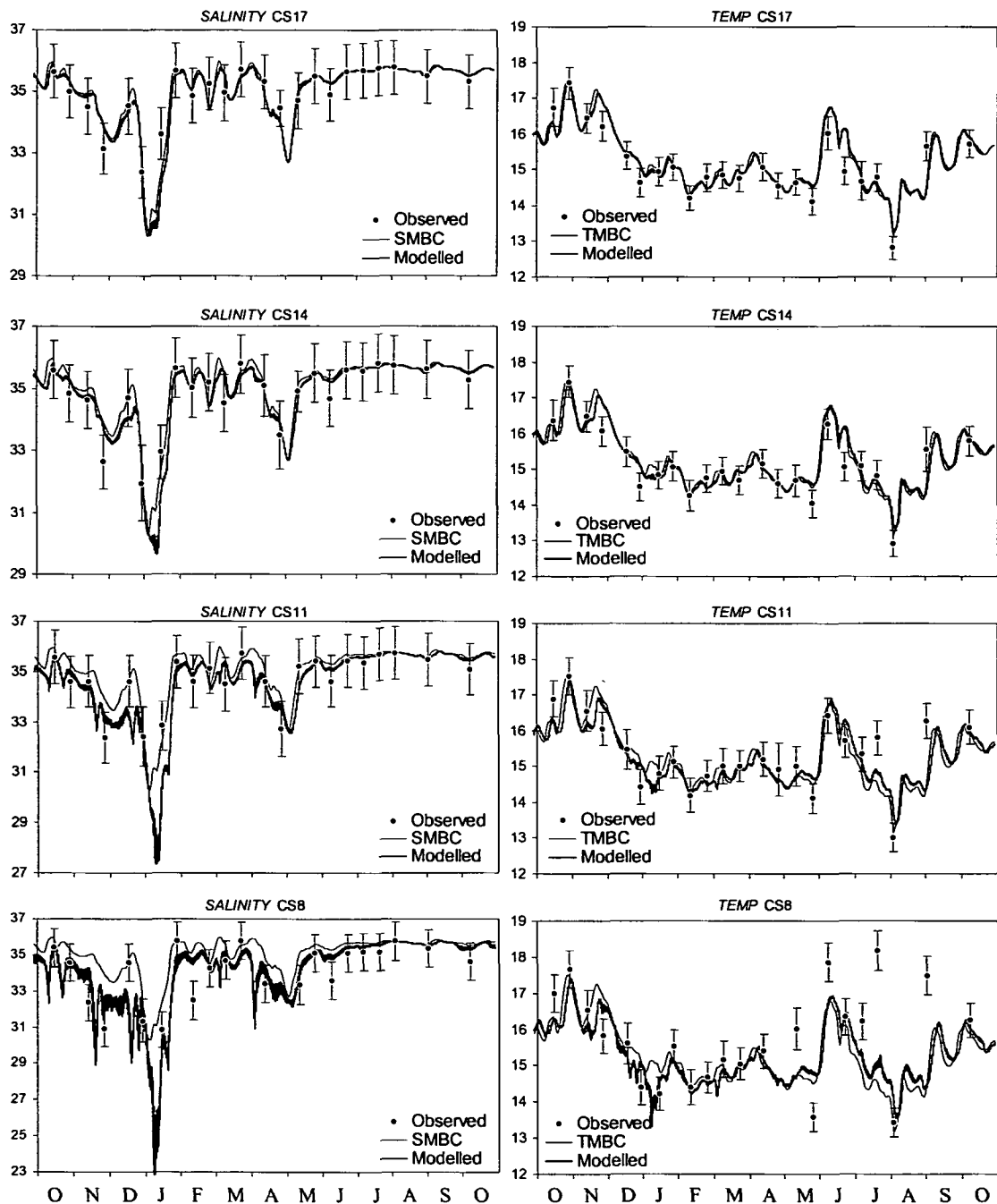
Fig. 5.11. Observed (points) and modelled *SALINITY* and *TEMP* (°C) in the Pontevedra Ria (heavy lines) at CS21, CS14, CS11 and CS8. The light line represents the *SALINITY* and *TEMP* mouth boundary condition, S_{MBC} and T_{MBC}, respectively.

The semi-diurnal widening of the simulated profiles during high runoff qualifies the tidal variability in salinity and, to a lesser extent, temperature. At CS8 this amounts to a semi-diurnal variability of ±1 for salinity and ±0.2

°C for temperature. Further seaward, the tidal variability is generally negligible. It can therefore be concluded that the state of the tide can be ignored when applying box models at the CS21 and CS14 boundaries in the ria.

Álvarez-Salgado et al. [1996a,b] observed that the hydrochemical dynamics of the central and internal Arosa Ria are different, showing strong oceanic and riverine signals, respectively. This suggests that separate dispersion coefficients for the central and internal parts of the ria may give a better representation of SALINITY rather than a single dispersion coefficient. This hypothesis is supported by the deviation of modelled from observed salinity at CS11 during high runoff events, although the low sampling resolution must also be considered. Similarly, *Harris et al.* [1984] found that K_X in the Tamar estuary (UK) was axially variable and dependant on freshwater flow. *Steen et al.* [2002] and *Pham et al.* [1997] also parameterised K_X with river flow in the Scheldt and Gironde estuaries, respectively. However, in the Pontevedra Ria K_X was not only dependant on river flow, but also winds and upwelling index, the latter two being relatively hard to quantify in terms of water exchange. Moreover, the model fits to the observed data were generally good. In addition, since K_X has been parameterised with I_w, W_L and Q_Z, the effect of upwelling has been included in the model.

Due to the low longitudinal variability in thermohaline gradients, the question arises as to the sensitivity of ECoS in detecting these small changes in salinity and temperature during upwelling and downwelling. Therefore, a sensitivity analysis of is paramount, since although SALINITY and TEMP appear to be adequately modelled, particulate constituents, e.g. phytoplankton, will behave very differently under variable K_X.

5.1.6. SENSITIVITY ANALYSIS OF THE PHYSICAL MODEL

Despite the obvious effort devoted to constructing hydrodynamic models, it is perhaps surprising that a sensitivity analysis of model variables to key parameters is often overlooked, or at least unreported. If model predictions are heavily biased toward the sensitivity of one or more parameters, then the model output will be unreliable. Where no discussion of model sensitivity or corresponding arguments of model predictions are provided, the model results are generally of little value to the scientific community.

The physical ECoS model of the Pontevedra Ria was perturbed by a variation in the parameters considered fundamental to conservation of momentum or those which cannot be verified by other means. Accordingly, the parameters tested are the Manning coefficient, n [Eq. 5.9], the major semi-diurnal harmonic constant, M_2 [Eq. 5.10], river runoff, Q_R [Fig. 2.4], the longitudinal dispersion coefficient, K_X [Eq. 5.2], and net surface heat exchange, H [Eq. 4.14]. The additional attraction of a sensitivity analysis of this type allows possible consequences of climate change via increased rainfall (=Q_R), sea-level rise (=M_2) and irradiance (=H) to be qualitatively assessed.

Fig. 5.12 shows the results of the sensitivity analysis with distance from the limit of tidal influence, varying one parameter for each model run. The size of the perturbation is indicated on the individual figures, and sensitivity is recorded as percentage deviation in SALINITY and TEMP from the reference model settings [Fig. 5.11]. It is clear that n, M_2 and Q_R had little effect on SALINITY and TEMP in the ria (CS7-CS21 km), and are only

important in the Lérez estuary. An increase in M_2 is negligible throughout. *SALINITY* shows ±4% variability with ±10% variability in Q_R.
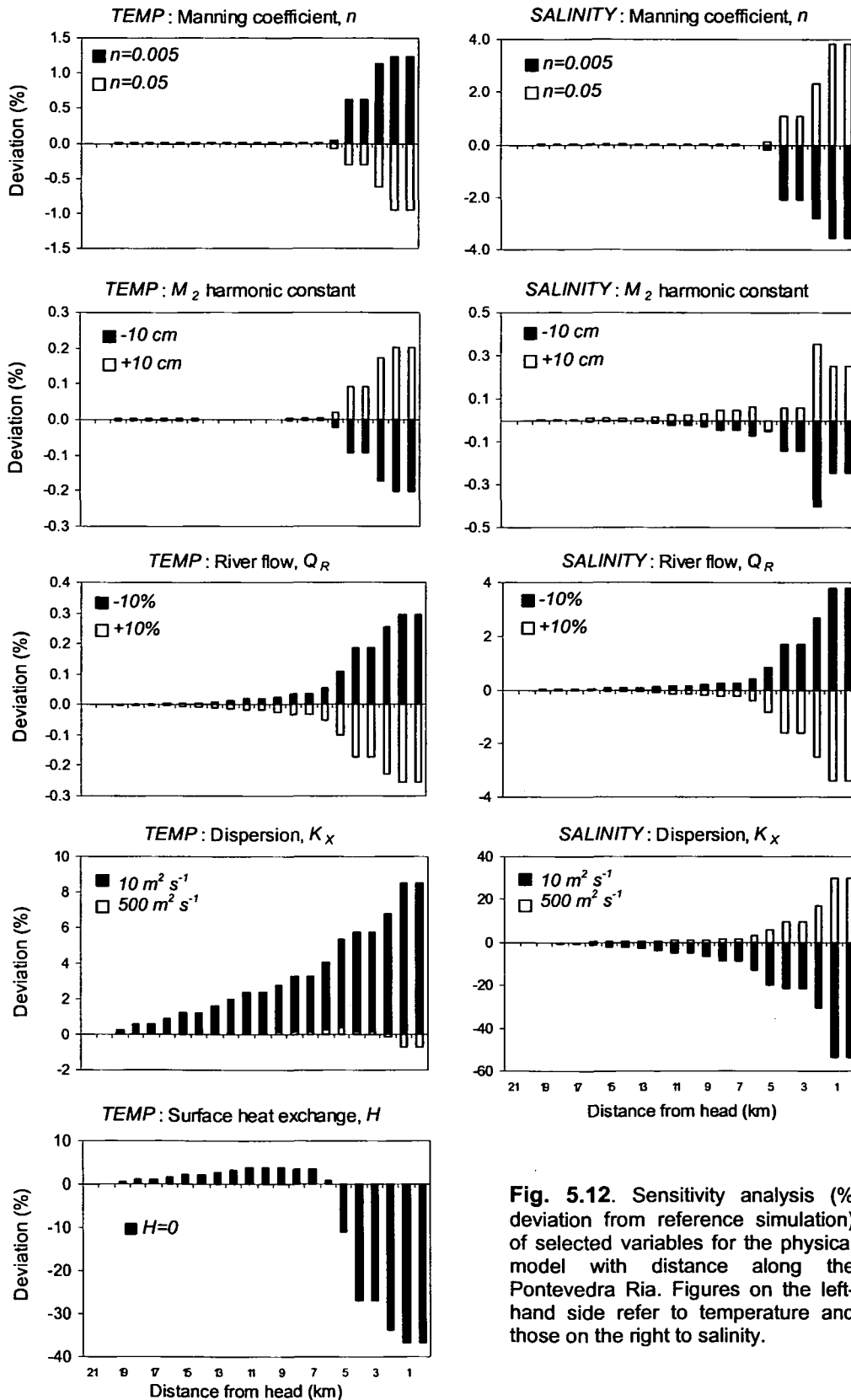
Fig. 5.12. Sensitivity analysis (% deviation from reference simulation) of selected variables for the physical model with distance along the Pontevedra Ria. Figures on the left-hand side refer to temperature and those on the right to salinity.

H had no effect on salinity, and is not included in Fig. 5.12. However, by removing H from the model (H=0) TEMP increased in the ria, and decreased in the estuary. From this observation it can be concluded that the ria was a net exporter of heat across the water surface whereas the estuary normally showed a net heat gain from the atmosphere. This bi-modal heat import-export pattern has not previously been observed in the Rias Bajas. An interesting aspect of future work would be quantify the importance of heat transfer from the estuary to the ria over an annual cycle. In the ria, however, the influence of surface and heating processes was generally low (~4%), illustrating the importance of advection and mixing processes. *Uncles and Stephens* [2001] reported similar findings for the Tamar Estuary (UK).

SALINITY and TEMP showed most sensitivity to the longitudinal dispersion coefficient, K_X, which increased toward the limit of tidal influence. The analysis tested the deviation of K_X=10 and K_X=500 m² s⁻¹. The variability with K_X=10 m² s⁻¹ was less than for K_X=500 m² s⁻¹, especially for TEMP, suggesting that S and T distributions showed an exponential-type relationship with K_X, which is expected. It is interesting to note that increasing dispersion resulted in an increase in SALINITY ($S_{OCEAN} > S_{RIA}$). Lower K_X permitted a greater build up of freshwater toward the ria head.

To summarise, the analysis has shown good model performance for the ria, and within an acceptable level considering the 1-D nature of the model. Conversely, the present model is unsuitable for the Lérez estuary which shows high sensitivity to key model parameters. The effect of the uncertainty in estuarine SALINITY and TEMP on the ria SALINITY and TEMP remains to be quantified. In addition, although SALINITY and TEMP in the ria were simulated to within the accuracy of the observed data, the transportation of particulate material has not been addressed. The sensitivity of particulates to K_X will undoubtedly be an important issue for the biogeochemical model, particularly since biogeochemical processes are rate-dependent. For example, the ria residence time, via its interaction with K_X, is a fundamental aspect of determining primary production in dynamic upwelling systems [*Huntsman and Barber*, 1977; *Minas et al.*, 1982].

5.2. MODELLING BIOGEOCHEMICAL CYCLES

5.2.1. OBJECTIVES AND MODELLING STRATEGY

The objective of this Chapter was to further explore the processes contributing to the nutrient dynamics in the Pontevedra Ria and Rias Bajas. As with any modelling study, the goals must be kept to a realistic level. Aside from the temporal resolution of the data, the number of state variables within the data set determines model complexity. It is thus imprudent to attempt to model, say, the microbial loop, without dissolved organic carbon data. Consequently, the Pontevedra Ria model was somewhat confined to inorganic nutrient dynamics, and processes restricted to those which mainly control temporal and spatial nutrient fluxes. Observed data can be used to validate the inorganic nutrient concentrations, and published phytoplankton and primary production data for the neighbouring Rias Bajas can be used semi-quantitatively to verify the biological model results. In short, the model will be used heuristically.

A specific objective of this work was to test our current understanding and relative importance of the critical biogeochemical processes in the Rias Bajas. Initially, a zero-dimensional (0-D) nutrient model was constructed in ECoS for the Pontevedra Ria, implying no advection or transportation of material. Spatial boundary conditions were absent and the state variables solely depended on internal exchange transfers. The strength of 0-D models lies in their ability to isolate biogeochemical from hydrodynamical effects [Dyke, 1996].

The pelagic nutrient 0-D sub-model was developed from first principles, starting with particulate organic dynamics and primary production. Dissolved inorganic nutrients were then superimposed to form a pelagic 0-D nutrient biogeochemical model using observed and literature parameter values. Subsequently, the pelagic model was coupled to a benthic biogeochemical model developed separately. The biogeochemical model was initially simplified by decoupling the hydrodynamic shell, thus allowing the sensitivity and importance of each parameter, transfer and state variable to be assessed. By gradually increasing model complexity the verification of each transfer and state variable concentration was facilitated. Finally, when the model outputs were suitably verified, the model was coupled to the physical shell to give a hydrodynamic-biogeochemical model of nutrient dynamics in the Pontevedra Ria.

The major processes modelled were photosynthesis, particulate organic matter, and early diagenesis of benthic organic material. These energy transfers are directly associated with the uptake or release of dissolved organic nutrients. Therefore, nutrient boundary conditions must be carefully considered due to the variability introduced to the system by upwelling, and parameterised with real data wherever possible. A summary of the modelling stages developed here is shown in Fig. [5.13].

5.2.2. FORMULATIONS AND VISUALISATIONS

5.2.2.1. MODEL CONSTRUCTION

The appearance or disappearance of constituents in marine reservoirs can be generally grouped into those which result from biological transformation

(e.g. nutrient uptake or regeneration), changes in redox potentials (e.g. mobility of metallic species) or radioactivity (e.g. radioactive decay of ^{137}Cs). Ultimately, reaction kinetics and the magnitude of the rate-determining step, k, determine the relative abundance of one species over another within each group of chemical transfers.

SUB-MODELS

```
┌──────────────────┐  ┌──────────────────┐  ┌──────────────────┐
│ PHYTOPLANKTON &  │  │ PELAGIC DISSOLVED │  │ PARTICULATE &    │
│ PARTICULATE      │  │ INORGANIC        │  │ DISSOLVED        │
│ ORGANIC MATTER   │  │ NUTRIENTS        │  │ BENTHIC NUTRIENTS│
└──────────────────┘  └──────────────────┘  └──────────────────┘
```
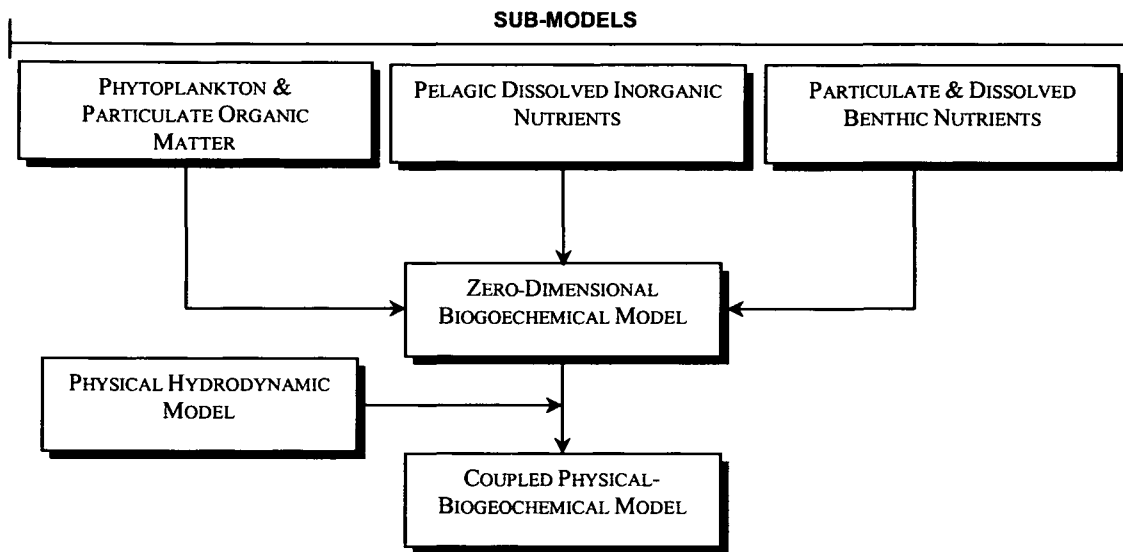

Fig. 5.13. Modelling strategy adopted for the Pontevedra Ria showing construction and coupling of individual sub-models.

The simplest case is that of spontaneous irreversible decomposition of a species N_1 to N_2:

$$N_1 \xrightarrow{\ k\ } N_2 \qquad\qquad [5.16]$$

The reaction is first order in N_1, where the loss of N_1 is described as:

$$rate = \frac{-d[N_1]}{dt} = k[N_1] \qquad\qquad [5.17]$$

By integrating from time zero, t_0, when $[N_1]=[N_1]_0$, to time t, when $[N_1]=[N_1]_t$, it follows that:

$$[N_1]_t = [N_1]_0 e^{-kt} \qquad\qquad [5.18]$$

where $[N_1]$ is a function of its initial concentration, the rate constant k, and the reaction time t. The mathematical relationship between $[N_1]_t$ and t is exponential, where the size of the exponential is equal to k for a given t. This is a useful concept in marine modelling since the appearance or disappearance of a species serves as the analytical parameter. In addition, since transfers are often are mediated by an abundance of microbes, they can be described as first order or pseudo first order. For example, inputs, outputs or exchange transfers between defined species in ECoS are defined as a proportion of the source amount. This allows a proportional loss/gain

of the source/sink constituent equal to the first-order rate constant multiplied by time, kt. Therefore, an output from a defined source of 0.1 (time)$^{-1}$ will result in the source concentration to fall by 10% per unit time.

Before constructing the 0-D model, it is worthwhile to provide a brief overview of the general way in which model transfers are parameterised in dynamic ecosystem models. Example 1 below provides a two-species interaction in a closed system and Example 2 extends the problem to a three-compartment model. In the third example, the fundamental modelling techniques are applied to the interaction of simple nutrient cycle.

5.2.2.2. EXAMPLE 1: CLOSED SYSTEM - TWO COMPARTMENT MODEL

Suppose two species N_1 and N_2 interact reversibly, where the initial concentration of $[N_1]_0=[N_2]_0=0.1$ arbitrary units [Fig. 5.14]. The forward and reverse reactions are determined by the first order rate constants k_1 and k_2, respectively.

$$N_1 \underset{k_2}{\overset{k_1}{\rightleftharpoons}} N_2$$
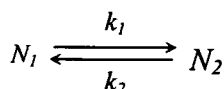
Fig. 5.14. Representation of a two-species reversible interaction.

Fig. 5.15a [RUN 1] shows the modelled concentrations of N_1 and N_2 where $k_1=k_2=0.1$ (time)$^{-1}$. Since k_1 and k_2 are identical, the concentration of N_1 and N_2 at any t will also be identical, and equal to 0.1. Accordingly, $[N_1]$ and $[N_2]$ are represented by a horizontal line.

Consider now where $[N_2]_0=0$. The simulation [Fig. 5.15a, RUN 2] shows how the concentration of N_1 and N_2 exponentially decrease and increase, respectively, to the steady state concentrations $[N_1]_{ss}=[N_2]_{ss}=0.05$ units.

In the final scenario, $[N_1]_0=[N_2]_0=0.1$ units and $k_1=0.05$ (time)$^{-1}$ and $k_2=0.1$ (time)$^{-1}$ [Fig. 5.15a, RUN 3]. The total concentration of both species at any point is 0.2 units, and the partial concentration is determined by the exchange rates. Since the loss of N_2 ($k_2=0.1$) is twice the loss of N_1 ($k_1=0.05$), at steady state $[N1]_{ss}=0.133$, and $[N_2]_{ss}=0.067$.

5.2.2.3. EXAMPLE 2: CLOSED SYSTEM - THREE COMPARTMENT MODEL

A third reactive species can be added to the above example, forming a closed non-reversible exchange cycle [Fig. 5.16].

$$N_1 \xleftarrow{\ k_3\ } N_3$$
$$k_1 \searrow \qquad \nearrow k_2$$
$$N_2$$
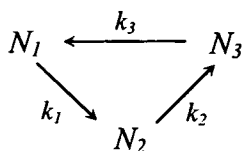
Fig. 5.16. Representation of a three-species irreversible interaction.

Consider the case where $[N_1]_0=0.1$ units and $[N_2]_0=[N_3]_0=0$, with transfers $k_1=0.1$ (time)$^{-1}$, $k_2=0.05$ (time)$^{-1}$ and $k_3=0.1$ (time)$^{-1}$. Accordingly, since k_2 is the slowest step, Fig. 5.15b shows that at steady state $[N_2]_{ss}=[N_1]_{ss}+[N_3]_{ss}$ where $[N_1]_{ss}=[N3]_{ss}=0.025$ units.

Subsequently, a constant external input of 0.01 (time)$^{-1}$ is added to N_1. The model results for each variable are shown in Fig. 5.15c. At steady state a constant increase in each nutrient is observed, where the sum of the individual increase for each variable equals 0.01 units (time)$^{-1}$, equal to the external input. In addition, the linear increase of $[N_2]_{ss}$ at equilibrium equals $[N_1]_{ss}+[N_3]_{ss}$.
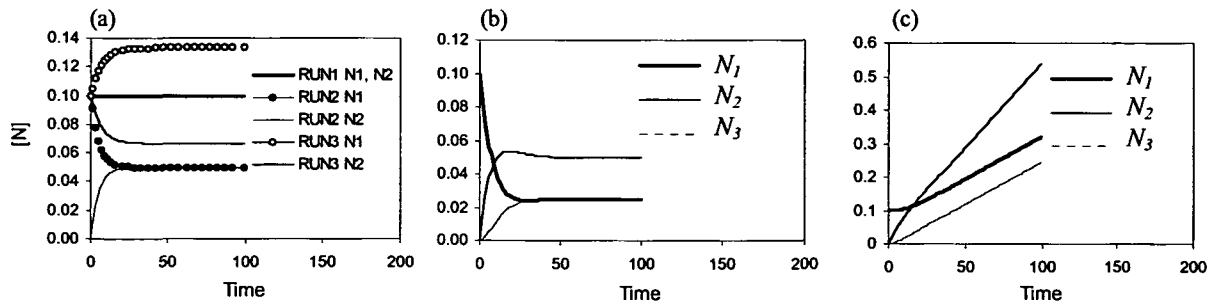
Fig. 5.15. Model simulations for (a) a closed two-compartment model, and (b) a closed three-compartment model, and (c) a, open three-compartment model.

5.2.2.4. EXAMPLE 3: APPLICATION TO A DYNAMIC NUTRIENT CYCLE

The basic principles addressed in Examples 1 and 2 are adaptable to nutrient dynamics. Taking a simplified marine nitrogen cycle as an example, a number of state variables must be selected to model nitrogen effectively. These could be dissolved inorganic nitrogen in the water column (DIN), suspended particulate organic nitrogen (PON), sediment particulate organic nitrogen ($PONSED$) and sediment dissolved inorganic nitrogen ($DINSED$). The conceptual model is shown schematically in Fig. 5.17. The exchanges between variables represent an external input (k_{in}), photosynthesis (k_1), sedimentation (k_2), remineralisation (k_3), and efflux (k_4). An additional DIN loss via denitrification (k_5) is also conceivable.
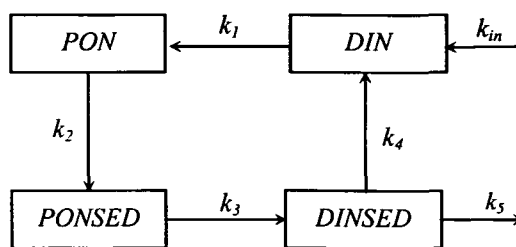
Fig. 5.17. Basic marine nitrogen cycle.

Consider a closed system ($k_{in}=k_5=0$), where $[DIN]_0=0.1$ and $[PON]_0=[PONSED]_0=[DINSED]_0=0$. The model simulation using transfers $k_1=k_3=k_4=0.1$ (time)$^{-1}$, and $k_2=0.05$ (time)$^{-1}$ is shown in Fig. 5.18a. At steady state ($\sim t=80$), DIN nitrogen is distributed within the model. Highest steady

state concentrations are predicted for *PON* since $k_2=0.5 \times k_{1,3,4}$. As a result, $[PON]_{ss}=2 \times [PONSED]_{ss}=2 \times [DIN]_{ss}=2 \times [DINSED]_{ss}=0.04$ units.

Fig. 5.18b shows the effect of including denitrification as an output from *DINSED* equal to the rate of efflux ($k_4=k_5=0.1$ (time)$^{-1}$). *PON* and *PONSED* concentrations increase up to $t=20$ as before, but show an inflection as nitrogen is consumed by denitrification. Consequently, all variables show an exponential loss to zero concentration at $t=\infty$.
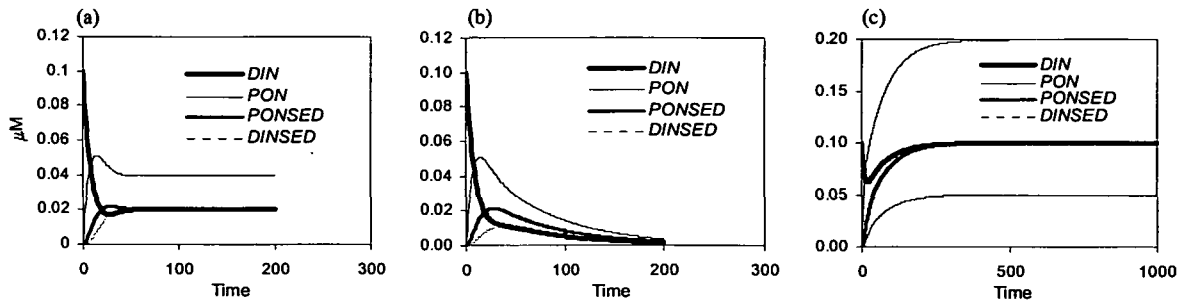
Fig. 5.18. Model simulations for (a,b) a closed four-compartment model, and (c) an open four-compartment model.

In the final example, an external input is added to DIN at $k_{in}=0.01$ (time)$^{-1}$ [Fig. 5.18c]. At $t=\sim400$ $[DINSED]_{ss}=0.5 \times [PONSED]_{ss}=0.5 \times [DIN]_{ss}$, since 50% *DINSED* is denitrified. The total nitrogen in the model at steady state will be a function of the rate of external nitrogen gains or losses, whereas the proportion of nitrogen within each pool is a function of internal exchanges between variables. It is clear that an enormous scope for model complexity is quickly generated from only four model components. In addition, external nutrient exchanges and boundary conditions are, in general, temporally variable. Marine modelling, therefore, is a challenging aspect of ecosystem analysis, and must be approached systematically.

123

5.2.3. 0-D MODEL OF THE PONTEVEDRA RIA

The biogeochemical model is adapted from the productivity template supplied with the ECoS package [*Harris and Gorley*, 1998b]. A summary of the state variables used in the final hydrodynamic biogeochemical model is given in Table 5.2. Table 5.3 presents the transfers between variables with a cross-reference to the corresponding formulae in the text. Table 5.4 lists the functional parameters used throughout this section. Table 5.5 summarises all the formulae used for the hydrodynamic biogeochemical model, indicating where modifications have been made to the default ECoS template. In this chapter, state variables [Table 5.2] and transfers [Table 5.3] are reported in italics, with all capital letters for variables and only the first letter capitalised for transfers. Parameters are also italicised.

5.2.3.1. PHYTOPLANKTON PRODUCTION AND PARTICULATE TRANSFER

The principal state variables for particulate material in the default ECoS biogeochemical template are phytoplankton *(PHYTO)*, particulate organic matter *(POM)*, and benthic particulate organic matter, *(POMSED)*. Fig. 5.19 shows a conceptual diagram of the default ECoS transfers between these state variables. The model is driven by primary production, *Prodn*, via marine autotrophs leading to an increase in *PHYTO* biomass. Phytoplankton mortality, *Mort*, is treated as an input to *POM*, which may then fall to the sediment via the transfer function *Dropout* and return to the water column by resuspension, *Resus*. Losses from the compartments include aerobic respiration, *Respn*, and remineralisation of organic matter in the water column, *Miner*$_W$, and sediments, *Miner*$_S$.
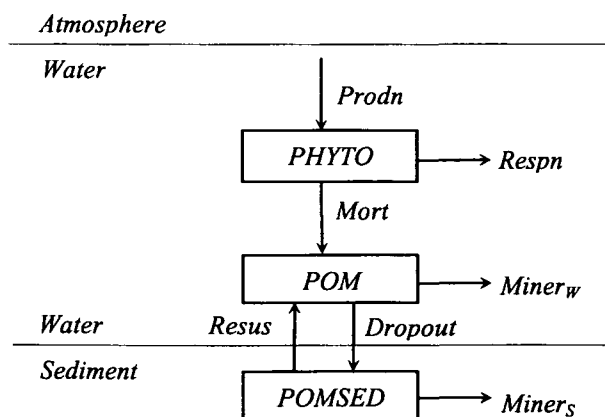
Fig. 5.19. Biogenic particulate transfers supplied with the ECoS package.

Table 5.2. Definition of the biogeochemical model state variables.

Symbol	Definition
Water column state variable	
PHYTO	Phytoplanktonic organic material
POM	Particulate organic material
NH4	Dissolved inorganic ammonium
NO3	Dissolved inorganic nitrate
PO4	Dissolved inorganic phosphate
Benthic state variable	
POMSED	Particulate organic material
NH4SED	Dissolved inorganic ammonium
NO3SED	Dissolved inorganic nitrate
PO4SED	Dissolved inorganic phosphate

Table 5.3. Processes used in the biogeochemical model.

Function	Definition	Formula
Denit	Denitrification in sediment	Eq. [5.58]
Dropout	Sedimentation of *POM*	Eq. [5.40]
NH4gen	Pelagic *NH4* remineralisation	Eq. [5.41]
NH4SEDgen	Benthic *NH4* remineralisation	Eq. [5.54]
NH4inc	Phytoplankton *NH4* uptake	Eq. [5.47]
NH4rinp	Fluvial *NH4* input	
Miner$_W$	Pelagic remineralisation of *POM*	Eq. [5.37]
Miner$_S$	Benthic remineralisation of *POM*	Eq. [5.53]
Mort	Phytoplankton mortality	Eq. [5.35]
Nitri$_W$	Pelagic nitrification	Eq. [5.45]
Nitri$_S$	Benthic nitrification	Eq. [5.56]
NO3inc	*NO3* uptake by phytoplankton	Eq. [5.48]
NO3rinp	Fluvial *NO3* input	
PO4gen	Pelagic *PO4* remineralisation	Eq. [5.42]
PO4SEDgen	Benthic *PO4* remineralisation	Eq. [5.55]
PO4inc	Phytoplankton *PO4* uptake	Eq. [5.49]
PO4rinp	Fluvial *PO4* input	
Prodn	Phytoplankton production	Eq. [5.23]
Respn	Phytoplankton respiration	Eq. [5.36]
Resus	Benthic resuspension	Eq. [5.52]
ZOOassm	Zooplankton secondary production	Eq. [5.60]

Table 5.4. Parameters used in the biogeochemical model.

Function	Definition	Rate/Units
α	Initial slope of light saturation curve	0.02 mg C (mg Chl a)$^{-1}$ h^{-1} (W m^{-2})$^{-1}$
α_{Ph}	Attenuation coefficient for phytoplankton	0.05 m^{-1}
α_{H2O}	Attenuation coefficient for water	0.1 m^{-1}
α_{SPM}	Attenuation coefficient for SPM	500 l g^{-1} m^{-1}
$anit$	Nitrification constant	0.01
$bnit$	Nitrification constant	0.15
β	Maximum rate of photosynthesis	1 d^{-1}
$Chl\ a{:}\ C$	Chl a to carbon ratio in phytoplankton	0.35 mg Chl a (mmol C)$^{-1}$
$C{:}N$	Carbon-nitrogen ratio in phytoplankton	5.36 g g^{-1}
$C{:}P$	Carbon-phosphorus ratio in phytoplankton	38.7 g g^{-1}
C_{Sshad}	Half saturation of phytoplankton self-shading	40 μmol C l^{-1}
$Depth$	Water depth	m
f_{Denit}	Maximum rate of sediment denitrification	0.1 d^{-1}
$f_{Dropout}$	Maximum POM sedimentation in 0-D model	0.5 d^{-1}
f_{MinerW}	Maximum rate of pelagic remineralisation	0.04 d^{-1}
f_{MinerS}	Maximum rate of benthic remineralisation	0.07 d^{-1}
f_{Mort}	Maximum rate of phytoplankton mortality	0.012 d^{-1}
f_{NitriS}	Maximum rate of sediment nitrification	d^{-1}
f_{NitriW}	Maximum rate of water column nitrification	d^{-1}
f_{Respn}	Maximum rate of phytoplankton respiration	0.04 d^{-1}
f_{Resus}	Maximum rate of POM resuspension	0.5 d^{-1}
H_{SW}	Light intensity at water surface	W m^{-2}
KI	Depth integrated light attenuation coefficient	m^{-1}
KM_{NH4}	Half saturation of $NH4$	0.25 μmol l^{-1}
KM_{NO3}	Half saturation of $NO3$	0.35 μmol l^{-1}
KM_{PO4}	Half saturation of $PO4$	0.20 μmol l^{-1}
$Mlight$	Light intensity in water column	W m^{-2}
$Nulim$	Photosynthesis inhibition by nutrient conc.	0 to 1
Nup	Nitrogen limitation	0 to 1
Pup	Phosphorus limitation	0 to 1
ρ_{ria}	Density of ria water	kg m^{-3}
ρ_{ENACW}	Density of core ENACW	1027 kg m^{-3}
$S_{Dropout}$	Particulate sinking rate	10 m d^{-1}
S_{shad}	Photosynthesis light inhibition by biomass	0 to 1
t	Time	d
T	Water temperature	°C
Ψ	Total attenuation coefficient	0.3 m^{-1}

Table 5.5. ECoS default formualtions and modifications used for the Pontevedra Ria.

Process	ECoS default formula	Modifications
Benthic denitrification	none	$Denit = f_{Denit} \times NO3SED$
Sinking rate of *POM*	$S_{Dropout} = POS\left[V_s \times \left(1 - \left(\frac{U}{U_d}\right)^2\right)\right]$	$S_{Dropout}$ = first-order kinetics
Phytoplankton mortality	$Mort = f_{mort} \times PHYTO$	as default
Pelagic *NH4* remineralisation	$NH4gen = \frac{Respn + POC.Miner}{C:N}$	as default
Benthic *NH4* remineralisation	$NH4SEDgen = \frac{POC.Miner_S}{C:N}$	as default
Phytoplankton *NH4* uptake	$NH4inc = \frac{Prodn \times PHYTO}{NH4 \times C:N} \times \frac{\frac{NH4}{KM_{NH4}}}{\left(\frac{NH4}{KM_{NH4}} + \frac{NO3}{KM_{NO3}}\right)}$	as default
Benthic remineralisation	$Miner_S = f_{MinerS} \times POCSED$	as default
Pelagic remineralisation	$Miner_W = f_{MinerW} \times POC$	as default
Pelagic nitrification	$Nitri_w = \frac{(a_N + b_N \times SPM)}{NH4}$	$Nitri_w = f_{NitriW} \times NH4$, $f_{NitriW} = anit \times e^{bnit \times T}$
Benthic nitrification	none	$Nitri_s = f_{NitriS} \times NH4SED$, $f_{NitriS} = anit \times e^{bnit \times T}$
Phytoplankton *NO3* uptake	$NO3inc = \frac{Prodn \times PHYTO}{NO3 \times C:N} \times \frac{\frac{NO3}{KM_{NO3}}}{\left(\frac{NH4}{KM_{NH4}} + \frac{NO3}{KM_{NO3}}\right)}$	as default
Pelagic *PO4* remineralisation	$PO4gen = \frac{Respn + POC.Miner}{C:P}$	as default
Benthic *PO4* remineralisation	$PO4SEDgen = \frac{POC.Miner_S}{C:P}$	as default
Phytoplankton *PO4* uptake	$PO4inc = \frac{Prodn \times PHYTO}{PO4 \times C:P}$	as default
Phytoplankton production	$Prodn = \beta \times TANH(\alpha \times Mlight) \times Nu\,lim$	as default
Phytoplankton respiration	$Respn = f_{respn} \times PHYTO$	as default
Resuspension of *POM* and nutrients	$Resus = POS\left[Me \times \left(\left(\frac{U}{Ue}\right)^2 - 1\right)\right]$	$Resus = f_{Resus} \times POM \times [1 + TANH(\rho_{ria} - \rho_{ENACW})]$

The rate of change of each variable can be expressed as:

$$\frac{d[PHYTO]}{dt} = growth - losses = Pr\,odn - Mort - Re\,spn \qquad [5.19]$$

$$\frac{d[POM]}{dt} = Mort + Re\,sus - Miner_W - Dropout \qquad [5.20]$$

$$\frac{d[POMSED]}{dt} = Dropout - Miner_S - Re\,sus \qquad [5.21]$$

Prodn introduces organic carbon to the system by removal of dissolved inorganic carbon (*DIC*) and nutrients from the water column. *DIC* is not explicitly modelled in ECoS, and the *DIC* stock is assumed to be infinitely large. The default stoichiometry of the organic matter in ECoS is $C_{100}N_{16}P$. However, according to IGBP-LOICZ protocols [*Gordon et al.*, 1996], the composition of organic matter generally follows the stoichiometry of the so-called Redfield ratios [$C_{106}N_{16}P$, *Redfield et al.*, 1963]. Accordingly, the charged balanced net phytoplankton photosynthesis reaction can be represented by:

$$106CO_2 + 16H^+ + 16NO_3^- + H_3PO_4 + 122H_2O \rightarrow (CH_2O)_{106}(NH_3)_{16}H_3PO_4 + 138O_2 \quad [5.22]$$
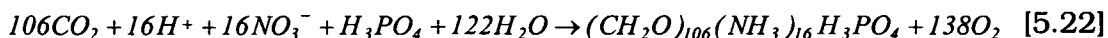
The C:N:P ratio in the ECoS template was thus modified to agree with Eq. 5.22. Therefore, *PHYTO* and *POM* is biogenic organic matter of Redfieldian stoichiometry. This is an important aspect of the modelling, since remineralisation of *POM* will also regenerate dissolved inorganic carbon and nutrients in Redfield stoichiometry.

Prodn is based on the light-saturation curve relating photosynthesis per unit biomass to the irradiance experienced by phytoplankton within the water column *Mlight* (W m⁻²):

$$Pr\,odn = \beta \times TANH(\alpha \times Mlight) \times Nu\,lim \qquad [5.23]$$

where β is the maximum rate of photosynthesis or assimilation number [typically mg C (mg Chl a)⁻¹ h⁻¹; *Platt and Jassby*, 1976; *Jassby et al.*, 2002] and α is the initial slope of the light saturation curve or the photosynthetic efficiency (mg C (mg Chl a)⁻¹ h⁻¹ (W m⁻²)⁻¹); equivalent to the rate at which β is reached as *Mlight* increases. The hyperbolic tangent function for *Prodn* is shown in Fig. 5.20 with different values for β and α. *Prodn* in ECoS is defined as a proportional increase of *PHYTO* where β is the first-order kinetic constant for *PHYTO* growth. The default values for β and α are 1.54×10^{-5} s⁻¹ (i.e. 1.33 d⁻¹) and 0.0217 mg C (mg Chl a)⁻¹ h⁻¹ [W m⁻²]⁻¹, respectively. In the present model, a value of α=0.02 was used, based on bio-optical experiments in the Vigo Ria by *Tilstone et al.* [1999] and *Arbones et al.* [2000]. There is considerable variability in the literature with regard to β, which ranges from to 0.02 to 3.0 d⁻¹ [*Tett*, 1990; *Chapelle et al.*, 1994; *Savchuk and Wulff*, 1996; *Tyrrell*, 1999; *Humborg et al.*, 2000; *Ianson and Allen*, 2002; *Wild-Allen et al.*, 2002]. Some of these authors included a temperature dependence of phytoplankton growth. Initial modelling of the Pontevedra Ria uses a value of β=1 d⁻¹. Clearly, there may well be inter-

specie and seasonal variability of α and β [Tilstone et al., 1999], as well as complications arising from species succession and seasonal variability of photosynthetically active radiation (PAR). At this stage, however, it was prudent to opt for simplification over complication, and therefore a single value for α and β was used.

(a)   **(b)**
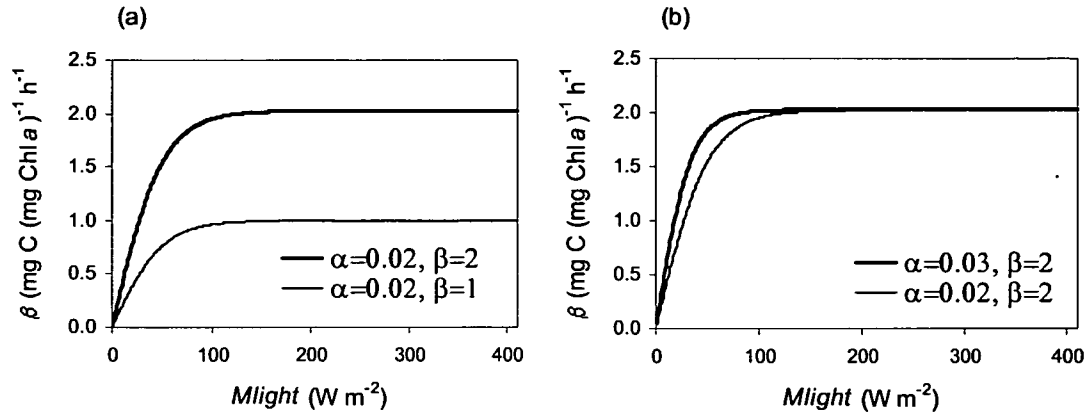
Fig. 5.20. Relationship between β and Mlight [Eq. 5.23] with different values for (a) β and (b) α.

Mlight is a function of the light intensity at the water surface, H_{SW} [W m^{-2}, Fig. 2.3a], the attenuation coefficient for water (α_{H2O}, m^{-1}) and SPM (α_{SPM}, m^{-1}), and water depth (Depth, m):

$$Mlight = H_{SW} \times \frac{(1 - e^{-\Psi})}{\Psi}$$ [5.24]

$$\Psi = Depth \times KI$$ [5.25]

$$KI = \alpha_{H2O} + \alpha_{SPM}$$ [5.26]

α_{H2O} was defined as 0.1 m^{-1}, and α_{SPM} was 500 l g^{-1} m^{-1} [Miller and Zepp, 1979]. H_{SW} was scaled between 0 and 100% by the attenuation and Depth at any point. Unfortunately, there is no supporting SPM data for the Pontevedra Ria. The mean±SD SPM concentration of the incoming river water is 22.5±35.6 mg l^{-1} [Ibarra and Prego, 1997]. Further, given that the salinity range of the Pontevedra Ria was between 31-35 [Ruiz Villarreal et al., 2002], the turbidity of the Pontevedra Ria was assumed to equal to that of coastal seawater [~3×10^{-4} g l^{-1}; R. Prego, Pers. Comm.].

With increased phytoplankton numbers, less light will penetrate the lower depths of the ria, thus reducing β. Therefore, an additional light inhibition was formulated on the basis of phytoplankton self-shading in the water column, S_{shad}. A Michaelis-Menten expression was used to describe S_{shad}, assuming that assimilation decreases to 50% when PHYTO reaches a defined concentration C_{Sshad}:

$$S_{shad} = 1 - \frac{PHYTO}{C_{Sshad} + PHYTO}$$ [5.27]

However, after initial modelling this formulation was neglected since it was unclear what *PHYTO* concentration could best represent C_{Sshad}, although a value of 2 µmol l^{-1} for *PON* (~13 µmol l^{-1} *POM*) has been suggested [*Gordon et al.*, 1996]. *Savchuk and Wulff* [1996] proposed that light absorption from zooplankton and phytoplankton (α_{Ph}) in the Baltic Sea was <3% of α_{H2O}. In addition, α_{Ph} has been reported to be generally within the range 0.01-0.1 m^{-1} in the Rias Bajas, depending on the wavelength of the incoming radiation [*Arbones et al.*, 1996]. Assuming that α_{Ph} = 0.05 m^{-1}, *KI* transforms to:

$$KI = \alpha_{H2O} + \alpha_{SPM} + \alpha_{Ph} \qquad [5.28]$$

where *KI* is the total attenuation and equal to 0.30 m^{-1} using the parameterisations above. This value is in good agreement with the Secchi disc-derived *KI* values in Fig. 2.3b and those by *Figueiras and Niell* [1986] for the Pontevedra Ria.

The final term in Eq. 5.23, *Nulim*, represents nutrient limitation of photosynthesis. In ECoS, *Nulim* switches between nitrogen (*Nup*) and phosphorus limitation (*Pup*) depending on which has the minimum concentration:

$$Nu\,lim = MIN(\,Nup, Pup\,) \qquad [5.29]$$

Competition between ammonium and nitrate is represented by the hyperbolic dependence of concentration and the half-saturation Michaelis-Menten constants for ammonium (KM_{NH4}) and nitrate (KM_{NO3}):

$$Nup = NupNH4 + NupNO3 \qquad [5.30]$$

$$NupNH4 = \frac{\left(\dfrac{NH4}{KM_{NH4}}\right)}{\left(1 + \left(\dfrac{NO3}{KM_{NO3}}\right) + \left(\dfrac{NH4}{KM_{NH4}}\right)\right)} \qquad [5.31]$$

$$NupNO3 = \frac{\left(\dfrac{NO3}{KM_{NO3}}\right)}{\left(1 + \left(\dfrac{NO3}{KM_{NO3}}\right) + \left(\dfrac{NH4}{KM_{NH4}}\right)\right)} \qquad [5.32]$$

Similarly for phosphate limitation, with no competing nutrient and a half-saturation constant KM_{PO4}:

$$Pup = \frac{\left(\dfrac{PO4}{KM_{PO4}}\right)}{\left(1 + \left(\dfrac{PO4}{KM_{PO4}}\right)\right)} \qquad [5.33]$$

A graphical representation of how *Pup* depends on *PO4* concentration for various *KM* coefficients is shown in Fig. 5.21. Low *KM* are associated with

higher Pup and less nutrient limitation of $Prodn$. The greater the ratio of the ambient nutrient concentration to its half-saturation constant, Pup or Nup and hence by implication, $Nulim$, will tend toward 1. The default values for KM_{NH4}, KM_{NO3} and KM_{PO4} are 0.7, 0.7 and 0.3 μmol l^{-1}, respectively. However, KM_{NH4} is likely to be lower than KM_{NO3} since phytoplankton have a greater affinity for ammonium compared to nitrate [$Lomas$ and $Gilbert$, 1999]. Metabolic energy must be spent on reducing nitrate to ammonium before the nitrogen it can be utilised by phytoplankton enzymes, which requires energy. Based on a range of literature vales, KM_{NH4}, KM_{NO3} and KM_{PO4} for the Pontevedra Ria were defined as 0.25, 0.35 and 0.2 μmol l^{-1}, respectively. Supposing a typical phosphate concentration of 0.40 μmol l^{-1} [Fig. 4.14], Pup would equal 0.66. Similarly, with nitrate and ammonium concentrations of 5.0 and 1.0 μmol l^{-1}, respectively, Nup would equal 0.95. Accordingly, under these conditions, phosphorus limitation would reduce $Prodn$ by 34%.
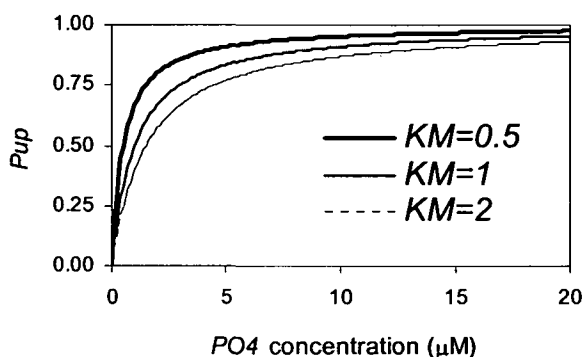
Fig. 5.21. Dependence of Pup (Eq. 5.33) on $PO4$ concentration (μM) with various Michaelis-Menten half-saturation constants.

Organic material lost from $PHYTO$ via $Mort$ is transferred to the POM state variable [Fig. 5.19]. $PHYTO$ biomass is also decreased by autotrophic respiration, $Respn$. POM and $POMSED$ are consumed by remineralisation, $Miner_W$ and $Miner_S$, respectively. $Miner_S$ is discussed in the benthic sub-model below. The equation for remineralisation can generally be written as an electron transfer from organic material (CH_2O) via an electron acceptor ($e.a.$) to give CO_2 and remineralised inorganic nutrients as products:

$$CH_2O + e.a. \rightarrow CO_2 + Ninorg, Pinorg...$$ [5.34]

Carbon output from $PHYTO$ and POM via $Respn$ and $Miner_W$ is lost from the system unless, of course, there is supporting data to permit a state variable for dissolved inorganic carbon.

Maximum rates of mortality, f_{Mort}, respiration, f_{Respn}, and remineralisation, f_{Miner_W}, in the literature are generally represented by first-order kinetics:

$$Mort = f_{Mort} \times PHYTO$$ [5.35]

$$Respn = f_{Respn} \times PHYTO$$ [5.36]

$$Miner_W = f_{MinerW} \times POM \qquad \qquad [5.37]$$

The rate constants for these processes are listed in Table 5.4. The default ECoS value for f_{Mort} was 0.009 d^{-1}, which is approximately 25% lower than recent literature values [*Anderson and Williams*, 1999; *Humborg et al.*, 2000; *Tian et al.*, 2001]. Thus, a value of 0.012 was used for f_{Mort} for the Pontevedra Ria. f_{Respn} was encoded in ECoS as 0.04 d^{-1} and agrees with the L3VMP model of the North Sea by *Tett* [1990]. f_{MinerW} was equal to 0.04 d^{-1}.

POM is transferred to the bed sediment from the water column by particulate *Dropout* [Fig. 5.19]. In the default ECoS model, *Dropout* represents a first order loss of POM as a function of the particulate sinking velocity, $S_{Dropout}$ (m d^{-1}), *Depth* (m) and water velocity, U (m d^{-1}):

$$Dropout = \frac{S_{Dropout}}{Depth} \qquad \qquad [5.38]$$

$$S_{Dropout} = POS\left[V_S \times \left(1 - \left(\frac{U}{U_d}\right)^2 \right) \right] \qquad POS(a) = a \text{ if } a{>}0, \; 0 \text{ otherwise} \qquad [5.39]$$

where V_S is the sinking rate of particles in suspension (m d^{-1}) and U_d is the upper threshold velocity for deposition (m d^{-1}). When $U > U_d$ deposition is zero. However, for the 0-D model, hydrodynamics are absent and a parameterisation of $S_{Dropout}$ was required. In other ecosystem models [e.g. *Lee et al.*, 2002], detrital material is often defined as fast sinking (~100 m d^{-1}) or slow sinking (~0.1 m d^{-1}). A sinking rate of $S_{Dropout}$=10 m d^{-1} would appear to be an appropriate compromise for general particulate material on the Galician shelf [*Halvorsen et al.*, 2001]. For the 0-D model, assuming the mean depth of the Pontevedra Ria to be 20 m, then from Eq. 5.38 the first-order *Dropout* rate loss, $f_{Dropout}$, is 0.5 d^{-1}:

$$Dropout = f_{Dropout} \times POM \qquad \qquad [5.40]$$

Clearly, in the hydrodynamic model, the magnitude of *Dropout* at any location in the ria will depend on the water depth at that point.

Model results. Fig. 5.22 shows simulated PHYTO, POM and POMSED for the conceptual 0-D model [Fig. 5.19] using the transfer rates detailed above. In view of the fact that these components are derived from phytoplanktonic material, they can be modelled on the basis of their *C*, *N* or *P* content. In these examples they are modelled as *C*, although it should be remembered that there will be a concomitant draw-down and regeneration of *N* and *P*.

Example 1 [Fig. 5.22a]. Consider a closed system whereby all particulate matter was contained within the model (*Prodn*=*Respn*=*Miner*=0) and *[PHYTO]₀*=40 μmol C l^{-1}, *[POM]₀*=20 μmol C l^{-1} and *[POMSED]₀*=0 μmol C l^{-1}. It was assumed that 50% of POMSED was resuspended daily, *Resus* (0.5 d^{-1}). The first order decrease in PHYTO was attributable to *Mort* transfer to the POM pool. POM, however, is subsequently consumed by a first order *Dropout* to POMSED. At *t*=∞, PHYTO tended to zero since it had no associated input.
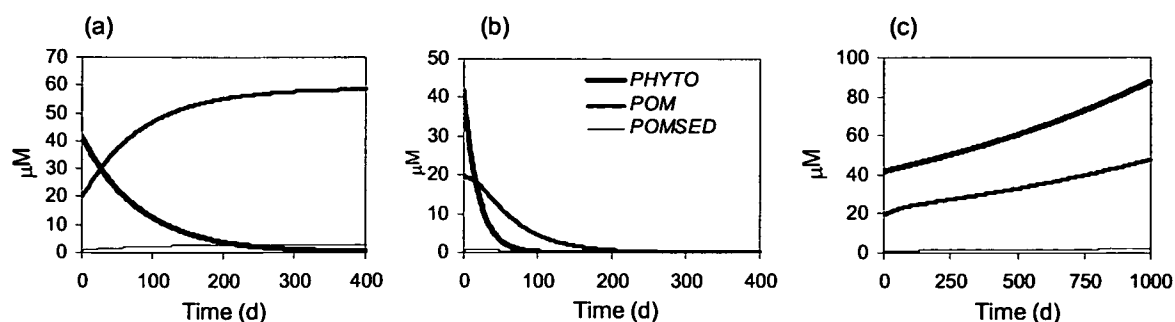
Fig. 5.22. Simulated particulate material for the zero-dimensional model. (a) and (b) are closed systems and (c) is open.

Example 2 [Fig. 5.22b]. In this case proportional loss terms for *Respn* [Eq. 5.34] and *Miner$_W$* [Eq. 5.35] were included [Table 5.4]. As a result, all particulate material was gradually transformed into dissolved inorganic nutrients and carbon. To reiterate, dissolved inorganic carbon is not a state variable, and respired carbon is lost from the model leading to a decrease to zero for [*PHYTO*], [*POM*] and [*POMSED*] at $t=\infty$.

Example 3 [Fig. 5.22c]. A carbon input was added to the *PHYTO* variable to represent photosynthesis [Eq. 5.23]. *Prodn* was initially parameterised with β only ($\beta = 0.05$ d^{-1}) in order to facilitate the relative transfers of carbon through the system without the added complication of light inhibition and nutrient limitation. In this simplified sub-model, *PHYTO* increase via *Prodn* was a source of local instability [*Laws*, 1997]. Therefore, the value for β used in this example differed from the value in Table 5.4 (1 d^{-1}) since *Prodn-Respn-Mort* must be kept to a minimum to avoid a rapid exponential growth of *PHYTO*. These controlling terms can be added at a later stage to calibrate the hydrodynamic model. Without these loss terms, Fig. 5.22c shows an exponential increase in each compartment, although the exponent of each increase will depend on the transfer rate between each compartment.

5.2.3.2. WATER COLUMN NUTRIENT DYNAMICS

The 0-D model outputs for the particulate variables in the previous section are laudable and rational, given the main trophic energy transfers employed. Therefore, the inorganic nutrients *NH4*, *NO3* and *PO4* can now be incorporated into the successive modelling shell [Fig. 5.23].

NH4 and *PO4* in the water column have an input from phytoplankton respiration, *Respn* [Eq. 5.36], and *Miner$_W$* [Eq. 5.37]. Therefore, where *C:N* and *C:P* are the elemental carbon-nitrogen and carbon-phosphorus phytoplanktonic nutrient ratios (g g^{-1}), the total in situ regeneration for *NH4* and *PO4* is:

$$NH4gen = \frac{Re\,spn + Miner_W}{C:N}$$

[5.41]

$$PO4gen = \frac{Re\,spn + Miner_W}{C:P}$$

[5.42]
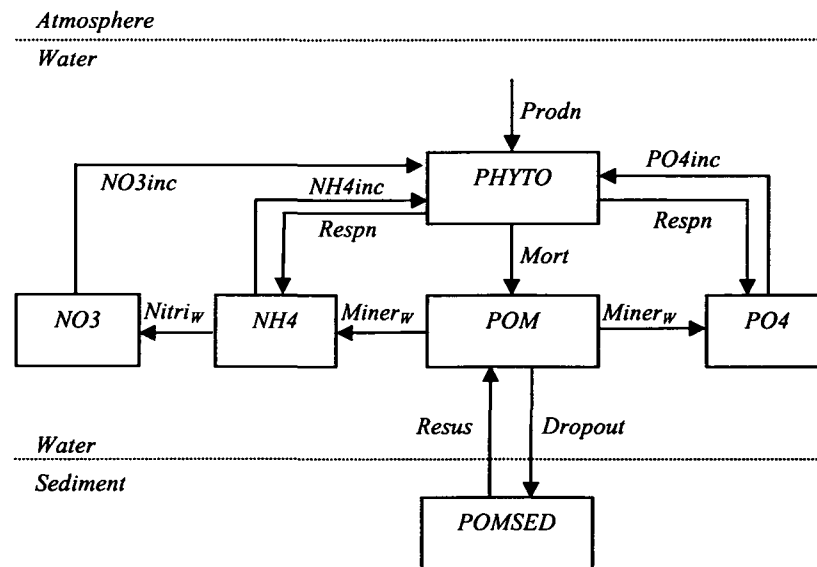
Fig. 5.23. Conceptual model of pelagic nutrient dynamics of the Pontevedra Ria used in the 0-D model.

$NO3$ generation in the water column occurs via nitrification of $NH4$ ($Nitri_W$). In modelling studies $Nitri_W$ has been defined as being proportional to the concentration of $NH4$ and limited by oxygen availability [$Tett$, 1990; Regnier et $al.$, 1997]. $Nitri_W$ is a two-step reaction involving the oxidation of $NH4$ to $NO2$, and the subsequent oxidation of $NO2$ to $NO3$. The overall reaction can be summarised as follows:

$$NH_4^+ + 2O_2 + 2HCO_3^- \rightarrow NO_3^- + 2CO_2 + 3H_2O$$ [5.43]
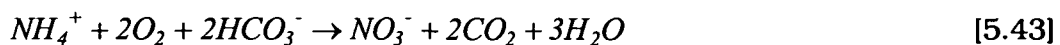
The nitrification template in ECoS was constructed from observations of nitrifying bacteria attached to suspended SPM in the turbid Tamar estuary, UK [$Owens$, 1986]. The default ECoS formula is given in Eq. 5.44, where a_N and b_N are constants [$Owens$, 1986]:

$$Nitri_W = \frac{(a_N + b_N \times SPM)}{NH4}$$ [5.44]

SPM concentrations may reach values of up to 1 g l^{-1} in the Tamar estuary [$Uncles$ et $al.$, 1985a,b], implying that this formulation is probably not applicable to the Pontevedra Ria. Thus, the single temperature-dependent process given by $Savchuk$ and $Wulff$ [1996] was used here, assuming no oxygen limitation or photo-inhibition of nitrifying microbes:

$$Nitri_W = f_{NitriW} \times NH4$$ [5.45]

$$f_{NitriW} = anit \times e^{bnit \times T}$$ [5.46]

where *anit* and *bnit* are constants [Table 5.4]. Thus, at a mean temperature of the Pontevedra Ria (16 °C), f_{Nitriw}=0.11 d^{-1}. A similar temperature dependence of nitrification was adopted by *Chapelle et al.* [1994] and *Humborg et al.* [2000]. For the 0-D model (temperature not considered) a first order constant of 0.11 d^{-1} was used.

Incorporation of nutrients into *PHYTO* occurs simultaneously with *Prodn*, and is defined as a stoichiometric proportional output from each nutrient pool depending on the size of the phytoplankton biomass and the rate of photosynthesis:

$$NH4inc = \frac{Prodn \times PHYTO}{NH4 \times C:N} \times \frac{\dfrac{NH4}{KM_{NH4}}}{\left(\dfrac{NH4}{KM_{NH4}} + \dfrac{NO3}{KM_{NO3}}\right)} \qquad [5.47]$$

$$NO3inc = \frac{Prodn \times PHYTO}{NO3 \times C:N} \times \frac{\dfrac{NO3}{KM_{NO3}}}{\left(\dfrac{NH4}{KM_{NH4}} + \dfrac{NO3}{KM_{NO3}}\right)} \qquad [5.48]$$

$$PO4inc = \frac{Prodn \times PHYTO}{PO4 \times C:P} \qquad [5.49]$$

The second term in Eqs. 5.47 and 5.48 represents the Michaelis-Menten kinetic competition between *NH4* and *NO3* uptake. The half-saturation constants are the same as previously [Table 5.4].

Model results. Suppose initial nutrient concentrations of $[NH4]_0=[NO3]_0=10$ μmol l^{-1}, and $[PO4]_0=5$ μmol l^{-1}. *Prodn*, *Minerw*, *Respn* and *Resus* remain unchanged from *Example 3* in the previous section, and f_{Nitriw} = 0.11.

The evolution of pelagic nutrient concentrations is shown in Fig. 5.24a-c, along with the absolute transfer for *PO4inc*, *PO4gen*, *NH4inc*, *NH4gen*, *NO3inc* and *Nitriw* in Fig. 5.24d-f. Fig. 5.24g-h shows the evolution of the uptake and limitation terms. The rapid increase in *NO3* and decrease in *NH4* was due to the initial transfer from *NH4* to *NO3* by in situ nitrification. *NH4* increased after *t*=400 since *NH4gen* > *NH4inc* [Fig. 5.24e]. *PO4* displayed a steady decrease in concentration over the simulation engendered by a slightly larger *PO4inc* than *PO4gen* [Fig. 5.24f]. Since *PO4* has no competing nutrient, its rate of decrease was a reflection of the size difference between *PO4inc* and *PO4gen*.

From Fig. 5.24g, *NO3* rather than *NH4* was initially observed as the nitrogenous nutrient favoured by phytoplankton due to the large *Nitriw* output from *NH4*. Fig. 5.24h illustrates how nitrogen rapidly became the limiting nutrient in the model as *NO3* and *NH4* concentrations fell below their *KM* concentrations. At this point, *Prodn* would be totally nitrogen limited. It is also worth noting that $[NH4]+[NO3]$ fell to zero before *PO4* since the initial N:P concentrations were below Redfield stoichiometry, as observed in the field [Fig. 4.14].
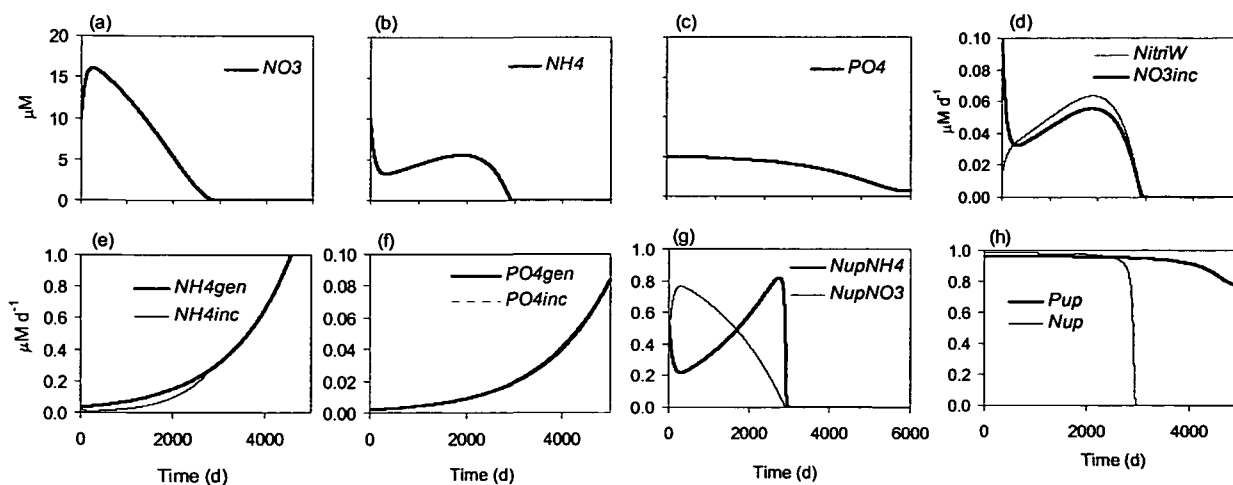
Fig. 5.24. Simulated pelagic nutrient dynamics for the zero-dimensional model [Note: *PO4gen* and *PO4inc* are superimposed].

5.2.3.3. BENTHIC NUTRIENT CYCLING

The benthic surface layer tends to be dominated by recently-settled, reactive detritus composed of organic, opaline and calcareous material. The structure of *POM* depends on the degree of degradation and particulate surface area [*Beaulieu*, 2002], both of which contribute to the overall settling velocity. Phytogenic detritus has a low settling velocity [*Beaulieu*, 2002], and may be held in suspension above the bed sediments as quasi-benthic fluff [*Jago and Jones*, 1998]. With residence times of the order of days to weeks, benthic fluff layers are ephemeral features of the sediment-water interface [*Jago et al.*, 1993; *Beaulieu*, 2002]. In some areas, fluff thickness may exceed 20 cm [*Laima et al.*, 2002].

In this thesis, based on the results of Chapter 4, the modelling of the benthic biogeochemistry concentrated on the biogenic fluff, using a vertically integrated dynamic sediment model. In a review of coupled benthic-pelagic biogeochemical models, *Soetaert et al.* [2000] classified benthic models by increasing complexity and accuracy from 0 to 4. The depth-integrated dynamic benthic model advocated here may be considered as level 3 according to the definition of these workers. A diagenetic model of benthic nutrient cycling used in the Pontevedra Ria model is shown in Fig. 5.25.

Resuspension and nutrient efflux. It has recently been argued that benthic effluxes of remineralised organic matter and biogenic fluff play an important role in the net ecosystem nutrient budget of the Pontevedra Ria [*Dale and Prego*, 2002]. *Álvarez-Salgado et al.* [1996a] hypothesised that *NH4* effluxes are synchronised to the upwelling stress-relaxation cycle. In Section 4.2 evidence was presented suggesting that high *NH4* effluxes of approximately 3.5 mg N m⁻² h⁻¹ are induced by stirring of benthic fluff during the rising upwelling cycle. Subsequently, during upwelling relaxation, the fluff settling velocity supersedes the water velocity leading to an increase in *POM* deposition and promotion of microbial degradation of benthic organic matter. The role of upwelling in the benthic *NO3* cycle is less clear on the

sampling time-scale in this work [*Dale and Prego*, 2002]. Maximum values of *NO3* efflux in the Pontevedra Ria are of the order 0.7 mg N m^{-2} h^{-1}.

Resuspension, sedimentation and bioturbation influence the efflux of nutrients across the sediment (fluff)-water interface. If the model values for *Resus*, *Dropout*, *Miner$_S$*, *Nitri$_S$* and *Denit* are correctly parameterised [Fig. 5.25], then in theory the nutrient efflux rate is the difference between these rates. This, of course, assumes that there is no nutrient accumulation in the sediment, which is likely to be permissible over the annual time scale of this study.
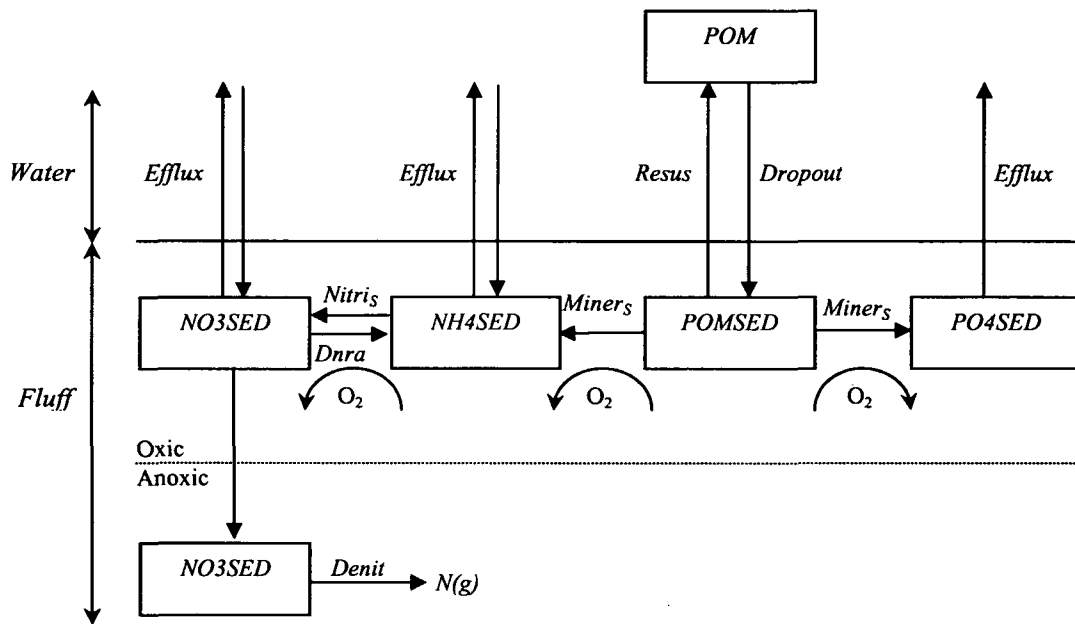
Fig. 5.25. Conceptual model of benthic nutrient dynamics of the Pontevedra Ria used in the 0-D model.

The diagenetic process begins with *POM Dropout* [Eq. 5.38]. Bioturbation is not considered. With high *Resus* the proportion of *POM* remineralised through the sediments will decrease. *POM* resuspension is thus intrinsically linked to upwelling. In the default ECoS model, *Resus* (f_{Resus}, kg m^{-2} d^{-1}) is calibrated with the erodibility Me (0.003 kg m^{-2} s^{-1}), water velocity U (m s^{-1}), the threshold water velocity for erosion *Ue* (m s^{-1}), and scaled to the amount of *POMSED* (kg m^{-2}):

$$Re\,sus = \frac{f_{Resus}}{POMSED} \qquad\qquad [5.50]$$

$$f_{Resus} = POS\left[Me\times\left(\left(\frac{U}{Ue}\right)^2 - 1\right)\right] \qquad POS(a) = a \text{ if } a>0, 0 \text{ otherwise} \qquad [5.51]$$

Elsewhere in the literature, *Resus* in coupled physical-microbiological models is a function of shear stress generated by tidal flows [*Jago et al.*, 1993; *Tett and Walne*, 1995; *Tappin et al.*, 1997]. However, in the Pontevedra Ria ECoS model, water velocity in the model is inferred from tidal elevation and runoff only, which is clearly unsuitable for enhanced

water currents due to upwelling. An underlying theme to oceanographic research in the Rías Bajas has been the tractability of ENACW on the basis of its thermohaline properties [Rosón et al. 1995]. It would therefore be advantageous to describe Resus of POM and nutrients (in this sense, nutrient Resus is synonymous with efflux) with the well-known TS signal of ENACW. Given that temperature and salinity contribute to the density, an expression for resuspension was developed employing the maximum resuspension rate f_{Resus} (d⁻¹), the density of the water in the ria, ρ_{ria}, and the density of core ENACW, ρ_{ENACW}:

$$Re\,sus = f_{Resus} \times NuSED \times \left[1 + TANH\left(\rho_{ria} - \rho_{ENACW}\right)\right]$$ [5.52]

where NuSED=NH4SED, NO3SED, PO4SED, POMSED. The maximum efflux rate for each nutrient, f_{Resus}, is equal to 0.5 d⁻¹ [Dale and Prego, 2002]. f_{Resus} depends on the relative strength of upwelling represented by the density at the mouth. PO4 is assumed to be remineralised and effluxed in stoichiometric agreement with DIN, despite possible impedance of PO4 release from sediments by the presence of a surface oxidised layer [van Raaphorst et al., 1988; Nedwell et al., 1993].

The hyperbolic tangent function varies between -1 and 0. The function tends toward zero as ρ_{ria} approaches ρ_{ENACW}, approximately 1027 kg m⁻³ [Fiúza et al., 1998], leading to maximum f_{Resus}. The function in brackets thus conveniently scales f_{Resus} to the density of the water in the ria. Fig. 5.26 presents the temporal evolution of daily ρ_{ria} at the mouth of the ria and [1+TANH(ρ_{ria}-ρ_{ENACW})]. Daily ρ_{ria} were derived from the salinity and temperature at the mouth (S$_{MBC}$ and T$_{MBC}$ used in the physical ECoS model [Fig. 5.10].
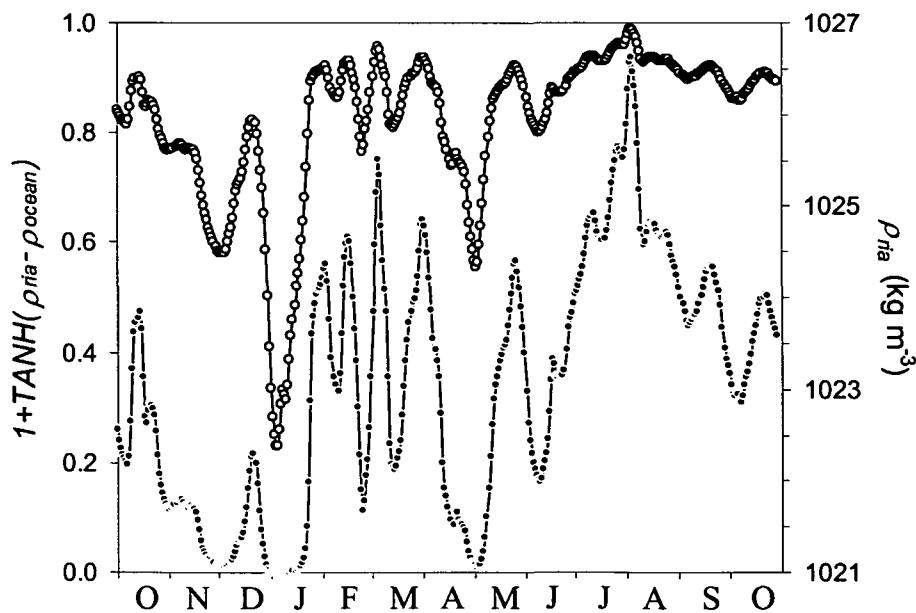
Fig. 5.26. Evolution of observed water density in the ria (ρ_{ria} open circles) and the hyperbolic function (Eq. 5.52, closed circles) over the study period (October 1997-1998).

A similar resuspension model was attempted using the Brunt-Väisälä stability of the water column [N; Eq. 2.3, Fig. 3.4]. Stability increases during upwelling relaxation and decreases during upwelling, leading to a inverse

relationship between upwelling and N. However, in contrast to density, N is strongly influenced by solar heating and runoff events. In addition, both upwelling and downwelling are characterised by low N, thus reducing the efficacy of N for predicting upwelling. Accordingly, density provides the most effective oceanographic parameterisation of upwelling than salinity, temperature or Brunt-Väisälä stability.

Nutrient remineralisation. Microbial degradation of organic matter in marine environments is the process by which organic substrate is transformed into inorganic material via a succession of basic enzymatic processes. These processes include hydrolysis of macromolecules, microbial uptake of the resulting monomeric substrates, respiration and biosynthesis of microbial biomass and degradation of this biomass by lysis or grazing by meiofauna [*Billen and Lancelot,* 1988]. This is represented in the 0-D pelagic model as a first order constant [f_{MinerW}, Eq. 5.37].

Billen and Lancelot [1988] cite literature values for first order degradation of organic matter in the sediment, f_{MinerS}, between 0.26 and 0.0087 d^{-1}. The large range of values arises from the differing lability of organic material in natural samples. In the Pontevedra Ria, *Dale and Prego* [2002] proposed values of up to 0.5 d^{-1} based on mass-balance calculations. Other workers used a Michaelis-Menten dependence of the organic load on organic matter oxidation in the water column [*Regnier et al.,* 1997]. At this stage, a first order constant was employed, taking the mean value of the listed values in *Billen and Lancelot* [1988] for the semi-labile fraction, f_{MinerS}=0.07 d^{-1} [Eq. 5.53]. It follows, therefore, that benthic regeneration of $NH4$ and $PO4$ are given by Eqs. 5.54 and 5.55:

$$Miner_S = f_{MinerS} \times POMSED \qquad [5.53]$$

$$NH4SEDgen = \frac{Miner_S}{C:N} \qquad [5.54]$$

$$PO4SEDgen = \frac{Miner_S}{C:P} \qquad [5.55]$$

Nitrification. Benthic nitrification of $NH4$ to $NO3$ ($Nitri_S$) is an aerobic process restricted to the sedimentary layers where oxygen is present, and may consume significant amounts of $NH4$ diffusing upward [*Blackburn and Henriksen,* 1983]. There is no default ECoS template for $Nitri_S$, and thus a formulation was developed. In a review of benthic nitrogen cycling, *Billen and Lancelot* [1988] stated that most values of $Nitri_S$ in the literature fall within the range 0.28-2.8 mg N m^{-2} h^{-1}. In recent kinetic models, $Nitri_S$ was expressed as a first-order reaction, proportional to the concentration of $NH4$ and limited by oxygen availability [*Savchuk and Wulff,* 1996; *Soetaert et al.,* 1996; *Kelly-Gerreyn et al.,* 1999]. If the principal control on the $Nitri_S$ is the concentration of $NH4$ or oxygen, then a first order kinetic model should be adequate. In a model of carbon degradation in sediments, *Westrich and Berner* [1984] showed experimentally that the degradation rate is essentially proportional to the organic carbon concentration in the case of excess oxygen, otherwise a Michaelis-Menten rate law must be used [*Rabouille and Gaillard,* 1991]. Due to lack of sediment oxygen data, the model $Nitri_S$ is restricted to a first-order description. Nevertheless, this may not prove to be

unrealistic as it has been suggested that upwelling provides a mechanism for ventilation of bottom waters and quasi-benthic fluff throughout the summer [*Dale and Prego*, 2002]. Therefore, $Nitri_S$ is assumed limited by $NH4SED$ only:

$$Nitri_S = f_{NitriS} \times NH4SED \qquad [5.56]$$

$$f_{NitriS} = anit \times e^{bnit \times T} \qquad [5.57]$$

where the maximum rate of $Nitri_S$ is f_{NitriS} and $anit$ and $bnit$ are temperature constants as before [Table 5.4].

Nitrate reduction. Nitrate in sediment can be either effluxed across the sediment-water interface or reduced. A possible product of nitrate reduction is ammonium via dissimilatory nitrate reduction (*Dnra*), or gaseous N_2 and N_2O via denitrification (*Denit*). ECoS lacks a template for nitrate reduction via *Dnra* or *Denit* [Fig. 5.25], and therefore suitable parameterisations was formulated. Early model studies defined *Denit* with first-order kinetics [*Vanderborght and Billen*, 1975; *Goloway and Bender*, 1982]. *Jenkins and Kemp* [1984] emphasised the importance of $NO3$ concentration in the sediments on the rate of *Denit*. Accordingly, several authors have recently recognised the importance of nitrate substrate and dissolved oxygen concentrations in both the sediment [*Soetaert et al.*, 1996; *Kelly-Gerreyn et al.*, 1999] and overlying water immediately above the sediment [*Savchuk and Wulff*, 1996]. Other workers have defined *Denit* as a proportion of $Nitri_S$ [*Humborg et al.*, 2000] or ignored *Denit* altogether [*Chapelle et al.*, 1994]. *Lancelot and Billen* [1985] proposed a model relating the first-order kinetic constant for *Denit* to the flux of organic matter to the sediments.

The potential for denitrification in the Pontevedra Ria is high due to regular inputs of nitrate rich oxygenated waters interspersed with sedimentation of fresh organic material. This means that *Denit: Dnra* may be higher than the typical 60:40 [e.g. *Nedwell*, 1982]. In spring, *Dale and Prego* [2002] [Section 4.2] reported that of the total PON remineralised in the sediments, approximately 25% was effluxed as $NH4$, 72% denitrified and 3% effluxed as $NO3$. To a first approximation, therefore, *Denit* appears to be important in the Pontevedra Ria. *Dnra* was not considered in the mass balance due to lack of data and thus its importance is unknown. Nevertheless, since *Dnra* is the reverse of $Nitri_S$, *Dnra* is included in the overall value for $Nitri_S$ [Eq. 5.54]. $Nitri_S$, therefore, is equal to net nitrification.

Dale and Prego [2002] found that 95% of the nitrified $NO3$ in the sediments was denitrified, permitting the first-order expression:

$$Denit = f_{Denit} \times NO3SED \qquad [5.58]$$

The maximum rate of denitrification, therefore, is 0.95 d^{-1}. For initial modelling, however, a more conservative estimate of denitrification of 0.1 d^{-1} was used.

Model results. The benthic sub-model simulations are shown in Fig. 5.27, where $[NH4SED]_0=[NO3SED]_0=[PO4SED]_0=[POMSED]_0=0$. β is again defined as 0.05 d^{-1} to avoid model instability. The simulations comprise the period October 1997-1998 and include the *Resus* transfer using observed values

for water density, ρ_{ria} [Eq. 5.50]. *POMSED* and *POM Resus* are inversely correlated [Fig. 5.27a]. Maximum resuspension occurs in August when upwelling stress is high, and *POMSED* falls to 0.12 µmol l^{-1} and the *POM Resus* rate is 0.06 µmol d^{-1}. The concentration of inorganic nutrients *NH4SED*, *NO3SED* and *PO4SED* in the sediment depend on the *POMSED* substrate. Therefore, the peaks in *NH4SED*, *NO3SED* and *PO4SED* [Fig. 5.27b] mirror those of *POMSED*. Using the same analogy, *Nitris* and *Denit* [Fig. 5.27c] depend on *NH4SED* and *NO3SED*. Nutrients are lost from the sediments at the same rate as *POMSED* [Fig. 5.27d].
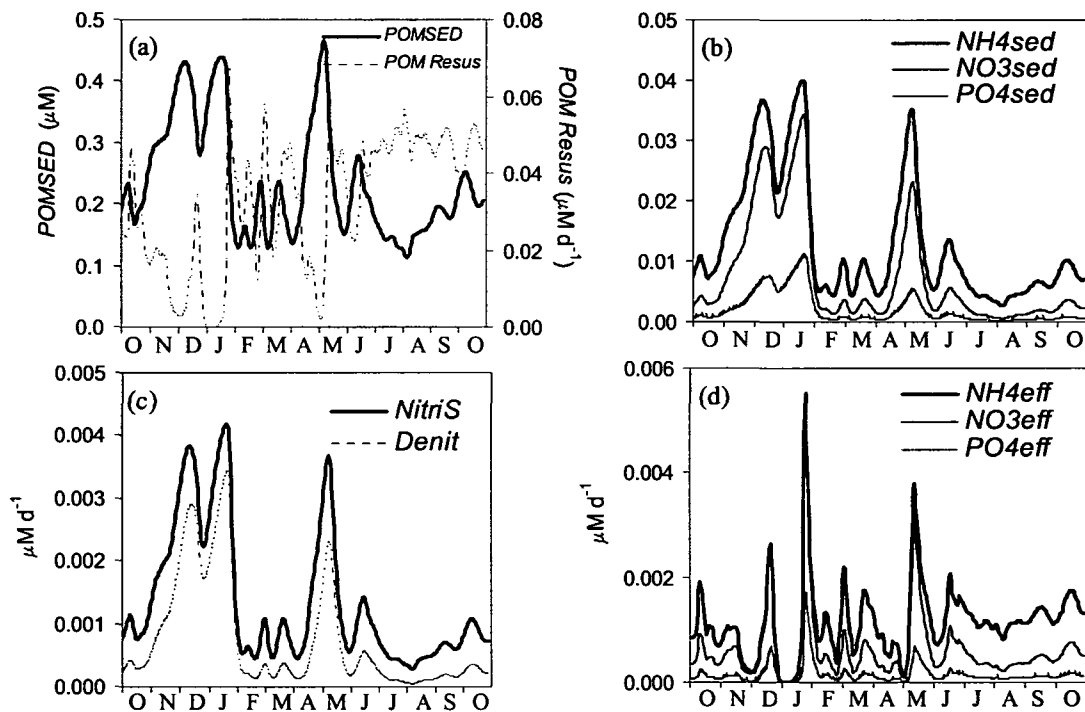
Fig. 5.27. Simulated benthic nutrient dynamics for the zero-dimensional model over the study period (October 1997-1998).

5.2.3.4. 0-D MODEL RESULTS FOR NUTRIENTS

The individual benthic, water column particulate and nutrient sub-models were subsequently coupled together to form a 0-D ecosystem model using observed and derived parameters applicable to the Pontevedra Ria. The conceptual diagram is shown in Fig. 5.28. Observed values of H_{sw} [Fig. 2.3] were included for light limitation of phytoplankton (*Mlight*), and β was again 0.053 d^{-1}. Nutrient limitation was also included [*Nulim*, Eq. 5.23]. In addition, to avoid exhaustion of nutrients, a constant nutrient input based on the values in Table 4.3. was added to represent fluvial inputs [*NH4rinp*, *NO3rinp*, *PO4rinp*; Table 5.4]. These inputs equated to 4.8×10^{-7} g *NO3-N* l^{-1} d^{-1} (0.034 µmol *NO3-N* l^{-1} d^{-1}), 1.43×10^{-7} g *NH4-N* l^{-1} d^{-1} (0.010 µmol *NH4-N* l^{-1} d^{-1}), 5.66×10^{-8} g *PO4-P* l^{-1} d^{-1} (1.83 nmol *PO4-P* l^{-1} d^{-1}). Observed temperatures at the ria mouth were encoded into the model for the benefit of *Nitriw* and *Nitris* efficiency [Eqs. 5.44 and 5.57].

The model simulations for the water column and sediment state variables are shown in Fig. 5.29. Phytoplankton biomass decreased with time throughout the simulation with a large decrease from October 1997-January 1998 followed by a lower decrease thereafter [Fig. 5.29a]. The absolute difference between *PHYTO* growth and losses (*Prodn-Respn-Mort=P-R-M*) was greatest in winter due to low irradiance [Fig. 5.29b]. Conversely, *Nup* and *Pup* were >0.96, suggesting that nutrient limitation was <4% of *Prodn*. As the light intensity increased in February, *Prodn* became less light limited, which explains the inflection in *PHYTO* biomass in Fig. 5.29a.

Water column nutrients showed contrasting behaviour over the simulation period [Fig. 5.29c]. The increase in *NO3* and decrease in *NH4* can be explained by previous arguments of the large initial $Nitri_W$ rate of 0.11 d^{-1} and lower KM_{NH4} than KM_{NO3}. Consequently, the Michaelis-Menten uptake functions *NupNO3* and *NupNH4* showed that phytoplankton nitrogen assimilation was exclusively based on *NO3* [Fig. 5.29d].
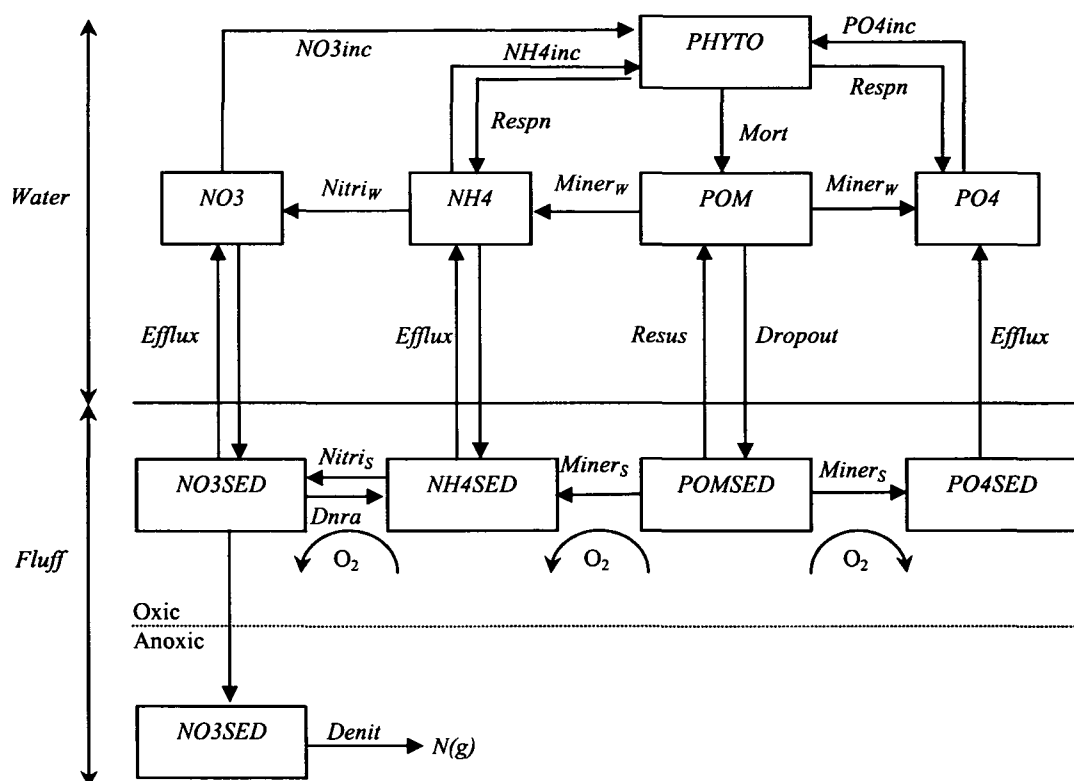
Fig. 5.28. Conceptual model of the zero-dimensional model of the Pontevedra Ria.

The evolution of benthic variables *POMSED*, *NH4SED*, *NO3SED* and *PO4SED* in Fig. 5.29e are similar to those in Fig. 5.27. The absolute efflux of nutrients and *POM* were also lower in summer [Fig. 5.27f], despite more frequent upwelling of ENACW. However, *POMSED*, *NH4SED*, *NO3SED* and *PO4SED* were low in summer due to persistent washout of the bed stock during spring, which leads to low effluxes.

The 0-D model could not be calibrated with real data since hydrodynamics were not included. Nevertheless, the model consistency was

verified by examining the conservation of *PO4*, *NO3* and *NH4* during simulations [*Lee et al.*, 2002]. The strategy required the integrated calculation of total *PO4*, *NO3* and *NH4* in all sub-models (dissolved/ particulate pelagic, benthic) for each day, setting the external nutrient input to zero and accounting for nutrient losses from denitrification. Conservation error was calculated as the difference between the total amount and initial amount. In all cases, the daily error was below 0.2%. Presumably [*Lee et al.*, 2002], rounding errors in the model were responsible for the small difference. Nevertheless, the model appeared to be consistent and the numerical scheme has not generated model instability or "leakage" of matter out of the model.
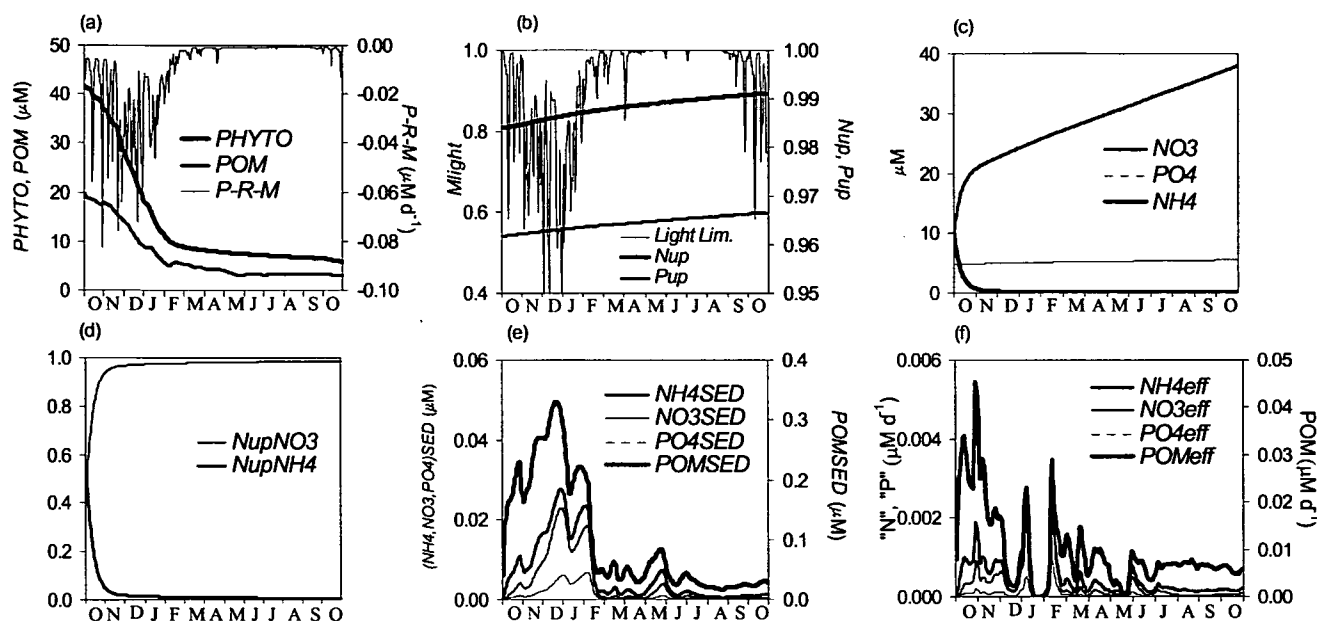
Fig. 5.29. Simulated model variables and processes using the zero-dimensional biogeochemical model over the study period (October 1997-1998).

5.2.3.5. SENSITIVITY ANALYSIS

A sensitivity analysis of the 0-D model variables [Table 5.2] to the individual model parameters will provide an initial insight of the relative importance of the model transfers [Table 5.3]. In view of the variability in the model induced by H_{SW} and ρ_{ria}, theoretical H_{SW} assuming 50% cloud cover [Fig. 2.3a] and a constant f_{Resus} of 0.2 d^{-1} was assumed for the sensitivity analysis. This provides more interpretable results than if observed daily data were used.

The sensitivity analysis should be based on a sound knowledge of the biogeochemical processes that are being modelled [*Dyke*, 1996]. The approach used was a ±10% perturbation of model parameters [Table 5.4], including *PO4rinp*, *NO3rinp* and *NH4rinp* [Table 5.3] to investigate the local instability of each variable. This value is a compromise between model stability and realistic natural variability in accordance with values reported in the literature. *Chapelle et al.* [1994] tested the sensitivity of the oxygen outputs from their biogeochemical model of Vilaine Bay, France, by removing a different oxygen-related process for a succession of model runs. This approach, however, is inconsistent with nature as it is unlikely that

individual biogeochemical processes will be totally inhibited under normal conditions, in particular for the Pontevedra Ria. With a ±10% variation the flux of material through the model will either be enhanced, reduced or unaffected, but not prevented.

Table 5.6 presents the results for the biogeochemical sensitivity analyses. For each analysis, the state variables are identified as a percentage change in concentration from the reference simulation [Fig. 5.29] on day 75 and 275. These days were chosen to coincide with the two distinct rates of *PHYTO* decrease over the simulation period [Fig. 5.29a].

The variables showed the expected increase or decrease in concentration with each parameter based on the exchanges defined within the model. The largest variability in the variables occurred with the parameters associated with phytoplankton production (β, f_{Respn} and f_{Mort}). With the exception of *PO4*, *NO3* and *NH4*, all variables showed approximately 20 and 230% increases on days 75 and 275, respectively, with a +10% increase in β. *PO4* and *NO3* presented a decrease with time in accordance with phytoplankton nutrient uptake. *NH4*, however, showed an increase since reduced nitrogen is more influenced by remineralisation of organic matter than are phosphate and nitrate, particularly since phytoplankton nitrogen uptake was almost exclusively as *NO3* [Fig. 5.29d].

Reducing β by 10% did not result in an equal loss in variable concentration. The explanation here is that the relationship with β and *PHYTO* is exponential rather than linear, suggesting that the initial phytoplankton concentration and definition of β will be important for the hydrodynamic-biogeochemical model. The sensitivity of the state variables to f_{Respn} was less than for β, and an increase in f_{Respn} provoked an increase in *PO4* and *NO3*.

NH4 showed considerable sensitivity to *bnit*, whereby a variability of approximately ±20% in *NH4* was engendered by ±10% *bnit*. In the benthic environment, however, *NH4SED* showed less sensitivity to *bnit*. Conversely, *NO3SED* was clearly dependent on *bnit* as nitrification provided the only source of *NO3SED*. f_{Resus} was important for all benthic variables, and a ±10% variability provoked a ~20% change. This may have important consequences for the hydrodynamic-biogeochemical model, where f_{Resus} varies from 0-0.5 d^{-1}, depending on the density of the water in the ria. Furthermore, a 10% reduction in benthic remineralisation, f_{Miners}, reduced *NO3SED* and *NH4SED* by up to 70% whereas an increase in f_{Miners} had relatively little effect. This suggests that benthic remineralisation was complete, and that f_{Miners} was a key parameter for determining benthic variable concentrations. In general, the sensitivity analysis of the 0-D model revealed that the most influential parameters are β, f_{Respn}, f_{Miners} and f_{Resus}. However, the exercise was essentially performed on a closed system. The sensitivity of the hydrodynamic model to variable nutrient boundary conditions is discussed in the following section.

Parameter	±10%	PHYTO 75	PHYTO 275	POM 75	POM 275	POMSED 75	POMSED 295	PO4 75	PO4 275	NO3 75	NO3 275	75	275	75	295	75	275	75	275
α	+10%	1.9	8.0	0.8	8.0	0.7	8.0	.	.	.	.	0.7	5.2	0.5	8.0	0.5	8.0	0.6	8.0
α	-10%	-2.8	-10.8	-1.3	-10.7	-1.1	-10.7	.	.	.	.	-1.2	-6.9	-0.9	-10.7	-0.8	-10.7	-1.0	-10.7
αPh	+10%	.	.	.	.	.	.	.	.	.	.	.	.	.	.	.	.	.	.
αPh	-10%	.	.	.	.	.	.	.	.	.	.	.	.	.	.	.	.	.	.
αH2O	+10%	.	.	.	.	.	.	.	.	.	.	.	.	.	.	.	.	.	.
αH2O	-10%	.	.	.	.	.	.	.	.	.	.	.	.	.	.	.	.	.	.
αSPM	+10%	.	.	.	.	.	.	.	.	.	.	.	.	.	.	.	.	.	.
αSPM	-10%	.	.	.	.	.	.	.	.	.	.	.	.	.	.	.	.	.	.
anit	+10%	.	.	.	.	.	.	.	.	.	.	-9.6	-8.9	.	.	6.3	6.3	-2.9	-2.9
anit	-10%	.	.	.	.	.	.	.	.	.	.	12.5	10.8	.	.	-6.8	-6.8	3.1	3.1
bnit	+10%	.	.	.	.	.	.	.	.	.	.	-20.8	-19.6	.	.	15.1	15.2	-7.0	-6.9
bnit	-10%	.	.	.	.	.	.	.	.	.	.	29.6	24.6	.	.	-14.1	-14.2	6.5	6.5
β	+10%	44.4	281.8	28.5	240.6	26.3	234.6	-0.4	-1.6	-1.8	-6.1	23.3	158.4	23.3	226.5	22.2	223.2	24.3	229.2
β	-10%	-30.8	-74.0	-21.3	-70.3	-19.9	-69.8	0.3	0.5	1.3	1.8	-17.4	-46.4	-18.0	-69.0	-17.3	-68.7	-18.7	-69.3
C:N	+10%	.	.	.	.	.	.	.	.	.	.	-6.5	-5.9	-9.1	-9.1	-9.1	-9.1	-9.1	-9.1
C:N	-10%	.	.	.	.	.	.	.	.	.	.	7.9	7.2	11.1	11.1	11.1	11.1	11.1	11.1
C:P	+10%	.	.	.	.	.	.	.	.	.	.	.	.	-9.1	-9.1	.	.	.	.
C:P	-10%	.	.	.	.	.	.	.	.	.	.	.	.	11.1	11.1	.	.	.	.
fDenit	+10%	.	.	.	.	.	.	.	.	.	.	.	.	.	.	-3.0	-3.0	.	.
fDenit	-10%	.	.	.	.	.	.	.	.	.	.	.	.	.	.	3.2	3.2	.	.
fDropout	+10%	.	.	-1.3	-1.3	8.5	8.5	.	.	.	.	.	.	8.5	8.5	8.5	8.5	8.5	8.5
fDropout	-10%	.	.	1.4	1.3	-8.7	-8.7	.	.	.	.	.	.	-8.7	-8.7	-8.7	-8.7	-8.7	-8.7
fMinerW	+10%	.	.	1.4	1.3	-8.7	-8.7	.	.	.	.	.	.	-8.7	-8.7	-8.7	-8.7	-8.7	-8.7
fMinerW	-10%	.	.	10.0	9.7	9.7	9.5	.	.	.	.	.	.	9.6	9.5	9.5	9.5	9.6	9.5
fMinerS	+10%	.	.	-1.07	-1.0	-3.7	-3.7	.	.	.	.	.	.	5.9	5.9	5.9	5.9	5.9	5.9
fMinerS	-10%	.	.	1.15	1.1	4.0	4.0	.	.	.	.	.	.	5.9	5.9	5.9	5.9	5.9	5.9
fMort	+10%	-8.5	-27.9	2.88	-18.4	3.2	-18.0	.	.	.	.	-3.3	-16.0	-6.4	-6.4	-90.1	-89.9	-67.9	-68.3
fMort	-10%	9.4	38.7	-3.64	21.4	-3.9	20.9	.	.	.	.	3.5	21.2	3.6	-17.5	-89.1	-91.2	-64.5	-72.0
fNitriS	+10%	.	.	.	.	.	.	.	.	.	.	.	.	3.6	-17.5	-89.9	-87.0	-67.2	-59.4
fNitriS	-10%	.	.	.	.	.	.	.	.	.	.	.	.	-4.2	20.2	.	.	.	.
fNitriW	+10%	.	.	.	.	.	.	.	.	0.9	1.5	12.4	10.8	.	.	6.3	6.3	-2.9	-2.9
fNitriW	-10%	.	.	.	.	.	.	.	.	-1.2	-4.0	.	.	.	.	-6.8	-6.8	3.1	3.1
fRespn	+10%	-25.4	-65.9	-17.5	-62.4	-16.4	-61.8	.	.	.	.	-10.1	-39.4	-14.8	-61.1	-14.2	-60.8	-15.3	-61.3
fRespn	-10%	34.2	193.6	22.2	168.5	20.6	164.8	.	.	.	.	11.3	97.8	18.3	159.7	17.4	157.7	19.0	161.4
fResus	+10%	.	.	1.0	1.0	-6.1	-6.1	.	.	.	.	.	.	-14.0	-13.9	-16.4	-16.2	-11.4	-11.3
fResus	-10%	.	.	-1.2	-1.2	6.9	6.9	.	.	.	.	.	.	18.1	17.8	21.2	21.0	13.9	13.8
KI	+10%	-0.3	.	-0.1	-1.3	-0.1	-1.3	.	.	.	.	.	.	-0.1	-1.3	.	.	-0.1	-1.3
KI	-10%	.	-1.3	0.1	1.3	0.1	1.3	.	.	.	.	.	.	0.1	1.3	.	.	0.1	1.3
KMNH4	+10%	.	.	.	.	.	.	.	.	.	.	.	.	.	.	.	.	.	.
KMNH4	-10%	.	.	.	.	.	.	.	.	.	.	.	.	.	.	.	.	.	.
KMNO3	+10%	.	.	.	.	.	.	.	.	.	.	.	.	.	.	.	.	.	.
KMNO3	-10%	.	.	.	.	.	.	.	.	.	.	.	.	.	.	.	.	.	.
KMPO4	+10%	-1.4	-4.8	-0.9	-4.4	-0.9	-4.3	.	.	.	.	-0.8	-2.9	-0.8	-4.2	-0.7	-4.2	-0.8	-4.3
KMPO4	-10%	1.4	5.1	0.9	4.6	0.9	4.5	.	.	.	.	0.8	3.1	0.8	4.5	0.7	4.4	0.8	4.5
PO4inp	+10%	.	.	.	.	.	.	.	.	.	.	.	.	.	.	.	.	.	.
PO4inp	-10%	.	.	.	.	.	.	.	.	.	.	.	.	.	.	.	.	.	.
NO3inp	+10%	.	.	.	.	.	.	.	.	1.1	2.9	.	.	.	.	.	.	.	.
NO3inp	-10%	.	.	.	.	.	.	.	.	-1.1	-2.9	.	.	.	.	.	.	.	.
NH4inp	+10%	.	.	.	.	.	.	.	.	.	.	2.5	3.5	.	.	.	.	.	.
NH4inp	-10%	.	.	.	.	.	.	.	.	.	.	-2.5	-3.5	.	.	.	.	.	.
T	+10%	.	.	.	.	.	.	.	.	.	.	-2.4	-2.2	.	.	1.5	1.5	.	.
T	-10%	.	.	.	.	.	.	.	.	.	.	2.5	2.2	.	.	-1.5	-1.5	.	.

5.2.4. COUPLING TO THE HYDRODYNAMIC MODEL

5.2.4.1. BIOGEOCHEMICAL BOUNDARY CONDITIONS AND INITIAL CONCENTRATIONS

In the Pontevedra Ria, the main nutrient inputs are from the ocean, the river Lérez and effluent discharge. Atmospheric input was ignored. The nutrient mouth boundary condition (*MBC*) was defined from the fortnightly observations at CS21. Intermediate data were interpolated linearly by ECoS. It may be argued that these data did not adequately represent the *MBC*, which depends on short-term runoff and upwelling events [*Nogueira et al.*, 1997a,b]. In a successive paper, *Nogueira et al.* [1998] showed statistically that inorganic nutrient concentrations in the surface and bottom layers of the Vigo Ria were significantly correlated with the thermohaline properties of the water and along-shore and offshore Ekman transport. In a similar way as for nutrient efflux [Eq. 5.50], an initial parameterisation of the nutrient boundary condition (*Nu*$_{MBC}$) was attempted using ρ_{ria}:

$$Nu_{MBC} = Nu_{ENACW} \times \left[1 + TANH\left(\rho_{ria} - \rho_{ENACW} \right) \right] \qquad [5.59]$$

where *Nu*$_{ENACW}$ is the concentration of a nutrient in core ENACW [*Castro et al.*, 1998]. A statistical comparison of observed and predicted *NO3* at the mouth was fairly robust in the upwelling season but statistically insignificant in winter. *PO4* and *NH4* were not significantly correlated with the prediction of Eq. 5.59 at any time. Parameterisation of the nutrient *MBC* with ENACW is compounded by the fact that over-shelf remineralisation and uptake modifies the nutrient concentrations. Therefore, the most logical approach for defining the *MBC* was to use observed values. A more complex parameterisation can be attempted when more data becomes available.

The initial nutrient and *POM* concentrations in the sediment were set to zero. In ECoS, sediment concentrations are defined on a w/w basis. Moreover, the sediment variable in ECoS is defined as a dynamic advective constituent, meaning that it can be transported up or down estuary depending on the water velocity and threshold velocity for resuspension and deposition [Eq. 5.51]. In this work, benthic fluff resuspension was not treated hydrodynamically due to the upwelling complication as discussed previously. In addition, *POM* and nutrient concentrations in the sediment fluff were not of interest here. The magnitude of sediment remineralisation, denitrification and resuspension were calibrated independently of sediment concentration.

5.2.4.2. MODEL SIMULATIONS

Pelagic and benthic nutrient dynamics. The model was run using the parameters specified for the 0-D model [Table 5.4], with the exception of β which was set to 1 d^{-1}. The model results in Fig. 5.30 correspond to the CS14 boundary between the central and internal ria. CS14 is assumed to be representative of the whole ria.

The model appears to satisfactorily hindcast the nutrient concentrations at CS14 [Fig. 5.30a-c]. The error bars on the nutrient concentrations represents a ±8% variability, equal to the change in cross-sectional area over a tidal cycle [see Section 4.4.2]. Qualitatively, the modelled and observed nutrient concentrations show higher concentrations in the wet

and dry season and lower concentrations in spring. This agrees with Fig. [4.14] and the findings of *Nogueira et al.* [1997a], and is attributable to runoff and upwelling cycles [*Nogueira et al.*, 1998]. Mean nutrient concentrations at CS14 were 0.26 ± 0.12 µmol $PO4$ l⁻¹, 4.64 ± 2.46 µmol $NO3$ l⁻¹, and 1.13 ± 0.46 µmol $NH4$ l⁻¹. Modelled nutrient concentrations were generally lower than observed values, suggesting that the model under-predicts the magnitude of remineralisation or resuspension in the ria. Moreover, despite the fact that nutrient concentrations were not statistically different from the long-term (1987-1992) mean surface and bottom nutrient data at the same location in the Vigo Ria [*Nogueira et al.*, 1997a], $NH4$ and $PO4$ concentrations in this study were approximately 50% lower than the long term means reported in *Nogueira et al.* [1997a]
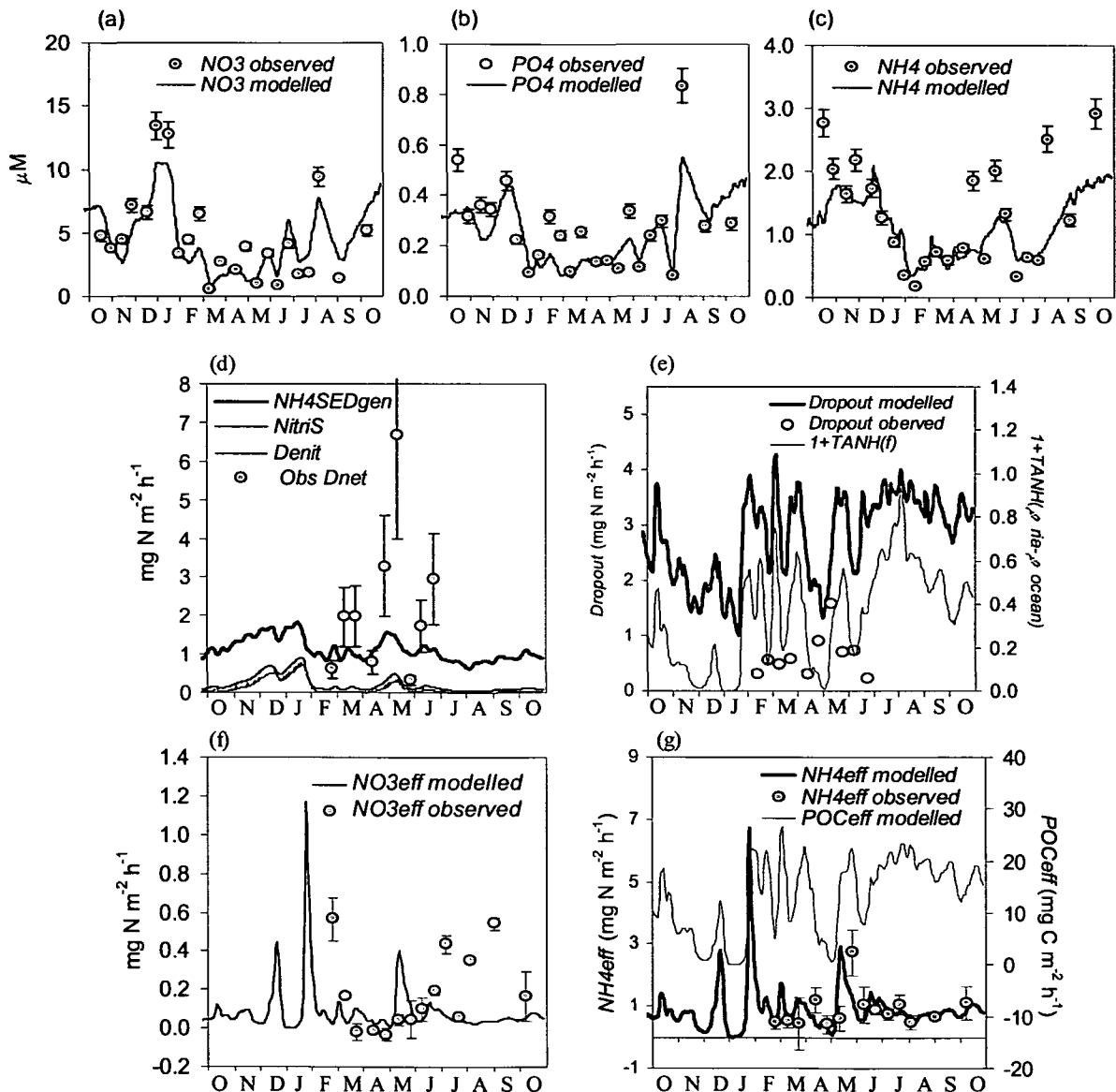
Fig. 5.30. Observed and simulated selected pelagic and benthic model variables and processes using the hydrodynamic biogeochemical model over the study period (October 1997-1998). Error bars on nutrients, assumed to represent the analytical and oceanographic error, are ±8% of the concentration. Error bars on Observed D_{net} are the same as in Chapter 4, and the errors on the nutrient effluxes represent the ±1 SD from the triplicate incubation experiments (n=3).

Fig. 5.30d-g presents the model results for benthic nitrogen dynamics and sedimentation. *NH4SEDgen* and *Nitris* [Fig. 5.30d] showed a maximum in November-January and April-May, where *NH4SEDgen* and *Nitris* in January reached approximately 1.6 mg N m^{-2} h^{-1} and 0.9 mg N m^{-2} h^{-1}, respectively. These were related to lower rates of resuspension and increased *Dropout* [Fig. 5.30e]. *NH4SEDgen* and *Dropout* were positively correlated ($r^2=0.75$, $n=410$, $p<0.001$). Consequently, *Denit* is also dependent on *Dropout* and *Resus*, and showed a slight temporal offset from *Nitris*. Qualitatively, the model results for *Denit* are in good agreement with the previous mass balance estimates for net denitrification [D_{net}, Eq. 4.2], showing promotion of *Denit* by increasing *Dropout*. Curiously, however, the mass-balance results were at least a factor of 10 higher than the modelled results. *Denit*, which is essentially gross denitrification, would be expected to be higher than D_{net}, implying that f_{Nitris} or f_{Denit} are too low or, conversely, that f_{Resus} is too high. Nevertheless, the benthic model predicted a negative relationship between *Resus* and *Denit*, confirming the previous hypothesis in Chapter 4.

The model predicted *Dropout* [Fig. 5.30d] showed no discernible correlation with the sediment trap depositional flux. This was of little concern at this stage, since the potential error in calculating sedimentation rates is well-known, particularly in coastal waters where horizontal transport of material may be important [*Sauchuk and Wulff*, 1996].

NO3eff and *NH4eff* across the sediment-water interface showed more favourable correlation to the experimental observations in Chapter 4 [Fig. 5.30f,g]. *NH4eff* showed a better fit against observed data than *NO3eff*, although experimental effluxes ought to be lower than model simulations since the incubations did not account for resuspension. Nevertheless, the results are encouraging. *NO3SED* production in the benthic model is via *Nitris*, despite observed influx of nitrate into the sediment during March-April [Fig. 4.9]. These benthic influxes are not accounted for in the model. High modelled *NO3eff* of 0.35-0.57 mg N m^{-2} d^{-1}, compared to experimental fluxes, may again be an artefact of the mesocosm incubations.

Phytoplankton, primary production and Chl a. PHYTO showed a pronounced seasonal variability, from 5 µmol C l^{-1} in winter to 13 µmol C l^{-1} in summer [Fig. 5.31a]. POC (derived from *POM*) showed a lower range of 1.5-6.5 µmol C l^{-1}. These values were lower than observations recorded at a similar location in the Vigo Ria [10-30 µmol POC l^{-1}; *Doval et al.*, 1997]. However, POC determinations from filtered water samples rarely differentiate between biogenic detritus, phytoplankton and inorganic carbonaceous material. Therefore, Chl *a* may be a more adequate tracer for drawing inter-ria comparisons of productivity. However, Chl *a* data in this study was not sufficient to verify model simulations. Chl *a* data were thus derived from POC data assuming, as stated previously, that POC was phytoplankton detritus. The Chl *a*: POC ratio was taken as 0.35 mg Chl *a* (mmol C)$^{-1}$ [*Rios et al.* 1998; *Lee et al.*, 2002]. Model predictions of Chl *a* are shown in Fig. 5.31b, with mean concentrations of 2.51±0.65 µg l^{-1} (range 1.7-4.1 µg l^{-1}). These were lower than 6.0±4.2 µg l^{-1} (range 0.2-17.5 µg l^{-1}) and 4.8±4.8 µg l^{-1} (range 0.2-22.2 µg l^{-1}) at the surface and at the 1% light level, respectively, observed by *Moncoiffé et al.* [2000] in the Vigo Ria. This is presumably because in ECoS constituents are depth averaged over the photic and aphotic zone. The predicted data were more comparable to those presented by *Doval et al.* [1998], and the long-term Vigo Ria mean of 3.33±2.65 µg l^{-1} [range 0.00-34.16 µg l^{-1}; *Nogueira et al.*, 1997a].
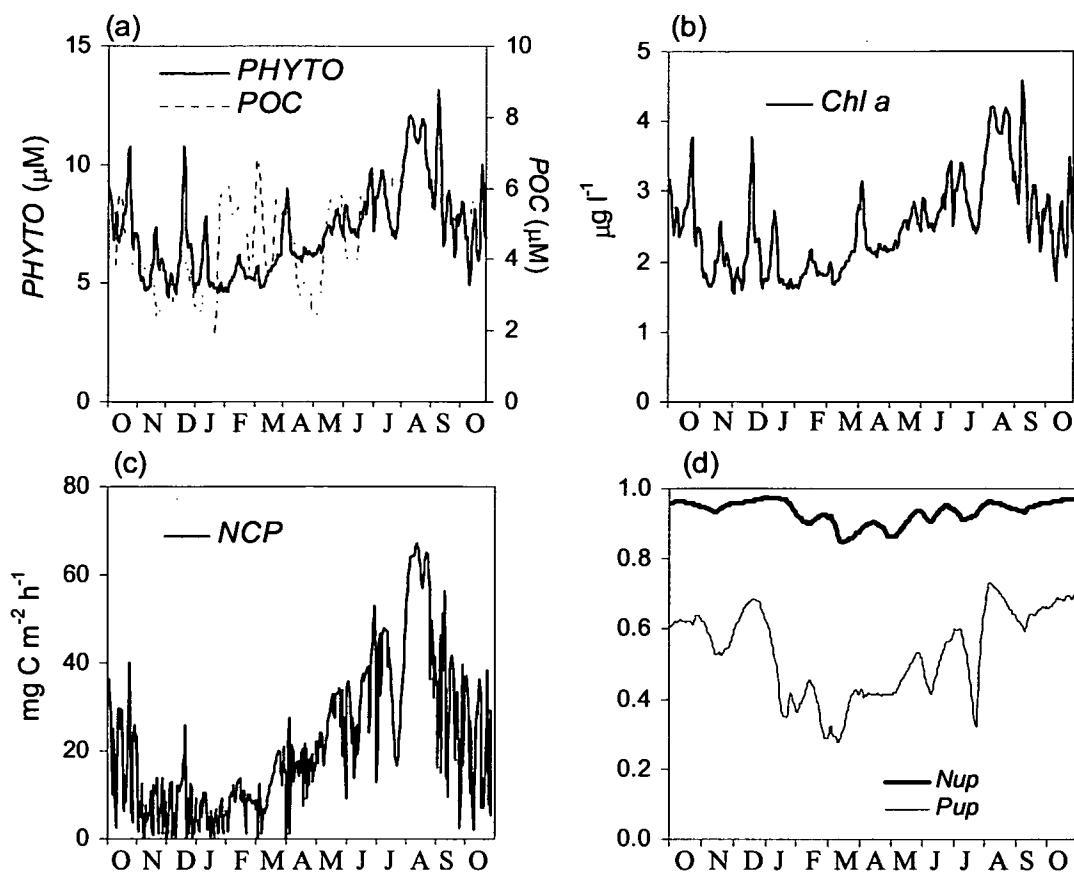
Fig. 5.31. Simulated selected primary production components using the hydrodynamic biogeochemical model over the study period (October 1997-1998).

A salient aspect of research into the Galician rias has focussed on accurate prediction of net community production [*NCP*; see references in Table 4.6]. In the model, *NCP* is calculated as *Prodn-Respn*. At this point, it must be noted that in this chapter *NCP* is positive for net production of organic matter and negative for net remineralisation of organic matter. In Chapter 4, by nature of the box model formulations, *NCP* was defined oppositely.

Fig. 5.31c shows a clear seasonal evolution of *NCP* in agreement with *PHYTO* biomass, with mean values of 9.0 ± 5.5 mg C m^{-2} h^{-1} for the wet season, 14.5 ± 5.8 mg C m^{-2} h^{-1} for spring and 39.3 ± 16.0 mg C m^{-2} h^{-1} for the dry season. These values show good agreement with the box model results in Table 4.6. A pronounced peak in *NCP* in August coincided with the gap in observed H_{SW} data, when theoretical H_{SW} were used [Fig. 2.3a]. In addition, spatially integrated dry season NCP_N and NCP_P for the Pontevedra Ria [Chapter 4] were 64.6 and 29.9 mg C m^{-2} h^{-1} (reported here as positive values, implying net autotrophy), respectively, again a good agreement. However, a box model *NCP* involves the integration of all uptake and remineralisation processes whereas *NCP* derived from ECoS is more comparable to direct ^{14}C incubations. Although algal respiration is accounted for in ^{14}C measurements, and DOM production may be significant [*Duarte and Cebrián*, 1996; *del Giorgio and Duarte*, 2002], large scale remineralisation processes on time-scales longer than the ^{14}C incubations are likely to affect the box model *NCP*. Therefore, ECoS *NCP* ought to be higher than box model estimates. *Tilstone et al.* [1999] reported

[14]C estimates for the Vigo Ria which were a factor of 2-3 higher than the values reported here. This confirms the underestimation of NCP with ECoS.

Fig. 5.29b shows that photosynthesis was not limited by light in summer. Moreover, in the 0-D model nutrient limitation was low (~4%). However, in the hydrodynamic model photosynthesis is limited by phosphate, by up to 70% in March 1998 and by approximately 50% in the dry season [Fig. 5.31d]. This is the first evidence of phosphate limitation in the Rias Bajas. The box-model results in this thesis, and supporting Rias Bajas references, all concluded that the rias were N-limited. This further illustrates the difference between box model and numerical model predictions. Numerical models provide a process-related approach to ecosystem dynamics, whereas box models integrate all nutrient remineralisation and uptake processes. Nitrogen limitation in the Pontevedra Ria predicted by the box model was thus an artefact of the data analysis and not a true representation of the real situation. Furthermore, given the large difference between Pup (0.52±0.12) and Nup (0.94±0.13), it is difficult to visualise under what conditions a switch to nitrogen limitation could be possible.

From this initial simulation, therefore, the model is able to predict qualitatively and semi-quantitatively nutrient distributions and, more importantly, NCP. However, it can be generally concluded that nutrients, POM, and NCP are lower than other reported values for the Rias Bajas. An examination of the variable sensitivity to perturbations in the model parameters is thus essential in order to simulate the behaviour of these variables with more accuracy.

5.2.4.3. SENSITIVITY ANALYSIS

The parameters and variables chosen for the sensitivity analysis were based on the results of the 0-D model [Table 5.6], and further included the nutrient MBC, dispersion (K_x) and density (ρ_{ria}). The mean annual value for each variable was calculated after a ±50% perturbation in each parameter. Sensitivity is expressed as a percentage change from the mean annual value of the simulation above [Fig. 5.30 and 5.31], defined as the reference simulation. The results are shown in Table 5.7.

Nutrient concentrations in the ria showed most sensitivity to their respective MBC [Table 5.7]. Therefore, the seemingly low modelled nutrient concentrations previously observed could be partly due to variability in MBC prior to each sampling survey, rather than an underestimation of remineralisation in the ria. In fact, PO3, NO3 and NH4 are insensitive to f_{Remin}.

A 50% increase in the nitrification parameters $anit$ and $bnit$ evoked a proportionate increase in NO3eff and Denit. Increasing $S_{Dropout}$ also favoured NO3eff and Denit. However, $anit$ and $bnit$ had relatively little effect on NH4eff (-2%), principally because the NH4SED pool was an order of magnitude greater than NO3SED (data not shown). Therefore, a recalibration of $anit$ or $bnit$ rather than $S_{Dropout}$ would be a logical approach for promoting higher NO3SED and Denit.

It has been suggested above that modelled NCP in the Pontevedra Ria was lower than in the neighbouring Rias Bajas. NCP showed high sensitivity to the parameters defining phytoplankton metabolism, α and β and, to a lesser extent, f_{Respn}. Increasing β by 50% resulted in a 125% increase in NCP, whereas for α+50% the increase in NCP was 32.8%. Of more concern

was the influence of K_X on NCP. SALINITY and TEMP exhibited low variability with K_X [Fig. 5.12]. Particulate material, however, is synthesised in situ and strongly affected by the residence time of the ria. Longer residence times led to increased PHYTO biomass and NCP [Table 5.7] since the phytoplankton doubling time becomes larger than the wash-out period [Huntsman and Barber, 1977; Minas et al., 1982]. Accordingly, with $K_X=10$ m² s⁻¹, mean PHYTO biomass increased by over 200% and NCP by 87%.

Table 5.7. Sensitivity analysis for the 1-D hydrodynamic biogeochemical model. Each variable (top row) was perturbed by ±50% variability in key model parameters (left column), with the exception of p_{ria} and K_X which were varied as indicated.

		PHYTO	POM	PO4	NO3	NH4	NCP	NO3eff	NH4eff	Denit	Nitri$_S$	Dropout
a	+50%	18.3	-	-3.5	-2.2	-2.3	32.8	-	-	-	-	-
	-50%	-23.5	-1.3	5.7	3.6	4.1	-54.3	-	-	-	-	-
anit	+50%	-	-	-	-	-1.2	-	47.7	-1.9	47.8	47.1	-
	-50%	-	-	-	-	1.3	-	-49.2	2.0	-49.1	-49.0	-
bnit	+50%	-	-	-	-	-1.0	-	43.4	-1.8	43.4	42.9	-
	-50%	-	-	-	-	-	-	-30.5	1.2	-30.6	-30.4	-
β	+50%	54.1	3.0	-13.2	-8.3	-9.1	125.6	-	-	-	-	1.4
	-50%	-30.2	-1.7	7.5	4.8	5.3	-68.1	-	-	-	-	-
f_{Mort}	+50%	-1.4	2.7	-	-	-	-1.0	-	-	-	-	1.6
	-50%	1.5	-2.7	-	-	-	1.0	-	-	-	-	-1.7
f_{Respn}	+50%	-4.5	-	-	-	2.3	-7.4	-	-	-	-	-
	-50%	4.9	-	-	-	-2.4	7.8	-	-	-	-	-
f_{Remin}	+50%	-	-6.3	-	-	1.4	8.4	-2.0	-2.4	-1.9	-2.4	-4.3
	-50%	-	7.0	-	-	-1.4	7.9	2.1	2.5	2.1	2.5	4.6
PO4rinp	+50%	-	-	-	-	-	-	-	-	-	-	-
	-50%	-	-	-	-	-	-	-	-	-	-	-
NO3rinp	+50%	-	-	-	-	-	-	-	-	-	-	-
	-50%	-	-	-	-	-	-	-	-	-	-	-
NH4rinp	+50%	-	-	-	-	-	-	-	-	-	-	-
	-50%	-	-	-	-	-	-	-	-	-	-	-
$PO4_{MBC}$	+50%	21.3	1.1	51.3	-2.2	-2.5	34.0	-	-	-	-	-
	-50%	-20.3	-1.2	-50.0	3.1	3.5	-44.8	-	-	-	-	-
$NO3_{MBC}$	+50%	-	-	-	52.6	2.9	-	-	-	-	-	-
	-50%	-	-	-	-52.0	-6.8	-	-	-	-	-	-
$NH4_{MBC}$	+50%	-	-	-	-	43.8	-	-	-	-	-	-
	-50%	-	-	-	-	-43.1	-	-	-	-	-	-
$S_{Dropout}$	+50%	-	-16.5	-	-	-	-	28.8	26.6	28.7	26.6	19.9
	-50%	-	25.5	-	-	-	-	-40.2	-38.9	-40.2	-38.9	-33.6
K_X*	10	220.7	11.6	-28.0	-17.6	-4.3	86.7	-	-	-	-	2.5
	500	-27.9	-1.6	5.7	3.6	-	-24.0	-	-	-	-	-
ρ_{ria}**	1027	-	36.2	-	-	-	-	-9.2	17.9	-67.1	-57.4	34.8
	1024	-	-47.4	-	-	-	-	-97.3	-97.6	103.3	77.3	-36.1

* Units: m² s⁻¹
** Units: kg m⁻³

The definition of K_X used in this work is thus questionable. In support of the present temporally variable K_X, PO4 and NO3 decreased to low levels throughout the year with $K_X=10$ m² s⁻¹ [Table 5.7]. With increasing K_X, the nutrient MBC dominated the nutrient concentrations in the ria. Therefore, the concentrations of NO3, NH4 and PO4 would suggest that the hydrodynamics were correctly parameterised, or at least more accurately parameterised than using $K_X=10$ m² s⁻¹. Estimates of $K_X=200-400$ m² s⁻¹

using Eq. 5.13 and diffusivities of 100-400 m² s⁻¹ in other ocean-dominated systems [*Largier et al.*, 1997] lend further confidence to the present K_x definition. Therefore, based on this argument, it would appear that the biological primary production parameters, rather than the hydrodynamics, require recalibration.

5.2.4.4. MODELLING NET COMMUNITY PRODUCTION

The primary production model [Eq. 5.23] was parameterised with a first-order expression of the light-saturated chlorophyll-specific rate of photosynthesis, β. In quantitative studies, β is expressed as mg C (mg Chl a)⁻¹ h⁻¹ and termed P_m^B [*Platt and Jassby*, 1976; *Jassby et al.*, 2002]. Therefore, P_m^B can be calculated as the rate of carbon production in the Pontevedra Ria (*Prodn*, mg C l⁻¹ h⁻¹) to the Chl a concentration (mg Chl a l⁻¹). Bio-optical experiments by *Tilstone et al.* [1999] under various hydrographic scenarios in the Vigo Ria provide directly quantified values of P_m^B for comparison.

Predicted values of P_m^B with the ECoS 1-D reference simulation are shown in Fig. 5.32. Mean P_m^B values ranged from 0.22±0.11 mg C (mg Chl a)⁻¹ h⁻¹ in the wet season, 0.34±0.11 mg C (mg Chl a)⁻¹ h⁻¹ in the spring, 0.63±0.18 mg C (mg Chl a)⁻¹ h⁻¹ in the dry season. In contrast, spring and summer values reported by *Tilstone et al.* [1999] for total phytoplankton were 1.77±0.96 mg C (mg Chl a)⁻¹ h⁻¹ and 2.70±0.87 mg C (mg Chl a)⁻¹ h⁻¹, respectively. Therefore, the model under-predicts P_m^B by at least a factor of 4-5. In ecosystem models of the Galician shelf during upwelling, *Halvorsen et al.* [2001] use a P_m^B value of 1.5 mg C (mg Chl a)⁻¹ h⁻¹. Similarly, *Slagstad and Wassmann* [2001] employed variable P_m^B (1.1-2.0 mg C (mg Chl a)⁻¹ h⁻¹) depending on the dominant phytoplankton species. P_m^B is Chl a-normalised production, and is therefore is increased when NCP is large relative to phytoplankton biomass, PHYTO. From Table 5.7, higher P_m^B was thus promoted by an increase in the parameters with which (% increase NCP) > (% increase PHYTO), which follow the order $\beta > a > PO4_{MBC} > f_{Respn}$. It is interesting to note that decreasing K_x lead to higher PHYTO and a decrease in P_m^B, since the proportionate increase in PHYTO is almost three-fold greater than the increase in NCP.
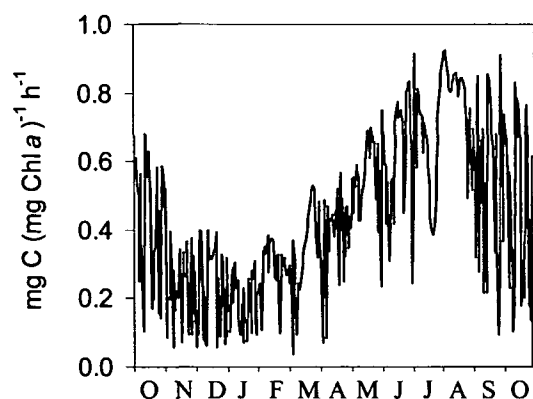
Fig. 5.32. Simulated chlorophyll a-normalised primary production (P_m^B) using the hydrodynamic biogeochemical model over the study period (October 1997-1998).

Therefore, β was increased to 2 d^{-1}. This increase is not arbitrary, but was chosen on the basis of contemporary literature values, specifically the upwelling model of *Ianson and Allen* [2002] and the North Sea model of *Tett* [1990]. The results for *PHYTO*, Chl a, *NCP* and P_m^B are shown in Fig. 5.33. *PHYTO* showed a dramatic increase to over 50 μmol C l^{-1} in August [Fig. 5.33a]. Mean Chl a in the dry season increased to 9.17±3.77 μg l^{-1}, and the annual mean was 7.14±3.73 μg l^{-1}. Although within the long-term range of 0.00-34.16 μg l^{-1} [*Nogueira et al.*, 1997a], the modelled values were double the long-term mean of 3.33±2.65 μg l^{-1} [*Nogueira et al.*, 1997a].

Mean spring and summer P_m^B increased to 0.72±0.23 and 1.19±0.37 mg C (mg Chl a)$^{-1}$ h^{-1}, respectively [Fig. 5.33b]. This is more agreeable with the other workers [*Tilstone et al.*, 1999; *Moncoiffé et al.*, 2000; *Halvorsen et al.*, 2001; *Slagstad and Wassmann*, 2001]. However, with no control over *PHYTO* biomass (other than *Nulim* and *Mlight*), *NCP* reached extremely high rates [Fig. 5.33c]. Mean dry season values were 231 mg C m^2 h^{-1}, with an isolated maximum of 580 mg C m^2 h^{-1}. The highest values of *GPP* reported in the literature are 148 mg C m^2 h^{-1} by *Tilstone et al.* [1999] and 113 mg C m^2 h^{-1} by *Moncoiffé et al.* [2000]. Modelled Chl a-normalised *NCP* was statistically equivalent to the experimental observations of *Tilstone et al.* [1999], and thus considered a satisfactory agreement. However, a zooplankton grazing component was required in order to limit the growth of *PHYTO* biomass and, by implication, *NCP*.
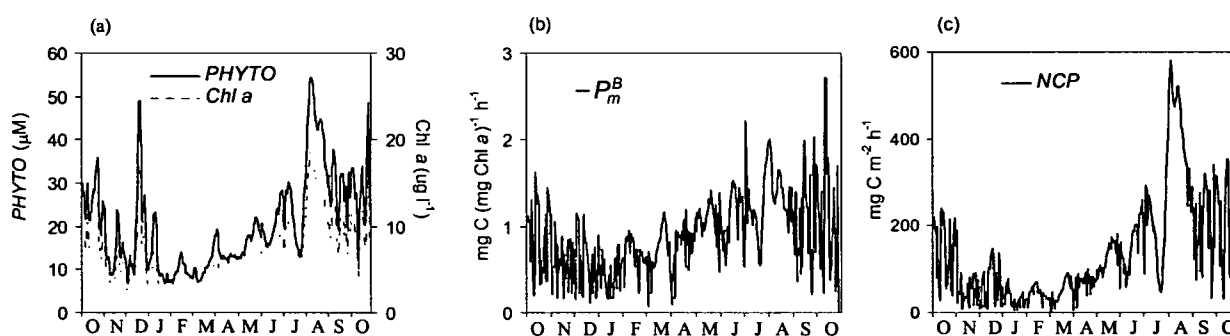
Fig. 5.33. Simulations of selected primary production components using the hydrodynamic biogeochemical model and a maximum phytoplankton growth rate of β=2 d^{-1} over the study period (October 1997-1998).

5.2.4.5. MICROZOOPLANKTON SECONDARY PRODUCTION

A microzooplankton variable (*ZOO*) was added to ECoS as a dynamic advected constituent. Due to lack of supporting data, some assumptions are necessary in order to quantify the rate of microzooplankton grazing. *ZOO* was defined as the sum of heterotrophic dinoflagellates, heterotrophic nanoflagellates and ciliates [*Halvorsen et al.*, 2001], and advected with the water. No account was made for zooplankton inter-species grazing rates, although model modification would be straightforward. Grazing of *PHYTO* follows the Ivlev function, assimilation was assumed to be a constant fraction of ingested food (100%), and microzooplankton faeces were included in the mortality function [0.33 d^{-1}, *Halvorsen et al.*, 2001]. *ZOO* respire at a rate of 0.05 d^{-1}. The temperature-dependent rate of ingestion, *ZOOassm*, was quantified as follows [*Chapelle et al.*, 1994]:

$$ZOOassm = ZOO \times f_{Ingest} \times e^{KT \times T} \times \left[1 - e^{-KZ \times MAX(0,PHYTO-PHYTHR)} \right]$$ [5.60]

where f_{Ingest} is the microzooplankton growth rate at 15 °C (0.5 d^{-1}), KT is the temperature coefficient (0.07 °C^{-1}), KZ is the Ivlev constant (0.008 l µmol C^{-1}) and $PHYTHR$ is the threshold $PHYTO$ concentration for zooplankton assimilation (1 µmol l^{-1}).

Model results. The revised model results for all variables and processes are shown in Fig. 5.34. Further modifications to the reference simulation, based on the sensitivity analysis, included an increase in *bnit* to 0.3, a decrease in f_{Resus} to 0.3 d^{-1}, and an increase in f_{Denit} to 0.5 d^{-1}, to test the validity of the box model D_{net} estimate. The results show that nutrients *NO3*, *PO4* and *NH4* continued to be under predicted by ECoS [Fig. 5.34a-c]. The largest difference occurred during the strong upwelling in August. Possible explanations have been discussed above.

The model denitrification results showed an improved agreement with the box model estimates of D_{net} [Fig. 5.34d]. *Denit* increased during upwelling relaxation and decreased during upwelling due to resuspension of detrital substrate [Fig. 5.34e]. *Denit* removed ~15 g C m^{-2} y^{-1} from the Pontevedra Ria, compared to 57-91 g C m^{-2} y^{-1} in the North Sea [*Lee et al.*, 2002]. Observed *Dropout* remained almost an order of magnitude lower than modelled results. The nature of the sediment trap deployment, the trap design and the sensitivity of *POM* to resuspension make it difficult to assess the integrity of observed and modelled *Dropout*. Net *Dropout* (*Dropout-Resus*), however, was 4.2±1.5 mg N m^{-2} h^{-1}, which is equivalent to box-model results net *Dropout* of 2.1±3.2 mg C m^{-2} h^{-1} in the Vigo Ria [*Prego*, 1994] and 4.4 mg N m^{-2} h^{-1} for the upwelling season in the Arosa Ria [*Álvarez-Salgado et al.*, 1996a]. This suggests that the sediment traps were inefficient. Moreover, their design may be questionable (4 bound plexiglass tubes each 10m diameter). There may also be a problem of increased laminar water flow over the opening of the traps, thus reducing sedimentation. A larger trap deposition area is commonly employed [*Kremling and Streu*, 1993].

POM was assumed to sediment directly to the fluff pool, although permanently suspended material may be important. Accordingly, *Lee et al.* [2002] and *Halvorsen et al.* [2001] used different sinking rates for fast and slow detritus, whereas *Savchuk* [2002] opted for a temperature dependent sinking rate. Nevertheless, *NO3eff* and *NH4eff* agreed well with model observations [Fig. 5.34g,h] although observed *NH4eff* was a factor of 3-4 lower than modelled *NH4eff* in the dry season. Reasons for this could be related to the size of the fluff pool or, as is more likely, due to the incubation core design within which diffusion dominated over advection.

The primary and secondary production components are shown in Fig. 5.34i-o. *PHYTO* and, by implication, *POC* showed seasonal variability as before, although in this revised model the Chl *a* concentrations were far more comparable to the results of *Moncoiffé et al.* [2000] and *Nogueira et al.* [1997a]. Mean Chl *a* concentration was 3.14±1.12 µg l^{-1}, and compared to the long-term mean of 3.33±2.65 µg l^{-1} [*Nogueira et al.*, 1997a]. Mean *NCP* was 46.5 mg C m^{-2} h^{-1} in spring and 147 mg C m^{-2} h^{-1} in the dry season. These values were higher than the box model *NCP* estimates [Table 4.6], but within the mean seasonal range of *Tilstone et al.* [1999] plotted on Fig. 5.34k. Mean seasonal values of P_m^B [Fig. 5.34l] were also statistically

equivalent to the data reported by *Tilstone et al* [1999]. As before, *Prodn* was clearly limited by *PO4* [Fig. 5.34n], with increasing severity in spring when upwelling nutrient input was limited. The predicted *f*-ratio of primary production [*NO3inc*/(*NO3inc*+*NH4inc*)] ranged from 0.43-0.87, and is close agreement with observations in the Rias Bajas [*Álvarez-Salgado et al*, 1996a; *Moncoiffé et al*, 2000] and on the shelf [*Álvarez-Salgado et al*, 2002].
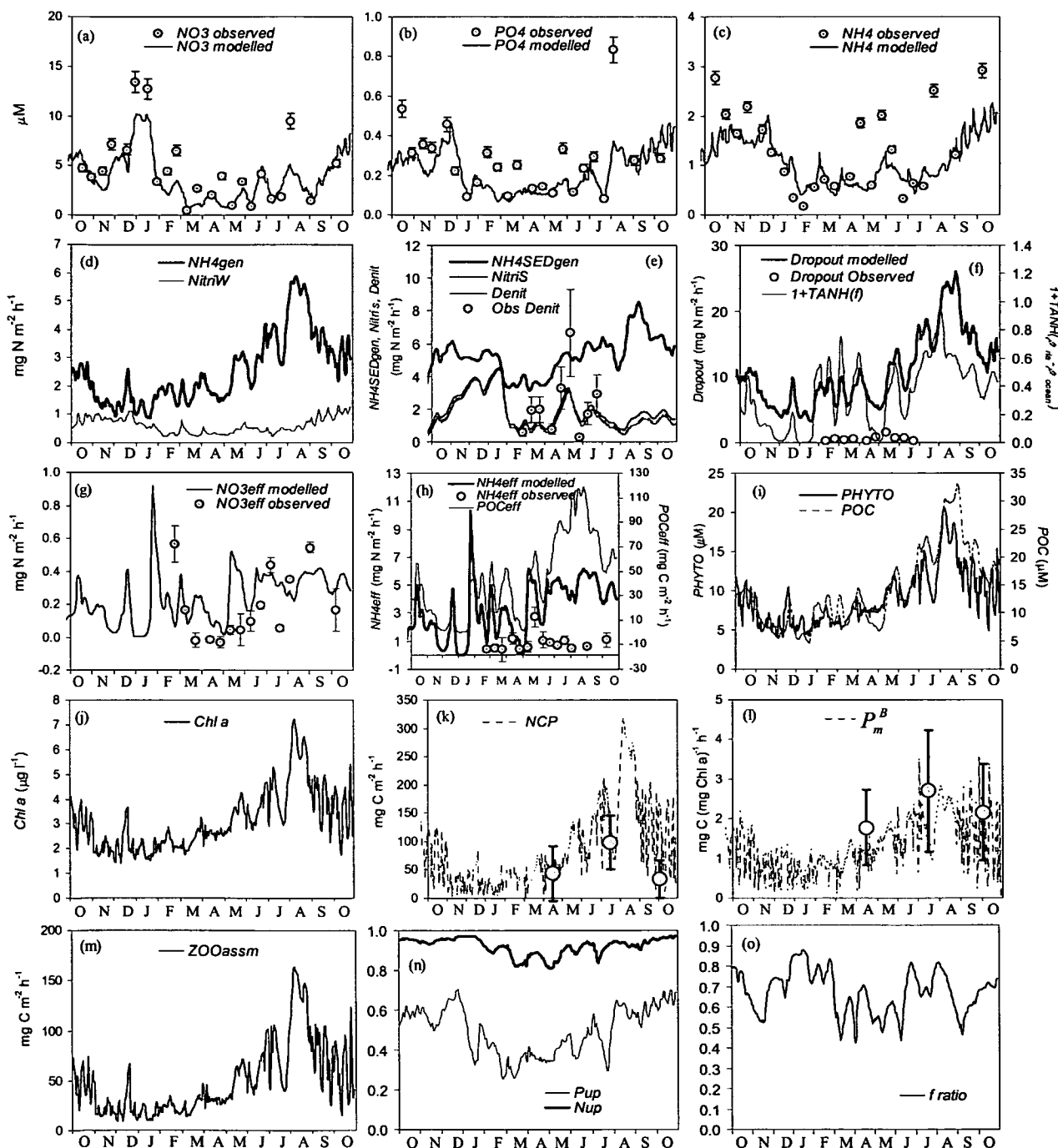
Fig. 5.34. Simulations of benthic and pelagic model variables and processes using the hydrodynamic biogeochemical model over the study period (October 1997-1998). Zooplankton secondary production is included in the model. For explanation of error bars on (a-c) and (e,g,h) see Fig. 5.30 legend. Grey points and ±SD on *NCP* (fig. h) and P_m^B (fig. l) are data from *Tilstone et al.* [1999] using ^{14}C incubations (n=6 for each datum).

Finally, it is necessary to examine *ZOO* secondary production [Fig. 5.34m]. This part of the model could not be verified due to lack of data, although recent studies on the adjacent shelf provided a means of semi-verifying *ZOOassm*. Mean spring and summer rates of *ZOOassm* are 25.5 and 76.1 mg C m^{-2} h^{-1}, respectively [Fig. 5.34m]. *Halvorsen et al.* [2001] reported carbon transfers from the phytoplankton to zooplankton pools in an upwelling filament off the Rias Bajas. Their mean values for *ZOOassm* of phytoplankton during the experiment were 250 mg C m^{-2} d^{-1}. Assuming a 24 h assimilation period (based on mean light intensity over 24h), these values are equal to 10.4 mg C m^{-2} h^{-1}, approximately a factor of 5 lower than the present model results. However, aside from the simplified zooplankton model in the present work, two important factors must be considered to rationalise this discrepancy. Firstly, there will presumably be notable differences in onshore and inshore *ZOOassm* rate [*Sutton et al.*, 2001]. Secondly, zooplankton feeding efficiency is rarely 100% and a large food proportion (~80%) may be excreted in faecal pellets [*Straile*, 1997; *Fileman and Burkhill*, 2001]. This second consideration alone would be sufficient to verify model data against literature values. Nevertheless, this hypothesis was tested by running the model with a revised zooplankton assimilation rate, *ZOOassm$_A$*, based on a 20% feeding efficiency (Z_{AE}=0.8). The remaining 80% of uningested phytoplanktonic material was encoded as a transfer to the *POM* pool.

$$ZOOassm_A = (1 - Z_{AE}) \times ZOOassm \qquad [5.61]$$

With reduced feeding efficiency, mean *ZOO* concentration over the simulation fell from 12.3 to 4.4 µmol C l^{-1}. *Halvorsen et al.* [2001] found that a decrease in assimilation efficiency on the Galician shelf gave mean mesozooplankton concentrations of 2 µmol C l^{-1}. The decrease in grazing rate, however, did not show the large expected decrease, and mean spring and summer rates of *ZOOassm* were 12.5 and 29.7 mg C m^{-2} h^{-1}, respectively. Nevertheless, this is still considered a good agreement with other workers and constitutes the first legitimate estimate of zooplankton production in the Rias Bajas. However, the gap in knowledge of secondary production in the Rias Bajas is clear. In addition, bacterial production has not been considered in the model, although studies suggests that bacterial dynamics are complex [*Zdanowski and Figueiras*, 1997]. Until further data becomes available, model accuracy will be constrained by surrogate rate constants of *ZOOassm*.

5.2.4.6. SEASONAL NUTRIENT BUDGET AND MODEL EVALUATION

To conclude the biogeochemical modelling of the Pontevedra Ria, the seasonal *PO4*, *NO3* and *NH4* budgets are presented in Fig. 5.35. Despite decreasing fluvial inputs from the wet to the dry season, the rate of pelagic nutrient transfer increased due to increasing nutrient uptake by *PHYTO*. The seasonal pelagic and benthic transfers were generally within the same order of magnitude. The benthic nutrient models showed less seasonal variation. Effluxes were greater in the dry season due to upwelling resuspension of bed fluff, which resulted in lower rates of *Denit* than in the wet season. Lowest levels of *Denit* were predicted in spring, when most resuspension of the previous seasonal benthic material occured with the

first upwelling events. *PO4* efflux rates were not measured in the incubation experiments, although from the results a first estimate of phosphate benthic recycling in the Rias Bajas can be proposed. The model suggests that 24% (0.88/3.68) of phytoplankton *PO4* requirements in the dry season were provided by the benthos. Past budgets, therefore, may therefore have seriously underestimated the *NCP* of the Rias Bajas, particularly since *PHYTO* growth appears to be P-limited [Fig. 5.34n].

The net exchanges across the mouth of the Pontevedra Ria are presented on the left hand side of the seasonal budgets. For each nutrient, the net flux at the mouth (negative = net export, positive = net import) is reported as (i) ECoS predictions in area units, (ii) ECoS predictions in mol s^{-1}, and (iii) box-model outgoing flux [mol s^{-1}; Table 4.3] for comparison with the ECoS model.
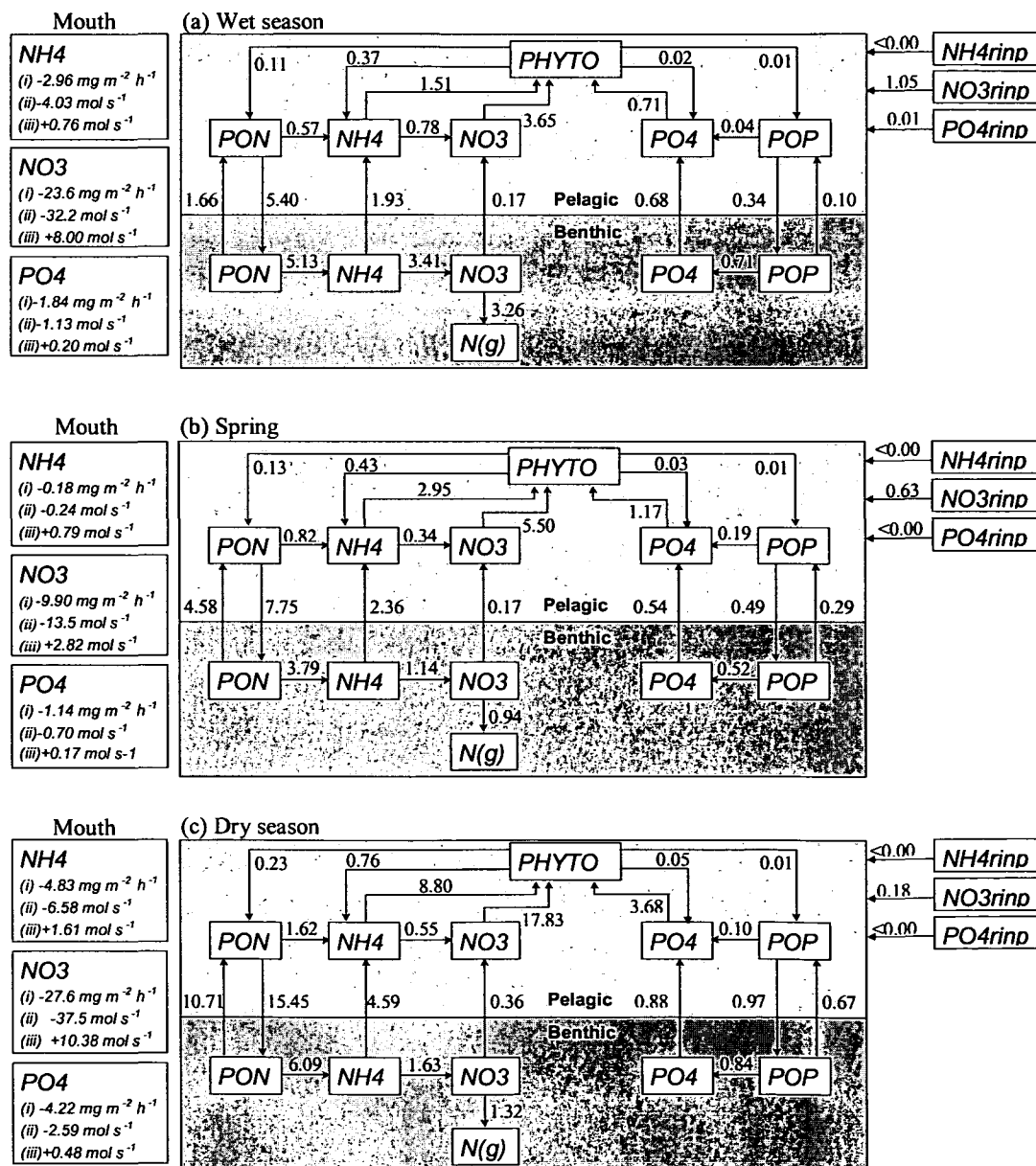
Fig. 5.35. ECoS-derived seasonal transfers (mg m^{-2} h^{-1}) of nitrogen and phosphorus through the pelagic and benthic compartments of the Pontevedra Ria over the study period (October 1997-1998). Mouth exchange is reported as ECoS predictions (i) and (ii), and box model predictions (iii). A negative mouth exchange denotes net export from the ria to the ocean.

It can be seen that whereas the box model dissolved inorganic nutrient budget was either positive or negative [Table 4.4], ECoS seasonal mean predictions were always negative. Moreover, ECoS fluxes across the mouth were a factor of 5-10 larger than the box model fluxes. In order to rationalise this difference, the integration scheme of the two approaches must be considered. The box model crudely constrains a complex partially mixed circulation [e.g. *Taboada et al.*, 1998; *Ruiz Villarreal et al.*, 2002] into a simplistic two-layer residual flow. Hydrodynamics are based on the distribution of salt only, creating a large potential for error as shown previously. Nevertheless, the box model appeared to be able to predict seasonal net uptake and remineralisation by the ria, but this was probably because low nutrient concentrations in the surface layer were assumed to exit the ria at a constant rate. ECoS, on the other hand, constrains a partially mixed flow into 1-D, and thus a nutrient-rich inflow at the bottom and low-nutrient outflow at the surface are averaged.

There is more scope for observing remineralisation processes with the ECoS model, although these must be defined. For the box model, all remineralisation processes, defined and undefined, are accounted for. This is presumably why the box model is able to more readily predict net nutrient import across the mouth than ECoS. The net export predicted by ECoS suggests that nutrient supply to the ria and nutrient regeneration therein are always greater than biological nutrient uptake. Remineralisation of defined allochthonous organic material and bacterially regenerated nutrients via the microbial loop [*Zdanowski and Figueiras*, 1997; *Álvarez-Salgado et al.*, 2001] would increase net nutrient export if these were included in the ECoS model. Clearly, these processes are indirectly incorporated in the box model. Therefore, it can be summarised that both approaches have their strengths and weaknesses, and each would be considerably strengthened, particularly for predicting NCP and nutrient export, with data for dissolved organic matter and microbial remineralisation and uptake [*Álvarez-Salgado et al.*, 2001].

Despite these obvious setbacks, the ECoS model was considered to be a good initial approximation of the biogeochemical nutrient cycle of the Pontevedra Ria. This does not undermine the predictability of box models, but rather illustrates the differences between the two approaches. The optimum model for the Rias Bajas may therefore be a compromise between box-models and hydrodynamic biogeochemical models. Coastal managers must decide which approach is most useful for decision making. The dynamic inter-annual hydrography exhibited by the rias suggests that box-models are more suitable than 1-D models during certain hydrographic scenarios (e.g. runoff-induced stratification, moderate upwelling). In contrast, 1-D representation is preferred during poorly stratified periods of low-runoff, and intense upwelling and downwelling when the water column is thoroughly mixed. A logical progression in model development would therefore be the construction of a stratified ECoS model.

Conclusions

6. Conclusions and future work

This thesis presented a multidisciplinary study of the oceanography of the Pontevedra Ria (NW Spain). Several important findings and ideas have been developed which will be of great interest to the scientific community and local environmental management bodies. An important conclusion has been to highlight the generic application of these results to the other Rias Bajas. These findings are discussed here in accordance with the corresponding chapters of the thesis.

6.1. CHAPTER 3: HYDROGRAPHY

The hydrographical variability of the Pontevedra Ria was largely dependent on freshwater inputs inasmuch as the wind regime of the North Atlantic high-pressure cell, the latter determining the extent of oceanic water upwelling. Local winds were capable of modifying tidal currents in the internal ria. Upwelling and runoff were the driving forces behind the residual circulation, although by the nature of their origin they were not superimposed, but rather occurred separately during the dry and wet seasons, respectively.

Four distinct water bodies penetrated inside the ria during the course of the study period: (1) an autumnal water body typically located on the shelf, (2) water transported by the poleward current in winter, (3) subsurface shelf water in May to September when upwelling relaxed, and (4) East North Atlantic Central Water (ENACW), whose regular upwelling into the ria in summer is well recognised. This ria-shelf interaction is an improvement of the state-of-the-art understanding of upwelling since the poleward current was not previously believed to upwell inside the rias. Favourable upwelling conditions in the wet season are a phenomenon, when the Icelandic depression briefly succumbs to anticyclonic conditions. A more detailed description is currently being published [*Álvarez et al.*, In press]. The succession of these changes occurred on a time-scale which was too rapid to be detected by the fortnightly resolution of the sampling frequency. Therefore, a detailed mechanism of the interchange of water bodies could not be described. Clearly, future studies on this topic must therefore consider a 2-3 d sampling frequency, which is equivalent to the inertia displayed by water masses on the shelf to upwelling favourable conditions.

During upwelling, oceanic water always entered the ria along the southern coastline, independent of fluvial or upwelling dominance in the ria. Conversely, water tended to leave the ria via the northern coast, except in the case of strong upwelling when water only exited through the southern mouth. This phenomenon was favoured by the presence of the islands in the mouth. During downwelling a deepening of the pycnocline inside the ria was observed, and was more pronounced on the northern coast. Isopycnal three-dimensional surface maps provided a means of visualising the complexity of ocean-ria mixing in the Pontevedra Ria.

A quantitative approach to water mass exchange was made with a mass-balance analysis. An iterative approach to the well-known fraction of freshwater method was employed to describe in detail the variable flushing time of the Pontevedra Ria, NW Spain. The water fluxes predicted by the water-salt budget were comparable with results from the neighbouring Rias Bajas. Highest incoming fluxes occurred periodically from January-February through to July, and were generally associated with large vertical water fluxes representing upwelling from the lower layer of the ria to the surface waters. However, negative vertical fluxes were occasionally predicted, which imply downwelling. Although these findings were agreeable with other studies on the Pontevedra Ria, and for the same year [*Pardo et al.*, 2001], the possible statistical weakness of the data used to construct the budget was highlighted. Nevertheless, there was a statistical relationship between upwelling flux and the upwelling index (I_W), albeit weak. Although it may be presumed that the robustness of this relationship will be increased with more data, the usefulness of a linear relationship between measurable upwelling flux and a single empirically-derived upwelling index is questionable. The interplay of many complex factors which contribute to upwelling implies that observed highly significant relationships between advective fluxes and I_W (e.g. *Álvarez-Salgado et al.*, 2000] are probably more fortuitous than scientifically sound.

The residence time appeared to be a highly variable function of upwelling with influences from river runoff. The largest water exchange fluxes were attributed to the large gravity flows during upwelling, resulting in a reduction in residence time. A statistically-robust quantitative relationship of the residence time in function of the external independent variables could not be obtained due to water exchange at the mouth acting on shorter time-scales than the sampling resolution. However, definite qualitative trends were observed. Residence time varied from ~4-9 d in the central ria and ~1-4 d in the internal ria. Accordingly, mean daily rates of water exchange were 20 and 50% for the central and internal ria, respectively.

These findings will be invaluable for biogeochemists wishing to ascertain the effect of the short-term ria flushing on geochemical kinetic activity and modification of bio-sensitive elements. Moreover, the socio-economic implications are obvious. Furthermore, an understanding of how upwelling affects density distribution and the salt dispersion is fundamental for ecosystem modelling. However, the results must be interpreted on the scientific quality of the data. It is thus proposed that a different approach is needed to accurately determine the water exchange time in the Rias Bajas. Techniques independent of steady- or non-steady assumptions such as dye dispersion or drogue tracking are possible methods of ascertaining downstream dispersion. An investigation of this type would make an attractive study, and challenge the existing dogma of the water exchange mechanism in the Galician Rias Bajas.

6.2. CHAPTER 4: CHEMICAL OCEANOGRAPHY

The spatial and temporal nutrient distributions in the Pontevedra Ria were consistent with other studies of the neighbouring Rias Bajas. In general, nutrient concentrations were dominated by the river during the wet season and by the ocean in the dry season. However, in contrast to previous studies, there was a clear zone of near-bed aerobic remineralisation in the

internal ria during the spring and dry seasons. In this thesis, the advantages of considering the hydrodynamical characteristics of the system have been highlighted. These findings were corroborated by nutrient flux experiments, and high rates of remineralisation, particularly for ammonium, were most observable during stirring of quasi-benthic phytodetrital fluff. A mass balance of nitrogen and silicon at the benthic-pelagic interface revealed that, aside from resuspension, denitrification was a major fate for particulate organic nitrogen in the sediment, averaging 2.5 mg N m^{-2} h^{-1} for the spring and dry season. However, the specific role of the quasi-benthic algal fluff in nutrient recycling was unclear. High rates of denitrification may have been provoked by regular organic matter deposition between upwelling cycles and coupled nitrification-denitrification across zones of distinct oxygen potential. Ventilation of bottom waters by upwelling may also be a key part of the denitrification processes. Future studies ought to consider assessing denitrification directly using, for example, isotope pairing or acetylene incubation techniques. In view of the uncertainty in the denitrification estimate proposed in this study, a direct quantification of denitrification would clearly be a worthwhile effort. Nonetheless, the direct effect of water advection on sediment nutrient cycling in the Galician Rias Bajas is undisputable. This must be considered when interpreting experimental incubation results.

A non-steady state nutrient budget revealed that the central and internal zones of the Pontevedra Ria displayed different biogeochemical characteristics. In the wet season the central ria was an area of notable uptake, whereas the internal ria showed equally high net remineralisation. By resolving the nutrient budgets in a stratified representation of the ria, net remineralisation was elucidated as a process occurring in both the upper and lower layers. However, net remineralisation continued in the surface layer of the internal ria throughout the year, whereas the lower layer showed clear net nutrient uptake in spring and the dry season. The upshot was an alternating spatial and temporal trend in net community production (NCP), which was well within the range of values reported for the Vigo and Arosa rias. Furthermore, this work has shown the importance of benthic nutrient inputs to the total NCP estimate. In spring, 41% and 29% of total ammonium and silicate inputs to the ria were from the benthos, and in the dry season up to 25% of NCP was due to the sediment nutrient flux. To date, this nutrient source has been neglected in published studies of nutrient dynamics in the Rias Bajas. However, the significance and interpretation of the NCP data would be significantly improved by supporting data of dissolved and particulate matter fluxes across the boundaries of the budget. For example, apparent net production of organic material may be offset by remineralisation of organic material. This secondary recycling via the microbial loop was not considered, and its significance in the Rias Bajas is unknown.

The nutrient budget was used to provide a second estimate of denitrification based on the uptake of inorganic nutrients between the model boundaries. To a first approximation, the results were in agreement with the benthic estimate of denitrification. Denitrification removed up to a third of NCP in the spring and dry season. However, similar to the benthic estimate, there was a large uncertainty associated with the box model denitrification estimate, which was hard determine qualitatively and, therefore, quantitatively. It is unfortunate that data for DIP benthic efflux were unavailable, as this would reveal the true extent of apparent nitrification or denitrification using the box model approach. These findings

again highlight the need for direct investigation of benthic nutrient chemistry.

Despite the efforts made in the budget calculations to gain a representative picture of the ria, the system description is, at best, an approximate representation of the real world since their predictions are inherently uncertain. On a local scale, uncertainty in the mass balance arises from the assumptions in the box model linear equations and interpolation of data between cruises. Moreover, the distribution of any chemical species is dependent, spatially and temporally, on many short-term physico-biogeochemical processes largely ignored in this thesis. It may be argued that inconsistencies engendered by the sampling time resolution were somewhat ameliorated over the 12 month data set. The box model is unlikely to have sufficiently captured these short-term hydrographic events due to the fortnightly resolved data. Nevertheless, the model results seem to be in good agreement with contemporary data. It is thus beyond the scope of this work to make far-reaching conclusions as to the complexity of nutrient cycles within the Pontevedra Ria. However, it can be confidently concluded that there is an urgent need for process-based research in the Rias Bajas in order to better parameterise nutrient distribution variability and hence confirm these and previous box model findings.

The robustness of the box model was questioned, and the statistical quality of the data used to construct the budget was explored in detail. By analysing the potential source of error in the salinity and temperature data at the model boundaries, it was concluded that the difference between surface and bottom salinity and temperature was small and within the analytical noise of the data. A re-examination of the data using a semi-theoretical approach showed that the water fluxes were substantially decreased by accounting for the analytical error in the budget. The implication for predicting net nutrient budgets to the coastal zone and NCP is clear. Nevertheless, combined salt-heat budgets do provide a promising means of deriving upwelling fluxes, although probably not in the Galician rias due to small longitudinal and lateral temperature differences. Moreover, budget accuracy was debilitated by the uncertainty in the empirical derivation of heat exchange across the water surface.

6.3. CHAPTER 5: HYDRODYNAMIC MODELLING WITH ECoS

The commercially available simulation environment, ECoS, has been encoded for the Pontevedra Ria upwelling system in NW Spain. Advected constituents were modelled using conservation of momentum to determine the hydrodynamic dispersion. The tidal exchange flux has been quantified and, depending on the phase of the spring-neap cycle, it can be concluded that tides in the Pontevedra Ria have a minor influence on water exchange. Salinity and temperature were simulated within the analytical error of the thermohaline data, and considered satisfactory given the non-steadiness and variability at the ria mouth. A sensitivity analysis showed that salinity and temperature in the ria were insensitive to ±10% variability in key model parameters, including the dispersion coefficient. On the other hand, ECoS failed to adequately simulate salinity and temperature in the Lérez estuary, presumably since the estuary is relatively shallow and tides and runoff show more dominance here than in the ria.

Several gaps in the understanding of the physical oceanography of the ria were apparent. ECoS was constructed using the meso-tidal Tamar Estuary (UK) as a template for hydrodynamics, where upwelling is absent. Water velocities in ECoS are calculated on the basis of tides and runoff only, and no allowance is made for enhancement or blockage of residual circulation due to hydrographic processes at the mouth. Therefore, a more sensitive method of calibrating upwelling and downwelling processes in the Rias Bajas is required. In this respect, it would be advantageous to proceed in 1-D (depth averaged) or 2-D (depth resolved) without resorting to complex 3-D models. Nevertheless, it is difficult to envisage how this could be achieved with the present ECoS hydrodynamic template. In addition, further fundamental questions about the upwelling process have become apparent. For example, how does upwelling interact with the tide? Is there an observable change in mean sea level at the mouth normally associated with wind-induced Ekman transport? How is tidal exchange modified by synergistic and antagonistic episodes of winds and upwelling? There is a paucity of information addressing these issues in the Rias Bajas, and studies into the physical oceanography of the rias are clearly under-represented.

A benthic and pelagic biogeochemical model of nutrient dynamics and productivity was coupled to the hydrodynamic model. This is believed to be the first time that ECoS has been used to predict benthic nutrient chemistry and net ecosystem production. The seaward boundary condition for nutrients was encoded with observed data due to a failure to predict boundary conditions on the basis of upwelling water masses. In addition, the lack of data covering the different annual hydrographic characteristics implied that all available data was used in calibrating the model for thermohaline and biogeochemical variables. Therefore, the model was not validated by an independent set of data. In short, the model could only be used heuristically.

Inorganic nutrient concentrations were qualitatively and quantitatively simulated against observed data. Moreover, nutrient efflux rates from sediment and benthic denitrification also showed encouraging parallels with field observations. Denitrification was relatively crudely parameterised as a first order rates loss of benthic nitrate concentration, and oxygen limitation of denitrification ought to be included in the subsequent model.

One of the most important findings of the model was that phytoplankton growth in the Pontevedra Ria was limited by phosphorus and not, as hitherto believed, by nitrogen. Although, remineralisation of allocthonous organic material was not included, there is a very clear case for phosphorus limitation in the Rias Bajas. A rapid exploration of this hypothesis could be achieved by defining an external input of organic material. In addition, faster remineralisation rates for organic phosphorus compared to organic nitrogen should be included in the revised model.

The annual evolution of NCP was successfully reproduced by examining the chlorophyll-normalised rate of organic carbon production. However, it was necessary to limit phytoplankton growth by adding a zooplankton constituent with literature values for grazing of phytoplankton. Although this reproduced realistic values for NCP, the uncertainty in the zooplankton component was acknowledged.

Compared to the box model, ECoS dissolved inorganic nutrient fluxes across the mouth were a factor of 5-10 larger than the box model fluxes. This was attributed to the different definitions of constituent uptake and remineralisation processes in each approach. It may be possible that the

163

depth averaged ECoS structure is an oversimplification of the ria hydrography. Equally, however, the same arguments apply to the box model, in particular given the potential for error in the box model-derived advective fluxes. Nevertheless, the box model was able to predict seasonal net uptake and remineralisation, presumably because all remineralisation processes, defined and undefined were accounted for. The accuracy and validity of hydrodynamic models are limited by the processes and parameters defined therein. Both approaches have their strengths and weaknesses, and each would be considerably strengthened with data for dissolved organic matter and microbial remineralisation and uptake. As a possible means of validation, it would be interesting to apply the current model to the data collected in the neighbouring Vigo Ria. This would provide a measure of the generic application of the model to the Galician Rias Bajas. Furthermore, future developments of the Pontevedra Ria ECoS model should include a parameter optimisation stage. However, give the spatial resolution of the data, it is uncertain to what extent this would be useful or realistic.

There is an abundance of publications of system-scale nutrient dynamics in the Rias Bajas. Although the results and conclusions therein are of scientific worth, advances in potential biogeochemical modelling are progressing at a slower rate. This leads to the salient conclusion of the modelling section, and equally applicable to all aspects of this thesis, in that the development of process-based research is notably lacking in the Rias Bajas. Future efforts ought to be directed towards bridging the knowledge gap in the key areas highlighted in this thesis. In this way, socio-economic demands from tourism and aquaculture can be managed more efficiently.

References

Abreu SN, Pereira ME, Duarte AC (1998) The use of a mathematical model to evaluate mercury accumulation in sediments and recovery time in a coastal lagoon (Ria de Aveiro, Portugal). Water Science and Technology 37:33-38

Ackroyd DR, Bale AJ, Howland RJM, Knox S, Millward GE, Morris AW (1986) Distributions and behaviour of dissolved Cu, Zn and Mn in the Tamar Estuary. Estuarine, Coastal and Shelf Science 23:621-640

Adams EE, Stolzenbach KD, Lee J-J, Caroli J, Funk D (1998) Deposition of contaminated sediments in Boston Harbor studied using fluorescent dye and particle tracers. Estuarine, Coastal and Shelf Science 46:371-382

Alber M, Sheldon JE (1999) Use of a date-specific method to examine variability in the flushing times of Georgia estuaries. Estuarine, Coastal and Shelf Science 49:469-482

Aller RC (1988) Benthic fauna and biogeochemical processes in marine sediments: the role of burrow structures. In Nitrogen cycling in coastal marine environments, T. H. Blackburn, J. Sørensen (eds), John Wiley & Sons Ltd, Chichester, pp 301-338

Álvarez I, deCastro M, Prego R, Gómez-Gesteira M. Hydrographic characterisation of a winter upwelling event in the Ria of Pontevedra (NW Spain). Estuarine, Coastal and Shelf Science. In Press.

Álvarez-Salgado XA, Fraga F, Pérez FF (1992) Determination of nutrient salts by automatic methods in seawater and brackish water: the phosphate blank. Marine Chemistry 39:311-319

Álvarez-Salgado XA, Rosón G, Pérez FF, Pazos Y (1993) Hydrographic variability off the Rías Baixas (NW Spain) during the upwelling season. Journal of Geophysical Research 98:14447-14455

Álvarez-Salgado XA, Rosón G, Pérez FF, Figueiras FG, Pazos Y (1996a) Nitrogen cycling in an estuarine upwelling system, the Ría de Arosa (NW Spain). 1. Short-time-scale patterns of hydrodynamic and biogeochemical circulation. Marine Ecology Progress Series 135:259-273

Álvarez-Salgado XA, Rosón G, Pérez FF, Figueiras FG, Ríos AF (1996b) Nitrogen cycling in an estuarine upwelling system, the Ría de Arosa (NW Spain). II. Spatial differences in the short-time-scale evolution of fluxes and net budgets. Marine Ecology Progress Series 135:275-288

Álvarez-Salgado XA, Castro CG, Pérez FF, Fraga F (1997) Nutrient remineralisation patterns in shelf waters of the Western Iberian upwelling. Continental Shelf Research 17:1247-1270

Álvarez-Salgado XA, Doval MD, Pérez FF (1999) Dissolved organic matter in shelf waters off the Ría de Vigo (NW Iberian upwelling system). Journal of Marine Systems 18:383-394

Álvarez-Salgado XA, Gago J, Míguez BM, Gilcoto M, Pérez FF (2000) Surface waters of the NW Iberian Margin: Upwelling on the shelf versus outwelling of upwelled waters from the Rías Baixas. Estuarine, Coastal and Shelf Science 51:821-837

Álvarez-Salgado XA, Gago J, Míguez BM, Pérez FF (2001) Net ecosystem production of dissolved organic carbon in a coastal upwelling system: the Ría de Vigo, Iberian margin of the North Atlantic. Limnology and Oceanography 46:135-147

Álvarez-Salgado XA, Beloso S, Joint I, Nogueira E, Chou L, Pérez FF, Groom S, Cabanas JM, Rees AP, Elskens M (2002) New production of the NW Iberian shelf during the upwelling season over the period 1982–1999. Deep-Sea Research I 49:1725-1739

Aminot A (1983) Dosage de l'oxygène dissous. In Manuel des Analyses Chimiques in Milieu Marin. A. Aminot and M. Chaussepied (eds), Centre National pour l'Explotation des Océans, Brest, pp. 75-92

Anderson TR, Williams PJleB (1999) A one-dimensional model of dissolved organic carbon cycling in the water column incorporating combined biological-photochemical decomposition. Global Biogeochemical Cycles 13:337-349

Arbones B, Figueiras FG, Zapata M (1996) Determination of phytoplankton absorption coefficient in natural seawater samples: Evidence of a unique equation to correct the path length amplification on glass-fiber filters. Marine Ecology Progress Series 137:293-304

Arbones B, Figueiras FG, Varela R (2000) Action spectrum and maximum quantum yield of carbon fixation in natural phytoplankton populations: implications for primary production estimates in the ocean. Journal of Marine Systems 26:97-114

Arbones MB, Andrade ML, Marcet MP, Montero MJ (1992) Niveles de materia orgánica, nitrógeno y fósforo depositados por effluentes en la zona de costa de la ría de Pontevedra. Thalassas 10:59-69

Asmus RM, Jensen MH, Jensen KM, Kristensen E, Asmus H, Wille A (1998) The role of water movement and spatial scaling for measurement of dissolved inorganic nitrogen fluxes in intertidal sediments. Estuarine, Coastal and Shelf Science 46:221-232

Bakun A (1973) Coastal upwelling indices, west coast of North America, 1946-1971. NOAA Technical Report NMFS SSRF-671, US Department of Commerce.

Bale AJ, Morris AW, Howland RJM (1985) Seasonal sediment movement in the Tamar estuary. Oceanologica Acta 8:1-6

Balls PW (1994) Nutrient inputs to estuaries from nine Scottish east coast rivers; influence of estuarine processes on inputs to the North Sea. Estuarine, Coastal and Shelf Science 39:329-352

Bao R, Varela M, Prego R (1997) Mesoscale distribution patterns of diatoms in surface sediments as tracers of coastal upwelling on the Galician shelf. Marine Geology 144:117-130

Barber RT, Smith RL (1981) Coastal upwelling systems. In Analysis of Marine Systems. A. R. Longhurst (ed), Academic Press, San Diego, pp. 31-68

Barciela MC, Bao R, Prego R, Herbello P (2000) Opal in the superficial sediment of the Pontevedra Ria: Distribution and comparison with the ria (Arosa and Vigo) and adjacent shelf. In A. Duarte, C. Vale, R. Prego (eds) Biogeochemical Studies in the Iberian Coastal Zone, IX Iberian Seminar of Marine Chemistry, University of Aveiro, pp 153-158

Beaulieu SE (2002) Accumulation and fate of phytodetritus on the sea floor. Oceanography and Marine Biology: an Annual Review 40:171-232

Bidle KD, Azam F (1999) Accelerated dissolution of diatom silica by marine bacterial assemblages. Nature 379:508-512

Billen G, Lancelot C (1988) Modelling benthic nitrogen cycling in temperate coastal ecosystems. In Nitrogen Cycling in Coastal Marine Environments. T. H. Blackburn, J. Sørensen (eds). John Wiley & Sons Ltd, Chichester, pp 341-378

Blackburn TH, Henriksen K (1983) Nitrogen cycling in different types of sediments from Danish waters. Limnology and Oceanography 28:477-493

Blanton JO, Atkinson LP, Castillejo F, Lavín A (1984) Coastal upwelling off the Rias Bajas, Galicia, Northwest Spain I: Hydrographic studies. Rapports et Process-verbaux Reunion Conseil International Exploration de la Mer 183:79-80

Blanton JO, Tenore KR, Castillejo. F., Atkinson LP, Schwing FB, Lavín A (1987) The relationship of upwelling to mussel production in the rias on the western coast of Spain. Journal of Marine Research 45:497-511

Bode A, Varela M (1998) Primary production and phytoplankton in three Galician Rias Altas (NW Spain): seasonal and spatial variability. Scientia Marina 62:319-330

Bowden KF (1980) Physical factors: salinity, temperature, circulation, and mixing processes. In Chemistry and Biogeochemistry of Estuaries. E. Olausson and I. Cato (eds), Wiley-Interscience, New York, pp. 37-70

Boyle E, Collier R, Dengler AT, Edmond JM, Ng AC, Stallard RF (1974) On the chemical mass-balance in estuaries. Geochimica et Cosmochimica Acta 38:1719-1728

Boynton WR, Kemp WM (1985) Nutrient regeneration and oxygen consumption by sediments along an estuarine salinity gradient. Marine Ecology Progress Series 23:44-55

Boynton WR, Kemp WM, Keefe CW (1982) A comparative analysis of nutrients and other factors influencing estuarine phytoplankton production. In Estuarine Comparisons. S. V. Kennedy (ed) Academic Press, San Diego, pp 69-90

Boynton WR, Garber JH, Summers R, Kemp WM (1995) Inputs, transformations, and transport of nitrogen and phosphorus in Chesapeake Bay and selected tributaries. Estuaries 18:285-314

Braga ES, Müller TJ (1998) Observation of regeneration of nitrate, phosphate and silicate during upwelling off Ubatuba, Brazil, 23 degrees S. Continental Shelf Research 18:915-922

Brooks DA, Baca MW, Lo YT (1999) Tidal circulation and residence time in a macrotidal estuary: Cobscook Bay, Maine. Estuarine, Coastal and Shelf Science 49:647-665

Brown J, Colling A, Park D, Phillips J, Rothery D, Wright J (1989) Ocean Circulation. G. Bearman (ed), Open university, Pergamon, Oxford, 238 pp

Bunker AF (1976) Computations of surface energy flux and annual air-sea interaction cycles of the North Atlantic Ocean. Monthly Weather Review. 104:1122-1140

Castro CG, Pérez FF, Álvarez-Salgado XA, Rosón G, Ríos AF (1994) Hydrographic conditions associated with the relaxation of an upwelling event off the Galician coast (NW Spain). Journal of Geophysical Research 99:5135-5147

Castro CG, Pérez FF, Holley SE, Ríos AF (1998) Chemical characterisation and modelling of water masses in the Northeast Atlantic. Progress in Oceanography 41:249-279

Chapelle A, Lazure P, Ménseguen A (1994) Modelling eutrophication events in a coastal ecosystem. Sensitivity analysis. Estuarine, Coastal and Shelf Science 39:529-548

Chase J (1975) Wind-driven circulation in a Spanish estuary. Estuarine and Coastal Marine Science 3:303-310

Christensen PB, Rysgaard S, Sloth NP, Dalsgaard T, Schwaerter S (2000) Sediment mineralization, nutrient fluxes, denitrification and dissimilatory nitrate reduction to ammonium in an estuarine fjord with sea cage trout farms. Aquatic Microbial Ecology 21:73-84

Cifuentes LA, Schemel LE, Sharp JH (1990) Qualitative and numerical-analyses of the effects of river inflow variations on mixing diagrams in estuaries. Estuarine, Coastal and Shelf Science 30:411-427

Clegg SL, Whitfield M (1995) A chemical model of seawater including dissolved ammonia and the stoichiometric dissociation constant of ammonia in estuarine water and seawater from 2 to 40°C. Geochimica et Cosmochimica Acta 59:2403-2421

Cloern JE (1991) Annual variations in river flow and primary production in the south San Francisco bay estuary (USA). In Estuaries and Coasts: Spatial and Temporal Intercomparisons, ECSA 19 Symposium, pp. 91-96

Codispoti LA (1983) Nitrogen in upwelling systems. In Nitrogen in the Marine Environment. E. J. Carpenter and D. G. Capone (eds), Academic Press, New York, pp. 513-564

Codispoti LA, Friedrich GE, Hood DW (1986) Variability in the inorganic carbon system over the southeastern Bering Sea shelf during spring 1980 and summer 1981. Continental Shelf Research 5:133-160

Conley DJ, Johnstone RW (1995) Biogeochemistry of N, P and Si in Baltic Sea sediments: response to a simulated deposition of a spring diatom bloom. Marine Ecology Progress Series 122:265-276

Cortéz L, Quevauviller P, Martin F, Donard OFX (1993) Survey of butyltin contaminants in Portuguese coastal environments. Environmental Pollution 82:57-62

Crosby SA, Millward GE, Butler EI, Turner DR, Whitfield M (1984) Kinetics of phosphate adsorption by iron oxyhydroxides in aqueous systems. Estuarine, Coastal and Shelf Science 19:257-270

Dale AW, Prego R (2002) Physico-biogeochemical controls on benthic-pelagic coupling of nutrient fluxes and recycling in a coastal upwelling system. Marine Ecology Progress Series 235:15-28

deCastro M, Gómez-Gesteira M, Prego R, Taboada JJ, Montero P, Herbello P, Pérez-Villar V (2000) Wind and tidal influence on water circulation in a Galician ria (NW Spain). Estuarine, Coastal and Shelf Science 51:161-176

del Giorgio PA, Duarte CM (2002) Respiration in the open ocean. Nature 420:379-384

Doval MD, Álvarez-Salgado XA, Pérez FF (1997) Dissolved organic matter in a temperate embayment affected by coastal upwelling. Marine Ecology Progress Series 157:21-37

Doval MD, Nogueira E, Pérez FF (1998) Spatio-temporal variability of the thermohaline and biogeochemical properties and dissolved organic carbon in a coastal embayment affected by upwelling: the Ría de Vigo (NW Spain). Journal of Marine Systems 14:135-150

Duarte CM, Cebrián J (1996) The fate of marine autotrophic pollution. Limnology and Oceanography 41:1758-1766

Dyer KR (1973) Estuaries: A Physical Introduction. First edition. John Wiley and Sons Ltd, Chichester, 140 pp

Dyer K (1997) Estuaries: A Physical Introduction. Second edition. John Wiley and Sons Ltd, Chichester, 195 pp

Dyke P (1996) Modelling Marine Processes. Prentice Hall, New Jersey, 152 pp

Edmond JM, Boyle EA, Grant B, Stallard RF (1981) The chemical mass balance in the Amazon plume. I. The nutrients. Deep-Sea Research 28:1339-1374

Edwards A, Jones K, Graham JM, Griffiths CR, MacDougall N, Patching J, Richard JM, Raine R (1996) Transient coastal upwelling and water circulation in Bantry Bay, a ria on the south-west coast of Ireland. Estuarine, Coastal and Shelf Science 42:213-230

Elliott M, McLusky DS (2002) The need for definitions in understanding estuaries. Estuarine, Coastal and Shelf Science 55:815-827

Enoksonn V (1993) Resuspension, ephemeral mud blankets and nitrogen cycling in Laholmsbukten, south east Kattegat. Hydrobiologia 176/177:61-75

Fairbridge RW (1980) The estuary: its definition and geodynamic cycle. In Chemistry and Biogeochemistry of Estuaries. E. Olausson, I. Cato (eds), John Wiley and Sons Ltd, Chichester, pp. 1-36

Fermín EG, Figueiras FG, Arbones B, Villarino ML (1996) Short-time evolution of Gymnodinium catenatum population in the Ria de Vigo. Journal of Phycology 32:212-221

Fernández-Reiriz MJ, Labarta U, Babarro JMF (1996) Comparative allometries in growth and chemical composition of mussel (*Mytillus galloprovincialis*) cultured in two zones in the ria Sada (Galicia, NW Spain). Journal of Shellfish Research 15:349-354

Figueiras FG, Niell FX (1986) Visibilidad del disco de secchi, clorofila a y materia orgánica particulada en la ría de Pontevedra (NO de España). Investigaciones Pesqueras 50:607-637

Figueiras FG, Niell FX (1987) Relaciones entre carbono, nitrógeno y chlorofila a en la ría de Pontevedra, NO de España. Investigaciones Pesqueras 51:3-21

Figueiras FG, Pazos Y (1991) Microplankton assemblages in three Rías Baixas (Vigo, Arosa and Muros, Spain) with a subsurface chlorophyll maximum: their relationships to hydrography. Marine Ecology Progress Series 76:219-233

Figueiras FG, Niell FX, Zapata M (1985) Hidrografía de la ria de Pontevedra (NO de España) con mención especial del banco de Placeres. Investigaciones Pesqueras 49:451-472

Figueiras FG, Niell FX, Mouriño C (1986) Nutrientes y oxígeno en la ría de Pontevedra (NO de España). Investigaciones Pesqueras 50 :97-115

Figueiras FG, Jones KJ, Mosquera AM, Álvarez-Salgado XA, Edwards A, MacDougall N (1994) Red tide assemblage formation in an estuarine upwelling ecosystem: Ria de Vigo. Journal of Plankton Research 16:857-878

Figueiras FG, Labarta U, Reiriz MJF (2002) Coastal upwelling, primary production and mussel growth in the Rias Baixas of Galicia. Hydrobiologia 484:121-131

Fileman E, Burkill P (2001) The herbivorous impact of microzooplankton during two short-term Lagrangian experiments off the NW coast of Galicia in summer 1998. Progress in Oceanography 51:361-383

Fischer HB, List EJ, Koh RCY, Imberger J, Brooks NH (1979) Mixing in Inland and Coastal Waters. Academic Press, New York, 483 pp

Fiúza AFG, Hamann M, Ambar I, Díaz del Río G, González N, Cabanas JM (1998) Water masses and their circulation off western Iberia during May 1993. Deep-Sea Research I 45:1127-1160

Floderus S, Håkansson L (1989) Resuspension, ephemeral mud blankets and nitrogen cycling in Laholmsbukten, south east Kattegat. Hydrobiologia 176/177:61-75

Fox LE (1989) A model for inorganic control of phosphate concentrations in river waters. Geochimica et Cosmochimica Acta 53:417-428

Fraga F (1976) Fotosíntesis en la Ría de Vigo. Investigaciones Pesqueras 40:151-167

Fraga F (1981) Upwelling off the Galician coast, northwest Spain. In Coastal Upwelling Series. F. A. Richards (ed), American Geophysical Union, Washington DC, pp. 176-182

Fraga F (1996) As rías. In As Augas de Galicia. F. Díaz-Fierros (ed), Consello de Cultura Galega, Santiago, pp. 215-280

Fraga F, Prego R (1989) Condiciones hidrográficas previas a la purga de mar. Cuadernos en la Area de Ciencia Marina 4:21-44

Fraga F, Mouriño C, Manríquez M (1982) Las masas de agua en la coasta de Galicia: junio-octubre. Resultados Expediciiones Cientificas 10:51-77

Friederich GE, Codispoti LA (1979) On some factors influencing dissolved silica distribution over the northwest African shelf. Journal of Marine Research 37:337-353

Friederich GE, Codispoti LA (1981) The effect of mixing and regeneration on the nutrient content of upwelling waters of Peru. In Coastal Upwelling Series. F. A. Richards (ed), American Geophysical Union, Washington DC, pp. 221-227

Froelich PN (1988) Kinetic control of dissolved phosphate in natural rivers and estuaries: A primer on the phosphate buffer mechanism. Limnology and Oceanography 33:649-668

Frouin R, Fiúza AFG, Ambar I, Botd TJ (1990) Observations of a poleward surface current off the coasts of Portugal and Spain during winter. Journal of Geophysical Research 95:679-691

Gago J, Gilcoto M, Pérez FF, Ríos AF (2003) Short-term variability of fCO_2 in seawater and air–sea CO_2 fluxes in a coastal upwelling system (Ria de Vigo, NW Spain). Marine Chemistry 80:247-264

Garber JH (1984) Laboratory study of nitrogen and phosphorus remineralisation during the decomposition of coastal plankton and seston. Estuarine, Coastal and Shelf Science 18:685-702

GESAMP Joint Group of Experts on the Scientific Aspects of Marine Pollution (1991) Coastal Modelling, GESAMP Reports and Studies 43, 192 pp

Geyer WR (1997) Influence of wind on dynamics and flushing of shallow estuaries. Estuarine, Coastal and Shelf Science 44:713-722

Gibbs RJ (1977) Effects of combustion temperature and time, and of the oxidation agent used in organic carbon and nitrigen analysis of marine sediments and dissolved organic material. Journal of Sedimentary Petrology 47:547-550

Gilcoto M, Álvarez-Salgado XA, Pérez FF (2001) Computing optimum residual estuarine fluxes with a multiparameter inverse method (OERFIM): application to the Ria of Vigo (NW Spain). Journal of Geophysical Research 106:31,303-31,318

Golloway F, Bender M (1982) Diagenetic models of interstitial nitrate profiles in deep sea suboxic sediments. Limnology and Oceanography 27:624-638

Gómez-Gesteira M, deCastro M, Prego R, Pérez-Villar V (2001) An unusual two layered tidal circulation induced by stratification and wind in the Ría of Pontevedra (NW Spain). Estuarine, Coastal and Shelf Science 52:555-563

Gordon DCJr, Boudreau PR, Mann KH, Ong JE, Silvert WL, Smith SV, Wattayakorn G, Wulff F, Yanagi T (1996) LOICZ (Land-Ocean Interactions in the Coastal Zone). Biogeochemical Modelling Guidelines. LOICZ Reports & Studies 5, 96 pp

Gorley RN, Harris JRW (1998) ECoS3 User Guide. Centre for Coastal and Marine Sciences. Plymouth Marine Laboratory, Plymouth, UK, 35 pp

Grasshoff K, Ehrhardt M, Kremling K (1983) Methods of Seawater Analysis (2nd edition). Verlag Chemie, Weinheim. 419 pp

Guo Q, Lordi GP (2000) Method for quantifying freshwater input and flushing time in estuaries. Journal of Environmental Engineering 126:675-683

Hagy JD, Sanford LP, Boynton WR (2000) Estimation of net physical transport and hydraulic residence times for a coastal plain estuary using box models. Estuaries 23:328-340

Halvorsen E, Pedersen OP, Slagstad D, Tande KS, Fileman ES, Batten SD (2001) Microzooplankton and mesozooplankton in an upwelling filament off Galicia: modelling and sensitivity analysis of the linkages and their impact on the carbon dynamics. Progress in Oceanography 51:499-513

Hansen DV, Rattray MJr (1966) Gravitational circulation in straits and estuaries. Journal of Marine Research 23:104-122

Hansen LS, Blackburn TH (1992) Effect of algal bloom deposition on sediment respiration and fluxes. Marine Biology 112:147-152

Harris JRW, Gorley RN (2003) ECoS, a framework for modelling hierarchical spatial systems. The Science of the Total Environment. In Press.

Harris JRW, Gorley RN (1998a) An Introduction to Modelling Estuaries with ECoS3. Centre for Coastal and Marine Sciences. Plymouth Marine Laboratory, Plymouth, UK, 39 pp

Harris JRW, Gorley RN (1998b) Estuary Quality Templates for ECoS3. Centre for Coastal and Marine Sciences. Plymouth Marine Laboratory, Plymouth, UK, 47 pp

Harris JRW, Bale AJ, Bayne BL, Mantoura RFC, Morris AW, Nelson LA, Radford PJ, Uncles RJ, Weston SA (1984) A preliminary model of the dispersal and biological effect of toxins in the Tamar Estuary, England. Ecological Modelling 22:253-284

Harrison SJ, Phizacklea AP (1985) Seasonal changes in heat flux and heat storage in the intertidal mudflats of the Forth estuary, Scotland. Journal of Climatology. 5:473-485

Head PC (1985) Data presentation and interpretation. In Practical Estuarine Chemistry. P. C. Head (ed), Cambridge University Press, New York, pp. 278-330

Helder W, de Vries RTP (1983) Estuarine nitrite maxima and nitrifying bacteria (Ems-Dollard Estuary). Netherlands Journal of Sea Research 17:1-18

Hilton ABC, McGillivary DL, Adams EE (1998) Residence time of freshwater in Boston's inner harbor. Journal of Waterway, Port, Coastal, and Ocean Engineering 124:82-89

Humborg C, Fennel K, Pastuszak M, Fennel W (2000) A box model approach for a long-term assessment of estaurine eutrophication, Szczecin Lagoon, southern Baltic. Journal of Marine Systems 25:387-403

Huntley DA, Leeks GJL, Walling DE (2001) From rivers to coastal areas: the background and context of the land-ocean interaction study. In Land-Ocean Interaction. Measuring and Modelling Fluxes from River Basins to Coastal Seas. D. A. Huntley, G. J. L. Leeks, D. E. Walling (eds), IWA Publishing, London, pp 1-7

Huntsman SA, Barber RT (1977) Primary production off northwest Africa: The relationship to wind and nutrient conditions. Deep-Sea Research 24:25-33

Hurd DC (1983) Physical and chemical properties of siliceous skeletons. In Silicon Geochemistry and Biogeochemistry. S. R. Aston (ed), Academic Press, New York, pp 187-244

Ianson D, Allen SE (2002) A two-dimensional nitrogen and carbon flux model in a coastal upwelling region. Global Biogeochemical Cycles 16:11

Ibarra E, Prego R (1997) La Ria de Pontevedra: Revisión de su conocimiento. Monografías de Química Oceanográfica 1:55-87

Inoue M, Wiseman WJJr (2000) Transport, mixing and stirring processes in a Louisiana estuary: a model study. Estuarine, Coastal and Shelf Science 50:449-466

Isshiki K, Sohrin Y, Nakayama E (1991) Form of dissolved silicon in seawater. 32:1-8

Jago CF, Jones SE (1998) Observation and modelling of the dynamics of benthic fluff resuspended from a sandy bed in the southern North Sea. Continental Shelf Research 18:1255-1282

Jago CF, Bale AJ, Green MO, Howarth MJ, Jones JE, McCave. I. N., Millward GE, Morris AW, Rowden AA, Williams JJ (1993) Resuspension processes and seston dynamics, southern North Sea. Philosophical Transactions of the Royal Society of London Series A 343:457-491

Jassby AD, Cloern JE, Cole BE (2002) Annual primary production: Patterns and mechanisms of change in a nutrient-rich tidal ecosystem. Limnology and Oceanography 47:698-712

Jenkins MC, Kemp WM (1984) The coupling of nitrification and denitrification in two estuarine sediments. Limnology and Oceanography 29:609-619

Jickells TD (1998) Nutrient biogeochemistry of the coastal zone. Science 281:217-222

Jiménez C, Niell FX, Figueiras FG, Clavero V, Algarra PBJ (1992) Green mass aggregations of Gyrodinium cf. aureolum Hulburt in the ria of Pontevedra (NW Spain). Journal of Plankton Research 14:705-720

Johns B, Rao AD, Dube SK, Sinha PC (1993) The effect of fresh-water discharge from the Godavari River on the occurrence of local upwelling off the east-coast of India. Estuarine, Coastal and Shelf Science 37:299-312

Joint I, Inall M, Torres R, Figueiras FG, Álvarez-Salgado XA, Rees AP, Woodward EMS (2001) Two Lagrangian experiments in the Iberian Upwelling System: tracking an upwelling event and an off-shore filament. Progress in Oceanography 51:221-248

Jones JE (2002) Coastal and shelf-sea modelling in the European context. Oceanography and Marine Biology: an Annual Review. 40:37-141

Kamp-Nielsen L (1992) Benthic-pelagic coupling of nutrient metabolism along an estuarine eutrophication gradient. Hydrobiologia 235/236:457-470

Karl DM, Christian JR, Dore JE, Hebel DV, Letelier RM, Tupas LM, Winn CD (1996) Seasonal and interannual variability in primary production and particle flux at Station ALOHA. Deep-Sea Research II 43:539-568

Kattner G (1999) Storage of dissolved inorganic nutrients in seawater: poisoning with mercuric chloride. Marine Chemistry 67:61-66

Kaul LW, Froelich PNJr (1984) Modeling estuarine nutrient geochemistry in a simple system. Geochimica et Cosmochimica Acta 48:1417-1433

Kelly-Gerreyn BA, Hydes DJ, Trimmer M, Nedwell DB (1999) Calibration of an early diagenesis model for high nitrate, low reactive sediments in a temperate latitude estuary (Great Ouse, UK). Marine Ecology Progress Series 177:37-50

Kemp WM, Sampou P, Caffrey J, Mayer M, Henriksen K, Boynton WR (1990) Ammonium recycling versus denitrification in Chesapeake Bay sediments. Limnology and Oceanography 35:1545-1563

Kiley KP, Welch CS (1989) The response of estuarine circulation to local wind events. In Estuarine Circulation, B. J. Neilson, A. Kuo, J. Brubaker (eds), Humana Press, New Jersey, pp. 97-112

Kjerfve B, Stevenson LH, Proehl JA, Chrzanowski TH, Kitchens WM (1981) Estimation of material fluxes in an estuarine cross section: A critical analysis of spatial measurement density and errors. Limnology and Oceanography 26:325-335

Klinck JM, Obrien JJ, Svendsen H (1981) A simple-model of fjord and coastal circulation interaction. Journal of Physical Oceanography 11:1612-1626

Knauer GA, Martin JH, Bruland KW (1979) Fluxes of particulate carbon, nitrogen and phosphorus in the upper water column of the northeast Pacific. Deep-Sea Research 26:97-108

Koike I, Sørensen J (1988) Nitrate reduction and denitrification in marine sediments. In Nitrogen Cycling in Coastal Marine Environments. T. H. Blackburn, J. Sørensen (eds), John Wiley & Sons Ltd, Chichester, pp 251-273

Kremling K, Streu P (1993) Saharan dust influenced trace element fluxes in deep North-Atlantic subtropical waters. Deep-Sea Research I 40:1155-1168

Laima M, Maksymowska-Brossard D, Sauriau PG, Richard P, Girard M, Gouleau D, Joassard L (2002) Fluff deposition on intertidal sediments: effects on benthic biota, ammonium fluxes and nitrification rates. Biogeochemistry 61:115-133

Lancelot C, Billen G (1985) Carbon-nitrogen relationships in nutrient metabolism of coastal marine ecosystems. Advances in Aquatic Microbiology 3:263-320

Largier JL, Hollibaugh JT, Smith SV (1997) Seasonally hypersaline estuaries in Mediterranean-climate regions. Estuarine, Coastal and Shelf Science 45:789-797

Lavín A, Diaz del Rio G, Cabanas JM, Casas G (1991) Afloramiento en el noroeste de la Península Ibérica. Índices de afloramiento para el punto 43 °N 11 °W periodo 1966-1989. Informe Técnico del Instituto Español de Oceanografia 91:1-39

Laws E (1991) Photosynthetic quotients, new production and net community production in the open ocean. Deep-Sea Research 38:143-167

Laws E (1997) Mathematical Methods for Oceanographers, John Wiley and Sons Ltd, New York, 343 pp

Lebo ME (1990) Phosphate uptake along a coastal-plain estuary. Limnology and Oceanography 35:1279-1289

Lebo ME (1991) Particle-bound phosphorus along an urbanized coastal-plain estuary. Marine Chemistry 34:225-246

Lebo ME, Sharp JH, Cifuentes LA (1994) Contribution of river phosphate variations to apparent reactivity estimated from phosphate-salinity diagrams. Estuarine, Coastal and Shelf Science 39:584-594

Lee J-Y, Tett P, Jones K, Jones S, Luyten P, Smith C, Wild-Allen K (2002) The PROWQM physical–biological model with benthic–pelagic coupling applied to the northern North Sea. Journal of Sea Research 48:287-331

Levasseur ME, Therriault J-C (1987) Phytoplankton biomass and nutrient upwelling dynamics in a tidally induced upwelling: the role of the NO_3 : SiO_4 ratio. Marine Ecology Progress Series 39:87-97

Lewis RE (1997) Dispersion in Estuaries and Coastal Waters. John Wiley and Sons Ltd, Chichester, 312 pp

Li YG, Mehta AJ, Hatfield K, Dortch MS (1997) Modulation of constituent release across the mud-water interface by water waves. Water Resources Research 33:1409-1418

Liu YP, Millward GE, Harris JRW (1998) Modelling the distributions of dissolved Zn and Ni in the Tamar Estuary using hydrodynamics coupled with chemical kinetics. Estuarine, Coastal and Shelf Science 47:535-546

Loder TC, Reichard RP (1981) The dynamics of conservative mixing in estuaries. Estuaries 4:64-69

Lohse L, Kloosterhuis KT, van Raaphorst W, Helder W (1996) Denitrification rates as measured by the isotope pairing method and the acetylene inhibition technique in continental shelf sediments of the North Sea. Marine Ecology Progress Series 132:169-179

Lomas MW, Gilbert PM (1999) Interactions between NH_4^+ and NO_3^- uptake and assimilation: comparison of diatoms and dinoflagellates at several growth temperatures. Marine Biology 133:541-551

López-Jamar E, Cal RM, González G, Hanson RB, Rey J, Santiago G, Tenore KR (1992) Upwelling and outwelling effects on the benthic regime of the continental shelf off Galicia, NW Spain. Journal of Marine Research 50:465-488

Maher W, Woo L (1998) Procedures for the storage and digestion of natural waters for the determination of filterable reactive phosphorus, total filterable phosphorus and total phosphorus. Analytica Chimica Acta 375:5-47

Malone TC, Conley DJ, Fisher TR, Gilbert PM, Harding LW, Sellner KG (1996) Scales of nutrient-limited phytoplankton productivity in Chesapeake Bay. Estuaries 19:371-385

Margalef R, Andreu B (1958) Componente vertical de los movimientos del agua en la ría de Vigo y su posible relación con la entrada de sardina. Investigaciones Pesqueras 11:105-126

Matsukawa Y, Suzuki T (1985) Box model analysis of hydrography and behaviour of nitrogen and phosphorus in a eutrophic estuary. Journal of the Oceanographic Society of Japan 41:407-426

McClain CR, Chao SY, Atkinson LP, Blanton JO, de Castillejo F (1986) Wind-driven upwelling in the vicinity of Cape Finisterre, Spain. Journal of Geophysical Research 91:8470-8486

McDowell DM, O'Connor BA (1977) Hydraulic Behaviour of Estuaries. Macmillan, London, 292 pp

McKelvie ID, Peat DMW, Worsfold PJ (1995) Techniques for the quantification and speciation of phosphorus in natural waters. Analytical Proceedings 32:437-445

Meybeck M (1982) Carbon, nitrogen and phosphorus transport by world rivers. American Journal of Science 282:401-450

Middelburg JJ, Nieuwenhuize J (2001) Nitrogen isotope tracing of dissolved inorganic nitrogen behaviour in tidal estuaries. Estuarine, Coastal and Shelf Science 53:385-391

Millard RC, Owens WB, Fofonoff NP (1990) On the calculation of the Brunt-Väisälä frequency. Deep Sea Research 37 (1):167-181

Miller GC, Zepp RG (1979) Effects of suspended sediments on photolysis rates of dissolved pollutants. Water Research 13:453-459

Millero FJ, Perron G, Desnoyers JE (1973) Heat capacity of seawater solutions from 5° to 35°C and 0.5 to 22 ppt chlorinity. Journal of Geophysical Research 78:449-4507

Millero FJ, Poisson A (1981) International one-atmosphere equation of state of seawater. Deep-Sea Research 28A:625-629

Millward GE, Morris AW, Tappin AD (1998) Trace metals at two sites in the southern North Sea: Results from a sediment resuspension study. Continental Shelf Research 18:1381-1400

Minas HJ, Packard TT, Minas M, Coste B (1982) An analysis of the production-generation system in the coastal upwelling area off NW Africa based on oxygen, nitrate, and ammonium distributions. Journal of Marine Research 40:615-641

Minas HJ, Minas M, Packard TT (1986) Productivity in upwelling areas deduced from hydrographic and chemical fields. Limnology and Oceanography 31:1182-1206

Moncoiffé G, Álvarez-Salgado XA, Figueiras FG, Savidge G (2000) Seasonal and short-time-scale dynamics of microplankton community production and respiration in an inshore upwelling system. Marine Ecology Progress Series 196:111-126

Mook DH, Hoskin CM (1982) Organic determinations by ignition: caution advised. Estuarine, Coastal and Shelf Science 15:697-699

Mora J, Planas M, Silva R (1989) Impacto de la contaminación orgánica en la Ensenada de Lourizán: El medio físico y la macrofauna bentónica. Cahiers de Biologie Marine 30:181-199

Moran MA, Sheldon WMJr, Sheldon JE (1999) Biodegradation of riverine dissolved organic carbon in five estuaries of the southeastern United States. Estuaries 22:55-64

Morris AW (1990) Kinetic and equilibrium approaches to estuarine chemistry. The Science of the Total Environment 97/98:253-266

Morris AW, Mantoura RFC, Bale AJ, Howland RJM (1978) Very low salinity regions of estuaries: important sites for chemical and biological reactions. Nature 274:678-680

Morris AW, Bale AJ, Howland RJM (1981) Nutrient distributions in an estuary: evidence of chemical precipitation of dissolved silicate and phosphate. Estuarine, Coastal and Shelf Science 12:205-216

Morris AW, Bale AJ, Howland RJM (1982a) The dynamics of estuarine manganese cycling. Estuarine, Coastal and Shelf Science 14:175-192

Morris AW, Bale AJ, Howland RJM (1982b) Chemical variability in the Tamar estuary, south-west England. Estuarine, Coastal and Shelf Science 14:649-661

Morris AW, Howland RJM, Woodward EMS, Bale AJ, Mantoura RFC (1985) Nitrite and ammonia in the Tamar Estuary. Netherlands Journal of Sea Research 19:217-222

Mortlock RA, Froelich PN (1989) A simple method for the rapid determination of biogenic opal in pelagic marine sediments. Deep-Sea Research 36:1415-1426

Mouriño C, Fraga F (1985) Determinacion de nitratos en agua de mar. Investigaciones Pesqueras 49:81-96

Mouriño C, Pérez FF, Ríos AF, Manríquez M, Estrada M, Marrase C, Prego R, Fraga F (1985) Campaña "Galicia VIII": Datos básicos, Datos Informativos. Instituto Investigaciones Pesqueras. 13:1-108

Murphy J, Riley JP (1962) A modified single solution method for the determination of phosphate in natural waters. Analytica Chimica Acta 27:31-36

Murray JW (1992) The oceans. In Global Biogeochemical Cycles. S. S. Butcher, R J. Charlson, G. H. Orians, G. V. Wolfe (eds), Academic Press, London, pp. 175-211

Nedwell DB (1982) Exchanges of nitrate and the products of bacterial nitrate reduction between seawater and sediments from a UK saltmarsh. Estuarine, Coastal and Shelf Science 14:557-566

Nedwell DB, Park RJ, Upton AC, Assinder DJ (1993) Seasonal fluxes across the sediemnt-water interface, and processes with sediments. Philosophical Transactions of the Royal Society of London Series A 343:519-529

Nelson DM, Tréguer P, Brzezinski MA, Leynaert A, Quéguiner B (1995) Production and dissolution of biogenic silica in the ocean: revised global estimates, comparison with regional data and relationship to biogenic sedimentation. Global Biogeochemical Cycles 9:359-372

Nielsen K, Nielsen LP, Rasmussen P (1995) Estuarine nitrogen retention independently estimated by the denitrification rate and mass balance methods: a study of Norsminde Fjord, Denmark. Marine Ecology Progress Series 119:275-283

Nielsen LP, Christensen PB, Revsbech NP, Sørensen J (1990) Denitrification and photosynthesis in stream sediment studied with microsensor and whole-core techniques. Limnology and Oceanography 35:1135-1144

Nixon SW (1981) Remineralisation and nutrient cycling in coastal marine systems. In Estuaries and Nutrients, B. J. Neilson, L. E. Cronin (eds), Humana Press, New Jersey, pp 111-138

Nogueira E, Pérez FF, Ríos AF (1997a) Seasonal patterns and long-term trends in an estuarine upwelling ecosystem (Ría de Vigo, NW Spain). Estuarine, Coastal and Shelf Science 44:285-300

Nogueira E, Pérez FF, Rios AF (1997b) Modelling thermohaline properties in an estuarine upwelling ecosystem (Ría de Vigo: NW Spain) using Box-Jenkins transfer function models. Estuarine, Coastal and Shelf Science 44:685-702

Nogueira E, Pérez FF, Ríos AF (1998) Modelling nutrients and chlorophyll a time series in an estuarine upwelling ecosystem (Ría de Vigo: NW Spain) using the Box-Jenkins approach. Estuarine, Coastal and Shelf Science 46:267-286

Officer CB (1981) Box models revisited. In Estuarine and Wetland Processes: With Emphasis on Modeling. P. Hamilton and K. B. Macdonald (eds), Plenum Press, New York, pp. 65-114

Otto L (1975) Oceanography of the Ria de Arosa NW Spain. Koninklijk Nederlands Meteorologisch Institut Mededelingen en Verhandelingen 96, 210 pp

Owens NJP (1986) Estuarine nitrification: A naturally occurring fluidized bed reaction? Estuarine, Coastal and Shelf Science 22:31-44

Owens NJP, Mantoura RFC, Burkill PH, Howland RJM, Pomroy AJ, Woodward EMS (1986) Nutrient cycling studies in Carmarthen Bay - phytoplankton production, nitrogen assimilation and regeneration. Marine Biology 93:329-342

Pardo PC, Gilcoto M, Pérez FF (2001) Short-time scale coupling between thermohaline and meteorological forcing in the Ría de Pontevedra. Scientia Marina 65:229-240

Parsons TR, Maita Y, Lalli CM (1984) A Manual of Chemical and Biological Methods for Seawater Analysis. Pergamon Press, Oxford, 173 pp

Pascual JR, Calpena V (1985) The tidal current in the Arosa Ria (Galicia, Spain). Revisiones de Geofisica. 41:149-158

Pennock JR, Sharp JH (1994) Temporal alteration between light- and nutrient-limitation of phytoplankton production in a coastal plain estuary. Marine Ecology Progress Series 111:275-288

Pereira ME, Duarte AC, Millward GE, Abreu SN, Vale C (1998) An estimation of industrial mercury stored in sediments of a confined area of the lagoon of Aveiro (Portugal). Water Science and Technology 37:125-130

Pérez FF, Álvarez-Salgado XA, Rosón G, Ríos AF (1992) Carbonic-calcium system, nutrients and total organic nitrogen in continental runoff to the Galician Rias Baixas, NW Spain. Oceanologica Acta 15:595-602

Pérez FF, Álvarez-Salgado XA, Rosón G (2000) Stoichiometry of the net ecosystem metabolism in a coastal inlet affected by upwelling. The Ría de Arousa (NW Spain). Marine Chemistry 69:217-236

Pérez FF, Castro CG, Álvarez-Salgado XA, Ríos AF (2001) Coupling between the Iberian basin - circulation and the Portugal boundary current system: a chemical study. Deep-Sea Research I 48:1519-1533

Pérez-Camacho A, Labarta U, Beiras R (1995) Growth of mussel (*Mytillus edulis galiprovincialis*) in cultivation raft. Influence of seed source, cultivation site and food availability. Aquaculture 138:349-362

Pham MK, Martin JM, Garnier JM, Li Z, Boutier B, Chiffoleau JF (1997) On the possibility of using the commercially available ECoS model to simulate Cd distribution in the Gironde estuary (France). Marine Chemistry 58:163-172

Pingree RD, Sinha B, Griffiths CR (1999) Seasonality of the European slope current (Goban Spur) and ocean margin exchange. Continental Shelf Research 19:929-975

Platt T, Jassby AD (1976) The relationship between photosynthesis and light for natural assemblages of coastal marine phytoplankton. Journal of Phycology 12:421-430

Pond S, Pickard GL (1983) Introductory Dynamical Oceanography. Second edition, Pergamon, UK, 329 pp

Prego R (1992) Flows and budgets of nutrient salts and organic carbon in relation to a red tide in the Ria of Vigo (NW Spain). Marine Ecology Progress Series 79:289-302

Prego R (1993a) General aspects of carbon biogeochemistry in the ria of Vigo, northwestern Spain. Geochimica et Cosmochimica Acta 57:2041-2052

Prego R (1993b) Biogeochemical pathways of phosphate in a Galician ria (North-western Iberian Peninsula). Estuarine, Coastal and Shelf Science 37:437-451

Prego R (1994) Nitrogen interchanges generated by biogeochemical processes in a Galician ria. Marine Chemistry 45:167-176

Prego R, Bao R (1997) Upwelling influence on the Galician coast: silicate in shelf water and underlying surface sediments. Continental Shelf Research 17:307-318.

Prego R, Cobelo-Garcia A (2003) Twentieth century overview of heavy metals in the Galician Rias (NW Iberian Peninsula). Environmental Pollution 121:425-452

Prego R, Fraga F (1992) A simple model to calculate the residual flows in a Spanish ria. Hydrographic consequences in the ria of Vigo. Estuarine, Coastal and Shelf Science 34:603-615

Prego R, Bao R, Howland R (1995) The biogeochemical cycling of dissolved silicate in a Galician ria. Ophelia 42:301-318

Prego R, Carmen Barciela M, Varela M (1999) Nutrient dynamics in the Galician coastal area (Northwestern Iberian Peninsula): Do the Rias Bajas receive more nutrient salts than the Rias Altas? Continental Shelf Research 19:317-334

Prego R, Dale AW, deCastro M, Gómez-Gesteira M, Taboada JJ, Montero P, Villareal MR, Pérez-Villar V (2001) Hydrography of the Pontevedra Ria: Intra-annual spatial and temporal variability in a Galician coastal system (NW Spain). Journal of Geophysical Research 106:19845-19857

Pritchard DW (1989) Estuarine circulation - a help or a hindrance. In Estuarine Circulation, B. J. Neilson, A. Kuo, and J. Brubaker (eds), Humana Press, Clifton, NJ, pp. 1-39

Punt AG (2000) Measurement and Modelling of Estuarine Chemistry. PhD Thesis, University of Plymouth, 232 pp

Rabouille C, Gaillard J-F (1991) A coupled model representing the deep-sea organic carbon mineralization and oxygen consumption in surficial sediments. Journal of Geophysical Research 96:2761-2776

Ragueneau O, Tréguer P (1994) Determination of biogenic silica in coastal waters: applicability and limits of the alkaline digestion method. Marine Chemistry 45:43-51

Rahm L, Wulff F (1992) Using parallel salinity and temperature profiles for calculations of estuarine fluxes with reference to the Baltic proper. Netherlands Journal of Sea Research 29:281-289

Raillard O, Menesguen A (1994) An ecosystem box model for estimating the carrying-capacity of a macrotidal shellfish system. Marine Ecology Progress Series 115:117-130

Rasmussen B, Josefson AB (2002) Consistent estimates for the residence time of micro-tidal estuaries. Estuarine, Coastal and Shelf Science 54:65-73

Redfield AC, Ketchum BH, Richards FA (1963) The influence of organisms on the composition of seawater. In The Sea. M. N. Hill (ed), Interscience, New York, pp 26-77

Regnier P, Wollast R, Steefel CI (1997) Long-term fluxes of reactive species in macrotidal estuaries: Estimates from a fully transient, multicomponent reaction-transport model. Marine Chemistry 58:127-145

Regnier P, O'Kane JP, Steefel CI, Vanderborght PA (2002) Modeling complex multi-component reactive-transport systems: towards a simulation environment based on the concept of a Knowledge Base. Applied Mathematical Modelling 26:913-927

Rio F, Rodriguez F (1982) Os Rios Galegos. Consello da Cultura Galega, Santiago de Compostela, 333 pp

Ríos AF, Pérez FF, Fraga F (1992) Water masses in upper and middle North Atlantic Ocean east of the Azores. Deep-Sea Research 39:645-658

Ríos AF, Fraga F, Pérez FF, Figueiras FG (1998) Chemical composition of phytoplankton and particulate organic matter in the Ria de Vigo (NW Spain). Scientia Marina 62:257-271

Robards K, McKelvie AD, Benson RL, Worsfold PJ, Blundell NJ, Casey H (1994) Determination of carbon, phosphorus, nitrogen and silicon species in waters. Analytica Chimica Acta 287:147-190

Rosón G, Pérez FF, Álvarez-Salgado XA, Figueiras FG (1995) Variation of both thermohaline and chemical properties in an estuarine upwelling ecosystem: Ria de Arousa. I. Time evolution. Estuarine, Coastal and Shelf Science 41:195-213

Rosón G, Álvarez-Salgado XA, Pérez FF (1997) A non-stationary box model to determine residual fluxes in a partially mixed estuary, based on both thermohaline properties: Application to the Ria de Arosa (NW Spain). Estuarine, Coastal and Shelf Science 44:249-262

Rosón G, Álvarez-Salgado XA, Pérez FF (1999) Carbon cycling in a large coastal embayment, affected by wind-driven upwelling: short-timescale variability and spatial differences. Marine Ecology Progress Series 176:215-230

Rowden AA, Jones MB, Morris AW (1998a) The role of *Callianassa subterranea* (Montagu) (THALASSINIDEA) in sediment resuspension in the North Sea. Continental Shelf Research 18:1365-1380

Rowden AA, Jago CF, Jones SE (1998b) Influence of benthic macrofauna on the geotechnical and geophysical properties of surficial sediment, North Sea. Continental Shelf Research 18:1347-1363

Ruiz Mateo A (1983) Dinámica marina de la ria de Pontevedra. MOPU Cuadernos de Investigacion 13, 22 pp

Ruiz-Villarreal M, Montero P, Taboada JJ, Prego R, Leita PC, Pérez-Villar V (2002) Hydrodynamic model study of the Ria de Pontevedra under estuarine conditions. Estuarine, Coastal and Shelf Science 54:101-113

Rysgaard S, Risgaard-Petersen N, Sloth NP, Jensen K, Nielsen LP (1994) Oxygen regulation of nitrification and denitrification in sediments. Limnology and Oceanography 39:1643-1652

Savchuk OP (2002) Nutrient biogeochemical cycles in the Gulf of Riga: scaling up field studies with a mathematical model. Journal of Marine Systems 32:253-280

Savchuk O, Wulff F (1996) Biogeochemical transformation of nitrogen and phosphorus in the marine environment - coupling hydrodynamic and biogeochemical processes in models for the Baltic proper. Systems Ecology Contributions 2, Stockholm University, 79 pp

Seitzinger SP (1988) Denitrification in fresh water and coastal marine ecosystems: Ecological and geochemical significance. Limnology and Oceanography 33:702-724

Seitzinger SP, Giblin AE (1996) Estimating, denitrification in North Atlantic continental shelf sediments. Biogeochemistry 35:235-260

Seitzinger SP, Sanders RW (1997) Contribution of dissolved organic nitrogen from rivers to estuarine eutrophication. Marine Ecology Progress Series 159:1-12

Seitzinger SP, Pilson MEQ, Nixon SW (1983) Nitrous oxide production in nearshore marine sediments. Science 222:1244-1246

Shaw PJ, Chapron C, Purdie DA, Rees AP (1998) Impacts of phytoplankton activity on dissolved nitrogen fluxes in the tidal reaches and estuary of the Tweed, UK. Marine Pollution Bulletin 37:280-294

Signell RP, Butman B (1992) Modeling tidal exchange and dispersion in Boston Harbor. Journal of Geophysical Research 97:15591-15606

Simpson JH, Brown J, Matthews J, Allen G (1990) Tidal straining, density currents and stirring in the control of estuarine stratification. Estuaries 13:125-132

Slagstad D, Wassmann P (2001) Modelling the 3-D carbon flux across the Iberian margin during the upwelling season in 1998. Progress in Oceanography 51:467-497

Sloth NP, Blackburn H, Hansen LS, Risgaard-Petersen N, Lomstein BA (1995) Nitrogen cycling in sediments with different organic loading. Marine Ecology Progress Series 116:163-170

Sloth NP, Riemann B, Nielsen LP, Blackburn T (1996) Resilience of pelagic and benthic microbial communities to sediment resuspension in a coastal ecosystem, Knebel Vig, Denmark. Estuarine, Coastal and Shelf Science 42:405-415

Smith EM, Kemp WM (1995) Seasonal and regional variations in plankton community production and respiration for Chesapeake Bay. Marine Ecology Progress Series 116:217-231

Smith NP (1985) The suitability of routine weather data for estimating local estuarine heat energy fluxes. Estuaries 8:270-278

Smith SV, Hollibaugh JT (1993) Coastal metabolism and the oceanic organic carbon balance. Reviews of Geophysics 31:75-89

Smith SV, Hollibaugh JT (1997) Annual cycle and intertidal variability of ecosystem metabolism in a temperate climate environment. Ecological Monographs 67:509-533

Smith SV, Hollibaugh JT (1998) Carbon-nitrogen-phosphorus cycling in Tomales Bay, California. Aquatic Geochemistry 4:395-402

Smith SV, Hollibaugh JT, Dollar SJ, Vink S (1989) Tomales Bay, California: A case for carbon-controlled nitrogen cycling. Limnology and Oceanography 34:37-52

Smith SV, Hollibaugh JT, Dollar SJ, Vink S (1991) Tomales Bay Metabolism: C-N-P stoichiometry and ecosystem heterotrophy at the land-sea interface. Estuarine, Coastal and Shelf Science 33:223-257

Soetaert K, Herman PMJ, Middelburg JJ (1996) A model of early diagentic processes from the shelf to abyssal depths. Geochimica et Cosmochimica Acta 60:1019-1040

Soetaert K, Middelburg JJ, Herman PMJ, Buis K (2000) On the coupling of benthic and pelagic biogeochemical models. Earth-Science Reviews 51:173-201

Sokal RR, Rohlf FJ (1995) Biometry: The Principals and Practice of Statistics in Biological Research. Third Edition, W.H. Freeman and Company, New York, 887 pp

Steen RJCA, Evers EHG, Van-Hattum B, Cofino WP, Brinkman UAT (2002) Net fluxes of pesticides from the Scheldt Estuary into the North Sea: a model approach. Environmental Pollution 116:75-84

Stolte W, Riegman R (1996) A model approach for size-selective competition of marine phytoplankton for fluctuating nitrate and ammonium. Journal of Phycology 32:732-740

Stolte W, McCollin T, Noordeloos AAM, Riegman R (1994) Effect of nitrogen source on the size distribution within marine phytoplankton populations. Journal of Experimental Marine Biology and Ecology 184:83-97

Straile D (1997) Gross growth efficiencies of protozoan and metazoan zooplankton and their dependence on food concentration, predator-prey weight ratio, and taxonomic group. Limnology and Oceanography 42:1375-1385

Sutton T, Hopkins T, Remsen A, Burghart S (2001) Multisensor sampling of pelagic ecosystem variables in a coastal environment to estimate zooplankton grazing impact. Continental Shelf Research 21:69-87

Taboada JJ, Prego R, Ruiz-Villarreal M, Gómez-Gesteira M, Montero P, Santos AP, Pérez-Villar V (1998) Evaluation of the seasonal variations in the residual circulation in the Ría of Vigo (NW Spain) by means of a 3D baroclinic model. Estuarine, Coastal and Shelf Science 47:661-670

Taboada JJ, Villarreal MR, Gómez-Gesteira M, Montero P, Santos AP, Pérez-Villar V, Prego R (2000) Estudio del transporte en la Ría de Pontevedra (NO España) mediante un modelo 3D. In A. Da Costa-Duarte, C. Vale, R. Prego (eds), Estudios de Biogeoquímica na Zona Costeira Ibérica, Universidade de Aveiro, Aveiro, Portugal, pp. 285-291

Tappin AD, Harris JRW, Uncles RJ (2003) The fluxes and transformations of suspended particles, particulate organic carbon, particulate nitrogen, nitrate, nitrite and ammonium in the Humber estuarine system (UK) from 1994 to 1996: results from an integrated observation and modelling study. The Science of the Total Environment. In Press.

Tappin AD, Gellers-Barkmann S, Burton JD, Statham PJ (1997) The use of NOSTRADAMUS, a numerical transport model, for simulating concentrations and distributions of chromium, cadmium and lead in the southern North Sea. Deutsche Hydrographische Zeitschrift 49:411-429

Tappin AD, Harris JRW, Uncles RJ, Boorman D (2002) Potential modification of the fluxes of nitrogen from the Humber Estuary catchment (U.K.) to the North Sea in response to changing agricultural inputs and climate patterns. Hydrobiologia 475:65-77

Taylor, A. H. and Stephens, J. A. Seasonal and year-to-year changes in the temperatures of the English Channel and the Southern North Sea, 1961-1976: a budget. Oceanologica Acta 6, 63-72. 83.

Teira E, Serret P, Fernández E (2001) Phytoplankton size-structure, particulate and dissolved organic carbon production and oxygen fluxes through microbial communities in the NW Iberian coastal transition zone. Marine Ecology Progress Series 219:65-83

Tenore KR, Boyer LF, Cal RM, Corral J, García-Fernández C, González N, González-Gurriaran E, Hanson RB, Iglesias J, Krom M, Lopez-Jamar E, McLain J, Pamatmat MM, Pérez A, Rhoads DC, de Santiago G, Tietjen J, Westrich J, Windom HL (1982) Coastal upwelling in the Rias Bajas, NW Spain: contrasting the benthic regimes of the Rias de Arosa and Muros. Journal of Marine Research 40:701-772

Tett P (1990) A Three Layer Vertical and Microbiological Processes Model for Shelf Seas. Proudman Oceanographic Laboratory, Report No. 14. 85 pp

Tett P, Walne A (1995) Observations and simulations of hydrography, nutrients and plankton in the southern North Sea. Ophelia 42:371-416

Tian RC, Vezina AF, Starr M, Saucier F (2001) Seasonal dynamics of coastal ecosystems and export production at high latitudes: A modeling study. Limnology and Oceanography 46:1845-1859

Tilstone GH, Figueiras FG, Fraga F (1994) Upwelling-downwelling sequences in the generation of red tides in a coastal upwelling system. Marine Ecology Progress Series 112:241-253

Tilstone G, Figueiras FG, Fermín EG, Arbones B (1999) Significance of nanophytoplankton photosynthesis and primary production in a coastal upwelling system (Ría de Vigo, NW Spain). Marine Ecology Progress Series 183:13-27

Tilstone GH, Míguez BM, Figueiras FG, Fermín EG (2000) Diatom dynamics in a coastal ecosystem affected by upwelling: coupling between species succession, circulation and biogeochemical processes. Marine Ecology Progress Series 205:23-41

Torres Lopez ST, Varela RA, Delhez E (2001) Residual circulation and thermohaline distribution of the Ria de Vigo: a 3-D hydrodynamical model. Scientia Marina 65:277-289

Tréguer P, Le Corre P (1979) The ratios of nitrate, phosphate and silicate during uptake and regeneration phases in the Moroccan upwelling regime. Deep-Sea Research 26:163-184

Trimmer M, Nedwell DB, Sivyer DB, Malcolm SJ (1998) Nitrogen fluxes through the lower estuary of the Great Ouse, England: the role of the bottom sediments. Marine Ecology Progress Series 163:109-124

Trimmer M, Nedwell DB, Sivyer DB, Malcolm SJ (2000) Seasonal benthic organic matter mineralisation measured by oxygen uptake and denitrification along a transect of the inner and outer River Thames estuary, UK. Marine Ecology Progress Series 197:103-119

Tyrrell T (1999) The relative influences of nitrogen and phosphorus on oceanic primary production. Nature 400:525-531

Tyrrell T, Law CS (1997) Low nitrate: phosphate ratios in the global ocean. Nature 387:793-796

Tyrrell T, Lucas MI (2002) Geochemical evidence of denitrification in the Benguela upwelling system. Continental Shelf Research 22:2497-2511

Uncles RJ, Stephens JA (2001) The annual cycle of temperature in a temperate estuary and associated heat fluxes to the coastal zone. Journal of Sea Research 46:143-159

Uncles RJ, Elliot RCA, Weston SA (1985a) Dispersion of salt and suspended sediment in a partially mixed estuary. Estuaries 8:256-269

Uncles RJ, Elliot RCA, Weston SA (1985b) Observed fluxes of water, salt and suspended sediment in a partly mixed estuary. Estuarine, Coastal and Shelf Science 20:147-167

Uncles RJ, Joint I, Stephens JA (1998a) Transport and retention of suspended particulate matter and bacteria in the Humber-Ouse estuary, UK, and their relationship to hypoxia and anoxia. Estuaries 21:597-612

Uncles RJ, Howland RJM, Easton AE, Griffiths ML, Harris C, King RS, Morris AW, Plummer DH, Woodward EMS (1998b) Seasonal variability of dissolved nutrients in the Humber-Ouse estuary. Marine Pollution Bulletin 37:234-246

UNESCO (1981) Background papers and supporting data on the International Equation of State of Seawater 1980. UNESCO Technical Papers in Marine Science 38.

UNESCO (1986) Progress on Oceanographic Tables and Standards 1983-1986. Work and recommendations of the UNESCO/SCOR/ICES/IAPSO joint panel. UNESCO Technical Papers in Marine Sciences 50:

UNESCO (1988) The acquisition, calibration and analysis of CTD data. UNESCO Technical Papers in Marine Science 54.

UNESCO (1994) Protocols for the Joint Global Ocean Flux Study (JGOFS), Core measurements. Inter-governmental Oceanographic Commission. Scientific Committee on Oceanographic Research. Manual and Guides 29.

United Kingdom Hydrographic Office. (2001) Admiralty Tide Tables 2002, Volume 2: Europe (excluding United Kingdom and Ireland), Mediterranean Sea and Atlantic Ocean, United Kingdom Hydrographic Office, Taunton, UK, 354 pp

Unnukrishnan AS, Shetye SR, Gouveia AD (1997) Tidal propagation in the Mandovi-Zuari estuarine network, west coast of India: impact of freshwater influx. Estuarine, Coastal and Shelf Science 45:737-744

Valle-Levinson A, Miller JL, Wheless GH (1998) Enhanced stratification in the lower Chesapeake Bay following northeasterly winds. Continental Shelf Research 18:1631-1647

Vallino JJ, Hopkinson CS (1998) Estimation of dispersion and characteristics mixing times in Plum Island Sound estuary. Estuarine, Coastal and Shelf Science 46:333-350

Van de Kreeke J, Robaczewska K (1989) Effect of wind on the vertical circulation and stratification in the Volkerak Estuary. Netherlands Journal of Sea Research 23:239-253

van Raaphorst W, Ruardil P, Brinkman AG (1988) The assessment of benthic phosphorus regeneration in an estuarine ecosystem model. Netherlands Journal of Sea Research 22:23-36

Vanderborght JP, Billen G (1975) Vertical distribution of nitrate in interstitial water of marine sediments with nitrification and denitrification. Limnology and Oceanography 20:953-961

Varela M, Prego R, Belzunce MJ, Salas FM (2001) Inshore-offshore differences in seasonal variations of phytoplankton assemblages: the case of a Galician Ria Alta (Ria de A Coruña) and its adjacent shelf (NW of Spain). Continental Shelf Research 21:1815-1838

Varney M (1992) Mixed reactions. Nature 355:122

Vergara J, Prego R (1997) Estimación de los aportes fluviales de nitrato, fosfato y silicato hacia las Rías Gallegas. In Procesos Biogeoquímicos en Sistemas Costeros Hispano-Lusos. R. Prego, and J. M. Fernandez (eds), Servicio de Publicaciones de la Diputación de Pontevedra, Pontevedra, pp. 33-40

Vezina AF, Gratton Y, Vinet P (1995) Mesoscale physical and biological variability during a summer phytoplankton bloom in the lower St. Lawrence estuary. Estuarine, Coastal and Shelf Science 41:393-411

Vilas F, García-Gil E, García-Gil S, Nombela MA, Alejo I, Rubio B, Pazos O (1996) Ría de Pontevedra: Cartografía de sedimentos submarinos, Xunta de Galicia, Santiago, 39 pp

Vorosmarty CJ, Loder TC (1994) Spring-neap tidal contrasts and nutrient dynamics in a marsh dominated estuary. Estuaries 17:537-551

Wainright SC (1987) Stimulation of heterotrophic microplankton production by resuspended marine sediments. Science 238:1710-1712

Walsh JJ (1988) On the Nature of Continental Shelves. Academic Press, San Diego, 520 pp

Wang DP, Elliot AJ (1978) Non-tidal variability in the Chesapeake Bay and Potomac River: Evidence for non-local forcing. Journal of Physical Oceanography 6:225-232

Webster IT, Smith SV, Parslow JS (2000) Implications of spatial and temporal variation for biogeochemical budgets of estuaries. Estuaries 23:341-350

Westrich JT, Berner RA (1984) The role of sedimentary organic matter in bacterial sulfate reduction: the G-model tested. Limnology and Oceanography 29:236-249

White KK, Dugdale RC (1997) Silicate and nitrate uptake in the Monterey Bay upwelling system. Continental Shelf Research 17:455-472

Wild-Allen K, Lane A, Tett P (2002) Phytoplankton, sediment and optical observations in Netherlands coastal water in spring. Journal of Sea Research 47:303-315

Wolanski E, King B, Galloway D (1997) Salinity intrusion in the Fly River estuary, Papua New Guinea. Journal of Coastal Research 13:983-994

Wooster WS, Bakun A, McLain DR (1976) The seasonal upwelling cycle along the eastern boundary of the North Atlantic. Journal of Marine Research 34:131-141

Yentsch CS, Menzel DW (1963) A method for the determination of phytoplankton chlorophyll and phaeophytin by fluorescence. Deep-Sea Research 10:221-231

Zdanowski MK, Figueiras FG (1997) Relationships between the abundance of bacteria and other biota and the hydrographic variability in the Ria de Vigo, Spain. Marine Ecology Progress Series 147:257-267